GRADUATE SCHOOL OF URBAN INNOVATION

YOKOHAMA NATIONAL UNIVERSITY

Development of a Benthic-Pelagic Coupled Numerical Model for Analyzing Water and Sediment Quality in Tokyo Bay

(東京湾の水質底質解析のための水中・堆積物結合数値モデルの開発)

by

A.A.W.R.R.M.K. AMUNUGAMA

A dissertation submitted in partial fulfillment of the requirements for the Doctoral Degree of Engineering

Academic Advisers:

Prof. Yoshiyuki Nakamura

Prof. Jun Sasaki

September, 2015

ABSTRACT

The occurrence of seasonal hypoxic and anoxic environment in shallow coastal and estuarine areas have been increased in recent past ensuing adverse effects to biodiversity, fisheries and food webs. To consider measures for improving hypoxia and anoxia, it is essential to develop a predictive model capable of reproducing long-term water and sediment quality considering their interactions. Many of the models have considered only seasonal and annual reproduction while some of the others have done decadal reproduction coupling with sediment models but mostly limited to two-layer or multi-layer models excluding the formation process of sedimentary bed itself. Hence, the objective of this study is to develop an integrated, layer resolved process-based, sediment-water coupled long-term predictive model aiming to reproduce long-term dynamics of water and sediment quality, including realistic process of sediment bed formation, and to analyze the principal mechanism of bed formation and thus its effect on water quality deterioration. Tokyo Bay is a good representation for seasonal hypoxic and anoxic environment in shallow coastal and estuarine areas, facing difficulties in controlling hypoxia and anoxia during summer even after considerable efforts during the past decades for reducing external loads into the bay and hence the model has been applied to Tokyo Bay.

Benthic-pelagic coupled ecosystem model is integrated with three dimensional hydrodynamic model, wave hindcasting model and bed shear stress model. Processes in water and sediment columns are considered independently and water column is coupled to sediment column through interaction layer flux. The state variables for the model are mainly temperature, salinity, three types of organic carbon, three types of phytoplankton, zooplankton, nutrients and dissolved oxygen. The model is forced by hourly meteorological data, daily river discharge data and instantaneous tidal motion. Initial conditions for all the state variables are given for water column and initial particulate organic carbon content is given except the zero initial values for all other state variables for sediment column. Boundary conditions are considered at the bay mouth, river mouths, free water surface and the bottom of the sediment layer. Three dimensional advection and diffusion equation in sigma coordinates is used for the water column while vertical advection and diffusion equation in Cartesian coordinates is used for sediment column. Control volume formulation with staggered grid system is adapted. Finite difference method with fourth order Runge-Kutta method is used to obtain the solution for governing differential equations. Model is

simulated for the period of April 1999 to March 2000 and long term computation with the same annual boundary conditions is continued until a reasonable steady state is achieved.

A set of data collected during the period of April 1999 to March 2000 at three locations in inner Tokyo Bay namely Chiba Light House (CLH), Keiyo Sea Birth (KSB) and Tokyo Light House (TLH) are used for verification of the water quality. The strongest blooming is during spring throughout the water column due to well mixed water while summer blooming is mainly in surface layers of the water column due to the effect of stratification. Even though the winter blooming is not as strong as spring blooming, well mixed water column resulted in blooming throughout the water column. Sediment oxygen demand which has been defined as the oxygen flux to sediment from water, reaches its lowest during summer validating anoxic decomposition in sediment and confirming hypoxia or anoxia in water column.

Spatial distribution of sediment quality such as water content (WC), particulate organic carbon content (POCC), total nitrogen content (TNC) and Total phosphorous content (TPC) are validated with the data collected for the year 2001. Model can reproduce the spatial distributions of sediment quality, such as WC, POCC, TNC and TPC showing the largest contents at the central part of the bay. Furthermore, it has been reproduced that the similar distribution of POCC in sediment and dissolved oxygen distribution in the bottom water confirming the phenomena of sediment pollution represented by POCC cause severe DO depletion (anoxia) in Tokyo Bay. Long term simulated results show the replacement of surface sediment with particulate organic carbon and the emergence of hypoxic water. Sensitivity analysis has been done to understand the effect of some important parameters of the model and to use them as tuning parameters of the model. Model is consistence and the multi-layered sediment model with maximum 1mm surface layer thickness gives the most realistic reproducibility of flux release in Tokyo Bay.

The model is confirmed to be robust for long term computations. After the validation of long term results, this model can be adopted to predict long term conditions and to propose measures against hypoxia in Tokyo Bay. Moreover, this modeling approach will be useful for considering long-term strategies to improve anoxia and hypoxia in polluted embayments in the world.

ACKNOWLEDGMENT

I would like to express my sincere gratitude to my academic adviser, Prof. Jun Sasaki for his valuable guidance and continuous dedication on supporting me towards the successful completion of this study. His vast knowledge on the fields of environmental research, numerical modeling and mathematical formulation showed me the precise approach to reach my research goals. My great acknowledgement must convey on his kind patience during all the weekly discussions on the model development. I believe that I could gain vast knowledge in numerous fields including way of thinking towards numerical model development, mathematical formulations, scientific paper writing and way of convincing research originalities. My research goals could never been achieved without his enormous support and dedication on research.

I greatly acknowledge my other academic supervisors Prof. Yoshiyuki Nakamura and Associate Prof. Takayuki Suzuki for giving me valuable advices during my research studies. Even though I started my research discussions with Prof. Nakamura at the mid way of my research, through his vast knowledge on the field of environmental research, I could improve my knowledge to obtain better outcomes of this research. I am very thankful to Associate Prof. Suzuki especially for his valuable comments on my work during the progress presentations. I indebted to their kind support in numerous ways and understanding my family situation when I couldn't attend for lab and sometime for some lab activities. I would like to express my sincere gratitude for other examiners of my doctoral defense Prof. Tatsuya Tsubaki and Associate Prof. Kimitoshi Hayano for their valuable comments.

I would like to thank our lab secretary Ms. Akiko Nakao for her kind support during my stay at YNU. It is my pleasure to thank Dr. Retno Wiyono, Dr. Chamila Niroshinie, and Dr. Morteza Attari, lab mates Mr. Muchebve Edwin and Mr. Yamamoto Shuji for their numerous supports during my study at YNU.

My special thanks go to my parents, siblings and in lows who gave me inspiration, endless support to continue this study. This study could never been started and could never been completed successfully if I haven't had a great husband like Mr. Sumith Thennakoon. My special thanks for his sacrifices, endless support, inspiration with loads of love and kind understanding during this study. I also present my special thanks to my lovely sons; Nadun Thennakoon, Matheesha Thennakoon and Sandul Thennakoon who sacrificed in many ways and gave me courage to compete this hard work.

This study was partially funded by JSPS KAKENHI Grant Number 25289152. I would like to acknowledge Japan Meteorological Agency, Ministry of Land, Infrastructure, Transport and Tourism, and Tokyo Metropolitan Government for providing meteorological and river discharge data for this study. I acknowledge Dr. Koibuchi, Y. for providing us water quality data and Dr. Okada, T. for providing us Tokyo Bay sediment quality data.

I appreciate all the others who could not mention here in names but encouraged me at least by a word.

CONTENTS

1. INTRODUCTION 1

1.1 BACKGROUND 1

1.2 OBJECTIVES OF THIS STUDY 3

1.3 LITERATURE REVIEW 4

1.4 ORGANIZATION OF THE DISSERTATION 15

2. MODEL FRAMEWORK 16

2.1 DEVELOPMENT OF A BENTHIC-PELAGIC COUPLE MODEL 16

2.2 APPLICATION OF MODEL TO TOKYO BAY 19

2.2.1 Model grid system 19

2.2.2 Initial conditions 19

2.2.3 Boundary conditions 20

2.2.4 Time step and output 27

2.2.5 Model forcing and validation 28

3. HYDRODYNAMIC, WAVE HINDCASTING AND BED SHEAR STRESS MODELS 32

3.1 HYDRODYNAMIC MODEL 32

3.1.1 Initial and boundary conditions 35

3.1.2 Numerical scheme 36

3.1.3 Grid system 37

3.2 WAVE HINDCASTING MODEL 38

3.3 BED SHEAR STRESS MODEL 41

4. PELAGIC MODULE IN ECOSYSTEM MODEL 42

4.1 GOVERNING DIFFERENTIAL EQUATIONS FOR ANY SCALAR PARAMETER 42

4.1.1 Discretization of advection and diffusion equation 47

4.1.2 Surface and bottom boundary conditions 54

4.1.3 Particulate matter settling 60

4.1.4 Source terms 68

5. BENTHIC MODULE IN ECOSYSTEM MODEL 81

5.1 POROSITY CHANGE WITH RESPECT TO PARTICULATE ORGANIC CARBON CONTENT 81

5.2 LAYER THICKNESS ADJUSTMENT 84
5.3 RENEWAL OF CONCENTRATIONS OF STATE VARIABLES 85
5.4 GOVERNING DIFFERENTIAL EQUATIONS FOR ANY SCALAR PARAMETER 86
5.4.1 Dissolved matter 87
5.4.2 Particulate matter 98
5.4.3 Surface and bottom boundary conditions 105
5.4.4 Solution for the discretized equations 122
5.4.5 Source terms 124
5.5 EVALUATION OF THE BURIAL RATE 130
6. BOUNDARY FLUX ANALYSIS AND BENTHIC-PELAGIC MODEL COUPLING 131
6.1 DISSOLVED OXYGEN FLUX AT THE WATER SURFACE 131
6.2 FLUX AT SEDIMENT-WATER INTERFACE 133
6.2.1 Dissolved matter 133
6.3 FLUX AT THE BOTTOM OF THE SEDIMENT 136
6.3.1 Dissolved matter 136
6.3.2 Particulate matter 137
6.4 BENTHIC-PELAGIC MODEL COUPLING AND BOTTOM BOUNDARY TREATMENT 138
6.4.1 Boundary flux treatment in pelagic model 138
6.4.2 Boundary flux treatment in benthic model 140
7. RESULTS AND DISCUSSION 143
7.1 WATER QUALITY 143
7.1.1 Salinity and temperature 143
7.1.2 Chlorophyll_ a 145
7.1.3 Dissolved oxygen 146
7.1.4 Phosphate phosphorous 150
7.1.5 Ammonia nitrogen 151
7.1.6 Nitrate nitrogen 152
7.1.7 Dissolved silica 153
7.2 SEDIMENT QUALITY 154
7.2.1 Spatial distributions of sediment quality 154
7.2.2 Vertical distribution of sediment quality 162

7.3 Effect of flux on water and sediment quality 171
7.4 Long term water and sediment quality 174
8. SENSITIVITY ANALYSIS 177
8.1 Consistency of the pelagic model on settling 177
8.2 Consistency of the benthic model under no flux condition 178
8.3 Consistency of the benthic-pelagic coupled model 179
8.4 Sensitivity analysis on discharge magnification factor 179
8.5 Sensitivity analysis on sediment layers 183
8.6 Sensitivity analysis on sorption and desorption 185
8.7 Sensitivity analysis of critical BSS on deposition and erosion 187
8.8 Sensitivity analysis of particulate organic carbon settling velocity on deposition 193
9. CONCLUSIONS 195

LIST OF FIGURES

Fig 1.1 Tokyo Bay topography 2
Fig 1.2 Distribution of sediment quality and water quality in Tokyo Bay 3
Fig 2.1 Schematic diagram of integrated process based multi layer benthic pelagic coupled ecosystem model 16
Fig 2.2 Schematic diagram of water and sediment processes 17
Fig 2.3 Numerical flow of the model 18
Fig 2.4 Locations of river and sewage point sources to Tokyo Bay at model grids 22
Fig 2.5 River discharges during one year period 26
Fig 2.6 Data collected locations 27
Fig 2.7 Meteorological conditions during one year period 31
Fig 3.1 Sigma coordinate transformation 33
Fig 3.2 Explicit and implicit approaches 36
Fig 3.3 Staggered grid system (a) x-sigma (b) y-sigma plane and (c) x-y plane 38
Fig 4.1 Spatial and vertical grid system for water column 42
Fig 4.2 Influx and efflux to the control volume 43
Fig 4.3 Settling of particles in water column at (a) any grid point, (b) at surface grid point and (c) at the bottom grid point 60
Fig 4.4 Bed shear stress on deposition or erosion 63
Fig 4.5 Algal growth limiting function for light 72
Fig 4.6 Algal growth limiting function for temperature 73
Fig 5.1 Vertical grid system for sediment column 81
Fig 5.2 Schematic diagram of sediment composition 82
Fig 5.3 Variation of porosity with respect to particulate organic carbon content 83
Fig 5.4 Effect of POCC on layer thickness change 84
Fig 5.5 Influx and efflux to the control volume 86
Fig 5.6 Movement of sediment material due to (a) deposition and (b) erosion 87
Fig 5.7 Sorption and desorption 89
Fig 5.8 2D Control volume 91
Fig 5.9 Advection term at CV faces 92
Fig 5.10 Upwind scheme approach 93
Fig 5.11 Porosity between two adjacent layers in sediment 94
Fig 5.12 Diffusion term at CV faces 94

Fig 5.13 Piecewise-linear profile assumption in vertical direction.....95
Fig 5.14 Advection term at CV faces.....101
Fig 5.15 Diffusion term at CV faces.....102
Fig 5.16 Advection term and diffusion term at CV faces.....106
Fig 5.17 Advection term and diffusion term at CV faces.....114
Fig 6.1 2D Control volume at water surface layer.....131
Fig 6.2 2D Control volume at sediment-water interface.....134
Fig 6.3 Boundary flux at sediment-water interface.....134
Fig 6.4 Boundary flux in water surface and bottom boundaries.....138
Fig 6.5 Boundary flux in sediment surface and bottom boundaries.....140
Fig 7.1 Observed and simulated salinity at (a) CLH, (b) KSB and (c) TLH.....143
Fig 7.2 Observed and simulated temperature at (a) CLH, (b) KSB and (c) TLH.....144
Fig 7.3 Observed and simulated Chl_*a* concentration at (a) CLH, (b) KSB and (c) TLH ...146
Fig 7.4 Observed and simulated DO concentration at (a) CLH, (b) KSB and (c) TLH 147
Fig 7.5 Bottom DO comparison with measured and computed at (a) CLH, (b) KSB and (c) TLH.....148
Fig 7.6 Simulate bottom DO at three stations.....149
Fig 7.7 Correlation of bottom DO between measured and computed at (a) CLH, (b) KSB and (c) TLH 149
Fig 7.8 Observed and simulated phosphorous concentration at (a) CLH, (b) KSB and (c) TLH.....150
Fig 7.9 Observed and simulated ammonia concentration at (a) CLH, (b) KSB and (c) TLH 151
Fig 7.10 Observed and simulated nitrate concentration at (a) CLH, (b) KSB and (c) TLH.152
Fig 7.11 Observed and simulated dissolved silica concentration at (a) CLH, (b) KSB and (c) TLH.....153
Fig 7.12 Observed (left) and simulated (right) spatial distributions of POCC 154
Fig 7.13 Simulated spatial distributions of POCC in every 5_year until model reaching a reasonable steady state.....156
Fig 7.14 Spatial distributions of (a) current induced bed shear stress, (b) wave induced bed shear stress and (c) total bed shear stress.....157
Fig 7.15 Distributions of BSS during 20-year period (a) at the inner part of the bay (b) at the bay mouth.....158
Fig 7.16 Observed (left) and simulated (right) spatial distributions of WC 159

Fig 7.17 Observed (left) and simulated (right) spatial distributions of (a) TP content and (b) TN content 160
Fig 7.18 Spatial distributions of POCC in sediment (left) and DO in bottom water (right) (a) data (b) simulated 162
Fig 7.19 Simulated vertical distributions of (a) DO, (b) ammonia (c) phosphorus (d) nitrate (e) dissolved silica (f) POC (g) Silt (h) particulate silica (i) POCC (j) WC (k) TPC (l) TNC (m) SiltC (n) porosity at CLH, KSB and TLH 167
Fig 7.20 Vertical distributions of phosphate (a) simulated and (b) data 168
Fig 7.21 Vertical distributions of ammonia (a) simulated and (b) data 169
Fig 7.22 Vertical distributions of nitrate (a) simulated and (b) data 169
Fig 7.23 Vertical distributions of POCC (a) simulated and (b) data 170
Fig 7.24 Vertical distributions of WC (a) simulated and (b) data 171
Fig 7.25 Simulated vertical distributions of (a) water nutrient, (b) water DO, (c) nutrient flux and (d) bed nutrient for phosphorous (left) and ammonia (right) at CLH 172
Fig 7.26 Simulated vertical distributions of (a) water nitrate, (b) water DO, (c) nitrate flux and (d) bed nitrate at CLH 173
Fig 7.27 Simulated vertical distributions of (a) water DO, (b) nutrient flux and (c) bed DO at CLH 174
Fig 7.28 20-year simulated vertical distributions of (a) POCC (b) Silt content and (c) WC in sediment column 175
Fig 7.29 20-year simulated vertical distributions of (a) *Chl_a* (b) DO in water column 176
Fig 8.1 Settling of suspended silt (a) with only diffusion (b) no diffusion 177
Fig 8.2 Sediment nutrients (a) ammonia and (b) phosphorous 178
Fig 8.3 Silt accumulation under no flux condition at the bottom boundary 179
Fig 8.4 Water salinity and temperature at CLH for different discharge magnification factors 180
Fig 8.5 Water salinity and temperature at KSB for different discharge magnification factors 181
Fig 8.6 Water salinity and temperature at TLH for different discharge magnification factors 182
Fig 8.7 (a) Simulated bottom ammonia variation in water column, (b) surface ammonia variation in sediment column, (c) bottom oxygen variation in water column with (1) 1mm, (2) 3mm and (3) 5mm surface layer thickness in sediment 183
Fig 8.8 Sediment oxygen demand 184

Fig 8.9 Ammonia flux 184
Fig 8.10 Observed and simulated (with 1mm surface layer thickness) dissolved oxygen concentration in water column at CLH 185
Fig 8.11 Simulated phosphorous and ammonia concentration in water column when (a) $D_p = 1\times10^{-5}$, (b) $D_p = 1\times10^{-6}$ and (c) $D_p = 1\times10^{-7}$ m^2/s 186
Fig 8.12 Variation of POCC with changing τ_D 187
Fig 8.13 Change of neutral zone with change of τ_D 188
Fig 8.14 Variation of POCC with changing τ_E 189
Fig 8.15 Change of neutral zone with the change of τ_E 190
Fig 8.16 Variation of POCC with changing both τ_D and τ_E 191
Fig 8.17 Change of possibility for deposition or erosion with change of τ_D and τ_E 192
Fig 8.18 vertical distribution of Silt content 192
Fig 8.19 Variation of POCC with changing POC settling velocity 194

LIST OF TABLES

Table 2.1 Nutrient concentrations of rivers and sewage point sources to Tokyo Bay (Japanese government sources) 21
Table 4.1 Stoichiometric relationships associated with biochemical processes 70

LIST OF SYMBOLS

Water	Sediment	Units	Description
salt		$[PSU]$	Salinity
tempt		$[°C]$	Temperature
C_{phy_1}		$[mgC/m\^3]$	Spring phytoplankton
C_{phy_2}		$[mgC/m\^3]$	Summer phytoplankton
C_{phy_3}		$[mgC/m\^3]$	Winter phytoplankton
C_{zoo}		$[mgC/m\^3]$	Zooplankton
C_{pocL}	B_{pocL}	$[mg/m\^3]$	Labile particulate organic carbon
C_{pocR}	B_{pocR}	$[mg/m\^3]$	Refractory particulate organic carbon
C_{pocI}	B_{pocI}	$[mg/m\^3]$	Inert particulate organic carbon
C_{NH_4}	B_{NH_4}	$[mMol/m\^3]$	Ammonium nitrogen
C_{PO_4}	B_{PO_4}	$[mMol/m\^3]$	Phosphate phosphorous
C_{NO_3}	B_{NO_3}	$[mMol/m\^3]$	Nitrate nitrogen
C_{Si}	B_{Si}	$[mMol/m\^3]$	Dissolved silica
C_{PSi}	B_{PSi}	$[mg/m\^3]$	Particulate biogenic silica
C_{DOX}	B_{DOX}	$[g/m\^3]$	Dissolved oxygen
C_{H_2S}	B_{H_2S}	$[g/m\^3]$	Sulfide
C_{silt}	B_{silt}	$[g/m\^3]$	Silt
Pelagic model parameters			
$R_{C_{phy}}$_PP		$[mgC/m\^3/s]$	Rate of primary production
$R_{C_{phy}}$_Met		$[mgC/m\^3/s]$	Rate of metabolism
$R_{C_{phy}}$_Mor		$[mgC/m\^3/s]$	Rate of mortality
$R_{C_{zoo}}$_G_each		$[mgC/m\^3/s]$	Rate of zooplankton grazing on each food
G_{Phy}		$[mgC/m\^3/s]$	Maximum rate of phytoplankton growth
TL_{phy}			Temperature limit for phytoplankton growth
LL_{phy}			Light limit for phytoplankton growth
NL_{phy}			Nutrient limit for phytoplankton growth
$K_{PO_4\_phy}$		$[mMol/m\^3]$	Half saturation constant of phosphorous

K_{nit_phy}	$[mMol/m\hat{}3]$	Half saturation constant of nitrogen
K_{SiO2_phy}	$[mMol/m\hat{}3]$	Half saturation constant of silica
$R_{C_{zoo}}$ _Gro	$[mgC/m\hat{}3/s]$	Rate of zooplankton growth
$R_{C_{zoo}}$ _Mor	$[mgC/m\hat{}3/s]$	Rate of zooplankton mortality
$R_{C_{zoo}}$ _Absor	$[mgC/m\hat{}3/s]$	Rate of zooplankton absorption
$R_{C_{zoo}}$ _ min_food	$[mgC/m\hat{}3/s]$	Rate of availability of minimum food for zooplankton
C_{zoo} _Absorb_portion		Maximum absorb portion of food by zooplankton
$R_{C_{zoo}}$ _G	$[mgC/m\hat{}3/s]$	Rate of zooplankton grazing
$R_{C_{zoo}}$ _G_pri	$[mgC/m\hat{}3/s]$	Grazing primitive of zooplankton
G_{zoo}	$[mgC/m\hat{}3/s]$	Maximum rate of zooplankton growth
TL_{zoo}		Temperature limit for zooplankton
FL_{zoo}		Food limit for zooplankton
$R_{C_{zoo}}$ _Fecal	$[mgC/m\hat{}3/s]$	Rate of zooplankton fecal
D_{zoo}	$[mgC/m\hat{}3/s]$	Maximum rate of zooplankton mortality
$R_{C_{pocL}}$ _dec_oxic	$[mgC/m\hat{}3/s]$	Rate of oxic decomposition for particulate organic carbon labile
$k_{C_{pocL},CpocL}$ _dec_oxic	$[mgC/m\hat{}3/s]$	Maximum rate of oxic decomposition for particulate organic carbon labile
$\theta_{C_{pocL}}$		Temperature coefficient for oxic decomposition of particulate organic carbon labile
$K_{O_2,Cpoc}$	$[gO_2/m\hat{}3]$	Oxygen half saturation constant for particulate organic carbon
$R_{C_{pocL}}$ _dec_anoxic_ $no3$	$[mgC/m\hat{}3/s]$	Rate of sub-oxic decomposition or denitrification for particulate organic carbon labile
$k_{C_{no3},CpocL}$ _denit	$[mgC/m\hat{}3/s]$	Maximum rate of sub-oxic decomposition for particulate organic carbon labile
$\theta_{C_{no3}}$		Temperature coefficient for sub-oxic decomposition of particulate organic carbon labile
$K_{dec,Cpoc}$	$[g/m\hat{}3]$	Half-saturation constant for denitrification of particulate organic carbon labile
$R_{C_{pocL}}$ _dec_anoxic_ $so4$	$[mgC/m\hat{}3/s]$	Rate of anoxic decomposition or sulfate as electron acceptor for particulate organic carbon labile

$k_{C_{pocL}}$ _dec_anoxic_so4	$[mgC/m\hat{}3/s]$	Maximum rate of anoxic decomposition for particulate organic carbon labile
$\theta_{C_{pocL}\_anoxic\_\_so4}$		Temperature coefficient for anoxic decomposition of particulate organic carbon labile
$K_{Cno3,\text{denit}}$	$[mMol/m\hat{}3]$	Half saturation constant for constant for nitrate in denitrification
$R_{C_{pocR}}$ _dec_oxic	$[mgC/m\hat{}3/s]$	Rate of oxic decomposition for particulate organic carbon refractory
$k_{C_{pocR},CpocR}$ _dec_oxic	$[mgC/m\hat{}3/s]$	Maximum rate of oxic decomposition for particulate organic carbon refractory
$\theta_{C_{pocR}}$		Temperature coefficient for oxic decomposition of particulate organic carbon refractory
$R_{C_{pocR}}$ _dec_anoxic_$no3$	$[mgC/m\hat{}3/s]$	Rate of sub-oxic decomposition or denitrification for particulate organic carbon refractory
$k_{C_{no3},CpocR}$ _denit	$[mgC/m\hat{}3/s]$	Maximum rate of sub-oxic decomposition for particulate organic carbon refractory
$R_{C_{pocR}}$ _dec_anoxic_$so4$	$[mgC/m\hat{}3/s]$	Rate of anoxic decomposition or sulfate as electron acceptor for particulate organic carbon refractory
$k_{C_{pocR}}$ _dec_anoxic_so4	$[mgC/m\hat{}3/s]$	Maximum rate of anoxic decomposition for particulate organic carbon refractory
$\theta_{C_{pocR}\_anoxic\_\_so4}$		Temperature coefficient for anoxic decomposition of particulate organic carbon refractory
$R_{C_{pocI}}$ _dec_oxic	$[mgC/m\hat{}3/s]$	Rate of oxic decomposition for particulate organic carbon inert
$k_{C_{pocI},CpocI}$ _dec_oxic	$[mgC/m\hat{}3/s]$	Maximum rate of oxic decomposition for particulate organic carbon inert
$\theta_{C_{pocI}}$		Temperature coefficient for oxic decomposition of particulate organic carbon inert
$R_{C_{pocI}}$ _dec_anoxic_$no3$	$[mgC/m\hat{}3/s]$	Rate of sub-oxic decomposition or denitrification for particulate organic carbon inert
$k_{C_{no3},CpocI}$ _denit	$[mgC/m\hat{}3/s]$	Maximum rate of sub-oxic decomposition for particulate organic carbon inert
$R_{C_{pocI}}$ _dec_anoxic_$so4$	$[mgC/m\hat{}3/s]$	Rate of anoxic decomposition or sulfate as electron acceptor for particulate organic carbon inert
$k_{C_{pocI}}$ _dec_anoxic_so4	$[mgC/m\hat{}3/s]$	Maximum rate of anoxic decomposition for particulate organic carbon inert
$\theta_{C_{pocI}\_anoxic\_\_so4}$		Temperature coefficient for anoxic decomposition of particulate organic carbon inert

$R_{C_{NH_4}}$ _nit	$[mMol/m\hat{}3/s]$	Rate of nitrification
$k_{C_{NH_4}}$ _nit	$[mMol/m\hat{}3/s]$	Maximum rate of nitrification
$K_{M,C_{NH_4}}$	$[mMol/m\hat{}3]$	Half-saturation constant for nitrification
$R_{C_{Si}}$ _pro	$[mMol/m\hat{}3/s]$	Rate of silica production
$k_{C_{Si}}$	$[mMol/m\hat{}3/s]$	Maximum rate of silica production
$\theta_{C_{Si}}$		Temperature coefficient for particulate silica dissolution
$K_{M,C_{PSi}}$	$[mMol/m\hat{}3]$	Half-saturation constant for particulate silica dissolution
$C_{Si,sat}$	$[mMol/m\hat{}3]$	Saturated concentration of silica
$R_{C_{H_2S}}$ _oxi	$[gS/m\hat{}3/s]$	Rate of sulfide oxidization
$k_{C_{H_2S}}$ _oxi	$[gS/m\hat{}3/s]$	Maximum rate of sulfide oxidization
$\theta_{C_{H_2S}}$		Temperature coefficient for sulfide oxidization
K_{M,C_{H_2S},O_2}	$[gS/m\hat{}3]$	Half saturation constant of oxygen for sulfide oxidization
Benthic model parameters		
$R_{B_{pocL}}$ _dec_oxic	$[mgC/m\hat{}3/s]$	Rate of oxic decomposition for particulate organic carbon labile
$k_{B_{pocL},BpocL}$ _dec_oxic	$[mgC/m\hat{}3/s]$	Maximum rate of oxic decomposition for particulate organic carbon labile
$\theta_{B_{pocL}}$		Temperature coefficient for oxic decomposition of particulate organic carbon labile
$K_{O_2,Bpoc}$	$[gO_2/m\hat{}3]$	Oxygen half saturation constant for particulate organic carbon
$R_{B_{pocL}}$ _dec_anoxic_$no3$	$[mgC/m\hat{}3/s]$	Rate of sub-oxic decomposition or denitrification for particulate organic carbon labile
$k_{B_{no3},BpocL}$ _denit	$[mgC/m\hat{}3/s]$	Maximum rate of sub-oxic decomposition for particulate organic carbon labile
$\theta_{B_{no3}}$		Temperature coefficient for sub-oxic decomposition of particulate organic carbon labile
$K_{dec,Bpoc}$	$[g/m\hat{}3]$	Half-saturation constant for denitrification of particulate organic carbon labile
$R_{B_{pocL}}$ _dec_anoxic_$so4$	$[mgC/m\hat{}3/s]$	Rate of anoxic decomposition or sulfate as electron acceptor for particulate organic carbon

		labile
$k_{B_{pocL}}$ _dec_anoxic_so4	$[mgC/m\hat{}3/s]$	Maximum rate of anoxic decomposition for particulate organic carbon labile
$\theta_{B_{pocL\_anoxic\_\_so4}}$		Temperature coefficient for anoxic decomposition of particulate organic carbon labile
$K_{Bno3,\text{denit}}$	[mMol/ $m\hat{}3$]	Half saturation constant for constant for nitrate in denitrification
$R_{B_{pocR}}$ _dec_oxic	$[mMol/m\hat{}3/s]$	Rate of oxic decomposition for particulate organic carbon refractory
$k_{B_{pocR},BpocR}$ _dec_oxic	$[mgC/m\hat{}3/s]$	Maximum rate of oxic decomposition for particulate organic carbon refractory
$\theta_{B_{pocR}}$		Temperature coefficient for oxic decomposition of particulate organic carbon refractory
$R_{B_{pocR}}$ _dec_anoxic_ $no3$	$[mgC/m\hat{}3/s]$	Rate of sub-oxic decomposition or denitrification for particulate organic carbon refractory
$k_{B_{no3},BpocR}$ _denit	$[mgC/m\hat{}3/s]$	Maximum rate of sub-oxic decomposition for particulate organic carbon refractory
$R_{B_{pocR}}$ _dec_anoxic_ $so4$	$[mgC/m\hat{}3/s]$	Rate of anoxic decomposition or sulfate as electron acceptor for particulate organic carbon refractory
$k_{B_{pocR}}$ _dec_anoxic_so4	$[mgC/m\hat{}3/s]$	Maximum rate of anoxic decomposition for particulate organic carbon refractory
$\theta_{B_{pocR\_anoxic\_\_so4}}$		Temperature coefficient for anoxic decomposition of particulate organic carbon refractory
$R_{B_{pocI}}$ _dec_oxic	$[mgC/m\hat{}3/s]$	Rate of oxic decomposition for particulate organic carbon inert
$k_{B_{pocI},BpocI}$ _dec_oxic	$[mgC/m\hat{}3/s]$	Maximum rate of oxic decomposition for particulate organic carbon inert
$\theta_{B_{pocI}}$		Temperature coefficient for oxic decomposition of particulate organic carbon inert
$R_{B_{pocI}}$ _dec_anoxic_ $no3$	$[mgC/m\hat{}3/s]$	Rate of sub-oxic decomposition or denitrification for particulate organic carbon inert
$k_{B_{no3},BpocI}$ _denit	$[mgC/m\hat{}3/s]$	Maximum rate of sub-oxic decomposition for particulate organic carbon inert
$R_{B_{pocI}}$ _dec_anoxic_ $so4$	$[mgC/m\hat{}3/s]$	Rate of anoxic decomposition or sulfate as electron acceptor for particulate organic carbon inert
$k_{B_{pocI}}$ _dec_anoxic_so4	$[mgC/m\hat{}3/s]$	Maximum rate of anoxic decomposition for particulate organic carbon inert

$\theta_{B_{pocI\_anoxic\_\_so4}}$		Temperature coefficient for anoxic decomposition of particulate organic carbon inert
$R_{B_{NH_4}}$ _nit	$[mMol/m\hat{}3/s]$	Rate of nitrification
$k_{B_{NH_4}}$ _nit	$[mMol/m\hat{}3/s]$	Maximum rate of nitrification
$K_{M,B_{NH_4}}$	$[mMol/m\hat{}3]$	Half-saturation constant for nitrification
$R_{B_{Si}}$ _pro	$[mMol/m\hat{}3/s]$	Rate of silica production
$k_{B_{Si}}$	$[mMol/m\hat{}3/s]$	Maximum rate of silica production
$\theta_{B_{Si}}$		Temperature coefficient for particulate silica dissolution
$K_{M,B_{PSi}}$	$[mMol/m\hat{}3]$	Half-saturation constant for particulate silica dissolution
$B_{Si,sat}$	$[mMol/m\hat{}3]$	Saturated concentration of silica
$R_{B_{H_2S}}$ _oxi	$[gS/m\hat{}3/s]$	Rate of sulfide oxidization
$k_{B_{H_2S}}$ _oxi	$[gS/m\hat{}3/s]$	Maximum rate of sulfide oxidization
$\theta_{B_{H_2S}}$		Temperature coefficient for sulfide oxidization
K_{M,B_{H_2S},O_2}	$[gS/m\hat{}3]$	Half saturation constant of oxygen for sulfide oxidization
Benthic - pelagic common parameters		
rPC_dec		Ratio of phosphorous to carbon for particulate organic carbon decomposition
rNC_dec		Ratio of nitrogen to carbon for particulate organic carbon decomposition
rSiC_phy		Ratio of silica to carbon for particulate organic carbon decomposition
rSi_PSi		Ratio of dissolved silica to particulate silica
rCS_dec		Rate of carbon to sulfur for particulate organic carbon anoxic decomposition
rCS_oxi		Rate of carbon to sulfur for sulfide oxidization
rOC_dec		Ratio of oxygen to carbon for particulate organic carbon decomposition
rON_nit		Ratio of oxygen to nitrogen for nitrification
rOS_oxi		Ratio of oxygen to sulfur for sulfide oxidization
Benthic-pelagic interaction parameters		

Jflux	$[g/m\hat{}2/s]$		Deposition/resuspension flux of any particulate state variable
Diffusion_flux_s2w	$[mMol/m\hat{}2/s]$ $[g/m\hat{}2/s]$	or	Diffusion flux of any diffusion state variable between sediment and water
flux_s2w	$[mMol/m\hat{}2/s]$ $[g/m\hat{}2/s]$	or	Advection flux of any state variable between sediment and water
flux_b2s	$[mMol/m\hat{}2/s]$ $[g/m\hat{}2/s]$	or	Advection flux of any state variable between active sediment and bed

1. INTRODUCTION

1.1 Background

Water quality management needs to understand key processes affecting environmental problems such as eutrophication due to excessive nutrient loadings, low dissolved oxygen (DO) conditions caused by waste water discharges and accumulation of toxic materials in the sediment bed. Estuaries and lakes are the most affected marine and fresh water systems, where water tends to stagnate and feel the impact of excessive nutrient loading, leading to organic rich sediment bed especially when the solar radiation increases and air temperature goes up in spring and summer.

The appearance of hypoxia in water is mainly related with the characteristics of the sediment and hence the accurate sediment model is an important component to predict water quality and to propose measures against hypoxia. Sediment not only changes the water turbidity but also affects the nutrient concentrations in water. Particulate organic matter settles down in the water column and accumulates on the surface of the sediment bed. Settled particulate organic carbon undergoes diagenesis through oxic decomposition ensuing hypoxic or anoxic conditions in water column. Furthermore, aerobic or anaerobic decomposition of those accumulated particulate organic carbon has resulted in building up of high concentrations of phosphate and ammonia in sediment, and under anoxic conditions those nutrients are released to overlying water. Release of nutrients mainly depends on the characteristics of the bed. Sandy bed contains relatively little organic matter while muddy bottom contains abundant nutrients to release. These released nutrients from the sediment bed under hypoxic and anoxic conditions have resulted in eutrophication considerably. Therefore, water quality is directly related with the sediment fluxes. Excess nutrients then lead to eutrophication extensively.

Even though the models can be used to support water quality management and decision-making, it increasingly depends on accurate modeling and hence models should be more realistic. Thus, the water quality modeling, especially for long term predictive models, should include the detailed sediment process model and then estimate the correct sediment flux release to water. Process based coastal ecosystem models mainly consider physical processes, bioprocesses and chemical processes. Other than those general processes, mechanism of changing porosity with respect to POCC in sediment has been emerged from field data

analysis (Okada and Furukawa, 2005). Moreover, a critical aspect of water quality modeling, particularly for long term predictions and considering measures against hypoxia and anoxia is the long-term estimation of sediment quality. Many of the models have considered only seasonal and annual reproductions (Sasaki and Isobe, 2000) and (Koibuchi et al., 2001) while some of the others have done decadal reproduction coupling with sediment models but mostly limited to two-layer or multi-layer models excluding the formation process of sedimentary bed itself: e.g. (Di Toro, 2001) and (Ji, 2008). To consider measures for improving hypoxia and anoxia, it is essential to develop a predictive model capable of reproducing long-term water and sediment quality considering their interactions.

Tokyo bay represents the occurrence of seasonal hypoxic and anoxic environment in shallow coastal and estuarine areas which have been increased in recent past ensuing adverse effects to biodiversity, fisheries and food webs. Tokyo Bay with an average depth of 15m **Fig 1.1** shows the water stratification from late spring to autumn controlling phytoplankton proliferation due to excess nutrients in surface layers and at the same time the emergence of hypoxic water in the bottom layers of the water column.

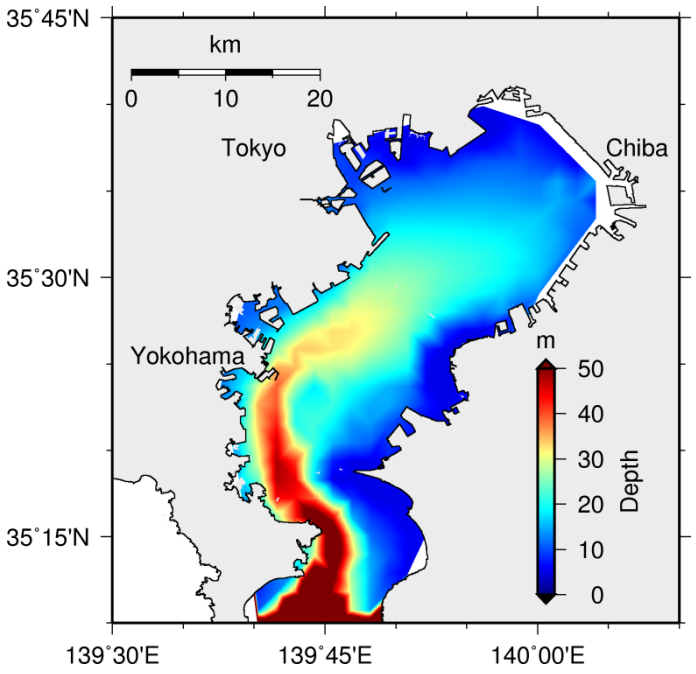

Fig 1.1 Tokyo Bay topography

Magnitude of the most dominant Phytoplankton species namely *S. costatum* in the bay is mostly limited by the variation of nutrients, specifically phosphate (Sasaki and Isobe, 2000). Even though the external loads to the bay have been reduced, nutrients released from the

sediment bed have resulted eutrophication significantly. Furthermore, Tokyo Bay shows increase of sediment WC at the central part of the bay. According to field data it has been proved that there exist not only high WC at the central part of the bay, but also some correlations between WC and other sediment quality parameters, such as POCC, TNC and TPC in sediment. Moreover, the spatial distribution of POCC in the sediment surface and the spatial distribution of dissolved oxygen concentration in bottom water show similar distributions as shown in the **Fig 1.2** confirming the active benthic pelagic coupling in the inner part of the bay. Even after considerable efforts during the past decades it is still facing difficulties in controlling hypoxia and anoxia especially during summer.

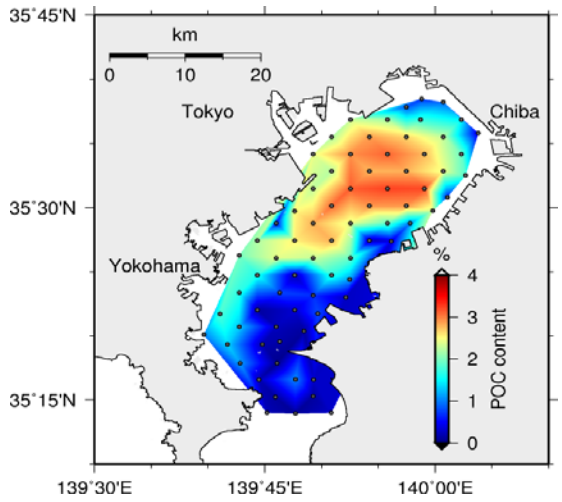

(a) POCC in the surface sediment (Okada and Furukawa, 2005)

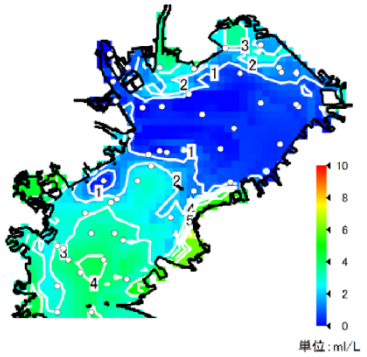

(b) Example of DO concentration in the bottom water ("Prediction of Bottom water hypoxia in Tokyo Bay", Chiba Prefecture., July 24, 2014)

Fig 1.2 Distribution of sediment quality and water quality in Tokyo Bay

1.2 Objectives of this study

The goal of this study is to develop an integrated, benthic-pelagic coupled, layer-resolved and process based a long-term predictive ecosystem model with sediment bed formation, which can be used to analyze water and sediment quality in Tokyo Bay, and to analyze the

principal mechanism of bed formation and thus its effect on water quality deterioration. This goal will be accomplished through the following achievements;

- Development of a robust and consistent pelagic model
- Development of a robust and consistent benthic model
- Coupling pelagic and benthic model through interaction layer flux
- Sensitivity analysis on critical parameters
- Validation of pelagic model
- Validation of benthic model

1.3 Literature review

Literature review has been mainly carried out on two different aspects; to understand the Tokyo Bay ecosystem through experimental research outcomes, and to understand methods for the development of numerical models to analyze water and sediment quality of coastal and inland environment.

Tokyo Bay ecosystem assessment

According to (Han et al., 1991) seasonally varying composition of red tides in Tokyo Bay has been comprised almost entirely of *Skeletonema costatum* during summer 1986 and 1987. The contribution of *S. costatum* has been analysed by species-specific photosynthetic rate (SSP). SSP of *S. costatum* has normalized with cell volume and considered as an indicator of growth activity. They have found that the volume-specific SSP is high in the initial phase of bloom while it decreases gradually with cell division, reaching a minimum at the peak of the bloom showing short-lived high volume -specific SSP.

(Han and Furuya, 2000) have conducted field investigations in Tokyo Bay from 1986 to 1987 to investigate the seasonal variation of phytoplankton dynamics through the methods of size fractionation and single-cell isolation. Period of red tide occurrence has been confirmed from spring to autumn. A diatom, *Skeletonema costatum* and a rapidophycean, Hetrosigma akashiwo have been identified as most important primary producers while small diatoms and flagellates have become dominant showing rapid changes of phytoplankton community structure within several days in summer. According to their observations nanoplankton

fraction has contributed most to Chlorophyll_*a* concentration and primary production during spring to autumn while microplankton contribution has become remarkable in winter. Moreover, picoplankton has remained relatively constant though out the year. They have further discussed the factors controlling the reduction of assimilation rates at the peak of the bloom, and changes in phytoplankton community structure.

(Fujiwara and Yamada, 2002) have analysed the temporal and spatial variations in the inflow of oceanic water into Tokyo Bay and its influence on hypoxia through the data collected during the summer 1998. Furthermore the accompanying changes in circulation within the bay have been studied by repeated measurements of the longitudinal distributions of hydrographic parameters and oxygen concentration from the bay head to off the bay mouth. According to them, density changes in the upper ocean induce inflow and outflow of oceanic water in the bay and hence when water density increased in the upper ocean, heavy saline water intruded into the lower layer of the bay. That inflow has forced a bottom hypoxic water mass to the bay head and, ultimately, lifted it up to a subsurface hypoxic water mass which then moved out as a thin layer just under a pycnocline, reaching beyond the bay mouth. According to the observations, as a result of intruding heavier deep water retreated and an intrusion of oceanic water at intermediate depth occurred, the hypoxic water mass has been displaced from the centre to the mouth of the bay.

Sediment condition of the shoreward area in Tokyo Bay has been mapped using sediment condition classification system based on echo features by (Okada and Furukawa, 2005). The sediment condition has been categorized by its moisture content, which has been correlated to the echo trace output. According to their conclusions, good condition sediments are intermittently spaced in the shoreward area that has previously presumed to be totally covered by sludge.

(Okada and Furukawa, 2005) have conducted field survey of sonar sounding of sediment as well as sediment sampling simultaneously in order to investigate benthic faunal distribution in Tokyo bay. They have shown the detailed spatial distribution of moisture content in Tokyo Bay. It has been revealed that sediments with relatively low moisture content whose value of 150% or less present even in highly stagnant basin in Yokohama/Kawasaki Port, Tokyo Port, Chiba and Ichihara ports areas. According to their field survey of benthic fauna, the number of species as well as the Index of biodiversity in Yokohama and Kawasaki Port has become comparable with those in sediment of Nakanose area, in which rich biodiversity had been well reported. Thus, they have been concluded that sea floor with relatively less moisture content of sediment, which are studded or distributed

locally in Yokohama and Kawasaki Port, serve as good habitat of benthos. Moreover it has been evidenced that sonar sounding technique employed in this study can be available for detecting such a missing small area with rich biodiversity.

Field observations done in 1999 spring by (Koibuchi and Isobe, 2007) have been aiming at the continuous measurements on short term variations in semi-enclosed bays. Toward the estimation of the conditions necessary for red tide occurrences in an area affected by eutrophication, they have carried out continuous measurements in the inner part of Tokyo Bay at three stations where red tide have been observed during spring. They have confirmed that blooms of phytoplankton occur under high solar radiation conditions, and in accounting for the levels of blooms, most important considerations are the mixed layer thickness and the vertical distribution of Photosynthetically Active Radiation (PAR). It has been found that phytoplankton can increase rapidly even under average solar radiation if optimum conditions of mixed-layer thickness and the eutrophic zone are met. As a consequence of north-wind induced outflow and vertical mixing have been identified as the causes for diluting phytoplankton and terminating blooms. Moreover, they have shown that the self shading effect of phytoplankton does not allow continuous blooming even there if there is not a strong wind.

(Nakane et al., 2008) have recoded data of water temperature, salinity, nutrient concentrations and the composition of the plankton community at three stations in inner Tokyo Bay over a period of 328 days with a sampling frequency of once per day. According to their data the period from June to October has been characterized as the development of stratification of temperature and salinity and November to March has been characterized as uniform salinity and temperature in water column due to vertical mixing. Moreover, it has been confirmed that the oxygen depleted water forms in the bottom layer during the stratification period. Nutrient loads have found to be high in the surface water due to the fresh water supply and occasionally phosphate has depleted due to pulses of primary production and that has suggested that the phosphate is the limiting nutrient during that period. *Skeletonema costatum* and several species of ciliates have shown significant fluctuations in their densities during short term periods. They have confirmed that the short term dynamics of the phytoplankton community are closely coupled to fluctuations in environmental forcing and the degree of coupling is stronger when the solar radiation is greater.

(Bouman et al., 2010) have examined the phytoplankton biomass and primary production in their environmental context, for a semi closed bay considering the case study of Tokyo Bay. Monthly collected data samples over a three year period have been analysed. According

to the data analysis, in the late spring and summer due to heavy precipitation and high surface temperatures, it gives rise to a highly stratified water column and consequently stimulated a series of phytoplankton bloom, whereas during the winter, a weakly-stratified and deeply-mixed water column leads to a rapid decline in phytoplankton biomass under light-limited growth conditions. According to them, as a result of high water turbidity and deep vertical mixing, both separately and in concert, light limit the algal growth over much of the year. They have assessed the relative influence of nutrient limitation and light limitation on algal growth.

Numerical modeling on water and sediment quality

Spatial and temporal hydrodynamic and water quality modeling analysis of a large reservoir on the south California (USA) coastal plain has done by (Tufford and McKellar, 1999). A 2D hydrodynamic model of Lake Marion has been developed using DYNHYD5 (WASP5) modeling package. EUTRO5 water quality model has been adopted. The model has been simulated a 12-month period representing 5-year average conditions. The model has been reproduced nutrients and phytoplankton dynamics of the lake. They have found that sediment sources of ammonia and phosphate are important to achieve model calibration, especially during high temperatures and low DO. Moreover, according to their study, ecological factors that influence phytoplankton productivity and nutrient dynamics are different in various parts of the lake.

A quasi-three-dimensional baroclinic hydrodynamic and water quality model has been developed by (Sasaki and Isobe, 2000). They have developed primitive equations with Boussinesq and hydrostatic approximations and then have transformed into sigma coordinates in order to overcome difficulties in handling irregular beds. They have developed a water quality model to compute oxygen depletion and applied it for Tokyo Bay. State variables of *S. Costatum* as the dominant species in the bay, DO, phosphate as the limiting nutrient have been considered in the model. Horizontal grid resolution of the model was 1km × 1km and vertically 20 sigma layers have been adopted. The Model has been forced by hourly meteorological data and instantaneous tidal motion. Computation was done during the spring and summer of 1994. The upwelling of anoxic water with high concentration of phosphate during the period which south wind had high velocity has been considered in the model. They have been able to reproduce the oxygen dynamics during the specific periods considered.

Two layer sediment model has been developed by (Di Toro, 2001) based on the principle of mass balance. That is the concept of change in the mass of any constituent within a volume must be the result of sources of mass to the volume, less the losses within the volume, and export from the volume. Two layers have considered as aerobic and anaerobic. Their main assumption was the POM settles to the bottom anaerobic layer since the aerobic layer is thinner enough. They have mainly considered four processes; (1) POM form the overlying water is deposited into the aerobic and anaerobic layers of the sediment which have referred as depositional flux, (2) The particulate organic matter mineralize in the sediment. This termed as diagenesis converts POM into soluble intermediates. Other than that sorption which converts a portion of the soluble species into particulate species has been considered. (3) Transported process of species by diffusion and particulate mixing into the aerobic layer from which they either transferred into the overlying water or, further react and consume DO or remixed into anaerobic layer. (4) Particulate and dissolved chemicals are buries via sedimentation. In this aspect they have assumed the layers are moving with the rate of burial velocity keeping their thicknesses constant. This general framework has been employed for each of the dependent variable.

(Sohma et al., 2001) have been developed a new coastal marine ecosystem model coupling with hydrodynamics and tidal flat ecosystem effects and applied to Mikawa Bay, Japan. They have resolved the flux dynamics of carbon, nitrogen, phosphorous and oxygen through the consideration of biochemical and physical interactions among them. They have found that the oxygen depleted water at the sea bottom especially during the summer has been resulted due to the increase of oxygen consumption in the benthic system and decrease of vertical mixing of water. They have concluded that the tidal flat has the potential to restrict the red tide effect in short term scale while it restricts the sedimentation of detritus in long term scale.

(Sasaki et al., 2002) has been developed an ecosystem model to reproduce water quality. They have considered pelagic sub model with two layered benthic sub-model. The two layers of sediment have been categorized as oxic surface layer and anoxic bottom layer. The thickness of each layer has been controlled by the rate of respiration of bacteria and the oxygen concentration in the bottom water. They have discussed the dynamic variation in nutrient concentrations by considering the effects of fresh water inflows, uptake by phytoplankton during blooms, degradation of sinking particulate organic materials, flux release from the bottom sediment and denitrification under anoxic condition.

(Kim et al., 2004) have constructed a coupled three dimensional hydrodynamic and ecotoxicological model and then applied into Tokyo Bay. The non-commercial Princeton Ocean model has been applied as the hydrodynamic model with some modifications to consider the effects such as tide, freshwater inflow and wind while ecotoxicological model based on finite difference method has been developed during their study. They have analyzed dissolved Bisphenol A and found that its concentration is highly sensitive for the biodegradation rate. Moreover, they have concluded that bioconcentration factor is the most important factor for Bisphenol A in phytoplankton while biodegradation rate and partition coefficient are most important for Bisphenol A in particulate organic carbon.

(Zheng et al., 2004) have been developed a 3D physical and water quality model for the Satilla River Estuary, Georgia. Physical model has been based on the Estuarine and coastal ocean model (ECOM-si) while 3D conventional water quality analysis simulation program (WASP5) has been modified to develop the water quality model. Concentrations of inorganic nutrients such as ammonia, nitrate plus nitrite and ortho-phosphorouse, Chlorophyll_*a* and DO have been predicted from the model. According to their findings the intertidal salt mash is the main sink for particulate material and the major consumer of DO making high sediment oxygen demand. Moreover they have concluded that the tidal mixing-induced bottom resuspension process plays a critical role in supplying nutrients to the water.

A hydrodynamic and water quality modeling study has been done by (Na and Park, 2006). They have applied the model to Lake Paldang, a lake in South Korea that is stratified by incoming flows. The Generalized, Longitudinal-Lateral-Vertical Hydrodynamic and Transport (GLLVHT) model has been embedded within the Generalized Environmental Modeling System for Surface waters (GEMSS). They have determined the spatial and temporal patterns of phytoplankton growth through the model. The model has been applied to examine the distributions of water quality and residence time in the lake and phytoplankton response to changes in nutrient loads. They have further analyzed the influence of the hydrodynamics on phytoplankton response. It has been concluded that the lake is phosphorus limiting, and limiting nutrient loadings and reducing phosphorous loading may be effective in controlling phytoplankton blooming.

(Ji, 2008) has developed water quality and sediment quality model with hydrodynamic model. Their 3D hydrodynamic model has based on the fundamental principles of conservation of momentum, mass and energy. Approximations of (1) Boussinesq approximation, (2) hydrostatic approximation, and (3) Quasi-3D approximation have made to simplify the complex conservation equations. . The sediment quality model was more or less

similar to the model developed by (Di Toro, 2001). Kinetic formulae which have been used for the source terms of water state variables follow a similar approach as sediment kinetic formulae. Their model considers not only particulate organic carbon (POC) but also particulate organic nitrogen (PON) and particulate organic phosphorous (POP) in both water and sediment.

A benthic-pelagic coupled ecosystem model has been developed by (Sohma et al., 2008) to evaluate the oxygen-carbon-nitrogen-phosphorous coupled cycle which was driven by physical and biochemical processes. They have considered not only benthic-pelagic coupling but also central bay-tidal flat ecosystem coupling. The model has been applied for a time frame of 100 years under seasonal forcing functions to achieve an annual periodical steady state. Seasonal dynamics in the central bay and daily tidal dynamics in the tidal flat have been analyzed. Other than that they have been reproduced the vertical distribution of dissolved oxygen profile especially in hypoxic season and oxygen fluxes at the sediment-water interface.

A model for the prediction of waves and currents as well as bed shear stress has been developed by (Achiari and Sasaki, 2007) and integrated with the coastal circulation model developed by (Sasaki and Isobe, 2000). The wave model has been consisted of a wave hindcasting sub-model for the whole Tokyo Bay and a wave propagation sub-model for detailed wave computation in Sanbanze shallows. The wave hindcasting model has been based on the Shore Protection Manual formulas for both shallow and deep water cases with additional modifications in fetch calculation. The random wave propagation model has been based on a modified energy balance equation. The model has been validated for wave and current at two stations in Sanbanze Shallows in September 1999. The model has been reproduced the trend of time variation in wave and current successfully. Moreover, they have concluded that the computed bed shear stress distribution, which has dominated by waves rather than currents, correlates with the bottom sediment grain size distribution.

(Lopes et al., 2008) have validated a water quality model for the Rio de Aveiro, in order to use it as a predictive tool in the study of main water quality processes in the lagoon. Physical model has solved the classical 2D vertically integrated hydrodynamic and transport equations, and integrated in a hydrodynamic module while the water quality model has solved a system of differential equations that describes the chemical and biological state of the coastal waters. The model sensitivity analysis have shown that the ocean remains the main source of oxygen as well as the main factor controlling the DO distribution throughout the main lagoon areas due to the exchanges between the ocean and the lagoon. According to

their conclusions, hypoxia situation at very far and sallow areas are possible when the oxygen consumption related processes are dominant: at the intertidal areas and at areas situated at the far end of the lagoon, the DO concentration has become very low due to low phytoplankton concentration and low metabolism.

(Sasaki et al., 2009) have aimed at reduction of hypoxia and anoxia through an application of a mechanical circulator in an estuarine trench. This has been numerically examined in the phase of required flow rate and direction along with the physical mechanism of its effectiveness. They have developed a prototype of the circulator generating downward flow via an impeller attached to its main body which floats on the surface and transport the surface water to the bottom through a flexible draft tube connected to the floating body. They have verified the effectiveness of this circulator applying it to the Tokyo Bay. They have concluded that the circulator could achieve the desired objectives by reducing hypoxia and improving the water and sediment quality in the trench.

(Pochai, 2009) has used two mathematical models to simulate pollution due to sewage effluent in the nonuniform flow of water in a stream with varied current flow. A hydrodynamic model has been used to compute the velocity field and the elevation of the water flow. Dispersion model has followed one-dimensional advection-dispersion-reaction equation that gives the pollutant concentration fields. According to the results, the model could provide the elevation of water and the pollutant concentration at the discharge point to the stream. Moreover the model has been used to analyze the better locations and periods of time of different discharge points to the stream.

(Missaghi and Hondzo, 2010) have applied a 3D hydrodynamic model: Estuary and Lake Computer Model (ELCOM) coupling with an ecological model: Computational Aquatic Ecosystem Dynamic Model (CAEDYM) to simulate water quality parameters in three bays of the morphologically complex Lake Minnetonka. They have tried to reproduce spatial and temporal dynamics of temperature, DO, total phosphorous and Chl *a* considering one algae group. Ecological application of the model for the lake has been examined considering two cases: the effect of spatial heterogeneity on coldwater fish habitat analysis in 3D, and under a scenario where horizontal spatial heterogeneity is eliminated (1D), and have showed that the need for a 3D analysis in depicting ecological hot spots such as unsuitable fish habitats in the lake.

Integrated modeling system which included models of circulation, wave, sediment transport, and water quality have been developed by (Kim et al., 2010). They have analyzed the annual hypoxia and water dynamics in a shallow estuary in Southwest Florida which has

strong vertical salinity stratification due to moderate to high river discharge resulting reduced vertical mixing supplying dissolved oxygen from surface water to bottom water. They have concluded that the very low bottom dissolved oxygen concentrations were found at locations near the mouth of the river due to significant vertical stratification and increased sediment oxygen demand during the summer.

(Massoudieh et al., 2010) have been developed a quasi-two-dimensional model for simulating transport and transformation of contaminant species in river waters and sediments by considering the effect of geochemical reactions on the contaminated fate and mobility. They have considered the downstream transport of dissolved and sediment-associated species, and the mass transfer with bed sediment due to erosion and resuspension, through the linked advection-dispersion-reaction equations. A set of one dimensional columns representing sediment layers that consider the reactive transport of chemicals, burial , sorption/desorption and the diffusive transport of aqueous species have been taken into account in the bed sediment phase computation. Two demonstration cases have been considered both in the Central Basin Drain in the Central Valley of California.

Sediment-bacteria interaction processes in the Severn estuary and Bristol Channel have been numerically modeled by (Gao et al., 2011). A combined one and two-dimensional hydrodynamic model and two-dimensional suspended sediment transport model have been developed together with sediment-bacteria interaction model. They have investigated the impact of suspended sediment fluxes on the corresponding fecal bacteria transport processes. According to their findings the effects of the sediment-bacteria interactions on the bacterial levels in the water column were significant.

A 3D water quality model has been developed for the St. Lucie Estuary, a small and shallow estuary, by (Wan et al., 2012). The model has been calibrated and verified using two years of measured data. The calibrated model has been applied to study the hydrodynamic and eutrophication processes in the estuary. According to their findings the high concentrations of algae in the estuary are a result excessive nutrients and algae supply from freshwater inflows. Moreover, they have concluded that algal blooms may have led to the reduced DO at the bottom of the water body and at the same time stratification and circulation induced by freshwater inflows may also have contributed significantly for the bottom water hypoxia in the estuary.

(Zhao et al., 2012) have been developed a 3D hydrodynamic and water quality model for simulating flow circulation and pollutant fate and transport of Lake Fuxian in China. They could accurately reproduce the observed water surface elevation, spatiotemporal variations in

temperature, and total nitrogen, total phosphorous, and chemical oxygen demand. Through those results they have analyzed the total maximum daily load using two interpretations of water quality standards; the maximum instantaneous surface and annual average surface water concentrations.

(Zhao et al., 2013) have developed a 3D water quality model to investigate the causes as well as examining the underlying mechanism of eutrophication of Lake Yilong in Southwestern China. They have simulated the flow circulation, pollutant fate and transport, and the interactions between nutrients, phytoplankton and macrophytes. The model has been adopted to understand the water quality response to various load reduction intensities and ecological restoration measures. The results have showed that even if the nutrient load is reduced by as much as 77%, the Chl *a* concentration decreased only by 50% and aquatic vegetation has strong interaction with phytoplankton.

A linked hydrodynamic, water quality and algal biomass model for a large, multi-basin lake has been developed by (Zhang et al., 2013) and applied to Lake of the Woods (LOW). The 3D hydrodynamic Princeton Ocean Model (POM) has adopted as hydrodynamic model. They have considered mass balance model for total phosphorous loadings and linked mass-balance empirical model has been used to compute Chl *a*. they have tried to predict spatial differences in nutrients in particular total phosphorous, and algal and cyanobacterial standing stock (Chl *a*, biovolume-derived biomass and cynobacterial dominance).

Modeling of cohesive sediment dynamics in tidal estuarine systems has been done by (Franz et al., 2014). They have applied an available water modeling system with some modifications. They have considered the transport of cohesive sediment depends only on the advection-diffusion equation with a settling velocity included in vertical advection. Considering the combined effect of wave and currents on the bottom shear stress, the dynamics of cohesive sediment during the fortnightly and daily erosion-sedimentation cycle has been properly reproduced by that model. They have concluded that although tidal currents are the major cause of cohesive sediment erosion, wind induced waves also play an important role.

Patterns of temporal and spatial variability in hypoxia on the inner Louisiana-upper Texas (LaTex) shelf have been analysed by (Justić and Wang, 2014) using a FVCOM, an unstructured grid, 3D, hydrodynamic-water quality model. They have modeled the dynamics of DO using an expanded and revised version of the Water Analysis Simulation Program (WASP) coupling to a Finite Volume Coastal Ocean Model (FVCOM). They have found that the hypoxia originates in the bottom waters on the mid-continental shelf, where isolated

pockets of hypoxic water develop during early spring and late join into a larger continuous hypoxic zone; the dynamics of the bottom-water hypoxia is clearly influenced by the bathymetric features of the LaTex shelf; the dynamics of hypoxia on the LaTex shelf is strongly modulated by the frequency and intensity of cold fonts and tropical storms.

A 3D fecal coliform transport model has been developed by (Liu et al., 2015) and coupled with a hydrodynamic model to obtain a better understanding of local microbiological water quality in the tidal Danshuei River estuarine system of northern Taiwan. According to their results the measured and simulated salinity and fecal coliform have shown good agreements. The model has been applied to investigate the effects of upstream freshwater discharge variation and fecal coliform loading reduction.

A 3D water quality model to determine the environmental capacity of nitrogen and phosphorous in Jiaozhou Bay has been developed by (Li et al., 2015). They have coupled a 3D hydrodynamic model; the estuarine, coastal, and oceanic modeling system with sediments (ECOMSED) with a water quality model which has the ability to evaluate the environmental capacity of the coastal area for nitrogen and phosphorous in terms of nutrient kinetics. The water quality model has been composed of dissolved inorganic nitrogen phosphate, phytoplankton, zooplankton, detritus, dissolved organic nitrogen, and dissolved organic nitrogen. The model has been effectively reproduced the spatiotemporal variability in nutrient concentration.

(Zhang et al., 2015) have developed a benthic sediment diagenesis module and integrated into a hydrodynamic and water quality model of CE-QUAL-W2. The benthic sediment diagenesis model has been based on the framework developed by (Di Toro, 2001) and have considered well mixed two layers: top oxic or anoxic layer depending on the DO concentration in water column and bottom anoxic layer. They have studied the ability of the model to correctly predict sediment-water nutrient fluxes and sediment oxygen demand over time. Moreover the effect of benthic sediment diffusive thickness and particle mixing coefficients on nutrient releases from sediments has been examined. They have applied the model for five test cases. In addition the model has been applied to study the nutrient release and sediment oxygen demand of the lower Minnesota River in United States.

Literature can be concluded as:

1. Even though, Tokyo Bay is still facing difficulties in controlling hypoxia and anoxia, considerable efforts have been made during last few decades towards the aspect of controlling hypoxia.

2. In estuarine and coastal waters, sediment dynamics and its quality play an important role in both pelagic and benthic zones. All the above models have basically considered only physical processes, bioprocesses and chemical processes. Thus, more realistic modeling of sediment quality through the application of natural phenomena of sediment is very essential.
3. Almost all of these numerical studies analyzed short-term variations, i.e. few months and at most one year. Hence, the long term prediction of water and sediment quality is impractical though it is essential for estuarine and coastal environment management.

1.4 Organization of the Dissertation

The dissertation is organized into six chapters which include following contents.

Chapter 1 describes the importance of this research giving some background understanding, pass research outcomes with literature and the objectives of this study.

Chapter 2 explains the methodology of this study in detail.

Chapter 3 elucidates the governing equations of the coupled models of hydrodynamic, wave hindcasting and bed shear stress models.

Chapter 4 describes the pelagic model development through governing equations of the pelagic model.

Chapter 5 describes the benthic model development through governing equations of the benthic model.

Chapter 6 explains the coupling of benthic-pelagic model through interaction layer flux and describes the diffusive boundary discretization.

Chapter 7 includes the validation of water quality results and validation of sediment quality results with a discussion on discrepancies and important outcomes.

Chapter 8 includes sensitivity analysis to understand the effect of critical parameters on overall results

Chapter 9 concludes the present work showing some major results.

2. MODEL FRAMEWORK

2.1 Development of a benthic-pelagic couple model

An integrated benthic-pelagic coupled, layer resolved and process based ecosystem model was developed to reproduce the water quality and sediment quality in Tokyo Bay and integrated with three dimensional hydrodynamic model which has been developed based on Navier-Strokes equations with the hydrostatic and Boussinesq approximations (Sasaki and Isobe, 2000), wave hindcasting model (Achiari and Sasaki, 2007) and bed shear stress model (Rasmeemasmuang and Sasaki, 2008) (**Fig 2.1**) .The state variables for the model are mainly temperature, salinity, three types of organic carbon which have been categorized on the decomposition rate, three types of phytoplankton which have been categorized on the seasonal blooms, zooplankton, dissolved oxygen and nutrients such as ammonia-nitrogen, nitrate-nitrogen, phosphate-phosphorus and two types of silica namely dissolved silica and particulate biogenic silica. Adopted expressions for biochemical kinetic processes were basically based on formulae adopted in conventional models (Di Toro, 2001) and (Ji, 2008).

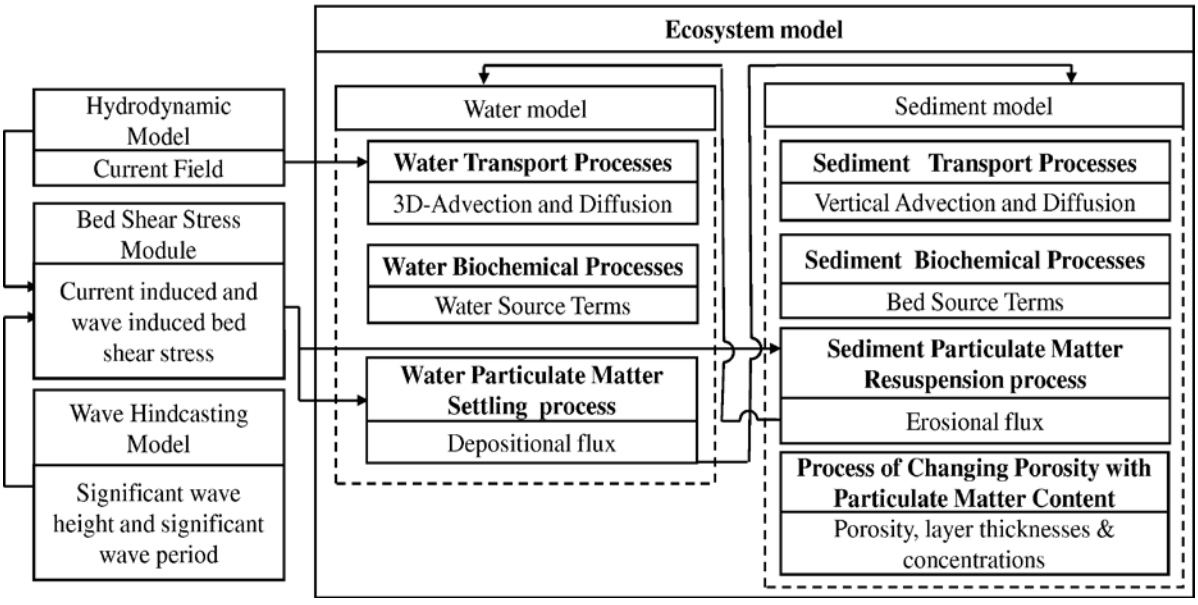

Fig 2.1 Schematic diagram of integrated process based multi layer benthic pelagic coupled ecosystem model

Process based coastal ecosystem models consider mainly physical processes which can be explained through material transport processes, bioprocesses which refer to systems that use living organisms to obtain desired results, and chemical processes which refer to transformation of reactants into products through breaking the bonds and creating new bonds. Other than those general processes, mechanism of changing porosity with respect to POCC in sediment which has been emerged from field data analysis (T Okada and Furukawa, 2005) has been considered in this study. With the change of porosity, change of the thickness of active sediment layer and then the change of nutrient concentrations in sediment have also been considered in this study. Processes in water and sediment columns were considered independently and water column was coupled to sediment column through interaction layer flux exchanges (**Fig 2.2**).

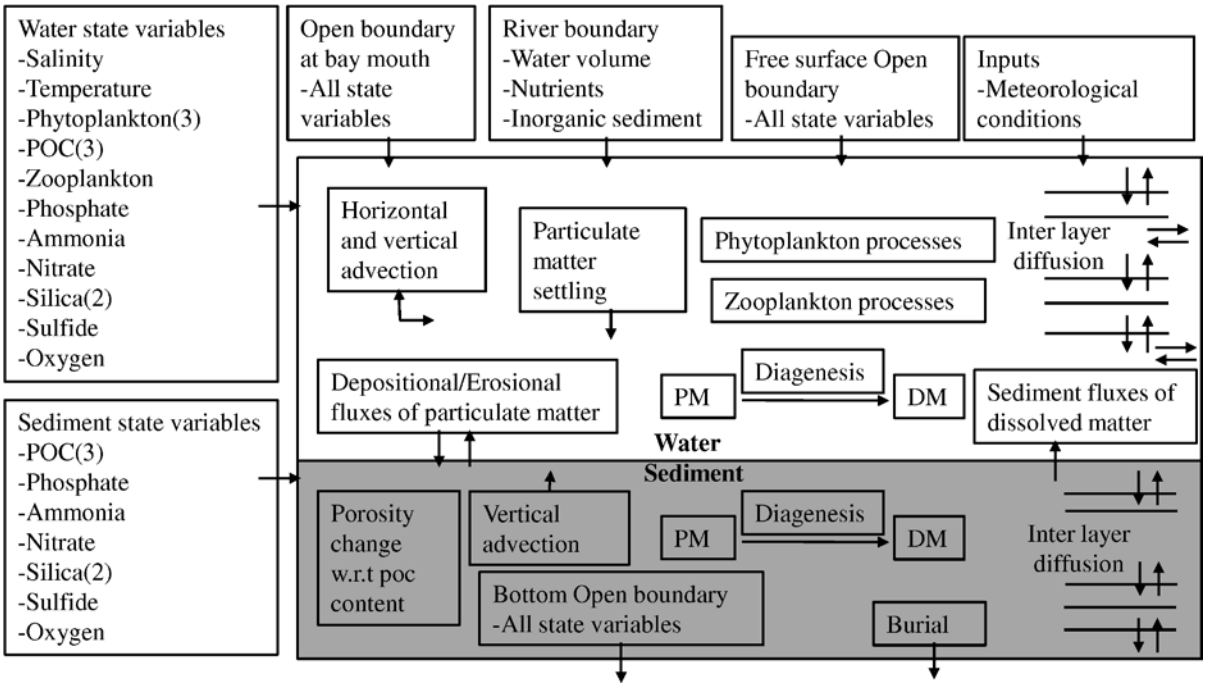

Fig 2.2 Schematic diagram of water and sediment processes

Numerical simulation flow with main sub-model components are shown in the (**Fig 2.3**). Independent computations for water column and sediment column are done and coupled through the independently computed flux. Basically, water model comprises with three modules: module_1 is the module to compute photosynthetically active radiation (PAR), module_2 is the module to compute three dimensional advection and diffusion and module_3 is the main module for water model which computes water source terms and calling all other

subroutines. Bed model comprises with two modules: module_1 is the module to compute vertical advection and diffusion and layer adjustment, and module_2 is the main module for sediment model which computes bed source terms and calling all other subroutines. Flux computation is done through the independent module which computes all the boundary flux. Coupling of water model to sediment model is through the boundary flux which has been considered in each water and sediment models during the computation of advection and diffusion.

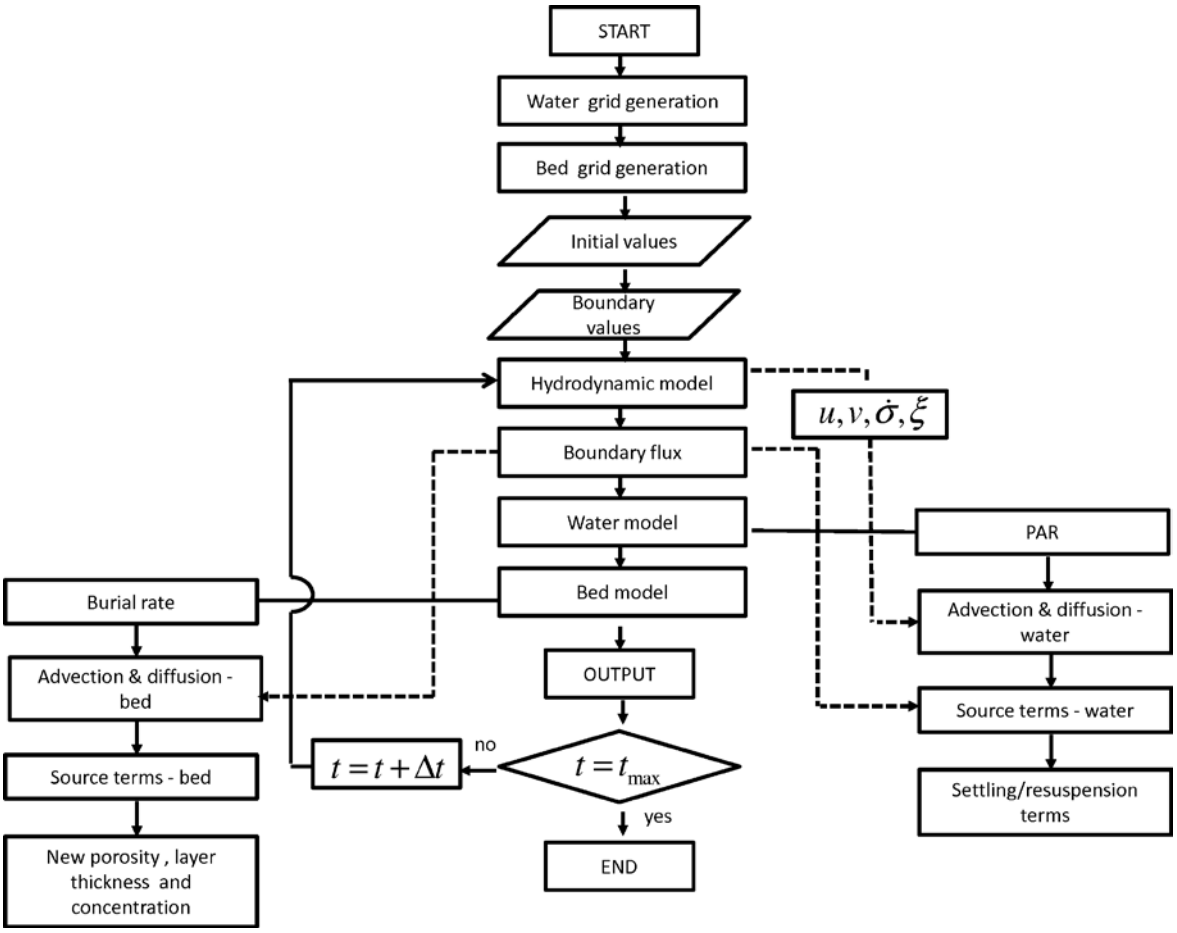

Fig 2.3 Numerical flow of the model

Time variable mass balance equations of each dependent variable have been developed and they are computed adopting a numerical integration method. A considerable effort is made in setting up the model and model parameters are set according to the published values and during the tuning process their sensitivity on results are analyzed. Moreover, the initial conditions - the values of concentrations of each dependent variable at each grid point at the

start of integration and boundary conditions - the values of concentrations of each dependent variable at open boundary are given.

2.2 Application of model to Tokyo Bay

2.2.1 Model grid system

Model gird systems for both benthic and pelagic sub models are generated to coincide to each other with (2 km × 2 km) horizontal resolution while the vertical grids are generated independently. Pelagic model compose of 10-sigma layers in vertical while it is 25 layers with different layer thicknesses in benthic model. Layer thicknesses in benthic are changing at every time step with respect to POCC. Sediment layer formation is discussed in detail under section **5.2**.

2.2.2 Initial conditions

Since the time variable solutions for both water and sediment state variables require initial conditions to start the computations they were given as the concentrations at $t = 0$. Initial conditions for hydrodynamic model have been discussed under section **3.1.1**. Pelagic model initial conditions for all the state variables are given uniformly based on the available data. Pelagic model is initialized with initial POCC and initial values for all other state variables were computed based on the POCC.

In order to compute initial concentrations of state variables in the sediment column, POCC has been assumed as 2% of the mass of sediment at the initial time step. Assuming $\rho_{st} = 2600.0$ kg/m^3, initial porosity is calculated form equation **5.12**. In order to obtain the initial POC concentration in sediment, bulk concentration of POC in mg/m^3 has been defined as B_{poc} while bulk concentration of sediment in g/m^3 has been defined as B_{st}.

$$\frac{m_{poc}}{m_{st}} = \frac{m_{poc} / V_b}{m_{st} / V_b} \tag{2.1}$$

$$\frac{m_{poc}}{m_{st}} = \frac{B_{poc}}{B_{st}} \tag{2.2}$$

Since $\left(\frac{m_{poc}}{m_{st}}\right)_{ini}$ is known, $\left(\frac{B_{poc}}{B_{st}}\right)_{ini}$ is known

$$B_{st} = \frac{m_{st}}{V_b} \quad 2.3$$

$$B_{st} = \frac{V_{st}\rho_{st}}{V_b} \quad 2.4$$

$$B_{st} = \frac{(V_b - V_w)\rho_{st}}{V_b} \times 10^3 \quad 2.5$$

$$B_{st} = \frac{(V_b - \phi V_b)\rho_{st}}{V_b} \times 10^3 \quad 2.6$$

$$B_{st} = (1-\phi)\rho_{st} \times 10^3 \quad 2.7$$

$$B_{st\_ini} = (1-\phi_{ini})\rho_{st} \times 10^3 \quad 2.8$$

From **2.8,** B_{st_ini} is computed in the model. Then, since $\left(\frac{B_{poc}}{B_{st}}\right)_{ini}$ and B_{st_ini} are known, B_{poc_ini} is computed. It is possible to separate this initial concentration of B_{poc_ini} into different types of POC, but totally inert initial POC has been considered in the model.

2.2.3 Boundary conditions

Boundary conditions are considered at the bay mouth, river and sewage mouths, free water surface and the bottom of the sediment layer. The locations of 12 river boundaries and 11 point sources at grid locations are shown in **Fig 2.4** while discharges and nutrient concentrations are shown in **Fig 2.5** and **Table 2.1** consequently. River and sewage data have been obtained from available government resources and river nutrient concentrations have been tuned during the model tuning process to overcome their inaccuracies.

Table 2.1 Nutrient concentrations of rivers and sewage point sources to Tokyo Bay (Japanese government sources)

River name	Grid point	Symbol	NH_4	NO_3	PO_4	SiO_2
Tsurumi	(6,20)	R10	5.0	300.0	1.5	175.0
Sumida	(9,29)	R12	5.0	300.0	1.5	175.0
Tama	(10,23)	R11	5.0	300.0	1.5	175.0
Ara	(11,29)	R1	5.0	300.0	1.5	175.0
Edo	(13,29)	R2	5.0	300.0	1.5	175.0
Mama	(17,31)	R3	5.0	300.0	1.5	175.0
Ebi	(19,30)	R4	5.0	300.0	1.5	175.0
Yoro	(21,23)	R7	5.0	300.0	1.5	175.0
Obitsu	(14,17)	R8	5.0	300.0	1.5	175.0
Koito	(11,13)	R9	5.0	300.0	1.5	175.0
Murata	(22,24)	R6	5.0	300.0	1.5	175.0
Hanami	(21,29)	R5	5.0	300.0	1.5	175.0
Sewage1	(12,28)	S1	1200.0	0.0	30.0	0.0
Sewage2	(10,26)	S10	1060.0	0.0	20.0	0.0
Sewage3	(9,28)	S11	1326.0	0.0	31.0	0.0
Sewage4	(21,24)	S3	1146.0	0.0	62.0	0.0
Sewage5	(21,28)	S2	1144.0	0.0	22.0	0.0
Sewage6	(10,22)	S9	3401.0	0.0	18.0	0.0
Sewage7	(5,10)	S6	1215.0	0.0	48.5	0.0
Sewage8	(4,20)	S8	911.0	0.0	35.0	0.0
Sewage9	(4,15)	S7	1051.0	0.0	35.0	0.0
Sewage10	(8,8)	S5	487.0	0.0	30.0	0.0
Sewage11	(10,13)	S4	4200.0	0.0	5.0	0.0

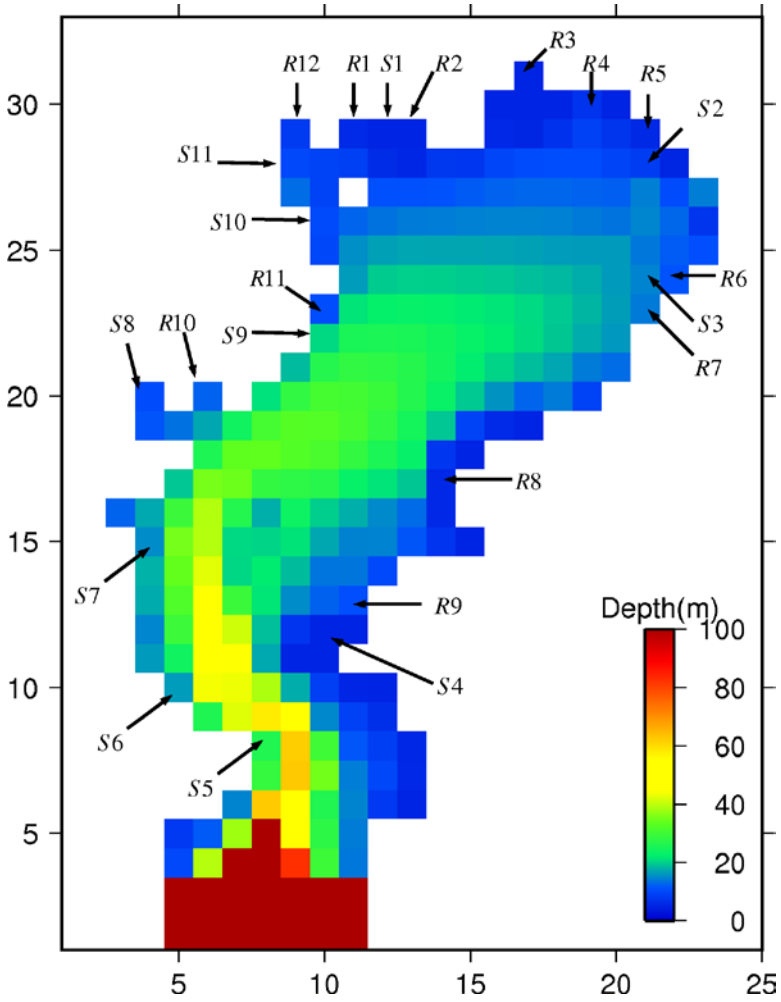

Fig 2.4 Locations of river and sewage point sources to Tokyo Bay at model grids

(a)

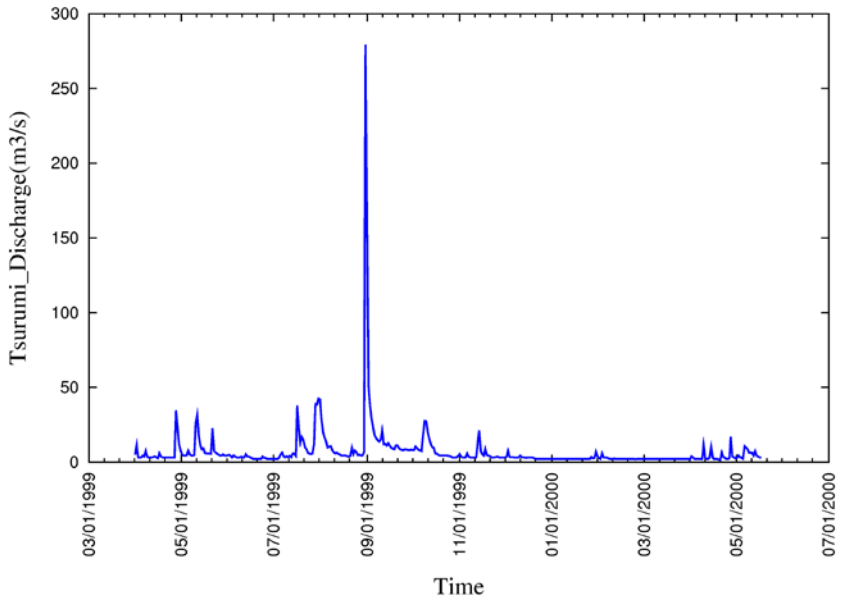

(b)

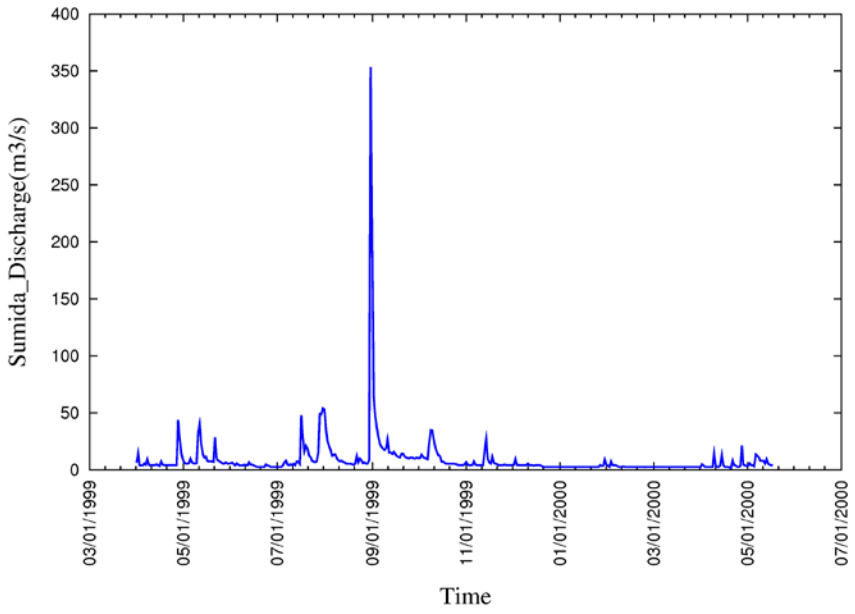
Sumida_Discharge(m3/s)
400
350
300
250
200
150
100
50
0
03/01/1999
05/01/1999
07/01/1999
09/01/1999
11/01/1999
01/01/2000
03/01/2000
05/01/2000
07/01/2000
Time

(c)

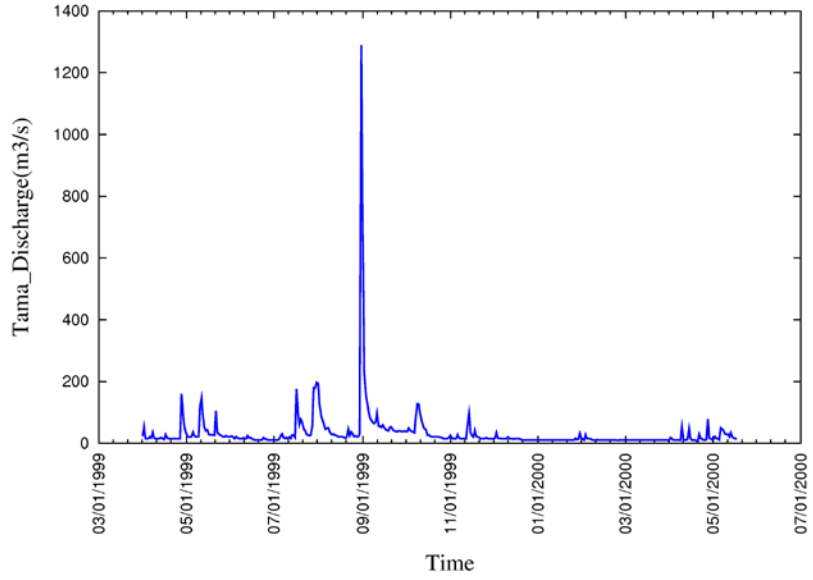
Tama_Discharge(m3/s)
1400
1200
1000
800
600
400
200
0
03/01/1999
05/01/1999
07/01/1999
09/01/1999
11/01/1999
01/01/2000
03/01/2000
05/01/2000
07/01/2000
Time

(d)

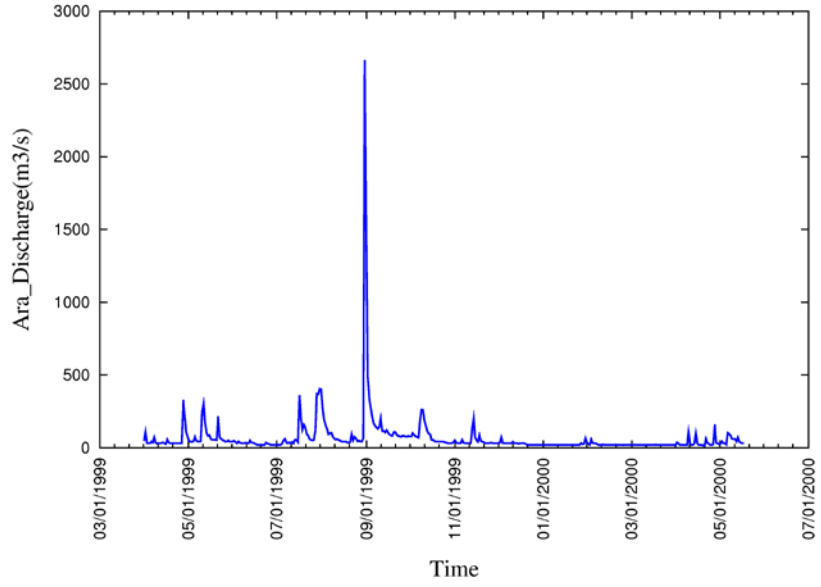
Ara_Discharge(m3/s)
3000
2500
2000
1500
1000
500
0
03/01/1999
05/01/1999
07/01/1999
09/01/1999
11/01/1999
01/01/2000
03/01/2000
05/01/2000
07/01/2000
Time

(e)

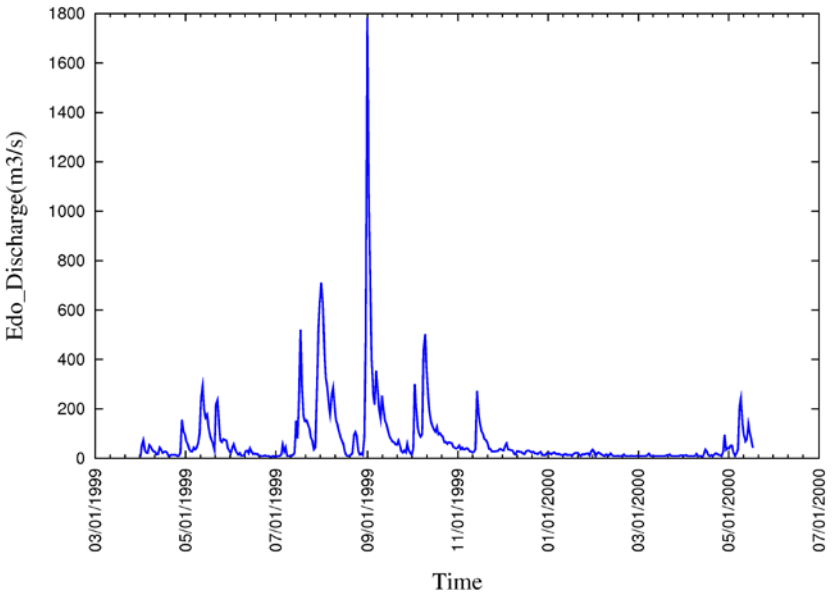
Edo_Discharge(m3/s)
1800
1600
1400
1200
1000
800
600
400
200
0
03/01/1999
05/01/1999
07/01/1999
09/01/1999
11/01/1999
01/01/2000
03/01/2000
05/01/2000
07/01/2000
Time

(f)

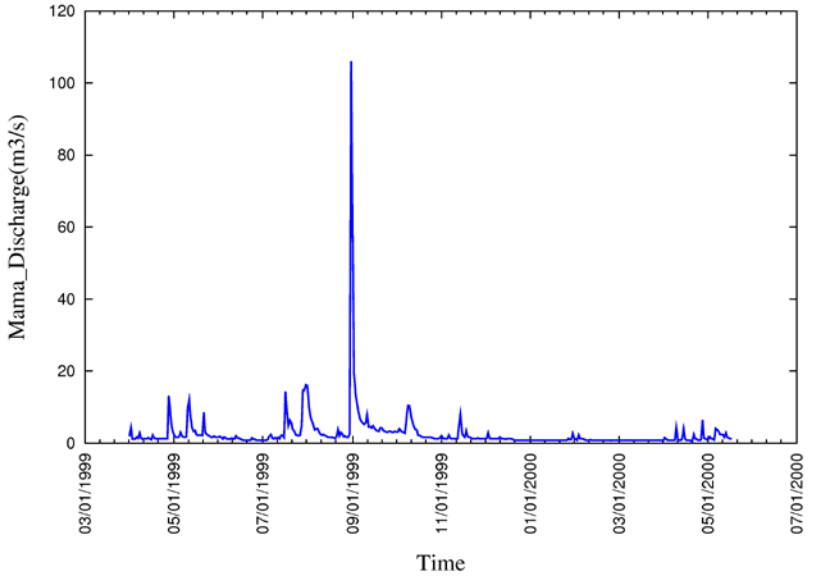
Mama_Discharge(m3/s)
120
100
80
60
40
20
0
03/01/1999
05/01/1999
07/01/1999
09/01/1999
11/01/1999
01/01/2000
03/01/2000
05/01/2000
07/01/2000
Time

(g)

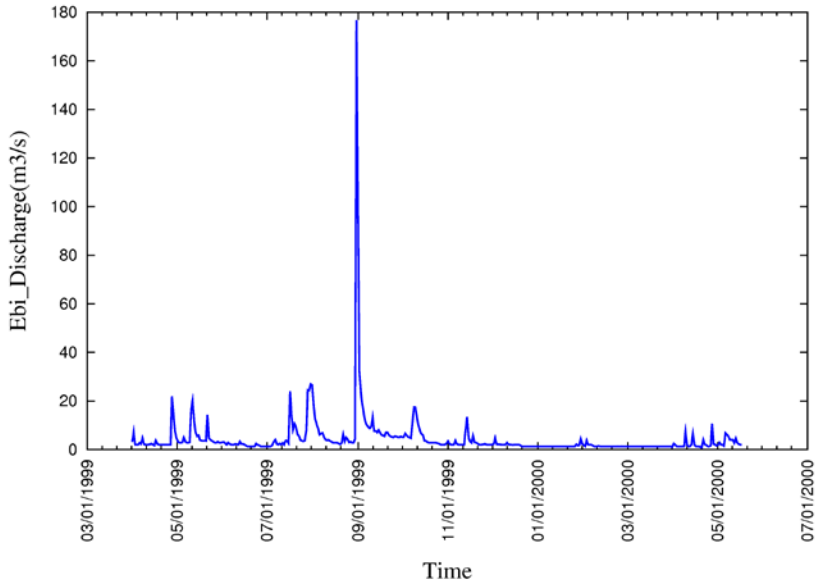
Ebi_Discharge(m3/s)
180
160
140
120
100
80
60
40
20
0
03/01/1999
05/01/1999
07/01/1999
09/01/1999
11/01/1999
01/01/2000
03/01/2000
05/01/2000
07/01/2000
Time

(h)

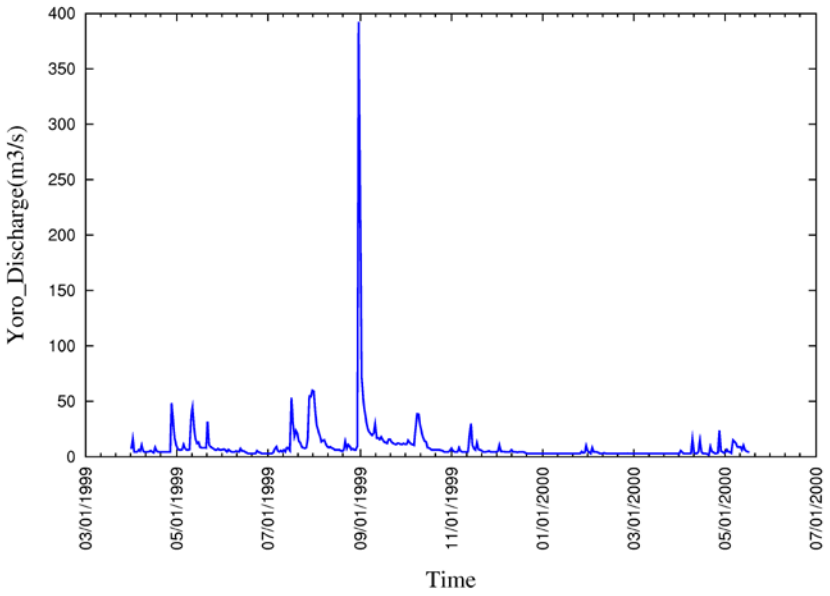
Yoro_Discharge(m3/s)
400
350
300
250
200
150
100
50
0
03/01/1999
05/01/1999
07/01/1999
09/01/1999
11/01/1999
01/01/2000
03/01/2000
05/01/2000
07/01/2000
Time

(i)

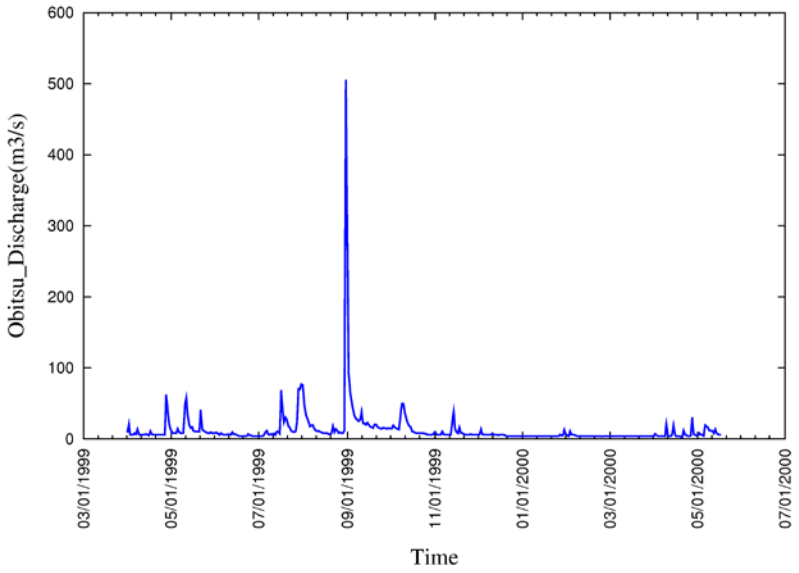
Obitsu_Discharge(m3/s)
600
500
400
300
200
100
0
03/01/1999
05/01/1999
07/01/1999
09/01/1999
11/01/1999
01/01/2000
03/01/2000
05/01/2000
07/01/2000
Time

(j)

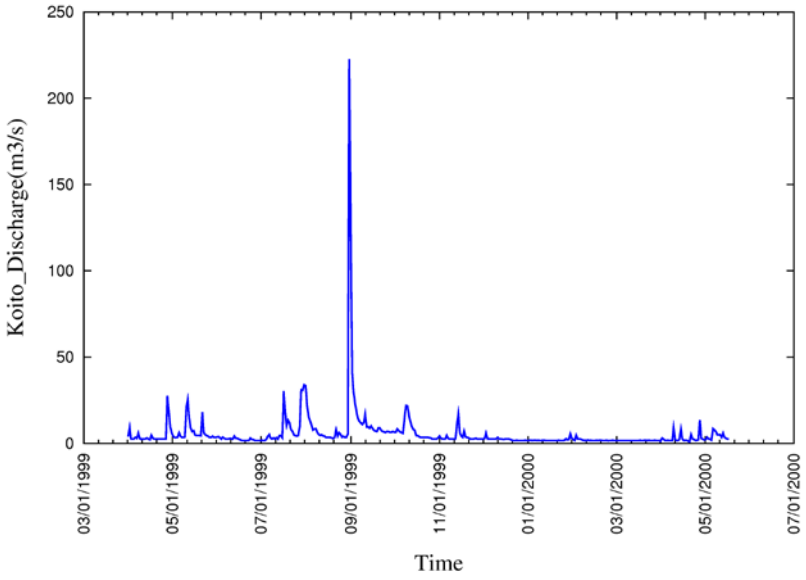
Koito_Discharge(m3/s)
250
200
150
100
50
0
03/01/1999
05/01/1999
07/01/1999
09/01/1999
11/01/1999
01/01/2000
03/01/2000
05/01/2000
07/01/2000
Time

(k)

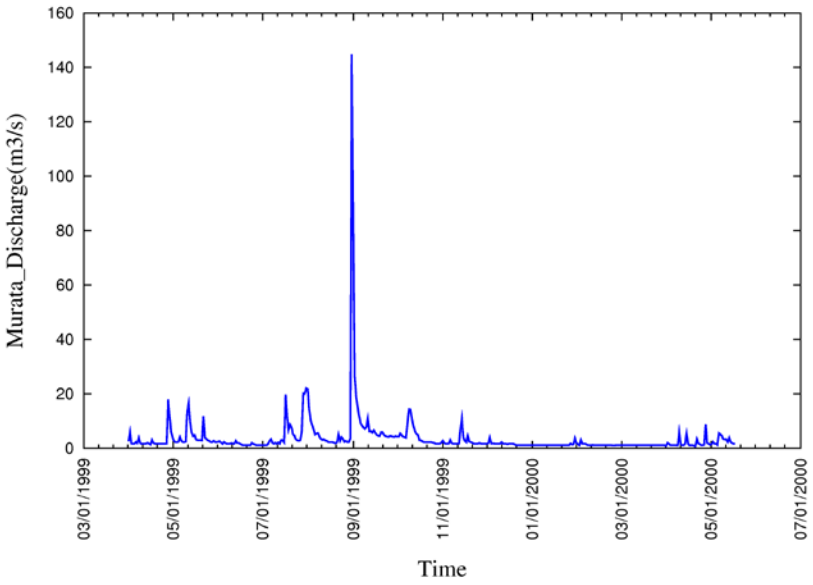

(l)

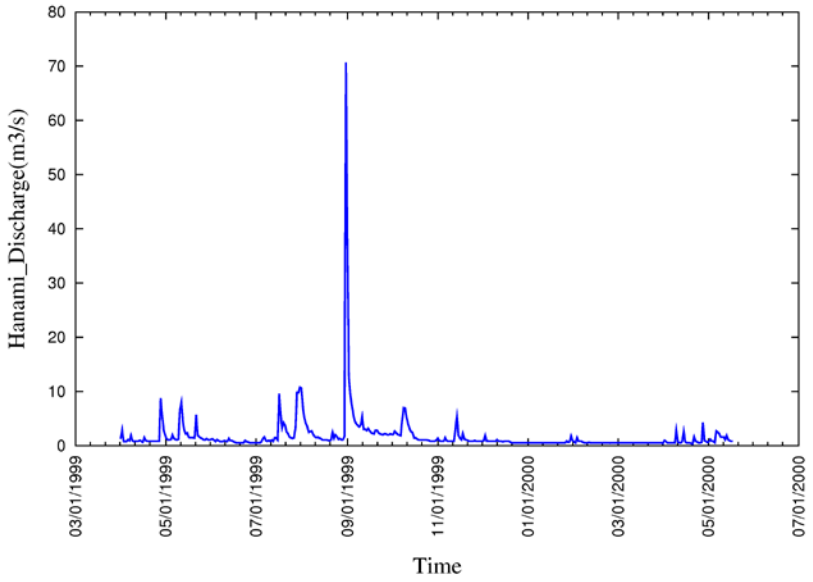

Fig 2.5 River discharges during one year period

Meteorological boundary conditions are shown under the section **2.2.5**. Other boundary conditions for hydrodynamic model are discussed in section **3.1.1**. Boundary conditions for ecosystem model have been discussed separately: boundary conditions at free water surface have been set to zero except for dissolved oxygen and this has been discussed in section **6.1** while boundary condition for the bottom of the sediment for dissolved and particulate state variables have been set as discussed in section **6.3**.

2.2.4 Time step and output

Time step of the computation is 100s which satisfies the Courant-Friedrich Levy (CFL) stability criterion in the form of;

$$\Delta t \leq \frac{\Delta L}{\sqrt{gD}} \qquad \textbf{2.9}$$

where ΔL is the computational length scale, D is the depth of water column and g is the gravitational acceleration.

With 2000m grid size and 15m water depth time step interval, Δt should be;

$$\Delta t \leq \frac{2000}{\sqrt{9.81 \times 15}} \qquad \textbf{2.10}$$

$$\Delta t \leq 165s \qquad \textbf{2.11}$$

Computation starts from 15 March 1999 and continued until acceptable steady state results are obtained. Three dimensional (3D) output is made for all the state variables at every noon with 5day interval. Output is made at three designated points where data has been collected namely Chiba Light House (CLH), Keiyo Sea Birth (KSB) and Tokyo Light House (TLH) as shown in the **Fig 2.6** at every one hour interval, and at designated dates where data has been collected.

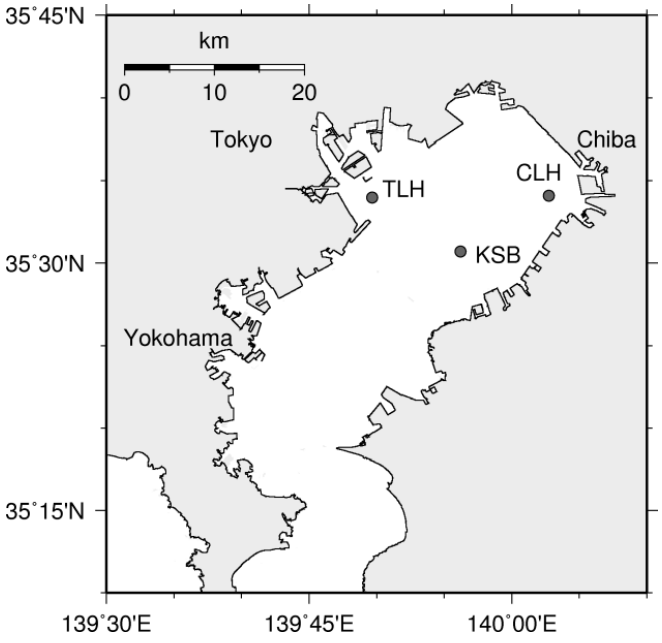

Fig 2.6 Data collected locations

2.2.5 Model forcing and validation

The model is forced by hourly meteorological data which includes air pressure, air temperature, vapor pressure, relative humidity, wind speed, wind direction, cloud cover, solar radiation and rainfall as shown in the **Fig 2.7**; daily river discharge data of 12 rivers which are located as in **Fig 2.4** and variations as shown in the **Fig 2.5**; and instantaneous tidal motion. Model parameters have been initially set according to reference values and during a comprehensive tuning process their sensitivity on results analyzed and required changes has been made.

Computation is made for the period of April 1999 to March 2000 and long term computation is continued with the same boundary conditions until reaching the steady state. During the long term simulation, initial conditions are renewed after each year of simulation. Since it is confirmed that the initial conditions affect the results during one year period of simulation until the steady state is obtained, the simulation is continued until the agreeable reproduction of data was obtained through realistic initial conditions. Model is validated with April 1999 to March 2000 water quality data and 2001 spatial distribution of sediment data.

(a)

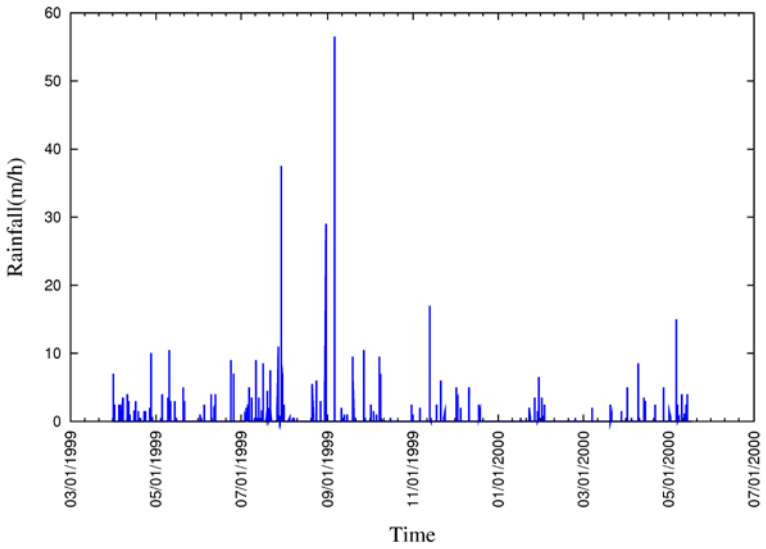

(b)

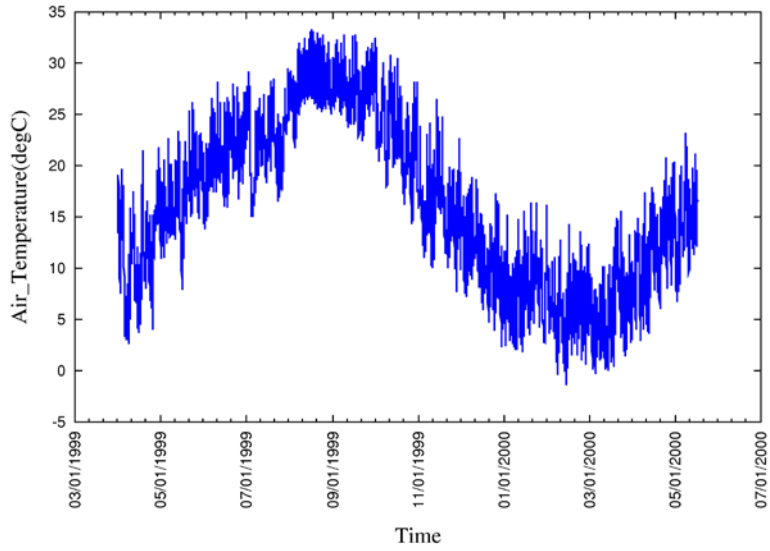
Air_Temperature(degC)
35
30
25
20
15
10
5
0
-5
03/01/1999
05/01/1999
07/01/1999
09/01/1999
11/01/1999
01/01/2000
03/01/2000
05/01/2000
07/01/2000
Time

(c)

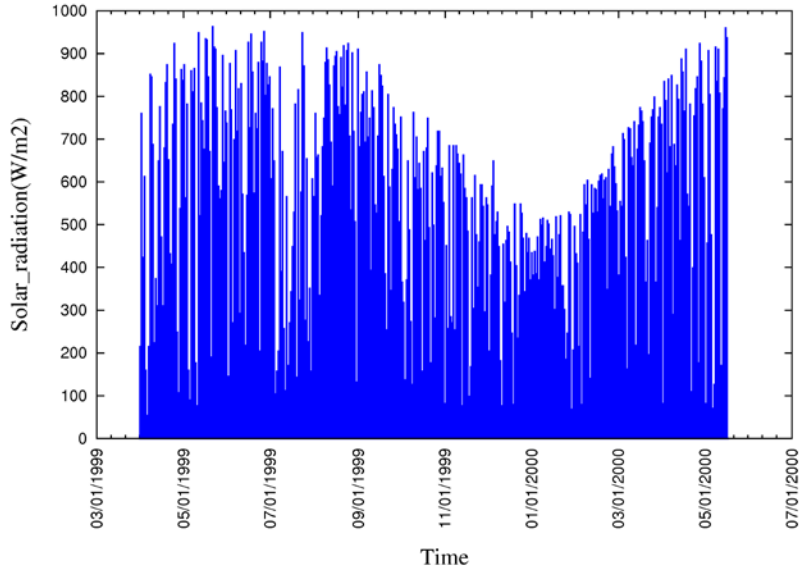
Solar_radiation(W/m2)
1000
900
800
700
600
500
400
300
200
100
0
03/01/1999
05/01/1999
07/01/1999
09/01/1999
11/01/1999
01/01/2000
03/01/2000
05/01/2000
07/01/2000
Time

(d)

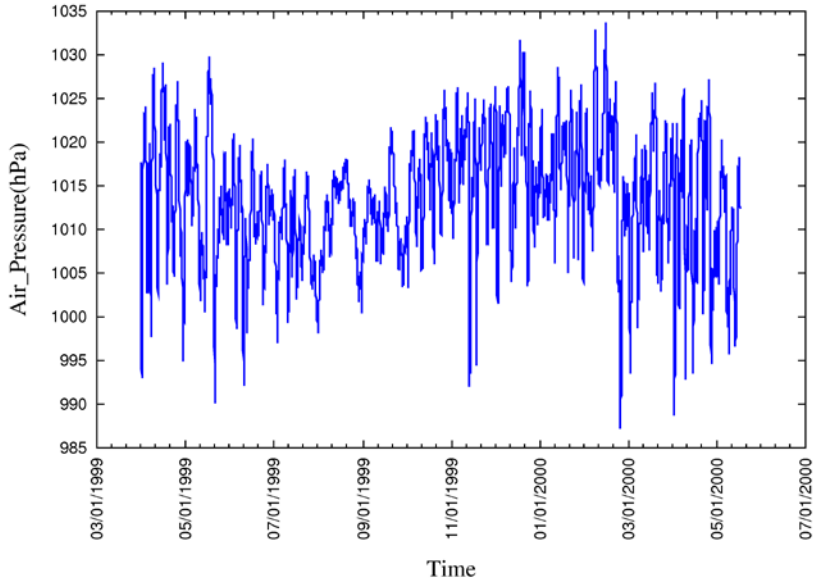
Air_Pressure(hPa)
1035
1030
1025
1020
1015
1010
1005
1000
995
990
985
03/01/1999
05/01/1999
07/01/1999
09/01/1999
11/01/1999
01/01/2000
03/01/2000
05/01/2000
07/01/2000
Time

(e)

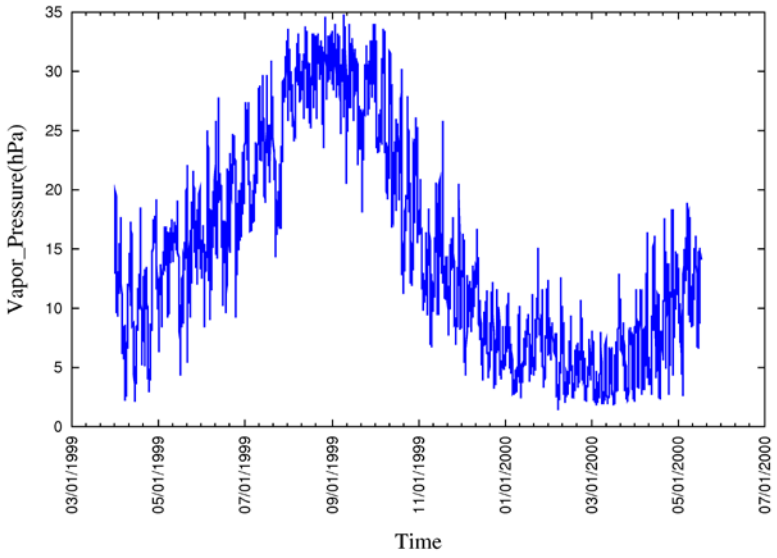
Vapor_Pressure(hPa)
35
30
25
20
15
10
5
0
03/01/1999
05/01/1999
07/01/1999
09/01/1999
11/01/1999
01/01/2000
03/01/2000
05/01/2000
07/01/2000
Time

(f)

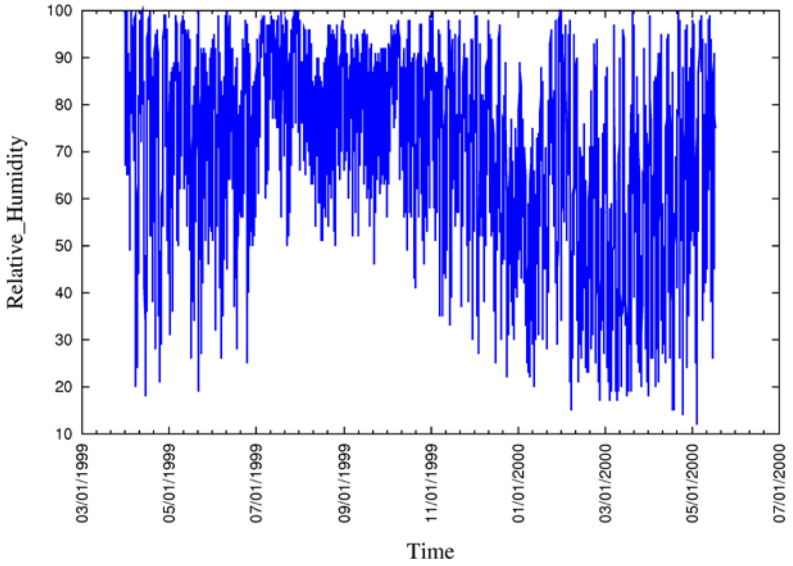
Relative_Humidity
100
90
80
70
60
50
40
30
20
10
03/01/1999
05/01/1999
07/01/1999
09/01/1999
11/01/1999
01/01/2000
03/01/2000
05/01/2000
07/01/2000
Time

(g)

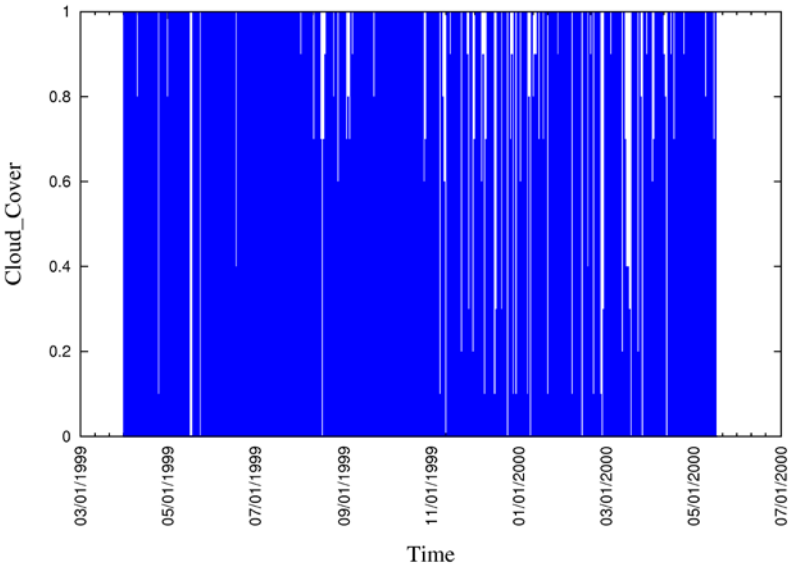
Cloud_Cover
1
0.8
0.6
0.4
0.2
0
03/01/1999
05/01/1999
07/01/1999
09/01/1999
11/01/1999
01/01/2000
03/01/2000
05/01/2000
07/01/2000
Time

(h)

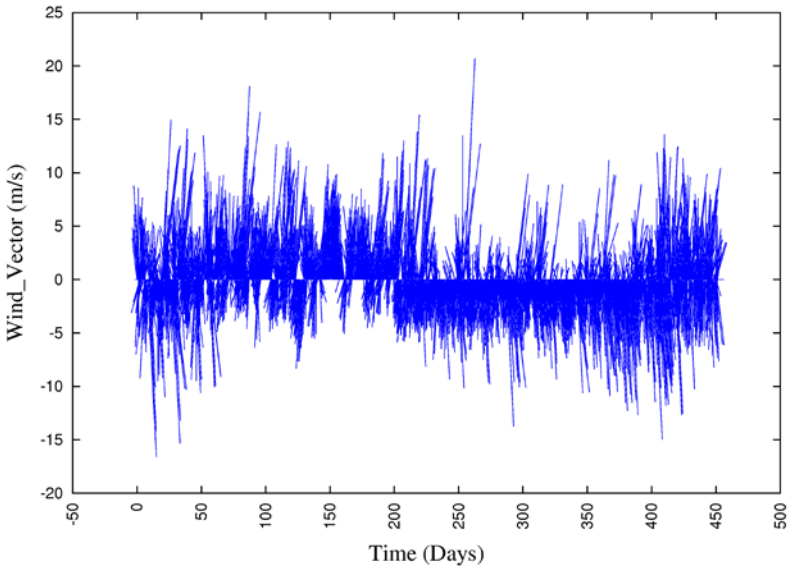

Fig 2.7 Meteorological conditions during one year period

3. HYDRODYNAMIC, WAVE HINDCASTING AND BED SHEAR STRESS MODELS

This chapter describes the basic concepts of previously developed models: hydrodynamic model, wave hindcasting model and bed shear stress model which have been coupled to the ecosystem model developed during this study.

3.1 Hydrodynamic model

A quasi-three-dimensional hydrodynamic model developed by (Sasaki and Isobe, 2000) is applied. Based on the momentum and continuity equations in Cartesian coordinates, the primitive equations with hydrostatic approximation: acceleration terms become negligible in the presence of gravity simplifying the pressure only as a function of surface elevation, and Boussinesq approximation: assume that changes in density are only a function of temperature and salinity.

Momentum equation in Cartesian coordinates;

$$\underbrace{\frac{\partial \vec{u}}{\partial t}}_{\substack{Time\_derivative \\ term}} + \underbrace{\frac{\partial(u\vec{u})}{\partial x}+\frac{\partial(v\vec{u})}{\partial y}+\frac{\partial(w\vec{u})}{\partial z}}_{Advection\_term} = \underbrace{f\begin{pmatrix}+v\\-u\end{pmatrix}}_{Coriolis\_term} \underbrace{-g\nabla_h\zeta-\frac{g}{\rho_0}\nabla_h\int_z^\zeta \rho' dz}_{Pressure\_gradient\_term} + \underbrace{A_h\left(\frac{\partial^2\vec{u}}{\partial x^2}+\frac{\partial^2\vec{u}}{\partial y^2}\right)+\frac{\partial}{\partial z}\left(A_v\frac{\partial\vec{u}}{\partial z}\right)}_{Diffusion\_term} \quad 3.1$$

Continuity equation in Cartesian coordinates;

$$\frac{\partial u}{\partial x}+\frac{\partial v}{\partial y}+\frac{\partial w}{\partial z}=0 \quad 3.2$$

where t is time, x and y are the horizontal coordinates, z is the vertical coordinate upward from the still water level, u, v and w are velocities in x, y and z directions respectively, $\vec{u}$ is the horizontal velocity vector of $(u,v)^T$, ζ is the water surface elevation from the still water level, ρ_0 and ρ' the constant reference density and deviation from it which gives the

sea water density $\rho(=\rho_0+\rho')$, ρ_h and ρ_v are the horizontal and vertical eddy viscosities, respectively, f is the Coriolis parameter, and $\nabla_h\left(=\partial/\partial x, \partial/\partial y\right)$ is the horizontal differential operator.

The density of the sea, $\rho\ (kg/m\hat{}3)$ water has been considered as a function of water salinity $S\ (psu)$ and temperature $T\ (^0C)$ and defined by the transport equation.

$$\begin{aligned}\rho &= 1000 + 20.99 + \left\{-4.3\times10^{-3}(T-20) - 0.256\right\}(T-20) \\ &+ \left\{2.3\times10^{-4}(S-30) - 1.53\times10^{-3}(T-20) + 0.7577\right\}(S-30)\end{aligned} \qquad 3.3$$

In order to overcome difficulties in manipulating irregular bottom topographies and to easily formulate surface and bottom boundary conditions, sigma coordinate system which has originally developed by (Phillips, 1957) has been used. According to the transformation the surface and bottom topographies have been defined as shown in **Fig 3.1**and translates;

$$\sigma = \frac{z+h}{h+\zeta} = \frac{z+h}{D} \qquad 3.4$$

where $D = h+\zeta$. According to this transformation

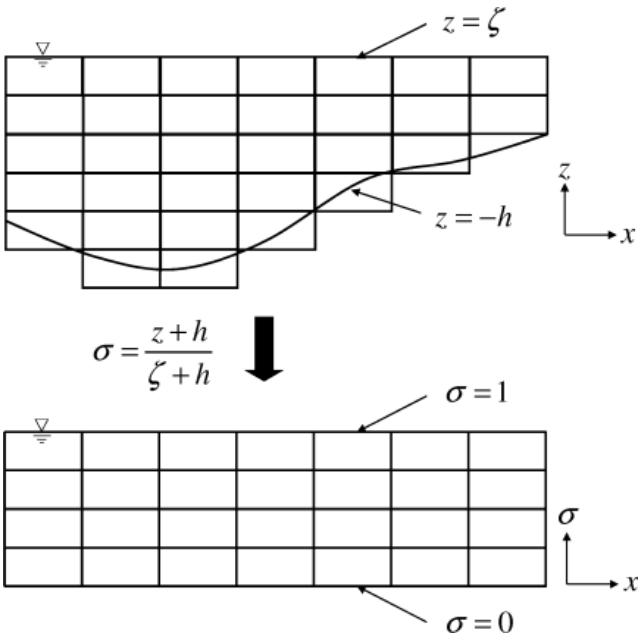

Fig 3.1 Sigma coordinate transformation

Then the momentum and continuity equations have been transformed into sigma coordinates as follows.

Momentum equation in sigma-coordinates;

$$\underbrace{\underbrace{\frac{\partial D\vec{u}}{\partial t}}_{\substack{Time\_derivative \\ term}} + \underbrace{\frac{\partial\left(Du\vec{u}\right)}{\partial x}+\frac{\partial\left(Dv\vec{u}\right)}{\partial y}+\frac{\partial\left(D\dot{\sigma}\vec{u}\right)}{\partial\sigma}}_{Advection\_term} = \underbrace{D\begin{pmatrix}+v\\-u\end{pmatrix}}_{Coriolis\_term}}$$

$$\underbrace{-\frac{gD}{\rho_0}\left\{\left(\rho_0+\rho'\sigma\right)\nabla_h\zeta-\rho'\left(\sigma-1\right)\nabla_h D-\nabla_h\left(D\int_\sigma^1\rho' d\sigma\right)\right\}}_{Pressure\_gradient\_term} \qquad 3.5$$

$$\underbrace{+DA_h\left(\frac{\partial^2\vec{u}}{\partial x^2}+\frac{\partial^2\vec{u}}{\partial y^2}\right)+\frac{1}{D}\frac{\partial}{\partial\sigma}\left(A_v\frac{\partial\vec{u}}{\partial\sigma}\right)}_{Diffusion\_term}$$

Continuity equation in sigma-coordinates;

$$\frac{\partial\zeta}{\partial t}+\frac{\partial\left(Du\right)}{\partial x}+\frac{\partial\left(Dv\right)}{\partial y}+\frac{\partial\left(D\dot{\sigma}\right)}{\partial z}=0 \qquad 3.6$$

where Pseudo velocity,

$$\dot{\sigma}=\frac{\partial\sigma}{\partial t}+u\frac{\partial\sigma}{\partial x}+v\frac{\partial\sigma}{\partial y}+w\frac{\partial\sigma}{\partial z} \qquad 3.7$$

and transport equations of temperature and salinity have been adopted as shown in the following equations.

$$\frac{\partial\left(DT\right)}{\partial t}+\frac{\partial\left(uDT\right)}{\partial x}+\frac{\partial\left(vDT\right)}{\partial y}+\frac{\partial\left(\dot{\sigma}DT\right)}{\partial\sigma}=\frac{1}{D^2}\frac{\partial}{\partial\sigma}\left(K_v\frac{\partial\left(HT\right)}{\partial\sigma}\right)$$
$$+DK_h\left(\frac{\partial^2T}{\partial x^2}+\frac{\partial^2T}{\partial y^2}\right)+\frac{1}{\rho C_p}\frac{dq\left(\sigma\right)}{d\sigma} \qquad 3.8$$

where K_h and K_v are the horizontal and vertical kinematic eddy diffusivities, and C_p and q are the specific heat and the short wave radiation respectively.

$$\frac{\partial(DS)}{\partial t}+\frac{\partial(uDS)}{\partial x}+\frac{\partial(vDS)}{\partial y}+\frac{\partial(\dot{\sigma}DS)}{\partial \sigma}=\frac{1}{D^2}\frac{\partial}{\partial \sigma}\left(K_v\frac{\partial(HS)}{\partial \sigma}\right)$$
$$+DK_h\left(\frac{\partial^2 S}{\partial x^2}+\frac{\partial^2 S}{\partial y^2}\right)-RS \qquad 3.9$$

where R is the river discharge which can be introduced at coastal nodes of the rivers.

3.1.1 Initial and boundary conditions

Initial conditions of salinity and temperature are given uniformly in space and depth and there is a room for setting them as a variable.

At the surface boundary, Pseudo velocity has set to zero and tangential stress at the free surface along a horizontal direction is equal to the wind stress.

$$\dot{\sigma}=0 \qquad 3.10$$

$$\rho A_v\frac{\partial u}{\partial \sigma}=D\rho_a C_f|W|W_x \qquad 3.11$$

$$\rho A_v\frac{\partial u}{\partial \sigma}=D\rho_a C_f|W|W_y \qquad 3.12$$

where C_f is the wind drag coefficient, ρ_a is the air density, W_x and W_y are the x and y components of the wind vector W at the latitude of 10m above the sea surface.

At the sea bottom boundary, Pseudo velocity has set to zero and quadratic dependence of the bottom stress on the velocity has been described as follows.

$$\dot{\sigma}=0 \qquad 3.13$$

$$\rho A_v\frac{\partial u}{\partial \sigma}=D\rho\gamma_b^2 u\sqrt{\left(u^2+v^2\right)} \qquad 3.14$$

$$\rho A_v\frac{\partial u}{\partial \sigma}=D\rho\gamma_b^2 v\sqrt{\left(u^2+v^2\right)} \qquad 3.15$$

where γ_b^2 is the bottom friction coefficient.

At lateral wall boundaries, normal velocities have set to zero and free-slip conditions have been applied for the friction terms.

At the bay mouth, tidal level has been estimated from the Meteorological agency data. Other than that wind direction, wind speed, solar radiation, air temperature, air pressure, vapor pressure, cloud cover and rain fall data obtained from Meteorological agency are given as boundary conditions. River and sewage discharge data have also been considered as boundary conditions as shown in the **Fig 2.4**, **Fig 2.5** and **Table 2.1**.

3.1.2 Numerical scheme

It has been found that the stability of the model is constrained by the time increment for bays with steep bottom slope and vertically high resolution. As shown in the **Fig 3.2** models can consider the variation of a parameter within a time step Δt in two ways. In explicit approach it assumes the variable keeps its value as its present value during the time step while in implicit approach it assumes the variable keeps its next time step value during the time step (Patankar, 1980). Considering these two approaches a more robust algorithm with semi-implicit scheme has been adopted. The sea surface elevation ζ and the vertical advection and vertical diffusion terms are discretized implicitly and the other terms are discretized explicitly.

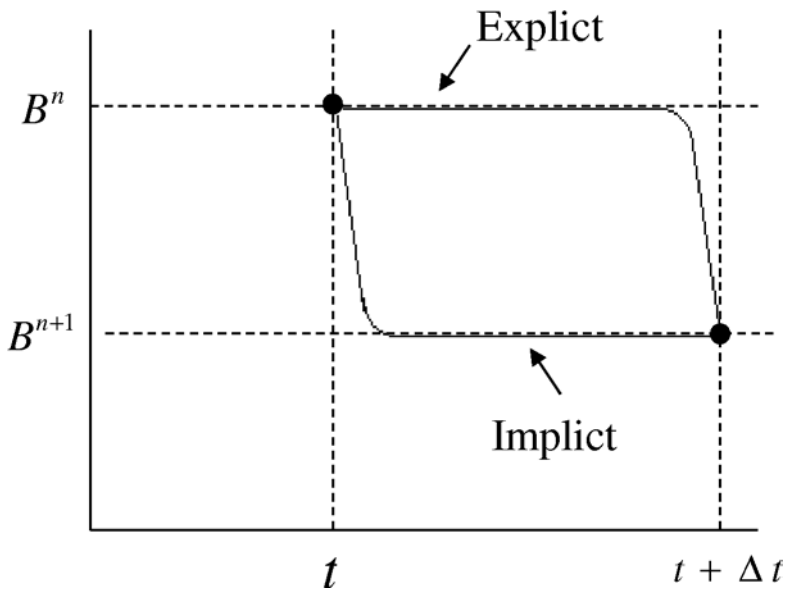

Fig 3.2 Explicit and implicit approaches

Difference between the explicit and explicit approach can be explained considering a simple differential equation for any state variable $C_{i,j,k}$ with a rate of change of λ ;

$$\frac{dC_{i,j,k}}{dt} = \lambda C_{i,j,k} \qquad 3.16$$

If explicit scheme is applied;

$$\frac{C_{i,j,k}^{n+1} - C_{i,j,k}^{n}}{\Delta t} = \lambda C_{i,j,k}^{n} \qquad 3.17$$

Where Δt is the time interval and n is the time step. Then the next time step value is;

$$C_{i,j,k}^{n+1} = \left(1 + \lambda \Delta t\right) C_{i,j,k}^{n} \qquad 3.18$$

If implicit scheme is applied;

$$\frac{C_{i,j,k}^{n+1} - C_{i,j,k}^{n}}{\Delta t} = \lambda C_{i,j,k}^{n+1} \qquad 3.19$$

Then the next time step value is;

$$C_{i,j,k}^{n+1} = \frac{C_{i,j,k}^{n}}{\left(1 - \lambda \Delta t\right)} \qquad 3.20$$

According to the equation **3.20**, in order to keep $C_{i,j,k}^{n+1} \rangle 0$; keep $\left(1 - \lambda \Delta t\right) \rangle 0$. That gives $\Delta t \langle \frac{1}{\lambda}$. Hence implicit scheme give a flexibility to keep the model stable by setting the time interval Δt .

3.1.3 Grid system

Staggered grid system defining scalars at the main grid points and velocities at the grid surfaces (with respect to the main grid points velocity components are staggered) have been used (**Fig 3.3**). This has twofold advantages:

1. The discretized continuity equation would contain the differences of adjacent velocity components, and that with a wavy velocity field is prevented.
2. Pressure difference between two adjacent grid points becomes natural driving force for velocity component which is located between these grid points.

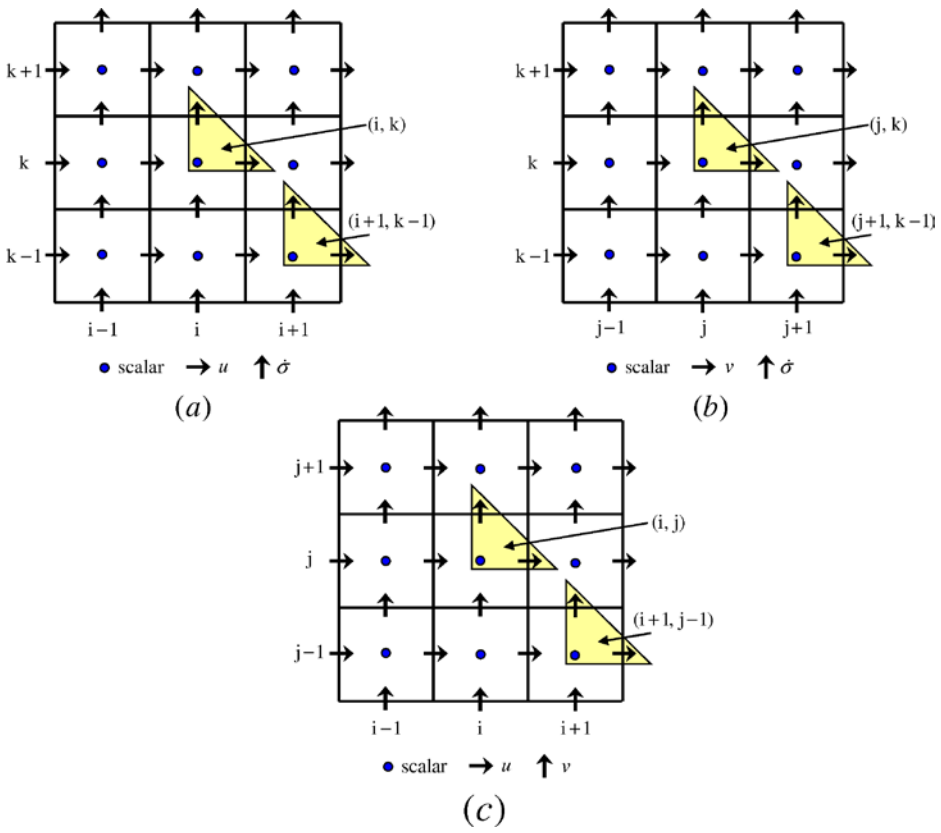

Fig 3.3 Staggered grid system (a) x-sigma (b) y-sigma plane and (c) x-y plane

3.2 Wave hindcasting model

The wave hindcasting model which has been developed and validated by (e.g. Achiari and Sasaki, 2007, Rasmeemasmuang and Sasaki, 2008, and Attari and Sasaki, 2012) is adopted. This wind-generated wave hindcasting model has been developed for both deep shallow and deep waters through a set of parametric equations which computes spatial and temporal variation in the significant wave height and period.

The wave growth pattern is considered as combine characteristics of fetch limited conditions and duration limited conditions. Under fetch limited conditions, it is considered that the wind has blown enough constantly long enough for wave heights at the end of the fetch to reach its equilibrium while under duration limited conditions, the length of the time that the wind has blown limits the wave height.

Under fetch limited condition the significant wave height H_w(m), significant wave period T_w (s) and wave duration t_w (s) are computed through the following equations **3.21**, **3.22** and **3.23**.

$$\frac{gH_w}{U_W^{\,2}} = 1.6\times10^{-3}\left(\frac{gF_W}{U_W^{\,2}}\right)^{1/2} \tag{3.21}$$

$$\frac{gT_w}{U_W} = 2.857\times10^{-1}\left(\frac{gF_W}{U_W^{\,2}}\right)^{1/3} \tag{3.22}$$

$$\frac{gt_w}{U_W} = 6.88\times10^{1}\left(\frac{gF_W}{U_W^{\,2}}\right)^{2/3} \tag{3.23}$$

where F_W is the fetch in meter at the location considered (Achiari and Sasaki, 2007), U_W is the wind speed at 10 m above the sea in meter per second and g is the gravitational acceleration in (m/s^2) The above equations are valid up to the fully developed wave conditions given by equations **3.24, 3.25** and **3.26** , and only when the real duration of wind blowing is longer than t_w .

$$\frac{gH_w}{U_W^{\,2}} = 2.433\times10^{-1} \tag{3.24}$$

$$\frac{gT_w}{U_W} = 8.134 \tag{3.25}$$

$$\frac{gt_w}{U_W} = 7.15\times10^{4} \tag{3.26}$$

The wave growth pattern in shallow waters is considered based on approximations in which wave energy is added due to wind stress and reduced due to bottom friction and percolation. These assumptions have ended up with following relationships to compute H_w (m), T_w (s) and t_w (s).

$$\frac{gH_w}{U_W^{\,2}} = 0.283 \tanh\left[0.530\left(\frac{gh}{U_W^{\,2}}\right)^{3/4} \tanh\left\{\frac{0.00565\left(\frac{gF_W}{U_W^{\,2}}\right)^{1/2}}{\tanh\left[0.530\left(\frac{gh}{U_W^{\,2}}\right)^{3/4}\right]}\right\}\right] \quad 3.27$$

$$\frac{gT_w}{U_W} = 7.54 \tanh\left[0.833\left(\frac{gh}{U_W^{\,2}}\right)^{3/8} \tanh\left\{\frac{0.0379\left(\frac{gF_W}{U_W^{\,2}}\right)^{1/3}}{\tanh\left[0.833\left(\frac{gh}{U_W^{\,2}}\right)^{3/8}\right]}\right\}\right] \quad 3.28$$

$$\frac{gt_w}{U_W} = 537\left(\frac{gT_W}{U_W}\right)^{7/3} \quad 3.29$$

Similarly as in deep water, the above equations **3.27**, **3.28** and **3.29** are valid only when the real duration of wind blowing is longer than t_w .

Moreover, the wave length L_w has been introduced applying the dispersion relationship in linear wave theory as shown in the equation **3.30.**

$$L_w = \frac{gT_w^{\,2}}{2\pi} \tanh\frac{2\pi h}{L_w} \quad 3.30$$

Since the equation **3.30** has to be solved through the iteration process and since it is not preferred in long-term computations, an explicit expression proposed by (Goda, 2010) is applied as shown in the equation **3.31**.

$$L_w = \frac{2\pi h}{\sqrt{\left(\Omega\left(\Omega + \frac{1}{\left(1 + \Omega\left(0.6522 + \Omega(0.4622 + \Omega^2(0.0864 + 0.0675\Omega)\right)\right)\right)}\right)\right)}} \quad 3.31$$

where,

$$\Omega = \frac{4\pi^2 h}{gT_w^{\,2}} \quad 3.32$$

(Rasmeemasmuang and Sasaki, 2008) have confirmed that the deviation of the results of the equations **3.30** and **3.31** are less than 0.1%.

3.3 Bed shear stress model

In order to model the spatial distribution of sediment quality, accurate modeling of Bed Shear Stress (BSS) is highly important and its sensitivity on the spatial distribution of sediment and water quality has been discussed in section **7.2.1**. BSS has been model adopting the method proposed by (e.g. Rasmeemasmuang and Sasaki, 2008, and Attari and Sasaki, 2012). The BSS, $\vec{\tau}_b$ has been computed based as a vector summation of Wave induced Bed Shear Stress (WBSS), $\vec{\tau}_w$ and Current induced Bed Shear Stress (CBSS), $\vec{\tau}_c$.

$$\vec{\tau}_b = \vec{\tau}_w + \vec{\tau}_c \tag{3.33}$$

The magnitudes of $\vec{\tau}_w$ and $\vec{\tau}_c$ are given by the following equations.

$$\tau_c = \rho C_d |U| U \tag{3.34}$$

$$\tau_w = \frac{1}{2}\rho f_w \left|\hat{U}_b\right|^2 \tag{3.35}$$

where U is the velocity of the mean current at reference height z_r, $\hat{U}_b$ is the amplitude of the wave induced oscillatory velocity, C_d and f_w are the drag coefficient or current-related friction factor and the wave-related friction factor, respectively. The amplitude of the wave induced oscillatory velocity $\hat{U}_b$ has been computed from the equation **3.36** using the wave characteristics obtained in section **3.2**.

$$\hat{U}_b = \frac{\pi H_w}{T_w \sinh(2\pi h / L_w)} \tag{3.36}$$

Wave related friction factor, f_w has been computed from the equation **3.37** where a_m represents the particle excursion which is given by the equation **3.38**.

$$f_w = \max\left[\exp\left\{5.213\left(\frac{a_m}{k_s}\right)^{-0.194} - 5.977\right\},\ 0.30\right] \tag{3.37}$$

$$a_m = \frac{H_w}{2\sinh(2\pi h / L_w)} \tag{3.38}$$

4. PELAGIC MODULE IN ECOSYSTEM MODEL

4.1 Governing differential equations for any scalar parameter

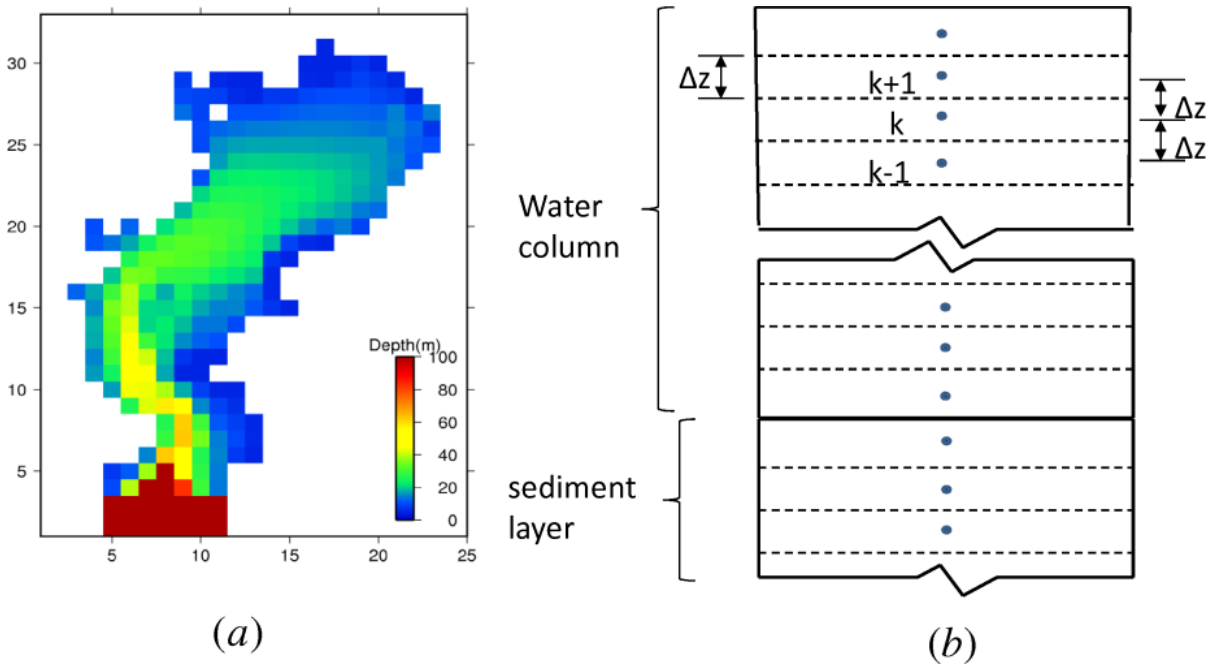

Fig 4.1 Spatial and vertical grid system for water column

This model has 2000 m × 2000 m horizontal grid resolution with 10 sigma layers in vertical direction in water column (**Fig 4.1**). In order to overcome difficulties in manipulating irregular bottom topographies and to easily formulate surface and bottom boundary conditions, sigma coordinate system which changes the surface and bottom topographies as shown in **Fig 3.1** has been used. Staggered grid system defining scalars at the main grid points and velocities at the grid surfaces (with respect to the main grid points velocity components are staggered) have been used (**Fig 3.3**).

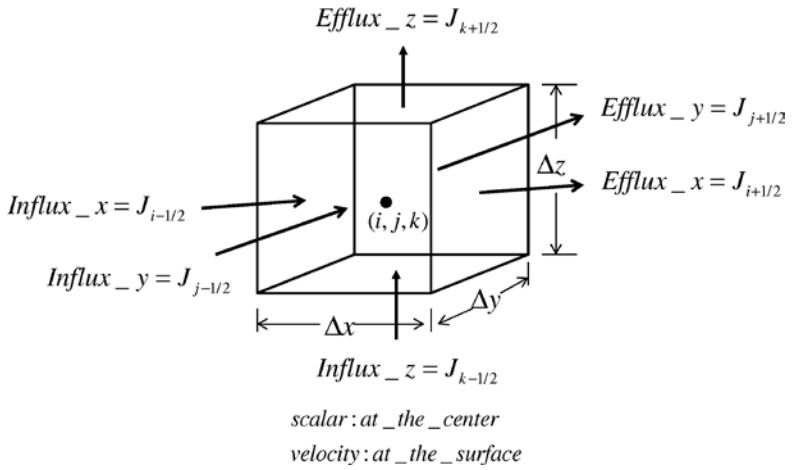

Fig 4.2 Influx and efflux to the control volume

Three dimensional layer-resolved advection and diffusion equation in sigma coordinates is developed for water column by adopting control volume formulation with staggered grid system. The conservation of mass over control volume V with dimensions $\Delta x, \Delta y, \Delta z$ is considered (**Fig 4.2**). The typical dependent variable C in the sediment has been defined as, $C_{\mathrm{i,j},k}$; the rate of change of mass per unit volume or the concentration of the material within the control volume V where, $i = 0 \sim (i\max+1)$: grid in x-direction, $j = 0 \sim (j\max+1)$: grid in y-direction and $k = 1 \sim (k\max)$: grid in z-direction. For the conservation of mass within the control volume, the net change of mass should be equivalent to the net mass influx due to advection and diffusion and the mass generation of species due to reactions. Hence, mass conservation equation can be written as;

$$Mass\_change + net\_mass\_advectiion\_flux = net\_mass\_diffusion\_flux + mass\_source\_gen \quad 4.1$$

The net change of mass during time period of Δt can be written as;

$$Mass\_change = \frac{\partial C_{\mathrm{i,j},k}}{\partial t} \Delta x.\Delta y.\Delta z.\Delta t \quad 4.2$$

Advection flux is the flux carried by the flow filed u, v, w and it can be written as;

$$net\_mass\_advectiion\_flux = \frac{\partial uC_{i,j,k}}{\partial t}\Delta x.\Delta y.\Delta z.\Delta t + \frac{\partial vC_{i,j,k}}{\partial t}\Delta x.\Delta y.\Delta z.\Delta t + \frac{\partial wC_{i,j,k}}{\partial t}\Delta x.\Delta y.\Delta z.\Delta t \quad 4.3$$

The flux $Influx\_x = J_{i-1/2,j,k}$ is entering to the control volume face dy, dz while the flux leaving the opposite face is $Efflux\_x = J_{i+1/2,j,k}$ after the time period of Δt. The flux $Influx\_y = J_{i,j-1/2,k}$ is entering to the control volume face dx, dz while the flux leaving the opposite face is $Efflux\_y = J_{i,j+1/2,k}$ after the time period of Δt. The flux $Influx\_z = J_{i,j,k-1/2}$ is entering to the control volume face dx, dy while the flux leaving the opposite face is $Efflux\_z = J_{i,j,k+1/2}$ after the time period of Δt. The net Influx over the control volume can be written as;

$$net\_mass\_diffusion\_flux = \left(Influx\_x - Efflux\_x\right)dy.dz.\Delta t + \left(Influx\_y - Efflux\_y\right)dx.dz.\Delta t + \left(Influx\_z - Efflux\_z\right)dx.dy.\Delta t \quad 4.4$$

$$net\_mass\_diffusion\_flux = \left(J_{i-1/2,j,k} - J_{i+1/2,j,k}\right)dy.dz.\Delta t + \left(J_{i,j-1/2,k} - J_{i,j+1/2,k}\right)dx.dz.\Delta t + \left(J_{i,j,k-1/2} - J_{i,j,k+1/2}\right)dx.dy.\Delta t \quad 4.5$$

Diffusion flux $J_{i,j,k}$ can be expressed by the Fick's law (Ji, 2008) as;

$$J_{i,j,k} = -K_{i,j,k}\frac{\partial C_{i,j,k}}{\partial z} \quad 4.6$$

where $K_{i,j,k}$ is the diffusion coefficient in z-direction (m^2/s)

$$Net\_mass\_dissfusion\_flux = \left[\left(-K_{i-1/2,j,k}\frac{\partial C_{i,j,k+1/2}}{\partial x}\right) - \left(-K_{i+1/2,j,k}\frac{\partial C_{i,j,k-1/2}}{\partial x}\right)\right]\Delta y\Delta z\Delta t + \left[\left(-K_{i,j-1/2,k}\frac{\partial C_{i,j,k+1/2}}{\partial y}\right) - \left(-K_{i,j+1/2,k}\frac{\partial C_{i,j,k-1/2}}{\partial y}\right)\right]\Delta x\Delta z\Delta t + \left[\left(-K_{i,j,k-1/2}\frac{\partial C_{i,j,k+1/2}}{\partial z}\right) - \left(-K_{i,j,k+1/2}\frac{\partial C_{i,j,k-1/2}}{\partial z}\right)\right]\Delta x\Delta y\Delta t \quad 4.7$$

$$Net\_\mathrm{mass}\_dissfusion\_flux = \frac{\partial}{\partial x}\left[K_x \frac{\partial C_{i,\mathrm{j},k}}{\partial x}\right]\Delta x\Delta y\Delta z\Delta t + \frac{\partial}{\partial y}\left[K_y \frac{\partial C_{i,\mathrm{j},k}}{\partial y}\right]\Delta x\Delta y\Delta z\Delta t + \frac{\partial}{\partial z}\left[K_z \frac{\partial C_{i,\mathrm{j},k}}{\partial z}\right]\Delta x\Delta y\Delta z\Delta t \quad 4.8$$

Let the rate of generation of chemical species over control volume is, $\sum_s R_s$. Then the generation of species over control volume during time period of Δt can be written as,

$$Sourec\_gen = \left[\sum_s R_s\right].\Delta x.\Delta y.\Delta z.\Delta t \quad 4.9$$

Equations **4.2, 4.3, 4.8** and **4.9** can be combined to make the mass conservation over the control volume,

$$\frac{\partial C_{i,\mathrm{j},k}}{\partial t}\Delta x\Delta y\Delta z\Delta t + \frac{\partial uC_{i,\mathrm{j},k}}{\partial t}\Delta x\Delta y\Delta z\Delta t + \frac{\partial vC_{i,\mathrm{j},k}}{\partial t}\Delta x\Delta y\Delta z\Delta t + \frac{\partial wC_{i,\mathrm{j},k}}{\partial t}\Delta x\Delta y\Delta z\Delta t = \frac{\partial}{\partial x}\left[K_x \frac{\partial C_{i,\mathrm{j},k}}{\partial x}\right]\Delta x\Delta y\Delta z\Delta t + \frac{\partial}{\partial y}\left[K_y \frac{\partial C_{i,\mathrm{j},k}}{\partial y}\right]\Delta x\Delta y\Delta z\Delta t + \frac{\partial}{\partial z}\left[K_z \frac{\partial C_{i,\mathrm{j},k}}{\partial z}\right]\Delta x\Delta y\Delta z\Delta t + \sum_s R_s\Delta x\Delta y\Delta z\Delta t \quad 4.10$$

Hence, the governing differential equation for any scalar parameter in the water column in Cartesian coordinates can be written as;

$$\frac{\partial C_{i,\mathrm{j},k}}{\partial t} + \frac{\partial uC_{i,\mathrm{j},k}}{\partial t} + \frac{\partial vC_{i,\mathrm{j},k}}{\partial t} + \frac{\partial wC_{i,\mathrm{j},k}}{\partial t} = \frac{\partial}{\partial x}\left[K_x \frac{\partial C_{i,\mathrm{j},k}}{\partial x}\right] + \frac{\partial}{\partial y}\left[K_y \frac{\partial C_{i,\mathrm{j},k}}{\partial y}\right] + \frac{\partial}{\partial z}\left[K_z \frac{\partial C_{i,\mathrm{j},k}}{\partial z}\right] + \sum_s R_s \quad 4.11$$

According to the sigma coordinate transformation;

$$\sigma = \frac{z+h}{\zeta+h} \quad 4.12$$

Then, the governing differential equation for any scalar parameter in the water column in sigma coordinates can be written as;

$$\frac{\partial(DC)}{\partial t}+\frac{\partial(uDC_{i,\mathrm{j},k})}{\partial x}+\frac{\partial(vDC_{i,\mathrm{j},k})}{\partial y}+\frac{\partial\left[(\dot{\sigma}+\dot{\sigma}_{\mathrm{sin}k})DC_{i,\mathrm{j},k}\right]}{\partial\sigma}$$
$$=DK_h\left(\frac{\partial^2 C_{i,\mathrm{j},k}}{\partial x^2}+\frac{\partial^2 C_{i,\mathrm{j},k}}{\partial y^2}\right)+\frac{1}{D}\frac{\partial}{\partial\sigma}\left(K_v\frac{\partial C_{i,\mathrm{j},k}}{\partial\sigma}\right)+D\sum_s R_s \qquad 4.13$$

where, D is the total depth which equals to the summation of still water depth h and the surface displacement, ζ . $\dot{\sigma}_{\mathrm{sink}}$ is the settling velocity in sigma coordinates given by $\dot{\sigma}_{\mathrm{sink}}=w_{\mathrm{sink}}/D$ (Sasaki and Isobe, 2000), using the settling velocity w_{sink} in Cartesian coordinates and the total depth D, and this will be zero for dissolved matters. K_h and K_v are the horizontal and vertical kinematic eddy diffusivities, respectively. For convenience decompose the above equation using the split operator;

Advection and diffusion only;

$$\frac{\partial(DC_{i,\mathrm{j},k})}{\partial t}+\frac{\partial(uDC_{i,\mathrm{j},k})}{\partial x}+\frac{\partial(vDC_{i,\mathrm{j},k})}{\partial y}+\frac{\partial(\dot{\sigma}DC_{i,\mathrm{j},k})}{\partial\sigma}$$
$$=DK_h\left(\frac{\partial^2 C_{i,\mathrm{j},k}}{\partial x^2}+\frac{\partial^2 C_{i,\mathrm{j},k}}{\partial y^2}\right)+\frac{1}{D}\frac{\partial}{\partial\sigma}\left(K_v\frac{\partial C_{i,\mathrm{j},k}}{\partial\sigma}\right) \qquad 4.14$$

Particulate matter settling only;

$$\frac{\partial(DC_{i,\mathrm{j},k})}{\partial t}+\frac{\partial(\dot{\sigma}_{\mathrm{sin}k}DC_{i,\mathrm{j},k})}{\partial\sigma}=0 \qquad 4.15$$

Source terms only;

$$\frac{\partial(DC_{i,\mathrm{j},k})}{\partial t}=D\sum_s R_s \qquad 4.16$$

Advection and diffusion equation (**4.14**) has been discretized in the sub section **4.1.1**. Solution for the equation of settling (**4.15**) has been discussed in detail in the sub section **4.1.3** while the solution for source term equation (**4.16**) has been discussed in the sub section 0**.** The hydrodynamic model with the hydrostatic and Boussinesq approximations (Sasaki and

Isobe, 2000) gives the three velocity components and surface displacement which is used in the ecosystem model.

4.1.1 Discretization of advection and diffusion equation

The vertical advection and vertical diffusion terms in the equation (**4.14**) are discretized implicitly and the others are discretized explicitly. Using three point scheme the finite difference equations of the each term of the above equation can, therefore, be written as follows.

1. Time derivative term

$$\frac{\partial(DC_{i,\mathrm{j},k})}{\partial t}=\frac{D_{i,j}^{n+1}C_{i,j,k}^{n+1}-D_{i,j}^{n}C_{i,j,k}^{n}}{\Delta t}=\frac{D_{i,j}^{n+1}}{\Delta t}C_{i,j,k}^{n+1}-\frac{D_{i,j}^{n}}{\Delta t}C_{i,j,k}^{n} \tag{4.17}$$

2. Advection term in x-direction

$$\begin{aligned}&\frac{\partial(uDC_{i,\mathrm{j},k})}{\partial x}=\frac{1}{\Delta x}\left(u_{i+1/2,j,k}^{n+1}D_{i+1/2,j}^{n+1}C_{i+1/2,j,k}^{n}-u_{i-1/2,j,k}^{n+1}D_{i-1/2,j}^{n+1}C_{i-1/2,j,k}^{n}\right)\\&-\frac{\lambda_x}{2\Delta x}\left(\left|u_{i+1/2,j,k}^{n+1}\right|D_{i+1/2,j}^{n+1}(C_{i+1,j,k}^{n}-C_{i,j,k}^{n})-\left|u_{i-1/2,j,k}^{n+1}\right|D_{i+1/2,j}^{n+1}(C_{i,j,k}^{n}-C_{i-1,j,k}^{n})\right)\end{aligned} \tag{4.18}$$

defining,

$$amdx_{i,j,k}=\lambda_x=\frac{\left|u_{i,j,k}\right|\Delta t}{\Delta x} \tag{4.19}$$

Then;

$$\begin{aligned}&\frac{\partial(uDC_{i,\mathrm{j},k})}{\partial x}=\frac{1}{\Delta x}\left(u_{i+1/2,j,k}^{n+1}D_{i+1/2,j}^{n+1}C_{i+1/2,j,k}^{n}-u_{i-1/2,j,k}^{n+1}D_{i-1/2,j}^{n+1}C_{i-1/2,j,k}^{n}\right)\\&-\frac{amdx_{i,j,k}}{2\Delta x}\left(\left|u_{i+1/2,j,k}^{n+1}\right|D_{i+1/2,j}^{n+1}(C_{i+1,j,k}^{n}-C_{i,j,k}^{n})-\left|u_{i-1/2,j,k}^{n+1}\right|D_{i+1/2,j}^{n+1}(C_{i,j,k}^{n}-C_{i-1,j,k}^{n})\right)\end{aligned} \tag{4.20}$$

$$\frac{\partial(uDC_{i,j,k})}{\partial x}=\left(\frac{u^{n+1}_{i+1/2,j,k}D^{n+1}_{i+1/2,j}}{\Delta x}\left(\frac{C^{n}_{i+1,j,k}+C^{n}_{i,j,k}}{2}\right)-\frac{u^{n+1}_{i-1/2,j,k}D^{n+1}_{i-1/2,j}}{\Delta x}\left(\frac{C^{n}_{i,j,k}+C^{n}_{i-1,j,k}}{2}\right)\right)$$
$$-\frac{amdx_{i+1/2,j,k}}{2\Delta x}\left|u^{n+1}_{i+1/2,j,k}\right|D^{n+1}_{i+1/2,j}(C^{n}_{i+1,j,k}-C^{n}_{i,j,k}) \qquad 4.21$$
$$+\frac{amdx_{i-1/2,j,k}}{2\Delta x}\left|u^{n+1}_{i-1/2,j,k}\right|D^{n+1}_{i-1/2,j}(C^{n}_{i,j,k}-C^{n}_{i-1,j,k})$$

$$\frac{\partial(uDC_{i,j,k})}{\partial x}=\left(\frac{u^{n+1}_{i+1/2,j,k}D^{n+1}_{i+1/2,j}}{2\Delta x}\right)\varphi^{n}_{i+1,j,k}+\left(\frac{u^{n+1}_{i+1/2,j,k}D^{n+1}_{i+1/2,j}}{2\Delta x}-\frac{u^{n+1}_{i-1/2,j,k}D^{n+1}_{i-1/2,j}}{2\Delta x}\right)\varphi^{n}_{i,j,k}$$
$$-\left(\frac{u^{n+1}_{i-1/2,j,k}D^{n+1}_{i-1/2,j}}{2\Delta x}\right)\varphi^{n}_{i-1,j,k}$$
$$-\left(\frac{amdx_{i+1/2,j,k}}{2\Delta x}\left|u^{n+1}_{i+1/2,j,k}\right|D^{n+1}_{i+1/2,j}\right)\varphi^{n}_{i+1,j,k}+\left(\frac{amdx_{i+1/2,j,k}}{2\Delta x}\left|u^{n+1}_{i+1/2,j,k}\right|D^{n+1}_{i+1/2,j}\right)\varphi^{n}_{i,j,k} \qquad 4.22$$
$$+\left(\frac{amdx_{i-1/2,j,k}}{2\Delta x}\left|u^{n+1}_{i-1/2,j,k}\right|D^{n+1}_{i-1/2,j}\right)\varphi^{n}_{i,j,k}-\left(\frac{amdx_{i-1/2,j,k}}{2\Delta x}\left|u^{n+1}_{i-1/2,j,k}\right|D^{n+1}_{i-1/2,j}\right)\varphi^{n}_{i-1,j,k}$$

3. Advection term in y-direction

$$\frac{\partial(vDC_{i,j,k})}{\partial x}=\frac{1}{\Delta y}\left(v^{n+1}_{i,j+1/2,k}D^{n+1}_{i,j+1/2}C^{n}_{i,j+1/2,k}-v^{n+1}_{i,j-1/2,k}D^{n+1}_{i,j-1/2}C^{n}_{i,j-1/2,k}\right)$$
$$-\frac{\lambda_y}{2\Delta y}\left(\left|v^{n+1}_{i,j+1/2,k}\right|D^{n+1}_{i,j+1/2}(C^{n}_{i,j+1,k}-C^{n}_{i,j,k})-\left|v^{n+1}_{i,j-1/2,k}\right|D^{n+1}_{i,j-1/2}(C^{n}_{i,j,k}-C^{n}_{i,j-1,k})\right) \qquad 4.23$$

defining,

$$amdy_{i,j,k}=\lambda_y=\frac{\left|v_{i,j,k}\right|\Delta t}{\Delta y} \qquad 4.24$$

Then;

$$\frac{\partial(vDC_{i,j,k})}{\partial x}=\frac{1}{\Delta y}\left(v^{n+1}_{i,j+1/2,k}D^{n+1}_{i,j+1/2}C^{n}_{i,j+1/2,k}-v^{n+1}_{i,j-1/2,k}D^{n+1}_{i,j-1/2}C^{n}_{i,j-1/2,k}\right)$$
$$-\frac{amdy_{i,j,k}}{2\Delta y}\left(\left|v^{n+1}_{i,j+1/2,k}\right|D^{n+1}_{i,j+1/2}(C^{n}_{i,j+1,k}-C^{n}_{i,j,k})-\left|v^{n+1}_{i,j-1/2,k}\right|D^{n+1}_{i,j-1/2}(C^{n}_{i,j,k}-C^{n}_{i,j-1,k})\right) \qquad 4.25$$

$$\frac{\partial(vDC_{i,\mathrm{j},k})}{\partial x}=\left(\frac{v^{n+1}_{i,j+1/2,k}D^{n+1}_{i,j+1/2}}{2\Delta y}\left(\frac{C^{n}_{i,j+1,k}+C^{n}_{i,j,k}}{2}\right)-\frac{v^{n+1}_{i,j-1/2,k}D^{n+1}_{i,j-1/2}}{2\Delta y}\left(\frac{C^{n}_{i,j,k}+C^{n}_{i,j-1,k}}{2}\right)\right)$$
$$-\frac{amdy_{i,j+1/2,k}}{2\Delta y}\left|v^{n+1}_{i,j+1/2,k}\right|D^{n+1}_{i,j+1/2}(C^{n}_{i,j+1,k}-C^{n}_{i,j,k})+\frac{amdy_{i,j-1/2,k}}{2\Delta y}\left|v^{n+1}_{i,j-1/2,k}\right|D^{n+1}_{i,j-1/2}(C^{n}_{i,j,k}-C^{n}_{i,j-1,k}) \quad 4.26$$

$$\frac{\partial(vDC_{i,\mathrm{j},k})}{\partial x}=\left(\frac{v^{n+1}_{i,j+1/2,k}D^{n+1}_{i,j+1/2}}{2\Delta y}\right)C^{n}_{i,j+1,k}+\left(\frac{v^{n+1}_{i,j+1/2,k}D^{n+1}_{i,j+1/2}}{2\Delta y}-\frac{v^{n+1}_{i,j-1/2,k}D^{n+1}_{i,j-1/2}}{2\Delta y}\right)C^{n}_{i,j,k}$$
$$-\left(\frac{v^{n+1}_{i,j-1/2,k}D^{n+1}_{i,j-1/2}}{2\Delta y}\right)C^{n}_{i,j-1,k}$$
$$-\left(\frac{amdy_{i,j+1/2,k}}{2\Delta y}\left|v^{n+1}_{i,j+1/2,k}\right|D^{n+1}_{i,j+1/2}\right)C^{n}_{i,j+1,k}+\left(\frac{amdy_{i,j+1/2,k}}{2\Delta y}\left|v^{n+1}_{i,j+1/2,k}\right|D^{n+1}_{i,j+1/2}\right)C^{n}_{i,j,k} \quad 4.27$$
$$+\left(\frac{amdy_{i,j-1/2,k}}{2\Delta y}\left|v^{n+1}_{i,j-1/2,k}\right|D^{n+1}_{i,j-1/2}\right)C^{n}_{i,j,k}-\left(\frac{amdy_{i,j-1/2,k}}{2\Delta y}\left|v^{n+1}_{i,j-1/2,k}\right|D^{n+1}_{i,j-1/2}\right)C^{n}_{i,j-1,k}$$

4. Advection term in sigma-direction

$$\frac{\partial(\dot{\sigma}DC_{i,\mathrm{j},k})}{\partial\sigma}=\frac{1}{\Delta\sigma}\left(\dot{\sigma}^{n+1}_{i,j,k+1/2}D^{n+1}_{i,j}C^{n+1}_{i,j,k+1/2}-\dot{\sigma}^{n+1}_{i,j,k-1/2}D^{n+1}_{i,j}C^{n+1}_{i,j,k-1/2}\right)$$
$$-\frac{\lambda_\sigma}{2\Delta\sigma}\left(\left|\dot{\sigma}^{n+1}_{i,j,k+1/2}\right|D^{n+1}_{i,j}(C^{n+1}_{i,j,k+1}-C^{n+1}_{i,j,k})-\left|\dot{\sigma}^{n+1}_{i,j,k-1/2}\right|D^{n+1}_{i,j}(C^{n+1}_{i,j,k}-C^{n+1}_{i,j,k-1})\right) \quad 4.28$$

$$\frac{\partial(\dot{\sigma}DC_{i,\mathrm{j},k})}{\partial\sigma}=\left(\frac{\dot{\sigma}^{n+1}_{i,j,k+1/2}D^{n+1}_{i,j}}{2\Delta\sigma}\right)C^{n+1}_{i,j,k+1}+\left(\frac{\dot{\sigma}^{n+1}_{i,j,k+1/2}D^{n+1}_{i,j}}{2\Delta\sigma}\right)C^{n+1}_{i,j,k}-\left(\frac{\dot{\sigma}^{n+1}_{i,j,k-1/2}D^{n+1}_{i,j}}{2\Delta\sigma}\right)C^{n+1}_{i,j,k}$$
$$-\left(\frac{\dot{\sigma}^{n+1}_{i,j,k-1/2}D^{n+1}_{i,j}}{2\Delta\sigma}\right)C^{n+1}_{i,j,k-1}$$
$$-\left(\frac{\lambda_\sigma D^{n+1}_{i,j}\left|\dot{\sigma}^{n+1}_{i,j,k+1/2}\right|}{2\Delta\sigma}\right)C^{n+1}_{i,j,k+1}+\left(\frac{\lambda_\sigma D^{n+1}_{i,j}\left|\dot{\sigma}^{n+1}_{i,j,k+1/2}\right|}{2\Delta\sigma}\right)C^{n+1}_{i,j,k} \quad 4.29$$
$$+\left(\frac{\lambda_\sigma D^{n+1}_{i,j}\left|\dot{\sigma}^{n+1}_{i,j,k-1/2}\right|}{2\Delta\sigma}\right)C^{n+1}_{i,j,k}-\left(\frac{\lambda_\sigma D^{n+1}_{i,j}\left|\dot{\sigma}^{n+1}_{i,j,k-1/2}\right|}{2\Delta\sigma}\right)C^{n+1}_{i,j,k-1}$$

defining,

$$amds_{i,j,k}=\lambda_\sigma=\frac{\left|\dot{\sigma}_{i,j,k}\right|\Delta t}{\Delta\sigma} \quad 4.30$$

Then;

$$\frac{\partial(\dot{\sigma}DC_{i,\mathrm{j},k})}{\partial\sigma}=\left(\frac{\dot{\sigma}^{n+1}_{i,j,k+1/2}D^{n+1}_{i,j}}{2\Delta\sigma}\right)C^{n+1}_{i,j,k+1}+\left(\frac{\dot{\sigma}^{n+1}_{i,j,k+1/2}D^{n+1}_{i,j}}{2\Delta\sigma}\right)C^{n+1}_{i,j,k}-\left(\frac{\dot{\sigma}^{n+1}_{i,j,k-1/2}D^{n+1}_{i,j}}{2\Delta\sigma}\right)C^{n+1}_{i,j,k}$$
$$-\left(\frac{\dot{\sigma}^{n+1}_{i,j,k-1/2}D^{n+1}_{i,j}}{2\Delta\sigma}\right)C^{n+1}_{i,j,k-1}$$
$$-\left(\frac{amdas_{i,j,k+1/2}D^{n+1}_{i,j}\left|\dot{\sigma}^{n+1}_{i,j,k+1/2}\right|}{2\Delta\sigma}\right)C^{n+1}_{i,j,k+1}+\left(\frac{amdas_{i,j,k+1/2}D^{n+1}_{i,j}\left|\dot{\sigma}^{n+1}_{i,j,k+1/2}\right|}{2\Delta\sigma}\right)C^{n+1}_{i,j,k} \quad 4.31$$
$$+\left(\frac{amdas_{i,j,k-1/2}D^{n+1}_{i,j}\left|\dot{\sigma}^{n+1}_{i,j,k-1/2}\right|}{2\Delta\sigma}\right)C^{n+1}_{i,j,k}-\left(\frac{amdas_{i,j,k-1/2}D^{n+1}_{i,j}\left|\dot{\sigma}^{n+1}_{i,j,k-1/2}\right|}{2\Delta\sigma}\right)C^{n+1}_{i,j,k-1}$$

5. Horizontal diffusion term

$$DK_h\left(\frac{\partial^2 C_{i,\mathrm{j},k}}{\partial x^2}+\frac{\partial^2 C_{i,\mathrm{j},k}}{\partial y^2}\right)=D_{i,j}\left[K_{hx}\frac{\partial^2 C}{\partial x^2}+K_{hy}\frac{\partial^2 C}{\partial y^2}\right] \quad 4.32$$

$$DK_h\left(\frac{\partial^2 C_{i,\mathrm{j},k}}{\partial x^2}+\frac{\partial^2 C_{i,\mathrm{j},k}}{\partial y^2}\right)=D^{n+1}_{i,j}\left[\frac{1}{\Delta x}\left(K_{hx\_i+1/2,j,k}\left.\frac{\partial C}{\partial x}\right|_{i+1/2,j,k}-K_{hx\_i-1/2,j,k}\left.\frac{\partial C}{\partial x}\right|_{i-1/2,j,k}\right)\right. \quad 4.33$$
$$\left.+\frac{1}{\Delta y}\left(K_{hy\_i,j+1/2,k}\left.\frac{\partial C}{\partial y}\right|_{i,j+1/2,k}-K_{hx,i,j-1/2,k}\left.\frac{\partial C}{\partial x}\right|_{i,j-1/2,k}\right)\right]$$

$$DK_h\left(\frac{\partial^2 C_{i,\mathrm{j},k}}{\partial x^2}+\frac{\partial^2 C_{i,\mathrm{j},k}}{\partial y^2}\right)=D^{n+1}_{i,j}\left[\frac{1}{\Delta x}\left(\begin{array}{l}K_{hx\_i+1/2,j,k}\dfrac{C_{i+1,j,k}-C_{i,j,k}}{\Delta x}\\ -K_{hx\_i-1/2,j,k}\dfrac{C_{i,j,k}-C_{i-1,j,k}}{\Delta x}\end{array}\right)\right. \quad 4.34$$
$$\left.+\frac{1}{\Delta y}\left(K_{hy\_i,j+1/2,k}\frac{C_{i,j+1,k}-C_{i,j,k}}{\Delta y}-K_{hx,i,j-1/2,k}\frac{C_{i,j,k}-C_{i,j-1,k}}{\Delta y}\right)\right]$$

$$DK_h\left(\frac{\partial^2 C_{i,\mathrm{j},k}}{\partial x^2}+\frac{\partial^2 C_{i,\mathrm{j},k}}{\partial y^2}\right)=\left(\frac{D^{n+1}_{i,j}K_{hx\_i+1/2,j,k}}{(\Delta x)^2}\right)C^n_{i+1,j,k}-\left(\frac{D^{n+1}_{i,j}K_{hx\_i+1/2,j,k}}{(\Delta x)^2}\right)C^n_{i,j,k}$$
$$-\left(\frac{D^{n+1}_{i,j}K_{hx\_i-1/2,j,k}}{(\Delta x)^2}\right)C^n_{i,j,k}+\left(\frac{D^{n+1}_{i,j}K_{hx\_i-1/2,j,k}}{(\Delta x)^2}\right)C^n_{i-1,j,k}$$
$$+\left(\frac{D^{n+1}_{i,j}K_{hy\_i,j+1/2,k}}{(\Delta y)^2}\right)C^n_{i,j+1,k}-\left(\frac{D^{n+1}_{i,j}K_{hy\_i,j+1/2,k}}{(\Delta y)^2}\right)C^n_{i,j,k} \quad 4.35$$
$$-\left(\frac{D^{n+1}_{i,j}K_{hy\_i,j-1/2,k}}{(\Delta y)^2}\right)C^n_{i,j,k}+\left(\frac{D^{n+1}_{i,j}K_{hy\_i,j-1/2,k}}{(\Delta y)^2}\right)C^n_{i,j-1,k}$$

6. Vertical diffusion term

$$\frac{1}{D}\frac{\partial}{\partial\sigma}\left(K_v\frac{\partial C_{i,\mathrm{j},k}}{\partial\sigma}\right)=\frac{1}{D_{i,j}^{n+1}}\cdot\frac{1}{\Delta\sigma}\left(K_{v_{i,j,k+1/2}}\frac{C_{i,j,k+1}^{n+1}-C_{i,j,k}^{n+1}}{\Delta\sigma}-K_{v_{i,j,k-1/2}}\frac{C_{i,j,k}^{n+1}-C_{i,j,k-1}^{n+1}}{\Delta\sigma}\right) \tag{4.36}$$

$$\begin{aligned}\frac{1}{D}\frac{\partial}{\partial\sigma}\left(K_v\frac{\partial C_{i,\mathrm{j},k}}{\partial\sigma}\right)&=\left(\frac{K_{v_{i,j,k+1/2}}}{D_{i,j}^{n+1}(\Delta\sigma)^2}\right)C_{i,j,k+1}^{n+1}-\left(\frac{K_{v_{i,j,k+1/2}}}{D_{i,j}^{n+1}(\Delta\sigma)^2}\right)C_{i,j,k}^{n+1}\\&-\left(\frac{K_{v_{i,j,k-1/2}}}{D_{i,j}^{n+1}(\Delta\sigma)^2}\right)C_{i,j,k}^{n+1}+\left(\frac{K_{v_{i,j,k-1/2}}}{D_{i,j}^{n+1}(\Delta\sigma)^2}\right)C_{i,j,k-1}^{n+1}\end{aligned} \tag{4.37}$$

Substituting equations **4.17**, **4.22**, **4.27**, **4.31**, **4.35** and **4.37** in equation **4.14**;

$$\begin{aligned}&\frac{D_{i,j}^{n+1}}{\Delta t}C_{i,j,k}^{n+1}-\frac{D_{i,j}^{n}}{\Delta t}C_{i,j,k}^{n}\\&+\left(\frac{u_{i+1/2,j,k}^{n+1}D_{i+1/2,j}^{n+1}}{2\Delta x}\right)C_{i+1,j,k}^{n}+\left(\frac{u_{i+1/2,j,k}^{n+1}D_{i+1/2,j}^{n+1}}{2\Delta x}-\frac{u_{i-1/2,j,k}^{n+1}D_{i-1/2,j}^{n+1}}{2\Delta x}\right)C_{i,j,k}^{n}-\left(\frac{u_{i-1/2,j,k}^{n+1}D_{i-1/2,j}^{n+1}}{2\Delta x}\right)C_{i-1,j,k}^{n}\\&-\left(\frac{amdx_{i+1/2,j,k}\left|u_{i+1/2,j,k}^{n+1}\right|D_{i+1/2,j}^{n+1}}{2\Delta x}\right)C_{i+1,j,k}^{n}+\left(\frac{amdx_{i+1/2,j,k}\left|u_{i+1/2,j,k}^{n+1}\right|D_{i+1/2,j}^{n+1}}{2\Delta x}\right)C_{i,j,k}^{n}\\&+\left(\frac{amdx_{i-1/2,j,k}\left|u_{i-1/2,j,k}^{n+1}\right|D_{i-1/2,j}^{n+1}}{2\Delta x}\right)C_{i,j,k}^{n}-\left(\frac{amdx_{i-1/2,j,k}\left|u_{i-1/2,j,k}^{n+1}\right|D_{i-1/2,j}^{n+1}}{2\Delta x}\right)C_{i-1,j,k}^{n}\\&+\left(\frac{v_{i,j+1/2,k}^{n+1}D_{i,j+1/2}^{n+1}}{2\Delta y}\right)C_{i,j+1,k}^{n}+\left(\frac{v_{i,j+1/2,k}^{n+1}D_{i,j+1/2}^{n+1}}{2\Delta y}-\frac{v_{i,j-1/2,k}^{n+1}D_{i,j-1/2}^{n+1}}{2\Delta y}\right)C_{i,j,k}^{n}-\left(\frac{v_{i,j-1/2,k}^{n+1}D_{i,j-1/2}^{n+1}}{2\Delta y}\right)C_{i,j-1,k}^{n}\\&-\left(\frac{amdy_{i,j+1/2,k}\left|v_{i,j+1/2,k}^{n+1}\right|D_{i,j+1/2}^{n+1}}{2\Delta y}\right)C_{i,j+1,k}^{n}+\left(\frac{amdy_{i,j+1/2,k}\left|v_{i,j+1/2,k}^{n+1}\right|D_{i,j+1/2}^{n+1}}{2\Delta y}\right)C_{i,j,k}^{n}\\&+\left(\frac{amdy_{i,j-1/2,k}\left|v_{i,j-1/2,k}^{n+1}\right|D_{i,j-1/2}^{n+1}}{2\Delta y}\right)C_{i,j,k}^{n}-\left(\frac{amdy_{i,j-1/2,k}\left|v_{i,j-1/2,k}^{n+1}\right|D_{i,j-1/2}^{n+1}}{2\Delta y}\right)C_{i,j-1,k}^{n}\\&+\left(\frac{\dot\sigma_{i,j,k+1/2}^{n+1}D_{i,j}^{n+1}}{2\Delta\sigma}\right)C_{i,j,k+1}^{n+1}+\left(\frac{\dot\sigma_{i,j,k+1/2}^{n+1}D_{i,j}^{n+1}}{2\Delta\sigma}\right)C_{i,j,k}^{n+1}-\left(\frac{\dot\sigma_{i,j,k-1/2}^{n+1}D_{i,j}^{n+1}}{2\Delta\sigma}\right)C_{i,j,k}^{n+1}-\left(\frac{\dot\sigma_{i,j,k-1/2}^{n+1}D_{i,j}^{n+1}}{2\Delta\sigma}\right)C_{i,j,k-1}^{n+1}\\&-\left(\frac{amdas_{i,j,k+1/2}D_{i,j}^{n+1}\left|\dot\sigma_{i,j,k+1/2}^{n+1}\right|}{2\Delta\sigma}\right)C_{i,j,k+1}^{n+1}+\left(\frac{amdas_{i,j,k+1/2}D_{i,j}^{n+1}\left|\dot\sigma_{i,j,k+1/2}^{n+1}\right|}{2\Delta\sigma}\right)C_{i,j,k}^{n+1}\\&+\left(\frac{amdas_{i,j,k-1/2}D_{i,j}^{n+1}\left|\dot\sigma_{i,j,k-1/2}^{n+1}\right|}{2\Delta\sigma}\right)C_{i,j,k}^{n+1}-\left(\frac{amdas_{i,j,k-1/2}D_{i,j}^{n+1}\left|\dot\sigma_{i,j,k-1/2}^{n+1}\right|}{2\Delta\sigma}\right)C_{i,j,k-1}^{n+1}\\&=\left(\frac{D_{i,j}^{n+1}K_{hx\_i+1/2,j,k}}{(\Delta x)^2}\right)C_{i+1,j,k}^{n}-\left(\frac{D_{i,j}^{n+1}K_{hx\_i+1/2,j,k}}{(\Delta x)^2}\right)C_{i,j,k}^{n}-\left(\frac{D_{i,j}^{n+1}K_{hx\_i-1/2,j,k}}{(\Delta x)^2}\right)C_{i,j,k}^{n}\\&+\left(\frac{D_{i,j}^{n+1}K_{hx\_i-1/2,j,k}}{(\Delta x)^2}\right)C_{i-1,j,k}^{n}+\left(\frac{D_{i,j}^{n+1}K_{hy\_i,j+1/2,k}}{(\Delta y)^2}\right)C_{i,j+1,k}^{n}-\left(\frac{D_{i,j}^{n+1}K_{hy\_i,j+1/2,k}}{(\Delta y)^2}\right)C_{i,j,k}^{n}\\&-\left(\frac{D_{i,j}^{n+1}K_{hy\_i,j-1/2,k}}{(\Delta y)^2}\right)C_{i,j,k}^{n}+\left(\frac{D_{i,j}^{n+1}K_{hy\_i,j-1/2,k}}{(\Delta y)^2}\right)C_{i,j-1,k}^{n}\\&+\left(\frac{K_{v_{i,j,k+1/2}}}{D_{i,j}^{n+1}(\Delta\sigma)^2}\right)C_{i,j,k+1}^{n+1}-\left(\frac{K_{v_{i,j,k+1/2}}}{D_{i,j}^{n+1}(\Delta\sigma)^2}\right)C_{i,j,k}^{n+1}-\left(\frac{K_{v_{i,j,k-1/2}}}{D_{i,j}^{n+1}(\Delta\sigma)^2}\right)C_{i,j,k}^{n+1}+\left(\frac{K_{v_{i,j,k-1/2}}}{D_{i,j}^{n+1}(\Delta\sigma)^2}\right)C_{i,j,k-1}^{n+1}\end{aligned} \tag{4.38}$$

$$
\begin{aligned}
&\left\{-\frac{K_{v_{i,j,k-1/2}}}{D_{i,j}^{n+1}(\Delta\sigma)^2}-\frac{D_{i,j}^{n+1}}{2\Delta\sigma}\left[\dot{\sigma}_{i,j,k-1/2}^{n+1}+amdas_{i,j,k-1/2}\left|\dot{\sigma}_{i,j,k-1/2}^{n+1}\right|\right]\right\}C_{i,j,k-1}^{n+1}\\
&+\left\{\left(\frac{D_{i,j}^{n+1}}{\Delta t}\right)-\left(-\frac{K_{v_{i,j,k-1/2}}}{D_{i,j}^{n+1}(\Delta\sigma)^2}-\frac{D_{i,j}^{n+1}}{2\Delta\sigma}\left[\dot{\sigma}_{i,j,k-1/2}^{n+1}+amdas_{i,j,k-1/2}\left|\dot{\sigma}_{i,j,k-1/2}^{n+1}\right|\right]\right)\right.\\
&\left.-\left(-\frac{K_{v_{i,j,k+1/2}}}{D_{i,j}^{n+1}(\Delta\sigma)^2}+\frac{D_{i,j}^{n+1}}{2\Delta\sigma}\left[\dot{\sigma}_{i,j,k+1/2}^{n+1}-amdas_{i,j,k+1/2}\left|\dot{\sigma}_{i,j,k+1/2}^{n+1}\right|\right]\right)\right.\\
&\left.-\left(\frac{D_{i,j}^{n+1}}{\Delta\sigma}\left[\dot{\sigma}_{i,j,k-1/2}^{n+1}-\dot{\sigma}_{i,j,k+1/2}^{n+1}\right]\right)\right\}C_{i,j,k}^{n+1}\\
&\left\{-\frac{K_{v_{i,j,k+1/2}}}{D_{i,j}^{n+1}(\Delta\sigma)^2}+\frac{D_{i,j}^{n+1}}{2\Delta\sigma}\left[\dot{\sigma}_{i,j,k+1/2}^{n+1}-amdas_{i,j,k+1/2}\left|\dot{\sigma}_{i,j,k+1/2}^{n+1}\right|\right]\right\}C_{i,j,k+1}^{n+1}\\
&=\left\{\frac{D_{i,j}^{n+1}K_{hx\_i-1/2,j,k}}{(\Delta x)^2}+\frac{1}{2\Delta x}\left(amdx_{i-1/2,j,k}\left|u_{i-1/2,j,k}^{n+1}\right|D_{i+1/2,j}^{n+1}+u_{i-1/2,j,k}^{n+1}D_{i-1/2,j}^{n+1}\right)\right\}C_{i-1,j,k}^{n}\\
&+\left\{-D_{i,j}^{n+1}\left(\frac{K_{hx\_i-1/2,j,k}}{(\Delta x)^2}+\frac{K_{hx\_i+1/2,j,k}}{(\Delta x)^2}+\frac{K_{hy\_i,j-1/2,k}}{(\Delta y)^2}+\frac{K_{hy\_i,j+1/2,k}}{(\Delta y)^2}\right)\right.\\
&+\frac{1}{2\Delta x}\begin{pmatrix}-amdx_{i-1/2,j,k}\left|u_{i-1/2,j,k}^{n+1}\right|D_{i-1/2,j}^{n+1}-amdx_{i+1/2,j,k}\left|u_{i+1/2,j,k}^{n+1}\right|D_{i+1/2,j}^{n+1}\\+u_{i-1/2,j,k}^{n+1}D_{i-1/2,j}^{n+1}-u_{i+1/2,j,k}^{n+1}D_{i+1/2,j}^{n+1}\end{pmatrix}\\
&+\frac{1}{2\Delta y}\begin{pmatrix}-amdy_{i,j-1/2,k}\left|v_{i,j-1/2,k}^{n+1}\right|D_{i,j-1/2}^{n+1}-amdy_{i,j+1/2,k}\left|v_{i,j+1/2,k}^{n+1}\right|D_{i,j+1/2}^{n+1}\\+v_{i,j-1/2,k}^{n+1}D_{i,j-1/2}^{n+1}-v_{i,j+1/2,k}^{n+1}D_{i,j+1/2}^{n+1}\end{pmatrix}+\frac{D_{i,j}^{n}}{\Delta t}\left.\right\}C_{i,j,k}^{n}\\
&+\left\{\frac{D_{i,j}^{n+1}K_{hx\_i+1/2,j,k}}{(\Delta x)^2}+\frac{1}{2\Delta x}\left(amdx_{i+1/2,j,k}\left|u_{i+1/2,j,k}^{n+1}\right|D_{i+1/2,j}^{n+1}-u_{i+1/2,j,k}^{n+1}D_{i+1/2,j}^{n+1}\right)\right\}C_{i+1,j,k}^{n}\\
&+\left\{\frac{D_{i,j}^{n+1}K_{hy\_i,j-1/2,k}}{(\Delta y)^2}+\frac{1}{2\Delta y}\left(amdy_{i,j-1/2,k}\left|v_{i,j-1/2,k}^{n+1}\right|D_{i,j+1/2}^{n+1}+v_{i,j-1/2,k}^{n+1}D_{i,j-1/2}^{n+1}\right)\right\}C_{i,j-1,k}^{n}\\
&+\left\{\frac{D_{i,j}^{n+1}K_{hy\_i,j+1/2,k}}{(\Delta y)^2}+\frac{1}{2\Delta y}\left(amdy_{i,j+1/2,k}\left|v_{i,j+1/2,k}^{n+1}\right|D_{i,j+1/2}^{n+1}-v_{i,j+1/2,k}^{n+1}D_{i,j+1/2}^{n+1}\right)\right\}C_{i,j+1,k}^{n}
\end{aligned}
\tag{4.39}
$$

This is written in the form of

$$
\begin{aligned}
&apkc_{i,j,k}C_{i,j,k-1}^{n+1}+bpkc_{i,j,k}C_{i,j,k}^{n+1}+cpkc_{i,j,k}C_{i,j,k+1}^{n+1}\\
&=auk_{i,j,k}C_{i-1,j,k}^{n}+buk_{i,j,k}C_{i,j,k}^{n}+cuk_{i,j,k}C_{i+1,j,k}^{n}+duk_{i,j,k}C_{i,j-1,k}^{n}+euk_{i,j,k}C_{i,j+1,k}^{n}
\end{aligned}
\tag{4.40}
$$

where,

$$apkc_{i,j,k} = \left\{ -\frac{K_{v_{i,j,k-1/2}}}{D_{i,j}^{n+1}(\Delta\sigma)^2} - \frac{D_{i,j}^{n+1}}{2\Delta\sigma}\left[\dot{\sigma}_{i,j,k-1/2}^{n+1} + amdas_{i,j,k-1/2} \left| \dot{\sigma}_{i,j,k-1/2}^{n+1} \right| \right] \right\} \tag{4.41}$$

$$\begin{aligned} bpkc_{i,j,k} = & \left\{ \left(\frac{D_{i,j}^{n+1}}{\Delta t} \right) - \left(-\frac{K_{v_{i,j,k-1/2}}}{D_{i,j}^{n+1}(\Delta\sigma)^2} - \frac{D_{i,j}^{n+1}}{2\Delta\sigma}\left[\dot{\sigma}_{i,j,k-1/2}^{n+1} + amdas_{i,j,k-1/2} \left| \dot{\sigma}_{i,j,k-1/2}^{n+1} \right| \right] \right) \right. \\ & \left. - \left(-\frac{K_{v_{i,j,k+1/2}}}{D_{i,j}^{n+1}(\Delta\sigma)^2} + \frac{D_{i,j}^{n+1}}{2\Delta\sigma}\left[\dot{\sigma}_{i,j,k+1/2}^{n+1} - amdas_{i,j,k+1/2} \left| \dot{\sigma}_{i,j,k+1/2}^{n+1} \right| \right] \right) - \left(\frac{D_{i,j}^{n+1}}{\Delta\sigma}\left[\dot{\sigma}_{i,j,k-1/2}^{n+1} - \dot{\sigma}_{i,j,k+1/2}^{n+1} \right] \right) \right\} \end{aligned} \tag{4.42}$$

$$cpkc_{i,j,k} = \left\{ -\frac{K_{v_{i,j,k+1/2}}}{D_{i,j}^{n+1}(\Delta\sigma)^2} + \frac{D_{i,j}^{n+1}}{2\Delta\sigma}\left[\dot{\sigma}_{i,j,k+1/2}^{n+1} - amdas_{i,j,k+1/2} \left| \dot{\sigma}_{i,j,k+1/2}^{n+1} \right| \right] \right\} \tag{4.43}$$

But equation **4.42** can be rewrite as;

$$bpkc_{i,j,k} = \left(\frac{D_{i,j}^{n+1}}{\Delta t} \right) - apkc_{i,j,k} - cpkc_{i,j,k} - \left(\frac{D_{i,j}^{n+1}}{2\Delta\sigma}\left[\dot{\sigma}_{i,j,k-1/2}^{n+1} - \dot{\sigma}_{i,j,k+1/2}^{n+1} \right] \right) \tag{4.44}$$

$$auk_{i,j,k} = \left(\frac{D_{i,j}^{n+1} K_{hx\_i-1/2,j,k}}{(\Delta x)^2} + \frac{1}{2\Delta x}\left(amdx_{i-1/2,j,k} \left| u_{i-1/2,j,k}^{n+1} \right| D_{i+1/2,j}^{n+1} + u_{i-1/2,j,k}^{n+1} D_{i-1/2,j}^{n+1} \right) \right) \tag{4.45}$$

$$\begin{aligned} buk_{i,j,k} = & \left\{ -D_{i,j}^{n+1} \left(\frac{K_{hx\_i-1/2,j,k}}{(\Delta x)^2} + \frac{K_{hx\_i+1/2,j,k}}{(\Delta x)^2} + \frac{K_{hy\_i,j-1/2,k}}{(\Delta y)^2} + \frac{K_{hy\_i,j+1/2,k}}{(\Delta y)^2} \right) \right. \\ & + \frac{1}{2\Delta x}\left(\begin{array}{l} -amdx_{i-1/2,j,k} \left| u_{i-1/2,j,k}^{n+1} \right| D_{i-1/2,j}^{n+1} - amdx_{i+1/2,j,k} \left| u_{i+1/2,j,k}^{n+1} \right| D_{i+1/2,j}^{n+1} \\ +u_{i-1/2,j,k}^{n+1} D_{i-1/2,j}^{n+1} - u_{i+1/2,j,k}^{n+1} D_{i+1/2,j}^{n+1} \end{array} \right) \\ & \left. + \frac{1}{2\Delta y}\left(\begin{array}{l} -amdy_{i,j-1/2,k} \left| v_{i,j-1/2,k}^{n+1} \right| D_{i,j-1/2}^{n+1} - amdy_{i,j+1/2,k} \left| v_{i,j+1/2,k}^{n+1} \right| D_{i,j+1/2}^{n+1} \\ +v_{i,j-1/2,k}^{n+1} D_{i,j-1/2}^{n+1} - v_{i,j+1/2,k}^{n+1} D_{i,j+1/2}^{n+1} \end{array} \right) + \frac{D_{i,j}^{n}}{\Delta t} \right\} \end{aligned} \tag{4.46}$$

$$cuk_{i,j,k} = \left\{ \frac{D_{i,j}^{n+1} K_{hx\_i+1/2,j,k}}{(\Delta x)^2} + \frac{1}{2\Delta x}\left(amdx_{i+1/2,j,k} \left| u_{i+1/2,j,k}^{n+1} \right| D_{i+1/2,j}^{n+1} - u_{i+1/2,j,k}^{n+1} D_{i+1/2,j}^{n+1} \right) \right\} \tag{4.47}$$

$$duk_{i,j,k} = \left\{ \frac{D_{i,j}^{n+1} K_{hy\_i,j-1/2,k}}{(\Delta y)^2} + \frac{1}{2\Delta y}\left(amdy_{i,j-1/2,k} \left| v_{i,j-1/2,k}^{n+1} \right| D_{i,j+1/2}^{n+1} + v_{i,j-1/2,k}^{n+1} D_{i,j-1/2}^{n+1} \right) \right\} \tag{4.48}$$

$$euk_{i,j,k} = \left\{ \frac{D_{i,j}^{n+1} K_{hy\_i,j+1/2,k}}{(\Delta y)^2} + \frac{1}{2\Delta y}\left(amdy_{i,j+1/2,k} \left| v_{i,j+1/2,k}^{n+1} \right| D_{i,j+1/2}^{n+1} - v_{i,j+1/2,k}^{n+1} D_{i,j+1/2}^{n+1} \right) \right\} \tag{4.49}$$

Equation **4.40** is further written as;

$$apkc_{i,j,k}C^{n+1}_{i,j,k-1} + bpkc_{i,j,k}C^{n+1}_{i,j,k} + cpkc_{i,j,k}C^{n+1}_{i,j,k+1} = dpkc_{i,j,k} \quad 4.50$$

where $dpkc_{i,j,k}$ denotes the coefficient for explicit terms.

$$dpkc_{i,j,k} = auk_{i,j,k}C^{n}_{i-1,j,k} + buk_{i,j,k}C^{n}_{i,j,k} + cuk_{i,j,k}C^{n}_{i+1,j,k} + duk_{i,j,k}C^{n}_{i,j-1,k} + euk_{i,j,k}C^{n}_{i,j+1,k} \quad 4.51$$

4.1.2 Surface and bottom boundary conditions

4.1.2.1 Surface boundary conditions

Define a dummy grid $C_{i,\mathrm{j},\mathrm{k}+1}$ above the surface of the water column where $C_{i,\mathrm{j},\mathrm{k}+1} = C_{i,\mathrm{j},\mathrm{k}}$ and $\dot{\sigma}^{n+1}_{i,j,k+1/2} = 0$ at the surface. Advection and diffusion on the surface sediment boundary has been considered as zero here since the boundary conditions are considered separately. Hence vertical advection and diffusion equations at the surface have been reconsidered as follows.

4a. Advection term in sigma-direction

$$\frac{\partial(\dot{\sigma}DC_{i,\mathrm{j},k})}{\partial\sigma} = \frac{1}{\Delta\sigma}\left(-\dot{\sigma}^{n+1}_{i,j,k-1/2}D^{n+1}_{i,j}C^{n+1}_{i,j,k-1/2}\right) - \frac{\lambda_\sigma}{2\Delta\sigma}\left(-\left|\dot{\sigma}^{n+1}_{i,j,k-1/2}\right|D^{n+1}_{i,j}(C^{n+1}_{i,j,k} - C^{n+1}_{i,j,k-1})\right) \quad 4.52$$

$$\begin{aligned}\frac{\partial(\dot{\sigma}DC_{i,\mathrm{j},k})}{\partial\sigma} &= -\left(\frac{\dot{\sigma}^{n+1}_{i,j,k-1/2}D^{n+1}_{i,j}}{2\Delta\sigma}\right)C^{n+1}_{i,j,k} - \left(\frac{\dot{\sigma}^{n+1}_{i,j,k-1/2}D^{n+1}_{i,j}}{2\Delta\sigma}\right)C^{n+1}_{i,j,k-1} \\ &+ \left(\frac{\lambda_\sigma D^{n+1}_{i,j}\left|\dot{\sigma}^{n+1}_{i,j,k-1/2}\right|}{2\Delta\sigma}\right)C^{n+1}_{i,j,k} - \left(\frac{\lambda_\sigma D^{n+1}_{i,j}\left|\dot{\sigma}^{n+1}_{i,j,k-1/2}\right|}{2\Delta\sigma}\right)C^{n+1}_{i,j,k-1}\end{aligned} \quad 4.53$$

defining,

$$amds_{i,j,k} = \lambda_\sigma = \frac{\left|\dot{\sigma}_{i,j,k}\right|\Delta t}{\Delta\sigma} \quad 4.54$$

Then;

$$\begin{aligned}\frac{\partial(\dot{\sigma}DC_{i,\mathrm{j},k})}{\partial\sigma} &= -\left(\frac{\dot{\sigma}^{n+1}_{i,j,k-1/2}D^{n+1}_{i,j}}{2\Delta\sigma}\right)C^{n+1}_{i,j,k} - \left(\frac{\dot{\sigma}^{n+1}_{i,j,k-1/2}D^{n+1}_{i,j}}{2\Delta\sigma}\right)C^{n+1}_{i,j,k-1} \\ &+ \left(\frac{amdas_{i,j,k-1/2}D^{n+1}_{i,j}\left|\dot{\sigma}^{n+1}_{i,j,k-1/2}\right|}{2\Delta\sigma}\right)C^{n+1}_{i,j,k} - \left(\frac{amdas_{i,j,k-1/2}D^{n+1}_{i,j}\left|\dot{\sigma}^{n+1}_{i,j,k-1/2}\right|}{2\Delta\sigma}\right)C^{n+1}_{i,j,k-1}\end{aligned} \quad 4.55$$

6a. Vertical diffusion term

$$\frac{1}{D}\frac{\partial}{\partial\sigma}\left(K_v\frac{\partial C_{i,\mathrm{j},k}}{\partial\sigma}\right)=\frac{1}{D_{i,j}^{n+1}}\cdot\frac{1}{\Delta\sigma}\left(-K_{v_{i,j,k-1/2}}\frac{C_{i,j,k}^{n+1}-C_{i,j,k-1}^{n+1}}{\Delta\sigma}\right) \tag{4.56}$$

$$\frac{1}{D}\frac{\partial}{\partial\sigma}\left(K_v\frac{\partial C_{i,\mathrm{j},k}}{\partial\sigma}\right)=-\left(\frac{K_{v_{i,j,k-1/2}}}{D_{i,j}^{n+1}(\Delta\sigma)^2}\right)C_{i,j,k}^{n+1}+\left(\frac{K_{v_{i,j,k-1/2}}}{D_{i,j}^{n+1}(\Delta\sigma)^2}\right)C_{i,j,k-1}^{n+1} \tag{4.57}$$

Substituting equations **4.17**, **4.22**, **4.27**, **4.31**, **4.35** and **4.37** in equation **4.14**;

$$\begin{aligned}
&\frac{D_{i,j}^{n+1}}{\Delta t}C_{i,j,k}^{n+1}-\frac{D_{i,j}^{n}}{\Delta t}C_{i,j,k}^{n}\\
&+\left(\frac{u_{i+1/2,j,k}^{n+1}D_{i+1/2,j}^{n+1}}{2\Delta x}\right)C_{i+1,j,k}^{n}+\left(\frac{u_{i+1/2,j,k}^{n+1}D_{i+1/2,j}^{n+1}}{2\Delta x}-\frac{u_{i-1/2,j,k}^{n+1}D_{i-1/2,j}^{n+1}}{2\Delta x}\right)C_{i,j,k}^{n}-\left(\frac{u_{i-1/2,j,k}^{n+1}D_{i-1/2,j}^{n+1}}{2\Delta x}\right)C_{i-1,j,k}^{n}\\
&-\left(\frac{amdx_{i+1/2,j,k}}{2\Delta x}\left|u_{i+1/2,j,k}^{n+1}\right|D_{i+1/2,j}^{n+1}\right)C_{i+1,j,k}^{n}+\left(\frac{amdx_{i+1/2,j,k}}{2\Delta x}\left|u_{i+1/2,j,k}^{n+1}\right|D_{i+1/2,j}^{n+1}\right)C_{i,j,k}^{n}\\
&+\left(\frac{amdx_{i-1/2,j,k}}{2\Delta x}\left|u_{i-1/2,j,k}^{n+1}\right|D_{i-1/2,j}^{n+1}\right)C_{i,j,k}^{n}-\left(\frac{amdx_{i-1/2,j,k}}{2\Delta x}\left|u_{i-1/2,j,k}^{n+1}\right|D_{i-1/2,j}^{n+1}\right)C_{i-1,j,k}^{n}\\
&+\left(\frac{v_{i,j+1/2,k}^{n+1}D_{i,j+1/2}^{n+1}}{2\Delta y}\right)C_{i,j+1,k}^{n}+\left(\frac{v_{i,j+1/2,k}^{n+1}D_{i,j+1/2}^{n+1}}{2\Delta y}-\frac{v_{i,j-1/2,k}^{n+1}D_{i,j-1/2}^{n+1}}{2\Delta y}\right)C_{i,j,k}^{n}-\left(\frac{v_{i,j-1/2,k}^{n+1}D_{i,j-1/2}^{n+1}}{2\Delta y}\right)C_{i,j-1,k}^{n}\\
&-\left(\frac{amdy_{i,j+1/2,k}}{2\Delta y}\left|v_{i,j+1/2,k}^{n+1}\right|D_{i,j+1/2}^{n+1}\right)C_{i,j+1,k}^{n}+\left(\frac{amdy_{i,j+1/2,k}}{2\Delta y}\left|v_{i,j+1/2,k}^{n+1}\right|D_{i,j+1/2}^{n+1}\right)C_{i,j,k}^{n}\\
&+\left(\frac{amdy_{i,j-1/2,k}}{2\Delta y}\left|v_{i,j-1/2,k}^{n+1}\right|D_{i,j-1/2}^{n+1}\right)C_{i,j,k}^{n}-\left(\frac{amdy_{i,j-1/2,k}}{2\Delta y}\left|v_{i,j-1/2,k}^{n+1}\right|D_{i,j-1/2}^{n+1}\right)C_{i,j-1,k}^{n}\\
&-\left(\frac{\dot\sigma_{i,j,k-1/2}^{n+1}D_{i,j}^{n+1}}{2\Delta\sigma}\right)C_{i,j,k}^{n+1}-\left(\frac{\dot\sigma_{i,j,k-1/2}^{n+1}D_{i,j}^{n+1}}{2\Delta\sigma}\right)C_{i,j,k-1}^{n+1}\\
&+\left(\frac{amdas_{i,j,k-1/2}D_{i,j}^{n+1}\left|\dot\sigma_{i,j,k-1/2}^{n+1}\right|}{2\Delta\sigma}\right)C_{i,j,k}^{n+1}-\left(\frac{amdas_{i,j,k-1/2}D_{i,j}^{n+1}\left|\dot\sigma_{i,j,k-1/2}^{n+1}\right|}{2\Delta\sigma}\right)C_{i,j,k-1}^{n+1}\\
&=\left(\frac{D_{i,j}^{n+1}K_{hx_i+1/2,j,k}}{(\Delta x)^2}\right)C_{i+1,j,k}^{n}-\left(\frac{D_{i,j}^{n+1}K_{hx_i+1/2,j,k}}{(\Delta x)^2}\right)C_{i,j,k}^{n}-\left(\frac{D_{i,j}^{n+1}K_{hx_i-1/2,j,k}}{(\Delta x)^2}\right)C_{i,j,k}^{n}\\
&+\left(\frac{D_{i,j}^{n+1}K_{hx_i-1/2,j,k}}{(\Delta x)^2}\right)C_{i-1,j,k}^{n}+\left(\frac{D_{i,j}^{n+1}K_{hy_i,j+1/2,k}}{(\Delta y)^2}\right)C_{i,j+1,k}^{n}-\left(\frac{D_{i,j}^{n+1}K_{hy_i,j+1/2,k}}{(\Delta y)^2}\right)C_{i,j,k}^{n}\\
&-\left(\frac{D_{i,j}^{n+1}K_{hy_i,j-1/2,k}}{(\Delta y)^2}\right)C_{i,j,k}^{n}+\left(\frac{D_{i,j}^{n+1}K_{hy_i,j-1/2,k}}{(\Delta y)^2}\right)C_{i,j-1,k}^{n}\\
&-\left(\frac{K_{v_{i,j,k-1/2}}}{D_{i,j}^{n+1}(\Delta\sigma)^2}\right)C_{i,j,k}^{n+1}+\left(\frac{K_{v_{i,j,k-1/2}}}{D_{i,j}^{n+1}(\Delta\sigma)^2}\right)C_{i,j,k-1}^{n+1}
\end{aligned} \tag{4.58}$$

$$
\begin{aligned}
&\left\{-\frac{K_{v_{i,j,k-1/2}}}{D_{i,j}^{n+1}(\Delta\sigma)^2}-\frac{D_{i,j}^{n+1}}{2\Delta\sigma}\left[\dot{\sigma}_{i,j,k-1/2}^{n+1}+amdas_{i,j,k-1/2}\left|\dot{\sigma}_{i,j,k-1/2}^{n+1}\right|\right]\right\}C_{i,j,k-1}^{n+1}\\
&+\left\{\left(\frac{D_{i,j}^{n+1}}{\Delta t}\right)-\left(-\frac{K_{v_{i,j,k-1/2}}}{D_{i,j}^{n+1}(\Delta\sigma)^2}-\frac{D_{i,j}^{n+1}}{2\Delta\sigma}\left[\dot{\sigma}_{i,j,k-1/2}^{n+1}+amdas_{i,j,k-1/2}\left|\dot{\sigma}_{i,j,k-1/2}^{n+1}\right|\right]\right)\right.\\
&\left.-\left(\frac{D_{i,j}^{n+1}}{\Delta\sigma}\left\lfloor\dot{\sigma}_{i,j,k-1/2}^{n+1}\right\rfloor\right)\right\}C_{i,j,k}^{n+1}\\
&+\{0\}C_{i,j,k+1}^{n+1}\\
&=\left\{\frac{D_{i,j}^{n+1}K_{hx\_i-1/2,j,k}}{(\Delta x)^2}+\frac{1}{2\Delta x}\left(amdx_{i-1/2,j,k}\left|u_{i-1/2,j,k}^{n+1}\right|D_{i+1/2,j}^{n+1}+u_{i-1/2,j,k}^{n+1}D_{i-1/2,j}^{n+1}\right)\right\}C_{i-1,j,k}^{n}\\
&+\left\{-D_{i,j}^{n+1}\left(\frac{K_{hx\_i-1/2,j,k}}{(\Delta x)^2}+\frac{K_{hx\_i+1/2,j,k}}{(\Delta x)^2}+\frac{K_{hy\_i,j-1/2,k}}{(\Delta y)^2}+\frac{K_{hy\_i,j+1/2,k}}{(\Delta y)^2}\right)\right.\\
&+\frac{1}{2\Delta x}\left(\begin{array}{l}-amdx_{i-1/2,j,k}\left|u_{i-1/2,j,k}^{n+1}\right|D_{i-1/2,j}^{n+1}-amdx_{i+1/2,j,k}\left|u_{i+1/2,j,k}^{n+1}\right|D_{i+1/2,j}^{n+1}\\+u_{i-1/2,j,k}^{n+1}D_{i-1/2,j}^{n+1}-u_{i+1/2,j,k}^{n+1}D_{i+1/2,j}^{n+1}\end{array}\right)\\
&\left.+\frac{1}{2\Delta y}\left(\begin{array}{l}-amdy_{i,j-1/2,k}\left|v_{i,j-1/2,k}^{n+1}\right|D_{i,j-1/2}^{n+1}-amdy_{i,j+1/2,k}\left|v_{i,j+1/2,k}^{n+1}\right|D_{i,j+1/2}^{n+1}\\+v_{i,j-1/2,k}^{n+1}D_{i,j-1/2}^{n+1}-v_{i,j+1/2,k}^{n+1}D_{i,j+1/2}^{n+1}\end{array}\right)+\frac{D_{i,j}^{n}}{\Delta t}\right\}C_{i,j,k}^{n}\\
&+\left\{\frac{D_{i,j}^{n+1}K_{hx\_i+1/2,j,k}}{(\Delta x)^2}+\frac{1}{2\Delta x}\left(amdx_{i+1/2,j,k}\left|u_{i+1/2,j,k}^{n+1}\right|D_{i+1/2,j}^{n+1}-u_{i+1/2,j,k}^{n+1}D_{i+1/2,j}^{n+1}\right)\right\}C_{i+1,j,k}^{n}\\
&+\left\{\frac{D_{i,j}^{n+1}K_{hy\_i,j-1/2,k}}{(\Delta y)^2}+\frac{1}{2\Delta y}\left(amdy_{i,j-1/2,k}\left|v_{i,j-1/2,k}^{n+1}\right|D_{i,j+1/2}^{n+1}+v_{i,j-1/2,k}^{n+1}D_{i,j-1/2}^{n+1}\right)\right\}C_{i,j-1,k}^{n}\\
&+\left\{\frac{D_{i,j}^{n+1}K_{hy\_i,j+1/2,k}}{(\Delta y)^2}+\frac{1}{2\Delta y}\left(amdy_{i,j+1/2,k}\left|v_{i,j+1/2,k}^{n+1}\right|D_{i,j+1/2}^{n+1}-v_{i,j+1/2,k}^{n+1}D_{i,j+1/2}^{n+1}\right)\right\}C_{i,j+1,k}^{n}
\end{aligned}
\tag{4.59}
$$

This can be written in the form of;

$$
apkc_{i,j,k}C_{i,j,k-1}^{n+1}+bpkc_{i,j,k}C_{i,j,k}^{n+1}+cpkc_{i,j,k}C_{i,j,k+1}^{n+1}=dpkc_{i,j,k} \tag{4.60}
$$

where,

$$
apkc_{i,j,k}=\left\{-\frac{K_{v_{i,j,k-1/2}}}{D_{i,j}^{n+1}(\Delta\sigma)^2}-\frac{D_{i,j}^{n+1}}{2\Delta\sigma}\left[\dot{\sigma}_{i,j,k-1/2}^{n+1}+amdas_{i,j,k-1/2}\left|\dot{\sigma}_{i,j,k-1/2}^{n+1}\right|\right]\right\} \tag{4.61}
$$

$$
cpkc_{i,j,k}=\{0\} \tag{4.62}
$$

$$bpkc_{i,j,k} = \left(\frac{D_{i,j}^{n+1}}{\Delta t}\right) - apkc_{i,j,k} - cpkc_{i,j,k} - \left(\frac{D_{i,j}^{n+1}}{2\Delta\sigma}\left[\dot{\sigma}_{i,j,k-1/2}^{n+1} - \dot{\sigma}_{i,j,k+1/2}^{n+1}\right]\right) \quad 4.63$$

$$dpkc_{i,j,k} = auk_{i,j,k}C_{i-1,j,k}^{n} + buk_{i,j,k}C_{i,j,k}^{n} + cuk_{i,j,k}C_{i+1,j,k}^{n} + duk_{i,j,k}C_{i,j-1,k}^{n} + euk_{i,j,k}C_{i,j+1,k}^{n} \quad 4.64$$

4.1.2.2 Bottom boundary conditions

Define a dummy grid $C_{i,\mathrm{j},\mathrm{k}-1}$ below the bottom of the water column where $C_{i,\mathrm{j},\mathrm{k}-1} = C_{i,\mathrm{j},\mathrm{k}}$ and $\dot{\sigma}_{i,j,k-1/2}^{n+1} = 0$ at the bottom of the water column. Advection and diffusion at the bottom water boundary has been considered as zero here since the boundary conditions are considered separately. Hence vertical advection and diffusion equations at the bottom have been reconsidered as follows.

4b. Advection term in sigma-direction

$$\frac{\partial(\dot{\sigma}DC_{i,\mathrm{j},k})}{\partial\sigma} = \frac{1}{\Delta\sigma}\left(\dot{\sigma}_{i,j,k+1/2}^{n+1}D_{i,j}^{n+1}C_{i,j,k+1/2}^{n+1}\right) - \frac{\lambda_\sigma}{2\Delta\sigma}\left(\left|\dot{\sigma}_{i,j,k+1/2}^{n+1}\right|D_{i,j}^{n+1}(C_{i,j,k+1}^{n+1} - C_{i,j,k}^{n+1})\right) \quad 4.65$$

$$\begin{aligned}\frac{\partial(\dot{\sigma}DC_{i,\mathrm{j},k})}{\partial\sigma} &= \left(\frac{\dot{\sigma}_{i,j,k+1/2}^{n+1}D_{i,j}^{n+1}}{2\Delta\sigma}\right)C_{i,j,k+1}^{n+1} + \left(\frac{\dot{\sigma}_{i,j,k+1/2}^{n+1}D_{i,j}^{n+1}}{2\Delta\sigma}\right)C_{i,j,k}^{n+1} \\ &- \left(\frac{\lambda_\sigma D_{i,j}^{n+1}\left|\dot{\sigma}_{i,j,k+1/2}^{n+1}\right|}{2\Delta\sigma}\right)C_{i,j,k+1}^{n+1} + \left(\frac{\lambda_\sigma D_{i,j}^{n+1}\left|\dot{\sigma}_{i,j,k+1/2}^{n+1}\right|}{2\Delta\sigma}\right)C_{i,j,k}^{n+1}\end{aligned} \quad 4.66$$

defining,

$$amds_{i,j,k} = \lambda_\sigma = \frac{\left|\dot{\sigma}_{i,j,k}\right|\Delta t}{\Delta\sigma} \quad 4.67$$

Then;

$$\begin{aligned}\frac{\partial(\dot{\sigma}DC_{i,\mathrm{j},k})}{\partial\sigma} &= \left(\frac{\dot{\sigma}_{i,j,k+1/2}^{n+1}D_{i,j}^{n+1}}{2\Delta\sigma}\right)C_{i,j,k+1}^{n+1} + \left(\frac{\dot{\sigma}_{i,j,k+1/2}^{n+1}D_{i,j}^{n+1}}{2\Delta\sigma}\right)C_{i,j,k}^{n+1} \\ &- \left(\frac{amdas_{i,j,k+1/2}D_{i,j}^{n+1}\left|\dot{\sigma}_{i,j,k+1/2}^{n+1}\right|}{2\Delta\sigma}\right)C_{i,j,k+1}^{n+1} + \left(\frac{amdas_{i,j,k+1/2}D_{i,j}^{n+1}\left|\dot{\sigma}_{i,j,k+1/2}^{n+1}\right|}{2\Delta\sigma}\right)C_{i,j,k}^{n+1}\end{aligned} \quad 4.68$$

6b.Vertical diffusion term

$$\frac{1}{D}\frac{\partial}{\partial\sigma}\left(K_v\frac{\partial C_{i,\mathrm{j},k}}{\partial\sigma}\right)=\frac{1}{D_{i,j}^{n+1}}\cdot\frac{1}{\Delta\sigma}\left(K_{v_{i,j,k+1/2}}\frac{C_{i,j,k+1}^{n+1}-C_{i,j,k}^{n+1}}{\Delta\sigma}\right) \tag{4.69}$$

$$\frac{1}{D}\frac{\partial}{\partial\sigma}\left(K_v\frac{\partial C_{i,\mathrm{j},k}}{\partial\sigma}\right)=\left(\frac{K_{v_{i,j,k+1/2}}}{D_{i,j}^{n+1}(\Delta\sigma)^2}\right)C_{i,j,k+1}^{n+1}-\left(\frac{K_{v_{i,j,k+1/2}}}{D_{i,j}^{n+1}(\Delta\sigma)^2}\right)C_{i,j,k}^{n+1} \tag{4.70}$$

Substituting equations **4.17**, **4.22**, **4.27**, **4.31**, **4.35** and **4.37** in equation **4.14**

$$\begin{aligned}
&\frac{D_{i,j}^{n+1}}{\Delta t}C_{i,j,k}^{n+1}-\frac{D_{i,j}^{n}}{\Delta t}C_{i,j,k}^{n}\\
&+\left(\frac{u_{i+1/2,j,k}^{n+1}D_{i+1/2,j}^{n+1}}{2\Delta x}\right)C_{i+1,j,k}^{n}+\left(\frac{u_{i+1/2,j,k}^{n+1}D_{i+1/2,j}^{n+1}}{2\Delta x}-\frac{u_{i-1/2,j,k}^{n+1}D_{i-1/2,j}^{n+1}}{2\Delta x}\right)C_{i,j,k}^{n}-\left(\frac{u_{i-1/2,j,k}^{n+1}D_{i-1/2,j}^{n+1}}{2\Delta x}\right)C_{i-1,j,k}^{n}\\
&-\left(\frac{amdx_{i+1/2,j,k}}{2\Delta x}\left|u_{i+1/2,j,k}^{n+1}\right|D_{i+1/2,j}^{n+1}\right)C_{i+1,j,k}^{n}+\left(\frac{amdx_{i+1/2,j,k}}{2\Delta x}\left|u_{i+1/2,j,k}^{n+1}\right|D_{i+1/2,j}^{n+1}\right)C_{i,j,k}^{n}\\
&+\left(\frac{amdx_{i-1/2,j,k}}{2\Delta x}\left|u_{i-1/2,j,k}^{n+1}\right|D_{i-1/2,j}^{n+1}\right)C_{i,j,k}^{n}-\left(\frac{amdx_{i-1/2,j,k}}{2\Delta x}\left|u_{i-1/2,j,k}^{n+1}\right|D_{i-1/2,j}^{n+1}\right)C_{i-1,j,k}^{n}\\
&+\left(\frac{v_{i,j+1/2,k}^{n+1}D_{i,j+1/2}^{n+1}}{2\Delta y}\right)C_{i,j+1,k}^{n}+\left(\frac{v_{i,j+1/2,k}^{n+1}D_{i,j+1/2}^{n+1}}{2\Delta y}-\frac{v_{i,j-1/2,k}^{n+1}D_{i,j-1/2}^{n+1}}{2\Delta y}\right)C_{i,j,k}^{n}-\left(\frac{v_{i,j-1/2,k}^{n+1}D_{i,j-1/2}^{n+1}}{2\Delta y}\right)C_{i,j-1,k}^{n}\\
&-\left(\frac{amdy_{i,j+1/2,k}}{2\Delta y}\left|v_{i,j+1/2,k}^{n+1}\right|D_{i,j+1/2}^{n+1}\right)C_{i,j+1,k}^{n}+\left(\frac{amdy_{i,j+1/2,k}}{2\Delta y}\left|v_{i,j+1/2,k}^{n+1}\right|D_{i,j+1/2}^{n+1}\right)C_{i,j,k}^{n}\\
&+\left(\frac{amdy_{i,j-1/2,k}}{2\Delta y}\left|v_{i,j-1/2,k}^{n+1}\right|D_{i,j-1/2}^{n+1}\right)C_{i,j,k}^{n}-\left(\frac{amdy_{i,j-1/2,k}}{2\Delta y}\left|v_{i,j-1/2,k}^{n+1}\right|D_{i,j-1/2}^{n+1}\right)C_{i,j-1,k}^{n}\\
&+\left(\frac{\dot\sigma_{i,j,k+1/2}^{n+1}D_{i,j}^{n+1}}{2\Delta\sigma}\right)C_{i,j,k+1}^{n+1}+\left(\frac{\dot\sigma_{i,j,k+1/2}^{n+1}D_{i,j}^{n+1}}{2\Delta\sigma}\right)C_{i,j,k}^{n+1}\\
&-\left(\frac{amdas_{i,j,k+1/2}D_{i,j}^{n+1}\left|\dot\sigma_{i,j,k+1/2}^{n+1}\right|}{2\Delta\sigma}\right)C_{i,j,k+1}^{n+1}+\left(\frac{amdas_{i,j,k+1/2}D_{i,j}^{n+1}\left|\dot\sigma_{i,j,k+1/2}^{n+1}\right|}{2\Delta\sigma}\right)C_{i,j,k}^{n+1}\\
&=\left(\frac{D_{i,j}^{n+1}K_{hx_i+1/2,j,k}}{(\Delta x)^2}\right)C_{i+1,j,k}^{n}-\left(\frac{D_{i,j}^{n+1}K_{hx_i+1/2,j,k}}{(\Delta x)^2}\right)C_{i,j,k}^{n}-\left(\frac{D_{i,j}^{n+1}K_{hx_i-1/2,j,k}}{(\Delta x)^2}\right)C_{i,j,k}^{n}\\
&+\left(\frac{D_{i,j}^{n+1}K_{hx_i-1/2,j,k}}{(\Delta x)^2}\right)C_{i-1,j,k}^{n}+\left(\frac{D_{i,j}^{n+1}K_{hy_i,j+1/2,k}}{(\Delta y)^2}\right)C_{i,j+1,k}^{n}-\left(\frac{D_{i,j}^{n+1}K_{hy_i,j+1/2,k}}{(\Delta y)^2}\right)C_{i,j,k}^{n}\\
&-\left(\frac{D_{i,j}^{n+1}K_{hy_i,j-1/2,k}}{(\Delta y)^2}\right)C_{i,j,k}^{n}+\left(\frac{D_{i,j}^{n+1}K_{hy_i,j-1/2,k}}{(\Delta y)^2}\right)C_{i,j-1,k}^{n}\\
&+\left(\frac{K_{v_{i,j,k+1/2}}}{D_{i,j}^{n+1}(\Delta\sigma)^2}\right)C_{i,j,k+1}^{n+1}-\left(\frac{K_{v_{i,j,k+1/2}}}{D_{i,j}^{n+1}(\Delta\sigma)^2}\right)C_{i,j,k}^{n+1}-\left(\frac{K_{v_{i,j,k-1/2}}}{D_{i,j}^{n+1}(\Delta\sigma)^2}\right)C_{i,j,k}^{n+1}+\left(\frac{K_{v_{i,j,k-1/2}}}{D_{i,j}^{n+1}(\Delta\sigma)^2}\right)C_{i,j,k-1}^{n+1}
\end{aligned} \tag{4.71}$$

$$
\begin{aligned}
&\{0\} C_{i,j,k-1}^{n+1} \\
&+\left\{\left(\frac{D_{i,j}^{n+1}}{\Delta t}\right)-\left(-\frac{K_{v_{i,j,k+1/2}}}{D_{i,j}^{n+1}(\Delta\sigma)^2}+\frac{D_{i,j}^{n+1}}{2\Delta\sigma}\left[\dot{\sigma}_{i,j,k+1/2}^{n+1}-amdas_{i,j,k+1/2}\left|\dot{\sigma}_{i,j,k+1/2}^{n+1}\right|\right]\right)\right. \\
&\left.-\left(\frac{D_{i,j}^{n+1}}{\Delta\sigma}\left[-\dot{\sigma}_{i,j,k+1/2}^{n+1}\right]\right)\right\} C_{i,j,k}^{n+1} \\
&\left\{-\frac{K_{v_{i,j,k+1/2}}}{D_{i,j}^{n+1}(\Delta\sigma)^2}+\frac{D_{i,j}^{n+1}}{2\Delta\sigma}\left[\dot{\sigma}_{i,j,k+1/2}^{n+1}-amdas_{i,j,k+1/2}\left|\dot{\sigma}_{i,j,k+1/2}^{n+1}\right|\right]\right\} C_{i,j,k+1}^{n+1} \\
&=\left\{\frac{D_{i,j}^{n+1}K_{hx\_i-1/2,j,k}}{(\Delta x)^2}+\frac{1}{2\Delta x}\left(amdx_{i-1/2,j,k}\left|u_{i-1/2,j,k}^{n+1}\right|D_{i+1/2,j}^{n+1}+u_{i-1/2,j,k}^{n+1}D_{i-1/2,j}^{n+1}\right)\right\} C_{i-1,j,k}^{n} \\
&+\left\{-D_{i,j}^{n+1}\left(\frac{K_{hx\_i-1/2,j,k}}{(\Delta x)^2}+\frac{K_{hx\_i+1/2,j,k}}{(\Delta x)^2}+\frac{K_{hy\_i,j-1/2,k}}{(\Delta y)^2}+\frac{K_{hy\_i,j+1/2,k}}{(\Delta y)^2}\right)\right. \\
&+\frac{1}{2\Delta x}\left(\begin{array}{l}-amdx_{i-1/2,j,k}\left|u_{i-1/2,j,k}^{n+1}\right|D_{i-1/2,j}^{n+1}-amdx_{i+1/2,j,k}\left|u_{i+1/2,j,k}^{n+1}\right|D_{i+1/2,j}^{n+1} \\ +u_{i-1/2,j,k}^{n+1}D_{i-1/2,j}^{n+1}-u_{i+1/2,j,k}^{n+1}D_{i+1/2,j}^{n+1}\end{array}\right) \\
&\left.+\frac{1}{2\Delta y}\left(\begin{array}{l}-amdy_{i,j-1/2,k}\left|v_{i,j-1/2,k}^{n+1}\right|D_{i,j-1/2}^{n+1}-amdy_{i,j+1/2,k}\left|v_{i,j+1/2,k}^{n+1}\right|D_{i,j+1/2}^{n+1} \\ +v_{i,j-1/2,k}^{n+1}D_{i,j-1/2}^{n+1}-v_{i,j+1/2,k}^{n+1}D_{i,j+1/2}^{n+1}\end{array}\right)+\frac{D_{i,j}^{n}}{\Delta t}\right\} C_{i,j,k}^{n} \\
&+\left\{\frac{D_{i,j}^{n+1}K_{hx\_i+1/2,j,k}}{(\Delta x)^2}+\frac{1}{2\Delta x}\left(amdx_{i+1/2,j,k}\left|u_{i+1/2,j,k}^{n+1}\right|D_{i+1/2,j}^{n+1}-u_{i+1/2,j,k}^{n+1}D_{i+1/2,j}^{n+1}\right)\right\} C_{i+1,j,k}^{n} \\
&+\left\{\frac{D_{i,j}^{n+1}K_{hy\_i,j-1/2,k}}{(\Delta y)^2}+\frac{1}{2\Delta y}\left(amdy_{i,j-1/2,k}\left|v_{i,j-1/2,k}^{n+1}\right|D_{i,j+1/2}^{n+1}+v_{i,j-1/2,k}^{n+1}D_{i,j-1/2}^{n+1}\right)\right\} C_{i,j-1,k}^{n} \\
&+\left\{\frac{D_{i,j}^{n+1}K_{hy\_i,j+1/2,k}}{(\Delta y)^2}+\frac{1}{2\Delta y}\left(amdy_{i,j+1/2,k}\left|v_{i,j+1/2,k}^{n+1}\right|D_{i,j+1/2}^{n+1}-v_{i,j+1/2,k}^{n+1}D_{i,j+1/2}^{n+1}\right)\right\} C_{i,j+1,k}^{n}
\end{aligned}
\tag{4.72}
$$

This can be written in the form of;

$$
apkc_{i,j,k}C_{i,j,k-1}^{n+1}+bpkc_{i,j,k}C_{i,j,k}^{n+1}+cpkc_{i,j,k}C_{i,j,k+1}^{n+1}=dpkc_{i,j,k} \tag{4.73}
$$

where,

$$
apkc_{i,j,k}=\{0\} \tag{4.74}
$$

$$
cpkc_{i,j,k}=\left\{-\frac{K_{v_{i,j,k+1/2}}}{D_{i,j}^{n+1}(\Delta\sigma)^2}+\frac{D_{i,j}^{n+1}}{2\Delta\sigma}\left[\dot{\sigma}_{i,j,k+1/2}^{n+1}-amdas_{i,j,k+1/2}\left|\dot{\sigma}_{i,j,k+1/2}^{n+1}\right|\right]\right\} \tag{4.75}
$$

$$
bpkc_{i,j,k}=\left(\frac{D_{i,j}^{n+1}}{\Delta t}\right)-apkc_{i,j,k}-cpkc_{i,j,k}-\left(\frac{D_{i,j}^{n+1}}{2\Delta\sigma}\left[\dot{\sigma}_{i,j,k-1/2}^{n+1}-\dot{\sigma}_{i,j,k+1/2}^{n+1}\right]\right) \tag{4.76}
$$

$$dpkc_{i,j,k} = auk_{i,j,k} C^{n}_{i-1,j,k} + buk_{i,j,k} C^{n}_{i,j,k} + cuk_{i,j,k} C^{n}_{i+1,j,k} + duk_{i,j,k} C^{n}_{i,j-1,k} + euk_{i,j,k} C^{n}_{i,j+1,k} \qquad 4.77$$

These simultaneous equations are solved using a Tri Diagonal Matrix Algorithm described in the sub-section **5.4.4**.

4.1.3 Particulate matter settling

Particulate organic matter settles down in the water column and accumulates on the surface of the sediment bed. Settled particulate organic carbon undergoes diagenesis through oxic decomposition ensuing hypoxic or anoxic conditions in water column. Moreover, aerobic or anaerobic decomposition of those accumulated particulate organic carbon has resulted in building up of high concentrations of phosphate and ammonia in sediment, and under anoxic conditions those nutrients are released to overlying water.. These released nutrients from the sediment bed under hypoxic and anoxic conditions have resulted in eutrophication in water column considerably. Hence, modeling of particulate matter settling in the water column is an important component in both water quality and sediment quality analysis.

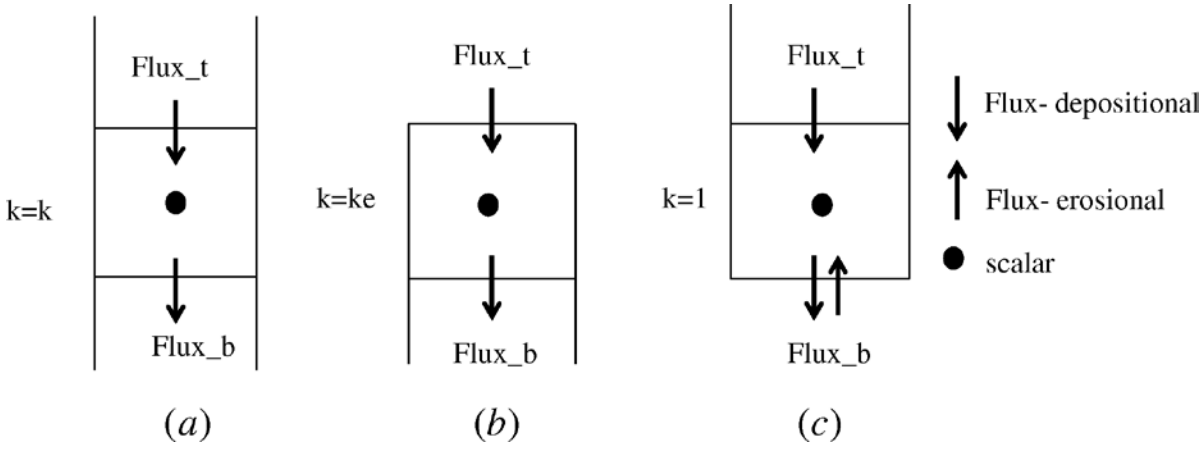

Fig 4.3 Settling of particles in water column at (a) any grid point, (b) at surface grid point and (c) at the bottom grid point

The discretization of governing equation for settling (4.15) is considered analyzing the flux at three different vertical grid points in the water column particularly, at any grid point,

at the surface grid point and at the bottom grid point. According to the governing equation of settling term (**4.15)** in sigma coordinates;

$$\frac{\partial(DC)}{\partial t}+\frac{\partial(D\dot{\sigma}_s C)}{\partial \sigma}=0 \tag{4.78}$$

$$\frac{\partial(DC)}{\partial t}+\frac{(Flux\_t-Flux\_b)}{\partial \sigma}=0 \tag{4.79}$$

Implicit upwind scheme is used for the discretization. According to the split operator, D always takes D_{ij}^{n+1}. From k=ke-1, to k=2 settling term is discretized as;

$$Flux\_t=D_{ij}^{n+1}\dot{\sigma}_{sij\left(k+\frac{1}{2}\right)}C_{ij\left(k+\frac{1}{2}\right)}^{n+1} \tag{4.80}$$

$$Flux\_b=D_{ij}^{n+1}\dot{\sigma}_{sij\left(k-\frac{1}{2}\right)}C_{ij\left(k-\frac{1}{2}\right)}^{n+1} \tag{4.81}$$

$$\frac{D_{ij}^{n+1}C_{ijk}^{n+1}-D_{ij}^{n+1}C_{ijk}^{n}}{\Delta t}+\frac{D_{ij}^{n+1}\dot{\sigma}_{sij\left(k+\frac{1}{2}\right)}C_{ij\left(k+\frac{1}{2}\right)}^{n+1}-D_{ij}^{n+1}\dot{\sigma}_{sij\left(k-\frac{1}{2}\right)}C_{ij\left(k-\frac{1}{2}\right)}^{n+1}}{\Delta \sigma}=0 \tag{4.82}$$

Adopting the upwind scheme, $C_{ij\left(k+\frac{1}{2}\right)}^{n+1}=C_{ij(k+1)}^{n+1}$ and $C_{ij\left(k-\frac{1}{2}\right)}^{n+1}=C_{ijk}^{n+1}$ 4.83

$$\frac{D_{ij}^{n+1}C_{ijk}^{n+1}-D_{ij}^{n+1}C_{ijk}^{n}}{\Delta t}+\frac{D_{ij}^{n+1}\dot{\sigma}_{sij\left(k+\frac{1}{2}\right)}C_{ij(k+1)}^{n+1}-D_{ij}^{n+1}\dot{\sigma}_{sij\left(k-\frac{1}{2}\right)}C_{ijk}^{n+1}}{\Delta \sigma}=0 \tag{4.84}$$

$$\left[\frac{D_{ij}^{n+1}}{\Delta t}-\frac{D_{ij}^{n+1}\dot{\sigma}_{sij\left(k-\frac{1}{2}\right)}}{\Delta \sigma}\right]C_{ijk}^{n+1}=\left[\frac{D_{ij}^{n+1}C_{ijk}^{n}}{\Delta t}-\frac{D_{ij}^{n+1}\dot{\sigma}_{sij\left(k+\frac{1}{2}\right)}C_{ij(k+1)}^{n+1}}{\Delta \sigma}\right] \tag{4.85}$$

$$C_{ijk}^{n+1}=\frac{\left[\frac{D_{ij}^{n+1}C_{ijk}^{n}}{\Delta t}-\frac{D_{ij}^{n+1}\dot{\sigma}_{sij\left(k+\frac{1}{2}\right)}C_{ij(k+1)}^{n+1}}{\Delta \sigma}\right]}{\left[\frac{D_{ij}^{n+1}}{\Delta t}-\frac{D_{ij}^{n+1}\dot{\sigma}_{sij\left(k-\frac{1}{2}\right)}}{\Delta \sigma}\right]} \tag{4.86}$$

$$C_{ijk}^{n+1}=\frac{\left[\frac{C_{ijk}^{n}}{\Delta t}-\frac{\dot{\sigma}_{sij\left(k+\frac{1}{2}\right)}C_{ij(k+1)}^{n+1}}{\Delta \sigma}\right]}{\left[\frac{1}{\Delta t}-\frac{\dot{\sigma}_{sij\left(k-\frac{1}{2}\right)}}{\Delta \sigma}\right]} \tag{4.87}$$

At the surface boundary assuming no flux at across the surface boundary, settling term is discretized as;

$$Flux\_t = 0 \tag{4.88}$$

$$Flux\_b = D_{ij}^{n+1}\dot{\sigma}_{sij\left(ke-\frac{1}{2}\right)}C_{ij\left(ke-\frac{1}{2}\right)}^{n+1} \tag{4.89}$$

$$\frac{D_{ij}^{n+1}C_{ijke}^{n+1} - D_{ij}^{n+1}C_{ijke}^{n}}{\Delta t} - \frac{D_{ij}^{n+1}\dot{\sigma}_{sij\left(ke-\frac{1}{2}\right)}C_{ij\left(ke-\frac{1}{2}\right)}^{n+1}}{\Delta\sigma} = 0 \tag{4.90}$$

Adopting the upwind scheme, $C_{ij\left(ke-\frac{1}{2}\right)}^{n+1} = C_{ijke}^{n+1}$ 4.91

$$\frac{D_{ij}^{n+1}C_{ijke}^{n+1} - D_{ij}^{n+1}C_{ijke}^{n}}{\Delta t} - \frac{D_{ij}^{n+1}\dot{\sigma}_{sij\left(ke-\frac{1}{2}\right)}C_{ijke}^{n+1}}{\Delta\sigma} = 0 \tag{4.92}$$

$$C_{ijke}^{n+1} = \frac{\left[\frac{D_{ij}^{n+1}C_{ijke}^{n}}{\Delta t}\right]}{\left[\frac{D_{ij}^{n+1}}{\Delta t} - \frac{D_{ij}^{n+1}\dot{\sigma}_{sij\left(ke-\frac{1}{2}\right)}}{\Delta\sigma}\right]} \tag{4.93}$$

$$C_{ijke}^{n+1} = \frac{\left[\frac{C_{ijke}^{n}}{\Delta t}\right]}{\left[\frac{1}{\Delta t} - \frac{\dot{\sigma}_{sij\left(ke-\frac{1}{2}\right)}}{\Delta\sigma}\right]} \tag{4.94}$$

At the bottom of the water column flux can be depositional or erosion depending on the bed shear stress (BSS) τ_b , the bed shear stress on deposition τ_D and the bed shear stress on erosion τ_E. Modeling of BSS is a critical parameter in calculating depositional or erosion flux which has been modeled in bed shear stress model as the vector summation of current induced bed shear stress (CBSS) and wave induced bed shear stress (WBSS) (Rasmeemasmuang and Sasaki, 2008). In this approach WBSS is obtained through the prediction of wave condition in wave hindcasting model (Achiari and Sasaki, 2007).

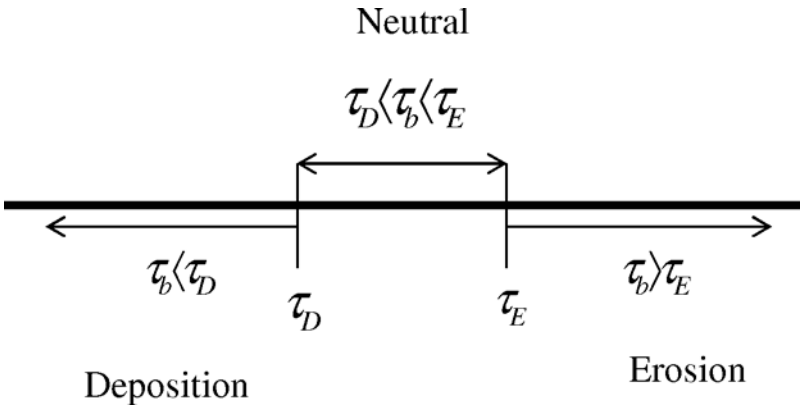

Fig 4.4 Bed shear stress on deposition or erosion

Considering the depositional bottom flux, settling term is discretized as;

$$Flux\_t = D_{ij}^{n+1} \dot{\sigma}_{sij\left(1+\frac{1}{2}\right)} C_{ij\left(1+\frac{1}{2}\right)}^{n+1} \tag{4.95}$$

$$Flux\_b = D_{ij}^{n+1} F_D \tag{4.96}$$

Depositional flux, F_D has been calculated from the following expression (Attari and Sasaki, 2012) based on the type of particulate matter.

$$\begin{aligned} F_D &= \dot{\sigma}_{sij\left(1-\frac{1}{2}\right)} C_{ij\left(1-\frac{1}{2}\right)}^{n+1} \left(1-\frac{\tau_b}{\tau_D}\right) \quad \text{if} \quad \tau_b < \tau_D \\ F_D &= 0 \qquad\qquad\qquad\qquad\quad \text{if} \quad \tau_b > \tau_D \end{aligned} \tag{4.97}$$

$$\frac{D_{ij}^{n+1} C_{ij1}^{n+1} - D_{ij}^{n+1} C_{ij1}^{n}}{\Delta t} + \frac{D_{ij}^{n+1} \dot{\sigma}_{sij\left(1+\frac{1}{2}\right)} C_{ij\left(1+\frac{1}{2}\right)}^{n+1} - D_{ij}^{n+1} \left[\dot{\sigma}_{sij\left(1-\frac{1}{2}\right)} C_{ij\left(1-\frac{1}{2}\right)}^{n+1} \left(1-\frac{\tau_b}{\tau_D}\right) \right]}{\Delta \sigma} = 0 \tag{4.98}$$

Adopting the upwind scheme, $C_{ij\left(1+\frac{1}{2}\right)}^{n+1} = C_{ij2}^{n+1}$ and $C_{ij\left(1-\frac{1}{2}\right)}^{n+1} = C_{ij1}^{n+1}$ 4.99

$$\frac{D_{ij}^{n+1} C_{ij1}^{n+1} - D_{ij}^{n+1} C_{ij1}^{n}}{\Delta t} + \frac{D_{ij}^{n+1} \dot{\sigma}_{sij\left(1+\frac{1}{2}\right)} C_{ij2}^{n+1} - D_{ij}^{n+1} \left[\dot{\sigma}_{sij\left(1-\frac{1}{2}\right)} C_{ij1}^{n+1} \left(1-\frac{\tau_b}{\tau_D}\right) \right]}{\Delta \sigma} = 0 \tag{4.100}$$

$$\left[\frac{D_{ij}^{n+1}}{\Delta t}-\frac{D_{ij}^{n+1}\dot{\sigma}_{sij\left(1-1/2\right)}\left(1-\frac{\tau_b}{\tau_D}\right)}{\Delta\sigma}\right]C_{ij1}^{n+1}=\left[\frac{D_{ij}^{n+1}C_{ij1}^{n}}{\Delta t}-\frac{D_{ij}^{n+1}\dot{\sigma}_{sij\left(1+1/2\right)}C_{ij2}^{n+1}}{\Delta\sigma}\right] \quad 4.101$$

$$C_{ij1}^{n+1}=\frac{\left[\frac{D_{ij}^{n+1}C_{ij1}^{n}}{\Delta t}-\frac{D_{ij}^{n+1}\dot{\sigma}_{sij\left(1+1/2\right)}C_{ij2}^{n+1}}{\Delta\sigma}\right]}{\left[\frac{D_{ij}^{n+1}}{\Delta t}-\frac{D_{ij}^{n+1}\dot{\sigma}_{sij\left(1-1/2\right)}\left(1-\frac{\tau_b}{\tau_D}\right)}{\Delta\sigma}\right]} \quad 4.102$$

$$C_{ij1}^{n+1}=\frac{\left[\frac{C_{ij1}^{n}}{\Delta t}-\frac{\dot{\sigma}_{sij\left(1+1/2\right)}C_{ij2}^{n+1}}{\Delta\sigma}\right]}{\left[\frac{1}{\Delta t}-\frac{\dot{\sigma}_{sij\left(1-1/2\right)}\left(1-\frac{\tau_b}{\tau_D}\right)}{\Delta\sigma}\right]} \quad 4.103$$

Considering the erosion bottom flux, settling term is discretized as;

$$Flux\_t=D_{ij}^{n+1}\dot{\sigma}_{sij\left(1+1/2\right)}C_{ij\left(1+1/2\right)}^{n+1} \quad 4.104$$

$$Flux\_b=-D_{ij}^{n+1}F_E \quad 4.105$$

Erosion flux, F_E has been calculated from the following expression (Rasmeemasmuang and Sasaki, 2008) where E_0 is the empirical erosion rate parameter.

$$F_E=E_0\left(\frac{\tau_b}{\tau_E}-1\right), \qquad \text{if} \quad \tau_b>\tau_E$$
$$F_E=0, \qquad \text{if} \quad \tau_b<\tau_E \quad 4.106$$

Since the erosion flux is computed as a total eroded material from sediment, it has been separated into corresponding particulate matter B according to their mass fraction , $F_{M,B}$. Mass fraction of each particulate matter is the ratio of the mass of each particulate matter to

the total mass eroded from sediment. Eroded total mass can be replaced with the bulk density and the total volume of eroded sediment. Mass fraction of any particulate matter in sediment can be written as;

$$F_{M,\mathrm{B}} = \frac{M_B}{M_T} \tag{4.107}$$

$$F_{M,\mathrm{B}} = \frac{M_B}{\rho_{bulk} V_T} \tag{4.108}$$

Since the concentration of state variables have been defined as the mass over unit control volume;

$$B = \frac{M_B}{V_T} \tag{4.109}$$

Hence mass fraction of each particulate matter which erodes from the sediment is computed as;

$$F_{M,\mathrm{B}} = \frac{B}{\rho_{bulk}} \tag{4.110}$$

Then;

$$\frac{D_{ij}^{n+1} C_{ij1}^{n+1} - D_{ij}^{n+1} C_{ij1}^{n}}{\Delta t} + \frac{D_{ij}^{n+1} \dot{\sigma}_{sij(1+1/2)} C_{ij(1+1/2)}^{n+1} - \left\{ -D_{ij}^{n+1} \left[E_0 \left(\frac{\tau_b}{\tau_E} - 1 \right) F_{M,B} \right] \right\}}{\Delta \sigma} = 0 \tag{4.111}$$

Adopting the upwind scheme, $C_{ij(1+1/2)}^{n+1} = C_{ij2}^{n+1}$ 4.112

$$\frac{D_{ij}^{n+1} C_{ij1}^{n+1} - D_{ij}^{n+1} C_{ij1}^{n}}{\Delta t} + \frac{D_{ij}^{n+1} \dot{\sigma}_{sij(1+1/2)} C_{ij2}^{n+1} + D_{ij}^{n+1} \left[E_0 \left(\frac{\tau_b}{\tau_E} - 1 \right) F_{M,B} \right]}{\Delta \sigma} = 0 \tag{4.113}$$

$$\left[\frac{D_{ij}^{n+1}}{\Delta t} \right] C_{ij1}^{n+1} = \left[\frac{D_{ij}^{n+1} C_{ij1}^{n}}{\Delta t} - \frac{D_{ij}^{n+1} \dot{\sigma}_{sij(1+1/2)} C_{ij2}^{n+1} + D_{ij}^{n+1} \left[E_0 \left(\frac{\tau_b}{\tau_E} - 1 \right) \right] F_{M,B}}{\Delta \sigma} \right] \tag{4.114}$$

$$C_{ij1}^{n+1} = \frac{\left[\frac{D_{ij}^{n+1} C_{ij1}^{n}}{\Delta t} - \frac{D_{ij}^{n+1} \dot{\sigma}_{sij\left(1+\frac{1}{2}\right)} C_{ij2}^{n+1} + D_{ij}^{n+1} \left[E_0 \left(\frac{\tau_b}{\tau_E} - 1 \right) F_{M,B} \right]}{\Delta \sigma} \right]}{\left[\frac{D_{ij}^{n+1}}{\Delta t} \right]} \qquad 4.115$$

$$C_{ij1}^{n+1} = \frac{\left[\frac{C_{ij1}^{n}}{\Delta t} - \frac{E_0 \left(\frac{\tau_b}{\tau_E} - 1 \right) F_{M,B} + \dot{\sigma}_{sij\left(1+\frac{1}{2}\right)} C_{ij2}^{n+1}}{\Delta \sigma} \right]}{\left[\frac{1}{\Delta t} \right]} \qquad 4.116$$

Hence, depositional or erosion flux at the bottom grid of the water column is considered with the combination of equations **4.103** and **4.116**.

$$C_{ij1}^{n+1} = \frac{\left[\frac{C_{ij1}^{n}}{\Delta t} - \frac{\dot{\sigma}_{sij\left(1+\frac{1}{2}\right)} C_{ij2}^{n+1}}{\Delta \sigma} \right]}{\left[\frac{1}{\Delta t} - \frac{\dot{\sigma}_{sij\left(1-\frac{1}{2}\right)} \left(1 - \frac{\tau_b}{\tau_D} \right)}{\Delta \sigma} \right]} f_D + \frac{\left[\frac{C_{ij1}^{n}}{\Delta t} - \frac{E_0 \left(\frac{\tau_b}{\tau_E} - 1 \right) F_{M,B} + \dot{\sigma}_{sij\left(1+\frac{1}{2}\right)} C_{ij2}^{n+1}}{\Delta \sigma} \right]}{\left[\frac{1}{\Delta t} \right]} f_E \qquad 4.117$$

$$f_D = 1 \text{ if } \tau_b < \tau_D \text{ and } f_D = 0 \text{ if } \tau_b > \tau_D$$

$$f_E = 1 \text{ if } \tau_b > \tau_E \text{ and } f_E = 0 \text{ if } \tau_b < \tau_E$$

For the stability of the model the equation **4.117** has been considered as;

$$C_{ij1}^{n+1}=\frac{\left[\frac{C_{ij1}^{n}}{\Delta t}-\frac{\dot{\sigma}_{sij\left(1+\frac{1}{2}\right)}C_{ij2}^{n+1}}{\Delta\sigma}\right]}{\left[\frac{1}{\Delta t}-\frac{\dot{\sigma}_{sij\left(1-\frac{1}{2}\right)}\times MAX\left\{\left(1-\frac{\tau_b}{\tau_D}\right),0.0\right\}}{\Delta\sigma}\right]}f_D+\frac{\left[\frac{C_{ij1}^{n}}{\Delta t}-\frac{E_0\times MAX\left\{\left(\frac{\tau_b}{\tau_E}-1\right),0.0\right\}F_{M,B}+\dot{\sigma}_{sij\left(1+\frac{1}{2}\right)}C_{ij2}^{n+1}}{\Delta\sigma}\right]}{\left[\frac{1}{\Delta t}\right]}f_E \qquad 4.118$$

Initially, the setting flux at the surface grid is computed using the equation **4.94** and from the next grid point until the bottom grid point settling flux is computed by using equation **4.87** and finally, the settling flux at the bottom grid point is computed by using the equation **4.118**.

Through the discretization of governing equation for settling interaction layer flux which transfers between water column and sediment column can be obtained as;

Depositional flux; $$Flux\_b=D_{ij}^{n+1}\left[\dot{\sigma}_{sij\left(1-\frac{1}{2}\right)}C_{ij1}^{n+1}\left(1-\frac{\tau_b}{\tau_D}\right)\right] \qquad 4.119$$

Erosion flux; $$Flux\_b=-D_{ij}^{n+1}\left[E_0\left(\frac{\tau_b}{\tau_E}-1\right)\right] \qquad 4.120$$

Combining both depositional and erosional flux, flux from water to sediment;

$$Flux\_b=D_{ij}^{n+1}\left[\dot{\sigma}_{sij\left(1-\frac{1}{2}\right)}C_{ij1}^{n+1}\left(1-\frac{\tau_b}{\tau_D}\right)\right]f_D-D_{ij}^{n+1}\left[E_0\left(\frac{\tau_b}{\tau_E}-1\right)\right]f_E \qquad 4.121$$

For the stability of the model this has been considered as;

$$Flux\_b = D_{ij}^{n+1}\left[\dot{\sigma}_{sij\left(1-\frac{1}{2}\right)}C_{ij1}^{n+1}\times MAX\left\{\left(1-\frac{\tau_b}{\tau_D}\right),0.0\right\}\right]f_D$$
$$-D_{ij}^{n+1}\left[E_0\times MAX\left\{\left(\frac{\tau_b}{\tau_E}-1\right),0.0\right\}\right]f_E \qquad 4.122$$

4.1.4 Source terms

Finite difference method with the fourth order Runge-Kutta method which gives the approximation of solutions of ordinary differential equations through explicit approach is used to obtain the solution for the source term equation **4.16**. For a source term C which is a function of C and time t;

$$\frac{dC}{dt} = f(t,C) \qquad 4.123$$

Define the coefficients,

$$k_1 = \Delta t\times f(t^n, C^n) \qquad 4.124$$

$$k_2 = \Delta t\times f(t^n+\frac{1}{2}\Delta t, C^n+\frac{1}{2}k_1) \qquad 4.125$$

$$k_3 = \Delta t\times f(t^n+\frac{1}{2}\Delta t, C^n+\frac{1}{2}k_2) \qquad 4.126$$

$$k_4 = \Delta t\times f(t^n+\Delta t, C^n+k_3) \qquad 4.127$$

For matrices of $[C]$ and $[F]$;

$$\frac{d[C]}{dt} = [F](t,[C]) \text{ where } [C]=\begin{bmatrix} C_1 \\ C_2 \\ \cdots \\ \cdots \\ C_m \end{bmatrix} \text{ and } [F]=\begin{bmatrix} f_1 \\ f_2 \\ \cdots \\ \cdots \\ f_m \end{bmatrix} \qquad 4.128$$

$$\begin{bmatrix} k_{11} \\ k_{12} \\ \cdots \\ \cdots \\ k_{1m} \end{bmatrix} = \begin{bmatrix} \Delta t \times f_1(t^n, C_1^n, C_2^n, ..., C_m^n) \\ \Delta t \times f_2(t^n, C_1^n, C_2^n, ..., C_m^n) \\ \cdots \\ \cdots \\ \Delta t \times f_m(t^n, C_1^n, C_2^n, ..., C_m^n) \end{bmatrix} \tag{4.129}$$

$$\begin{bmatrix} k_{21} \\ k_{22} \\ \cdots \\ \cdots \\ k_{2m} \end{bmatrix} = \begin{bmatrix} \Delta t \times f_1\left\{\left(t^n + \frac{1}{2}\Delta t\right), \left(C_1^n + \frac{1}{2}k_{11}\right) +, \left(C_2^n + \frac{1}{2}k_{12}\right), ..., \left(C_m^n + \frac{1}{2}k_{1m}\right)\right\} \\ \Delta t \times f_2\left\{\left(t^n + \frac{1}{2}\Delta t\right), \left(C_1^n + \frac{1}{2}k_{11}\right) +, \left(C_2^n + \frac{1}{2}k_{12}\right), ..., \left(C_m^n + \frac{1}{2}k_{1m}\right)\right\} \\ \cdots \\ \cdots \\ \Delta t \times f_m\left\{\left(t^n + \frac{1}{2}\Delta t\right), \left(C_1^n + \frac{1}{2}k_{11}\right) +, \left(C_2^n + \frac{1}{2}k_{12}\right), ..., \left(C_m^n + \frac{1}{2}k_{1m}\right)\right\} \end{bmatrix} \tag{4.130}$$

$$\begin{bmatrix} k_{31} \\ k_{32} \\ \cdots \\ \cdots \\ k_{3m} \end{bmatrix} = \begin{bmatrix} \Delta t \times f_1\left\{\left(t^n + \frac{1}{2}\Delta t\right), \left(C_1^n + \frac{1}{2}k_{21}\right) +, \left(C_2^n + \frac{1}{2}k_{22}\right), ..., \left(C_m^n + \frac{1}{2}k_{2m}\right)\right\} \\ \Delta t \times f_2\left\{\left(t^n + \frac{1}{2}\Delta t\right), \left(C_1^n + \frac{1}{2}k_{21}\right) +, \left(C_2^n + \frac{1}{2}k_{22}\right), ..., \left(C_m^n + \frac{1}{2}k_{2m}\right)\right\} \\ \cdots \\ \cdots \\ \Delta t \times f_m\left\{\left(t^n + \frac{1}{2}\Delta t\right), \left(C_1^n + \frac{1}{2}k_{21}\right) +, \left(C_2^n + \frac{1}{2}k_{22}\right), ..., \left(C_m^n + \frac{1}{2}k_{2m}\right)\right\} \end{bmatrix} \tag{4.131}$$

$$\begin{bmatrix} k_{41} \\ k_{42} \\ \cdots \\ \cdots \\ k_{4m} \end{bmatrix} = \begin{bmatrix} \Delta t \times f_1\left\{\left(t^n + \Delta t\right), \left(C_1^n + k_{31}\right) +, \left(C_2^n + k_{32}\right), ..., \left(C_m^n + k_{3m}\right)\right\} \\ \Delta t \times f_2\left\{\left(t^n + \Delta t\right), \left(C_1^n + k_{31}\right) +, \left(C_2^n + k_{32}\right), ..., \left(C_m^n + k_{3m}\right)\right\} \\ \cdots \\ \cdots \\ \Delta t \times f_m\left\{\left(t^n + \Delta t\right), \left(C_1^n + k_{31}\right) +, \left(C_2^n + k_{32}\right), ..., \left(C_m^n + k_{3m}\right)\right\} \end{bmatrix} \tag{4.132}$$

The solution for the differential equation comes as;

$$\begin{bmatrix} C_1^{n+1} \\ C_2^{n+1} \\ \cdots \\ \cdots \\ C_m^{n+1} \end{bmatrix} = \begin{bmatrix} C_1^n + \frac{1}{6}\left(k_{11} + 2k_{21} + 2k_{31} + k_{41}\right) \\ C_1^n + \frac{1}{6}\left(k_{12} + 2k_{22} + 2k_{32} + k_{42}\right) \\ \cdots \\ \cdots \\ C_1^n + \frac{1}{6}\left(k_{1m} + 2k_{2m} + 2k_{3m} + k_{4m}\right) \end{bmatrix} \tag{4.133}$$

4.1.4.1 Biochemical processes in water column

Biochemical processes combines both bioprocesses which refer to systems that use living organisms to obtain desired results, and chemical processes which refer to transformation of reactants into products through breaking the bonds and creating new bonds. All the Stoichiometric relationships associated with biochemical processes which have been adopted by many researchers, e.g. (Ji, 2008), (Di Toro, 2001) are shown in the **Table 4.1**.

Table 4.1 Stoichiometric relationships associated with biochemical processes

Photosynthesis - ammonia as electron accepter

$$106(CO_2)+16(NH_3)+H_3PO_4+106(H_2O)=(\mathrm{CH_2}\,O)_{106}(NH_3)_{16}(H_3PO_4)+106(O_2)$$

Photosynthesis - nitrate as electron accepter

$$106(CO_2)+16(NO_3^-)+H_3PO_4+122(H_2O)+16\,\mathrm{H^+}=(\mathrm{CH_2}\,O)_{106}(NH_3)_{16}(H_3PO_4)+138(O_2)$$

Oxic mineralization and metabolism

$$(\mathrm{CH_2}\,O)_{106}(NH_3)_{16}(H_3PO_4)+106(O_2)=106(CO_2)+16(NH_3)+H_3PO_4+106(H_2O)$$

Suboxic mineralization or Denitrification

$$(\mathrm{CH_2}\,O)_{106}(NH_3)_{16}(H_3PO_4)+\frac{424}{5}(HNO_3)=106(CO_2)+16(NH_3)+H_3PO_4+\frac{106}{5}(H_2O)+\frac{212}{5}(N_2)$$

Anoxic mineralization or H2S production

$$(\mathrm{CH_2}\,O)_{106}(NH_3)_{16}(H_3PO_4)+\frac{106}{2}(H_2SO_4)=106(CO_2)+16(NH_3)+H_3PO_4+106(H_2O)+\frac{106}{2}(\mathrm{H_2\,S})$$

Nitrification

$$NH_4^+ + 2O_2 = NO_3^- + H_2O + 2H^+$$

H2S oxidization

$$H_2S+2(O_2)=H_2SO_4$$

4.1.4.1.1 Modeling of Phytoplankton

Reproducibility of seasonal hypoxia in water column has a strong correlation with the reproducibility of Chlorophyll_*a* concentration. Hence, accurate modeling of phytoplankton is an important component in water quality modeling. Phytoplankton concentration controls by both physical transport which is similar to other water quality variables and only the effect

of biochemical processes are discussing in this section. Even though water quality models which intend to analyze short term variations of phytoplankton focuses on some specific types of phytoplankton, for long term simulations such as years or more, water quality processes are associated with different types of phytoplankton in different seasons. Hence, three seasonal blooms which have appeared every year in Tokyo Bay in particular spring, summer and winter are modeled based on three limiting factors such as light, temperature and nutrients. Respiration and excretion of phytoplankton have considered together as phytoplankton metabolism.

Since Chlorophyll_*a* (Chl_a) is the most commonly available to estimate algal biomass, and is considered to be directly promotional to the concentration of algal biomass Chl_a has been computed in the model with a Chl_a:C ratio of 1:27.

4.1.4.1.1.1 Nutrient Limit

Limiting nutrients for phytoplankton growth are mainly phosphorous and nitrogen except diatoms are limiting by additional nutrient of silicon. Diatoms consume dissolved silica in order to create their structural skeleton and hence silicon can limit the growth of diatoms. Carbon is also a major nutrient for phytoplankton growth and since its abundant availability carbon is not considered as a limiting nutrient for phytoplankton growth.

As many algal models directly link algal growth and nutrient uptake with fixed stoichiometry (Ji, 2008) , model has assumed that algae consume nutrients in a fixed stoichiometric ratio called Redfield-ratio of $C:N:P=106:16:1$. The growth limiting function for each nutrient has computed through the fixed stoichiometric approach, and combined together to form the growth limiting function due to nutrients. According to the Liebig's Law of the Minimum, growth is determined by the nutrient in least supply (Ji, 2008).

4.1.4.1.1.2 Light Limit

Algal primary production occurs through the photosynthesis or the metabolic process of plants which convert CO_2 and H_2O into carbon compounds and O_2 using light as the energy source. This is essential in one way to produce the food base in aquatic system and in another way as a source of O_2. Since the sunlight is the major driving force for the photosynthesis, light can limit the algal growth.

Light intensity in the water column has been calculated using Beer's law which states that light decreases with depth exponentially and can be explained by the equation **4.138** where k_e is the light extinction coefficient, PAR_{sur} is the light intensity at the surface and D is the depth in the water column (Ji, 2008). Light extinction coefficient k_e has been computed from equation **4.141** which has been considered as a function of Chl_a, suspendered sediment concentration and salinity (Attari et al., 2012). After computing the light intensity at each depth light limiting function on algal growth has been computed by using the equation **4.137** where PAR_{opt} is the optimum light intensity for the algal growth (Fennel and Neumann, 2004). Light limiting function reaches its maximum when $PAR = PAR_{opt}$ as shown in the **Fig 4.5**.

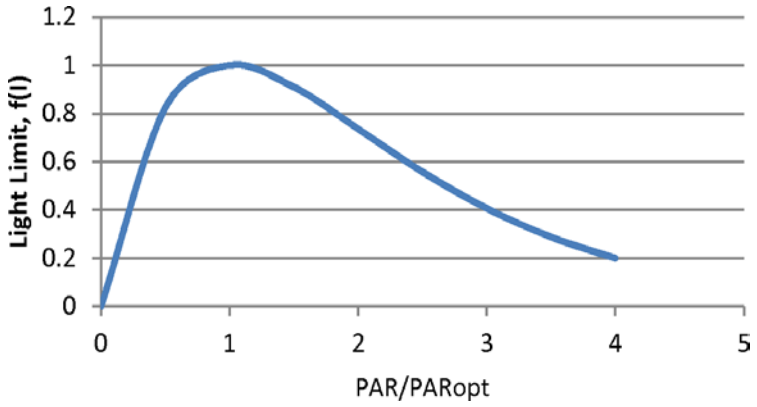

Fig 4.5 Algal growth limiting function for light

4.1.4.1.1.3 Temperature Limit

Temperature change is one of the major factors which control the seasonal variations of algae or the dominance during different seasons. Since different algal species have different optimum temperatures for their growth, different species can bloom in different seasons. This approach has been adopted in the model which gives three different dominant periods as shown in the **Fig 4.6**. This temperature effect has been computed from equation **4.136** where $LOTphy$ and $UOTphy$ are the lower and upper ends of optimum temperature while $BLOphy$ and $AUOphy$ represents the effect of temperature below $LOTphy$ and effect of temperature

above *UOTphy* respectively. It has been noticed that the *BLOphy* and *AUOphy* are very sensitive to control the specific algal dominance during a specific season.

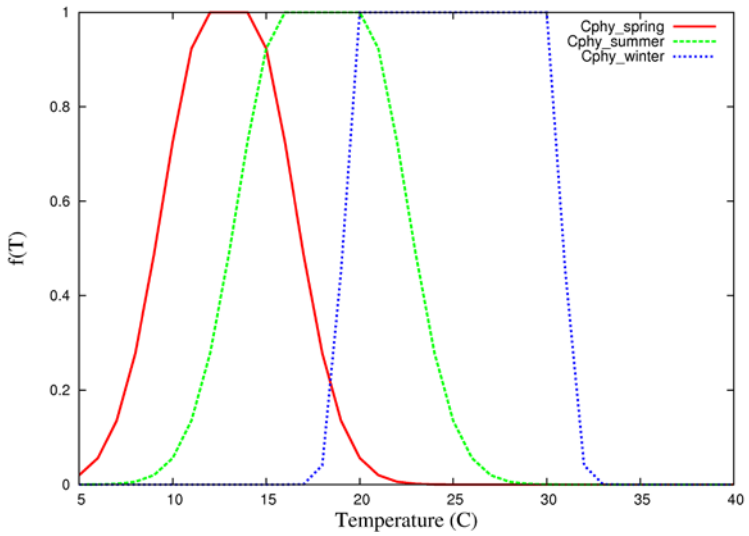

Fig 4.6 Algal growth limiting function for temperature

4.1.4.1.2 Kinetic Equations for source terms in pelagic model

The kinetic equations for source terms in pelagic model are adopted refering (Ji, 2008) and (Di Toro, 2001).

Phytoplankton

$$\frac{dC_{phy}(i,j,k,m)}{dt} = R_{C_{phy}}\_\mathrm{PP}(i,j,k,m) - R_{C_{phy}}\_\mathrm{Met}(i,j,k,m) - R_{C_{phy}}\_\mathrm{Mor}(i,j,k,m) - R_{C_{zoo}}\_\mathrm{G\_each}(i,j,\mathrm{k},m) \quad 4.134$$

$$R_{C_{phy}}\_\mathrm{PP}(i,j,k,m) = G_{Phy}(m)\times \mathrm{TL}_{phy}(i,j,k,m)\times \mathrm{LL}_{phy}(i,j,k,m)\times \mathrm{NL}_{phy}(i,j,k,m)\times C_{phy}(i,j,k,m) \quad 4.135$$

$$\mathrm{TL}_{phy}(i,j,k,m) = \begin{cases} e^{(-GKLphy(m)\times((tempt(i,j,k)-LOTphy(m))^2))} & if\,(tempt(i,j,k)\langle LOTphy(m)) \\ 1 & if\,(LOTphy(m)\langle tempt(i,j,k)\langle UOTphy(m)) \\ e^{(-GKLphy(m)\times((tempt(i,j,k)-UOTphy(m))^2))} & if\,(tempt(i,j,k)\rangle UOTphy(m)) \end{cases} \quad 4.136$$

$$\mathrm{LL}_{phy}(i,j,k,m) = \frac{PAR(i,\mathrm{j},k)}{PARopt(m)} \times e^{\left(1-\frac{PAR(i,j,k)}{PARopt(m)}\right)} \quad 4.137$$

$$PAR(i,j,k) = PAR\_sur(i,j,k)e^{-k_e D} \quad 4.138$$

$$k_e = 0.022 + (C_{Chl} + 27.C_{SS} + (35 - salt)5.5)0.0096 \quad 4.139$$

$$PARopt(m) = MAX\left(\frac{PAR(i,j,k)}{Photoinhibition}, PAR\min\_phy(m)\right) \quad 4.140$$

$$\mathrm{NL}_{phy}(i,j,k,m) = MIN(\mathrm{C}_{PO_4}\mathrm{NL}(i,j,\mathrm{k},\mathrm{m}), \mathrm{C}_{nit}\mathrm{NL}(i,j,\mathrm{k},\mathrm{m}), \mathrm{C}_{SiO_2}\mathrm{NL}(i,j,\mathrm{k},\mathrm{m})) \quad 4.141$$

$$\mathrm{C}_{PO_4}\mathrm{NL}_{phy}(i,j,\mathrm{k},\mathrm{m}) = f_{Monod}(\mathrm{C}_{PO_4}(\mathrm{i},\mathrm{j},k), K_{PO_4\_phy}(\mathrm{m})) \quad 4.142$$

$$\mathrm{C}_{nit}\mathrm{NL}_{phy}(i,j,\mathrm{k},\mathrm{m}) = f_{Monod}((C_{NH_4}(\mathrm{i},\mathrm{j},\mathrm{k}) + C_{NO3}(\mathrm{i},\mathrm{j},\mathrm{k})), \mathrm{K}_{\mathrm{nit\_phy}}(\mathrm{m})) \quad 4.143$$

$$\mathrm{C}_{SiO_2}\mathrm{NL}_{phy}(i,j,\mathrm{k},\mathrm{m}) = f_{Monod}(\mathrm{C}_{SiO2}(i,j,k), K_{SiO2\_phy}(\mathrm{m})) \quad 4.144$$

$$f_{Monod} = \frac{\mathrm{Nutrient}}{\mathrm{Hf\_Nutrient} + \mathrm{Nutrient}} \quad 4.145$$

$$\mathrm{r_f} = \frac{C_{NO_3}(i,j,k)}{C_{NO_3}(i,j,k) + C_{NH_4}(i,j,k)} \quad 4.146$$

$$R_{C_{phy}}\_\mathrm{Met}(i,j,k,m) = M_{Phy}(m) \times e^{(0.04\times(tempt(i,j,k)-20.0)} \times C_{phy}(i,j,k,m) \quad 4.147$$

$$R_{C_{phy}}\_\mathrm{Mor}(i,j,k,m) = D_{Phy}(m) \times C_{phy}(i,j,k,m) \quad 4.148$$

Zooplankton

$$\frac{dC_{zoo}(i,j,k)}{dx} = R_{C_{zoo}}\_\mathrm{Gro}(i,j,k) - R_{C_{zoo}}\_\mathrm{Mor}(i,j,k) \quad 4.149$$

$$R_{C_{zoo}}\_Gro(i,j,k) = R_{C_{zoo}}\_\mathrm{Absor}(i,j,k) - R_{C_{zoo}}\_\mathrm{min\_food}(i,j,k) \quad 4.150$$

$$R_{C_{zoo}}\_\mathrm{Absor}(i,j,k) = C_{zoo}\_\mathrm{Absorb\_portion} \times R_{C_{zoo}}\_G(i,j,k) \times f_{Monod}(C_{dox}(i,j,k), K_{dox}\_zoo) \quad 4.151$$

$$R_{C_{zoo}}\_G(i,j,k) = \sum_{foods\_iter=1}^{p} C_{zoo}\_G\_\mathrm{each}(\mathrm{foods\_iter}, i,j,k) \quad 4.152$$

$$R_{C_{zoo}}\_G\_\mathrm{each}(\mathrm{foods\_iter}, i,j,k) = R_{C_{zoo}}\_G\_\mathrm{pri}(i,j,k) \times \frac{\mathrm{Food\_each(foods\_iter)}}{\mathrm{Total\_Food}(i,j,\mathrm{k})} \quad 4.153$$

$$R_{C_{zoo}}\_G\_\mathrm{pri}(i,j,k) = G_{zoo} \times \mathrm{TL}_{zoo}(i,j,k) \times \mathrm{FL}_{zoo}(i,j,k) \times C_{zoo}(i,j,k) \quad 4.154$$

$$\mathrm{TL}_{zoo}(i,j,k) = e^{(0.035\times(tempt(i,j,k)-20.0))} \quad 4.155$$

$$\mathrm{FL}_{zoo}(i,j,k) = 1 - e^{(\mathrm{Ivlev}\times MIN((\mathrm{Food\_Threshold} - \mathrm{Total\_Food}(i,j,k)),0.0))} \quad 4.156$$

$$\text{Total\_Food}(i,j,k) = \sum_{foods\_iter=1}^{p} \text{Food\_each(foods\_iter)} \quad 4.157$$

$$\text{Food\_each(foods\_iter)} = C_{foods\_iter}(i,j,k) \quad 4.158$$

$$R_{C_{zoo}}\text{\_Mor}(i,j,k) = D_{zoo} \times C_{zoo}(i,j,k) \times \text{TL}_{zoo}(i,j,k) \times \frac{C_{zoo}(i,j,k)}{\text{Max\_zoo}} \quad 4.159$$

$$R_{C_{zoo}}\text{\_Fecal}(i,j,k) = R_{C_{zoo}}\text{\_G}(i,j,k) - C_{zoo}\text{\_Absor}(i,j,k) \quad 4.160$$

$$R_{C_{zoo}}\text{\_Met}(i,j,k) = MIN(\text{R}_{C_{zoo}}\text{\_Absor}(i,j,k), \text{R}_{C_{zoo}}\text{\_ min\_food}(i,j,k)) \quad 4.161$$

Particulate Organic Carbon Labile

$$\frac{dC_{pocL}(i,j,k)}{dt} = \left\{ \sum_{p=1}^{m} R_{C_{phy,p}}\text{\_Mor}(i,j,k) + R_{C_{zoo}}\text{\_Fecal}(i,j,k) + R_{C_{zoo}}\text{\_Mor}(i,j,k) \right\} \times F_{labile}$$
$$- R_{C_{zoo}}\text{\_}G\text{\_each}(4,i,j,k) - R_{C_{pocL}}\text{\_dec\_oxic}(i,j,k) - R_{C_{pocL}}\text{\_dec\_anoxic\_}no3(i,j,k) \quad 4.162$$
$$- R_{C_{pocL}}\text{\_dec\_anoxic\_}so4(i,j,k) + \left(\frac{Aflux\_s2w_{pocL}(i,j)}{\Delta\sigma} \right) \times flag1\_1$$

Oxic carbon diagenesis rate for labile POC

$$R_{C_{pocL},CpocL}\text{\_dec}(i,j,k) = k_{C_{pocL},CpocL}\text{\_dec} \times \theta_{C_{pocL}}^{(tempt(i,j,\text{k}-20)} \times C_{pocL}(i,j,k) \quad 4.163$$

Since oxic decomposition rate is controlled by the availability of oxygen:

$$R_{C_{pocL},CpocL}\text{\_dec\_oxic}(i,j,k) = k_{C_{pocL},CpocL}\text{\_dec\_oxic} \times \theta_{C_{pocL}}^{(tempt(i,j,k)-20)} \times \left[\frac{C_{dox}(i,j,k)}{K_{O_2,Cpoc} + C_{dox}(i,j,k)} \right] \quad 4.164$$
$$\times C_{pocL}(i,j,k)$$

Anoxic carbon diagenesis rate for labile POC or denitrification

Rate of nitrification $R_{C_{NO3},CpocL}\text{\_denit}(i,j,k)$ follows 1st order reaction rate constant $k_{C_{NO3},CpocL}\text{\_denit}$:

$$R_{C_{NO3},CpocL}\text{\_denit}(n,k) = k_{C_{NO3},CpocL}\text{\_denit}\left[C_{NO3}(i,j,k)\right] \quad 4.165$$

Since anoxic decomposition rate by the use of nitrate is controlled by the availability of oxygen and pock and temperature coefficient also applicable for the $R_{C_{NO3},CpocL}\text{\_denit}(i,j,k)$:

$$R_{C_{NO3},CpocL}\text{\_denit}(i,j,k) = k_{C_{no3},CpocL}\text{\_denit} \times \theta_{C_{no3}}^{(tempt(i,j,k)-20)}$$
$$\times MIN\left[\frac{K_{O_2,Cpoc}}{K_{O_2,Cpoc} + C_{dox}(i,j,k)}, \frac{C_{pocL}(i,j,k)}{K_{dec,Cpoc} + C_{pocL}(i,j,k)} \right] \times C_{no3}(i,j,k) \quad 4.166$$

$$R_{C_{pocL}}\_\text{dec\_anoxic\_no3}(i,j,k) = R_{C_{NO3},CpocL}\_\text{denit}(i,j,k)\times \text{rCN\_denit} \quad 4.167$$

Anoxic carbon diagenesis rate for labile POC or sulfate as electron acceptor

Since anoxic decomposition rate by the use of sulfate is controlled by the availability of oxygen and nitrate (Sulfate is abundant and has not considered as a limiting factor):

$$R_{C_{pocL}}\_\text{dec\_anoxic\_so4}(i,j,k) = k_{C_{pocL}}\_\text{dec\_anoxic\_so4}\times\theta_{C_{pocL}\_anoxic\_\_so4}^{(tempt(i,j,k)-20)}$$
$$\times MIN\left[\frac{K_{O_2,Cpoc}}{K_{O_2,Cpoc}+C_{dox}(i,j,k)},\frac{K_{Cno3,\text{denit}}}{K_{Cno3,\text{denit}}+C_{no3}(i,j,k)}\right]\times C_{pocL}(i,j,k) \quad 4.168$$

Particulate Organic Carbon Refractory

$$\frac{dC_{pocR}(i,j,k)}{dt} = \left\{\sum_{p=1}^{m} R_{C_{phy,p}}\_\text{Mor}(i,j,k) + R_{C_{zoo}}\_\text{Fecal}(i,j,k) + R_{C_{zoo}}\_\text{Mor}(i,j,k)\right\}\times F_{refrac}$$
$$-R_{C_{zoo}}\_G\_\text{each}(5,i,j,k) - R_{C_{pocR}}\_\text{dec\_oxic}(i,j,k) - R_{C_{pocR}}\_\text{dec\_anoxic\_}no3(i,j,k) \quad 4.169$$
$$-R_{C_{pocR}}\_\text{dec\_anoxic\_}so4(i,j,k) + \left(\frac{Aflux\_s2w_{pocR}(i,j)}{\Delta\sigma}\right)\times flag1\_1$$

Oxic carbon diagenesis rate for refractory POC

$$R_{C_{pocR}}\_\text{dec}(i,j,k) = k_{C_{pocR}}\_\text{dec}\times\theta_{C_{pocR}}^{(tempt(i,j,k)-20)}\times C_{pocR}(i,j,k)$$

Since oxic decomposition rate is controlled by the availability of oxygen:

$$R_{C_{pocR}}\_\text{dec\_oxic}(i,j,k) = k_{C_{pocR}}\_\text{dec\_oxic}\times\theta_{C_{pocR}}^{(tempt(i,j,k)-20)}\times\left[\frac{C_{dox}(i,j,k)}{K_{O_2,Cpoc}+C_{dox}(i,j,k)}\right]\times C_{pocR}(i,j,k) \quad 4.170$$

Anoxic carbon diagenesis rate for refractory POC or denitrification

Since anoxic decomposition rate by the use of nitrate is controlled by the availability of oxygen and pock and temperature coefficient also applicable for the $R_{C_{NO3},CpocR}\_\text{denit}(i,j,k)$:

$$R_{C_{NO3},CpocR}\_\text{denit}(i,j,k) = k_{C_{no3},CpocR}\_\text{denit}\times\theta_{C_{no3}}^{(tempt(i,j,k)-20)}$$
$$\times MIN\left[\frac{K_{O_2,Cpoc}}{K_{O_2,Cpoc}+C_{dox}(i,j,k)},\frac{C_{pocR}(i,j,k)}{K_{dec,Cpoc}+C_{pocR}(i,j,k)}\right]\times C_{no3}(i,j,k) \quad 4.171$$

$$R_{C_{pocR}}\_\text{dec\_anoxic\_no3}(i,j,k) = R_{C_{NO3},CpocR}\_\text{denit}(i,j,k)\times\text{rCN\_denit} \quad 4.172$$

Anoxic carbon diagenesis rate for refractory POC or sulfate as electron acceptor

Since anoxic decomposition rate by the use of sulfate is controlled by the availability of oxygen and nitrate (Sulfate is abundant and has not considered as a limiting factor):

$$R_{C_{pocR}}\_\text{dec\_anoxic\_so4}(i,j,k) = k_{C_{pocR}}\_\text{dec\_anoxic\_so4} \times \theta_{C_{pocR}\_anoxic\_so4}^{(tempt(i,j,k)-20)}$$
$$\times MIN\left[\frac{K_{O_2,Cpoc}}{K_{O_2,Cpoc}+C_{dox}(i,j,k)}, \frac{K_{Cno3,\text{denit}}}{K_{Cno3,\text{denit}}+C_{no3}(i,j,k)}\right] \times C_{pocR}(i,j,k) \quad 4.173$$

Particulate Organic Carbon Inert

$$\frac{dC_{pocI}(i,j,k)}{dt} = \left\{\sum_{p=1}^{m} R_{C_{phy,p}}\_\text{Mor}(i,j,k) + R_{C_{zoo}}\_\text{Fecal}(i,j,k) + R_{C_{zoo}}\_\text{Mor}(i,j,k)\right\} \times F_{inert}$$
$$-R_{C_{zoo}}\_G\_\text{each}(6,i,j,k) - R_{C_{pocI}}\_\text{dec\_oxic}(i,j,k) - R_{C_{pocI}}\_\text{dec\_anoxic\_}no3(i,j,k) \quad 4.174$$
$$-R_{C_{pocI}}\_\text{dec\_anoxic\_}so4(i,j,k) + \left(\frac{Aflux\_s2w_{pocI}(i,j)}{\Delta\sigma}\right) \times flag1\_1$$

Oxic carbon diagenesis rate for refractory POC

$$R_{C_{pocI}}\_\text{dec}(i,j,k) = k_{C_{pocI}}\_\text{dec} \times \theta_{C_{pocI}}^{(tempt(i,j,k)-20)} \times C_{pocI}(i,j,k)$$

Since oxic decomposition rate is controlled by the availability of oxygen:

$$R_{C_{pocI}}\_\text{dec\_oxic}(i,j,k) = k_{C_{pocI}}\_\text{dec\_oxic} \times \theta_{C_{pocI}}^{(tempt(i,j,k)-20)} \times \left[\frac{C_{dox}(i,j,k)}{K_{O_2,Cpoc}+C_{dox}(i,j,k)}\right] \times C_{pocI}(i,j,k) \quad 4.175$$

Anoxic carbon diagenesis rate for refractory POC or denitrification

Since anoxic decomposition rate by the use of nitrate is controlled by the availability of oxygen and pocI and temperature coefficient also applicable for the $R_{C_{NO3},CpocI}\_\text{denit}(i,j,k)$:

$$R_{C_{NO3},CpocI}\_\text{denit}(i,j,k) = k_{C_{no3},CpocI}\_\text{denit} \times \theta_{C_{no3}}^{(tempt(i,j,k)-20)}$$
$$\times MIN\left[\frac{K_{O_2,Cpoc}}{K_{O_2,Cpoc}+C_{dox}(i,j,k)}, \frac{C_{pocI}(i,j,k)}{K_{dec,Cpoc}+C_{pocI}(i,j,k)}\right] \times C_{no3}(i,j,k) \quad 4.176$$

$$R_{C_{pocI}}\_\text{dec\_anoxic\_no3}(i,j,k) = R_{C_{NO3},CpocI}\_\text{denit}(i,j,k) \times \text{rCN\_denit} \quad 4.177$$

Anoxic carbon diagenesis rate for refractory POC or sulfate as electron acceptor

Since anoxic decomposition rate by the use of sulfate is controlled by the availability of oxygen and nitrate (Sulfate is abundant and has not considered as a limiting factor):

$$R_{C_{pocI}}\_\text{dec\_anoxic\_so4}(i,j,k) = k_{C_{pocI}}\_\text{dec\_anoxic\_so4} \times \theta_{C_{pocI}\_anoxic\_so4}^{(tempt(i,j,k)-20)}$$
$$\times MIN\left[\frac{K_{O_2,Cpoc}}{K_{O_2,Cpoc}+C_{dox}(i,j,k)}, \frac{K_{Cno3,\text{denit}}}{K_{Cno3,\text{denit}}+C_{no3}(i,j,k)}\right] \times C_{pocI}(i,j,k) \quad 4.178$$

Phosphorous

$$\frac{dC_{PO_4}(i,j,k)}{dt} = \left\{\begin{array}{l} \sum_{p=1}^{m} R_{C_{phy,p}}\_\text{Met}(i,j,k) \\ +R_{C_{zoo}}\_\text{Met}(i,j,k) \\ -\sum_{p=1}^{m} R_{C_{phy,p}}\_\text{PP}(i,j,k) \\ +\sum_{q=1}^{3} R_{C_{poc,q}}\_\text{dec\_oxic}(i,j,k) \\ +\sum_{q=1}^{3} R_{C_{poc,q}}\_\text{dec\_anoxic\_no3}(i,j,k) \\ +\sum_{q=1}^{3} R_{C_{poc,q}}\_\text{dec\_anoxic\_so4}(i,j,k) \end{array}\right\} \times \text{rPC\_dec} \quad 4.179$$
$$+\left(\frac{Aflux\_s2w_{po4}(i,j)}{\Delta\sigma}\right) \times flag1\_1$$

Ammonia

$$\frac{dC_{NH_4}(i,j,k)}{dt} = \left\{\begin{array}{l} \sum_{p=1}^{m} R_{C_{phy,p}}\_\text{Met}(i,j,k) \\ +R_{C_{zoo}}\_\text{Met}(i,j,k) \\ -\sum_{p=1}^{m} R_{C_{phy,p}}\_\text{PP}(i,j,k) \times (1-\text{r\_f}) \\ +\sum_{q=1}^{3} R_{C_{poc,q}}\_\text{dec\_oxic}(i,j,k) \\ +\sum_{q=1}^{3} R_{C_{poc,q}}\_\text{dec\_anoxic\_no3}(i,j,k) \\ +\sum_{q=1}^{3} R_{C_{poc,q}}\_\text{dec\_anoxic\_so4}(i,j,k) \end{array}\right\} \times \text{rNC\_dec} \quad 4.180$$
$$+\left(\frac{Aflux\_s2w_{nh4}(i,j)}{\Delta\sigma}\right) \times flag1\_1$$
$$-R_{C_{NH_4}}\_\text{nit}(i,j,k)$$

Rate of Nitrification flux

Rate of nitrification $R_{C_{NH_4}}\_\text{nit}(i,j,k)$ follows 1st order reaction rate constant $k_{C_{NH_4}}\_\text{nit}$ $R_{C_{NH_4}}\_\text{nit}(i,j,k)$ decreases as the ammonia concentration increases $R_{C_{NH_4}}\_\text{nit}(i,j,k)$ follows Monod kinetics with respect to $C_{NH_4}(i,j,k)$:

$$R_{C_{NH_4}}\_\text{nit}(i,j,k) = k_{C_{NH_4}}\_\text{nit}\left[C_{NH_4}(i,j,k)\right]\left[\frac{K_{M,C_{NH_4}}}{K_{M,C_{NH_4}} + C_{NH_4}(i,j,k)}\right] \quad 4.181$$

$R_{C_{NH_4}}\_\text{nit}(i,j,k)$ decreases with decreasing oxygen concentration $R_{C_{NH_4}}\_\text{nit}(i,j,k)$ follows Michaelis-Menton expression:

$$R_{C_{NH_4}}\_\text{nit}(i,j,k) = k_{C_{NH_4}}\_\text{nit}\left[C_{NH_4}(i,j,k)\right]\left[\frac{K_{M,C_{NH_4}}}{K_{M,C_{NH_4}} + C_{NH_4}(i,j,k)}\right]\left[\frac{C_{dox}(i,j,k)}{K_{O_2,C_{NH_4}} + C_{dox}(i,j,k)}\right] \quad 4.182$$

Temperature coefficient also applicable to $R_{C_{NH_4}}\_\text{nit}(i,j,k)$:

Nitrate

$$\frac{dC_{NO3}(i,j,k)}{dt} = R_{C_{NH_4}}\_\text{nit}(i,j,k) - \left\{\sum_{p=1}^{m} R_{C_{phy,p}}\_\text{PP}(i,j,k)\times \text{r\_f}(i,j,\text{k})\right\}\times \text{rNC\_dec}$$
$$-\left\{\sum_{q}^{3} R_{C_{NO3},Cpoc,q}\_\text{denit}(i,j,k)\right\} + \left(\frac{Aflux\_s2w_{no3}(i,j)}{\Delta\sigma}\right)\times flag1\_1 \quad 4.183$$

Particulate Silica

$$\frac{dC_{PSi}(i,j,k)}{dt} = \sum_{p=1}^{2}\left\{R_{C_{phy,p}}\_\text{Mor}(i,j,k)\times \text{rSiC\_phy,p}\times \text{rSi\_PSi}\right\}$$
$$-R_{C_{Si}}\_\text{pro}(i,j,k)\times \text{rSi\_PSi} \quad 4.184$$

Dissolved silica production rate or Particulate silica dissolution rate

Rate of silica production $R_{C_{Si}}\_\text{pro}(i,j,k)$ follows 1st order reaction rate constant $k_{C_{Si}}\_\text{pro}$, $R_{C_{Si}}\_\text{pro}(i,j,k)$ is proportional to the silica solubility deficit $\left[C_{Si,sat} - C_{Si}(i,j,k)\right]$, $R_{C_{Si}}\_\text{pro}(i,j,k)$ is proportional to the particulate biogenic silica concentration, and $R_{C_{Si}}\_\text{pro}(i,j,k)$ follows the temperature coefficient:

$$R_{C_{Si}}\_\text{pro}(i,j,k) = k_{C_{Si}}\theta_{C_{Si}}^{(tempt(i,j,k)-20)}\left[C_{PSi}(i,j,k)\right]\left[C_{Si,sat} - C_{Si}(i,j,k)\right] \quad 4.185$$

$R_{C_{Si}}\_\text{pro}(i,j,k)$ follows Michaelis-Menton expression:

$$R_{C_{Si}}\_\text{pro}(i,j,k) = k_{C_{Si}}\theta_{C_{Si}}^{(tempt(i,j,k)-20)}\left[\frac{C_{PSi}(i,j,k)}{C_{PSi}(i,j,k)+K_{M,C_{PSi}}}\right]\left[C_{Si,sat}-C_{Si}(i,j,k)\right] \quad 4.186$$

Dissolved Silica

$$\frac{dC_{Si}(i,j,k)}{dt} = R_{C_{Si}}\_\text{pro}(i,j,k) - \sum_{p=1}^{2}\left\{\text{R}_{C_{phy,p}}\_\text{PP}(i,j,k)\right\}\times \text{rSiC\_phy,p} + \left(\frac{Aflux\_s2w_{si}(i,j)}{\Delta\sigma}\right)\times flag1\_1 \quad 4.187$$

Sulfide

$$\frac{dC_{H_2S}(i,j,k)}{dx} = \left\{\sum_{q=1}^{2} R_{C_{poc,q}}\_\text{dec\_anoxic\_so}4(i,j,k)\right\}\times \text{rCS\_dec} - R_{C_{H_2S}}\_\text{oxi}(i,j,k) + \left(\frac{Aflux\_s2w_{h2s}(i,j)}{\Delta\sigma}\right)\times flag1\_1 \quad 4.188$$

Sulfide oxidation rate

Rate of sulfide oxidation $R_{C_{H_2S}}\_\text{oxi}(i,j,k)$ follows 1st order reaction rate constant $k_{C_{H_2S}}\_\text{oxi}$, $R_{C_{H_2S}}\_\text{oxi}(i,j,k)$ depends on the concentration of oxygen:

$$R_{C_{H_2S}}\_\text{oxi}(i,j,k) = k_{C_{H_2S}}\_\text{oxi}\left[\frac{C_{dox}(i,j,k)}{K_{M,C_{H_2S},O_2}}\right]\frac{1}{\text{rCS\_oxi}} \quad 4.189$$

Temperature coefficient also applicable for $R_{C_{H_2S}}\_\text{oxi}(i,j,k)$:

$$R_{C_{H_2S}}\_\text{oxi}(i,j,k) = k_{C_{H_2S}}\_\text{oxi}\times\theta_{C_{H_2S}}^{(tempt(i,j,k)-20)}\left[\frac{C_{dox}(i,j,k)}{K_{M,C_{H_2S},O_2}}\right]\frac{1}{\text{rOS\_oxi}} \quad 4.190$$

Dissolved Oxygen

$$\frac{dC_{dox}(i,j,k)}{dx} = \left\{\begin{array}{l}\sum_{p=1}^{m} R_{C_{phy,p}}\_\text{PP}(i,j,k) \\ -\sum_{p=1}^{m} R_{C_{phy,p}}\_\text{Met}(i,j,k) \\ -R_{C_{zoo}}\_\text{Met}(i,j,k) \\ -\sum_{q=1}^{2} R_{B_{poc,q}}\_\text{dec\_oxic}(i,j,k)\end{array}\right\}\times \text{rOC\_dec} - R_{C_{NH_4}}\_\text{nit}(i,j,k)\times \text{rON\_nit} - R_{C_{H_2S}}\_\text{oxi}(i,j,k)\times \text{rOS\_oxi} + \left|\frac{K_{re}\times(\text{C}_{dox}\_sat - C_{dox}(i,j,k)}{\Delta\sigma}\right|_{k=ke} + \left(\frac{Aflux\_s2w_{dox}(i,j)}{\Delta\sigma}\right)\times flag1\_1 \quad 4.191$$

5. BENTHIC MODULE IN ECOSYSTEM MODEL

This model has 2000 m × 2000 m horizontal grid resolution which coincides on the horizontal grid system of water column. Initial thickness of the active sediment layer has considered as 50cm and it comprises with 25 multi-layers which have different layer thickness (**Fig 5.1)**. The relationship between porosity and POCC was derived based on the relationship which has been emerged between the water content and POCC through data analysis (Okada and Furukawa, 2005). Porosity was calculated in each time step based on the POCC. The thickness of each layer was renewed with respect to porosity.

Staggered grid system defining scalars at the main grid points and velocities at the grid surfaces (with respect to the main grid points velocity components are staggered) have been used (**Fig 3.3**).

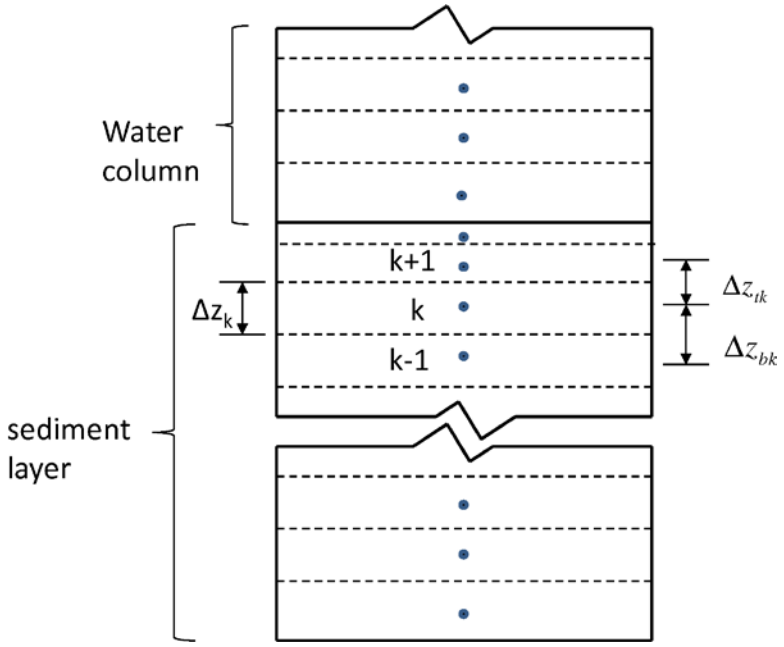

Fig 5.1 Vertical grid system for sediment column

5.1 Porosity change with respect to particulate organic carbon content

Sediment sample compose of inorganic sediment considered in this study as silt, particulate organic carbon, particulate silica and water as shown in the **Fig 5.2** where m_b is the bulk mass

of sediment, m_w is the mass of water, m_{st} is the mass of dry sediment, V_b is the bulk volume of sediment, V_w is the water volume, V_{st} is the volume of dry sediment, ρ_w is the density of water, ρ_{st} is the density of dry sediment, ϕ is the porosity and n is the time step. Assume the relationship developed by (T Okada and Furukawa, 2005) between POCC which has been considered as m_{poc}/m_{st} in (mg/g) and WC which has been considered as m_w/m_{st} in (%). m_{poc} is the mass of POC in gram.

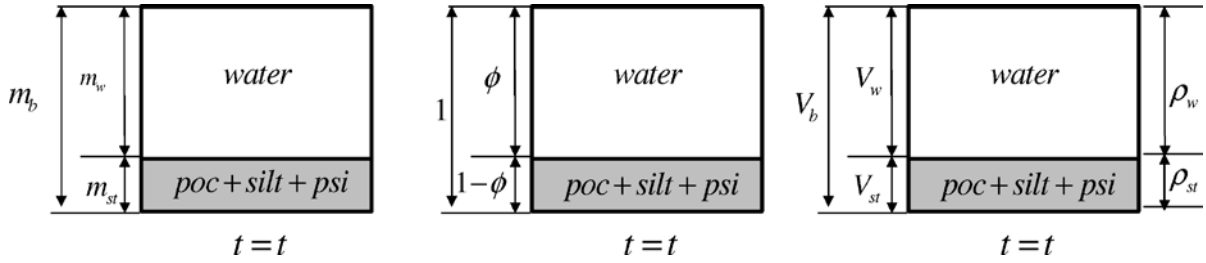

Fig 5.2 Schematic diagram of sediment composition

$$\frac{m_{poc}}{m_{st}} = 0.075 \times WC + 1.12 \tag{5.1}$$

$$WC = \frac{m_w}{m_{st}} \times 100 \tag{5.2}$$

$$WC = \frac{\rho_w V_w}{\rho_{st} V_{st}} \times 100 \tag{5.3}$$

$$WC = \frac{\rho_w \phi V_b}{\rho_{st} (1-\phi) V_b} \times 100 \tag{5.4}$$

$$WC = \frac{\phi}{(1-\phi)} \frac{\rho_w}{\rho_{st}} \times 100 \tag{5.5}$$

Substituting equation **5.5** in **5.1**:

$$\frac{m_{poc}}{m_{st}} = 0.075 \times \frac{\phi}{(1-\phi)} \frac{\rho_w}{\rho_{st}} \times 100 + 1.12 \tag{5.6}$$

$$\frac{m_{poc}}{m_{st}} - 1.12 = 7.5 \times \frac{\phi}{(1-\phi)} \frac{\rho_w}{\rho_{st}} \tag{5.7}$$

$$\left(\frac{m_{poc}}{m_{st}}-1.12\right)\frac{\rho_{st}}{7.5\rho_w}=\frac{\phi}{(1-\phi)} \tag{5.8}$$

$$\left(\frac{m_{poc}}{m_{st}}-1.12\right)\frac{\rho_{st}}{7.5\rho_w}=\phi\left[1+\left(\frac{m_{poc}}{m_{st}}-1.12\right)\frac{\rho_{st}}{75\rho_w}\right] \tag{5.9}$$

$$\phi=\frac{\left(\frac{m_{poc}}{m_{st}}-1.12\right)\frac{\rho_{st}}{7.5\rho_w}}{\left[1+\left(\frac{m_{poc}}{m_{st}}-1.12\right)\frac{\rho_{st}}{75\rho_w}\right]} \tag{5.10}$$

$$\phi=\frac{1}{\left[1+\frac{1}{\left(\frac{m_{poc}}{m_{st}}-1.12\right)\frac{\rho_{st}}{7.5\rho_w}}\right]} \tag{5.11}$$

In order to keep the model stability the porosity variation w.r.t. POCC is considered as:

$$\phi=\frac{1}{\left[1+\frac{1}{\left(\frac{m_{poc}}{m_{st}}+1.12\right)\frac{\rho_{st}}{7.5\rho_w}}\right]} \tag{5.12}$$

This variation has been plotted in **Fig 5.3**.

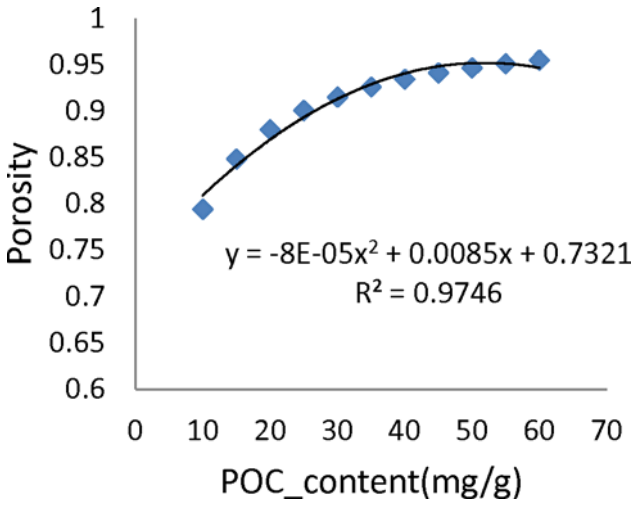

Fig 5.3 Variation of porosity with respect to particulate organic carbon content

5.2 Layer thickness adjustment

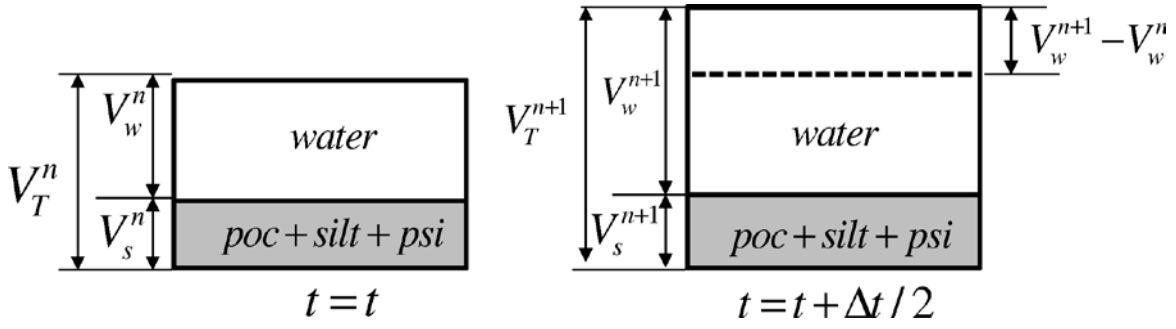

Fig 5.4 Effect of POCC on layer thickness change

It has been assumed that porosity increases after time $\Delta t / 2$ with the increase of POCC in sediment increasing porosity ($\phi^{n+1} \rangle \phi^n$). This increases the total volume of the control volume as from V_T^n to V_T^{n+1} as shown in the **Fig 5.4** when n is the time step considered.

At $t = t$, volume of dry sediment can be written as $V_s^n = (1 - \phi_n) V_T^n$

At $t = t + \Delta t / 2$, volume of dry sediment can be written as $V_s^{n+1} = (1 - \phi_{n+1}) V_T^{n+1}$

During the time step $\Delta t / 2$ ($\Delta t = 100s$) it has been assumed that the change of the volume of dry sediment is negligible and hence,

$$V_s^n = V_s^{n+1} \tag{5.13}$$

$$(1 - \phi^n) V_T^n = (1 - \phi^{n+1}) V_T^{n+1} \tag{5.14}$$

$$V_T^{n+1} = \frac{(1 - \phi^n)}{(1 - \phi^{n+1})} V_T^n \tag{5.15}$$

$$V_T^{n+1} = MF \times V_T^n \tag{5.16}$$

$$MF = \frac{(1 - \phi^n)}{(1 - \phi^{n+1})} \tag{5.17}$$

Then new layer thickness has been computed as;

$$\Delta z^{n+1} = MF \times \Delta z^{n} \qquad 5.18$$

5.3 Renewal of concentrations of state variables

With the change of layer thickness the concentrations of the state variables which have been defined with respect to the bulk volume of the control volume has to be renewed.

At $t = t$, concentration of any dependent variable B can be written as; $B^{n} = \frac{m_B^{n}}{V_T^{n}}$

At $t = t + \Delta t/2$, concentration of any dependent variable B can be written as; $B^{n+1} = \frac{m_B^{n+1}}{V_T^{n+1}}$

where, m_B^{n} is the mass of dependent variable at $t = t$ and m_B^{n+1} is the mass of dependent variable at $t = t + \Delta t/2$.

During the time step $\Delta t/2$ ($\Delta t = 100s$) mass conservation has to be satisfied and hence,

$$m_B^{n} = m_B^{n+1} \qquad 5.19$$

$$B^{n} V_T^{n} = B^{n+1} V_T^{n+1} \qquad 5.20$$

$$\text{Since, } V_T^{n+1} = MF \times V_T^{n} \qquad 5.21$$

$$B^{n} V_T^{n} = B^{n+1} \left(MF \times V_T^{n} \right) \qquad 5.22$$

Then, the new concentration of any state variable is computed as;

$$B^{n+1} = \frac{B^{n}}{MF} \qquad 5.23$$

5.4 Governing differential equations for any scalar parameter

Three dimensional layer-resolved advection and diffusion equation in Cartesian coordinates is developed for sediment column by adopting control volume formulation with staggered grid system. The conservation of mass over control volume V with dimensions $\Delta x, \Delta y, \Delta z$ is considered (**Fig 5.5**).

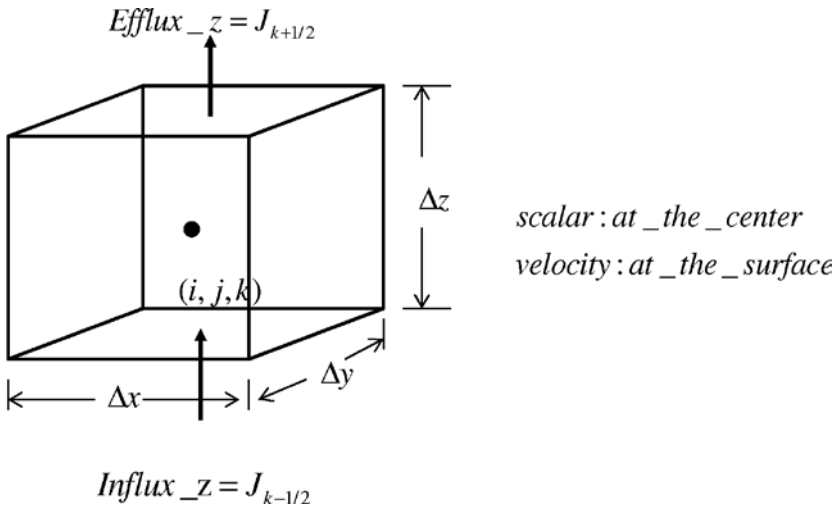

Fig 5.5 Influx and efflux to the control volume

The typical dependent variable B in the sediment has been defined as, $B_{\mathrm{i,j},k}$; the rate of change of mass per unit volume or the concentration of the material within the control volume V where, $i = 0 \sim (i\max+1)$: grid in x-direction, $j = 0 \sim (j\max+1)$: grid in y-direction and $k = (-kb\max) \sim 0$: grid in z-direction. Assume the porosity; $\phi_{\mathrm{i,j},k}$ in control volume V varies with the space and depth within the sediment. Advection flux has been considered as the flux due to burial effect. That is moving of some materials with a velocity ω_b by keeping the grid system constant. (This will be in some other way shifting of layers with a velocity ω_b to keep the grid system constant). ω is positive upwards and hence, in the case of accumulation $\omega_b = \omega_a$ will be negative while in the case of erosion $\omega_b = \omega_e$ will be positive. In case of no particle motion due to advection; $\omega_b = 0$. In the case of accumulation material with thickness $\omega_a \Delta t$ moves out from the computational domain while in the case of erosion material with thickness $\omega_e \Delta t$ added to the bottom of the active layer as shown in the **Fig 5.6**.

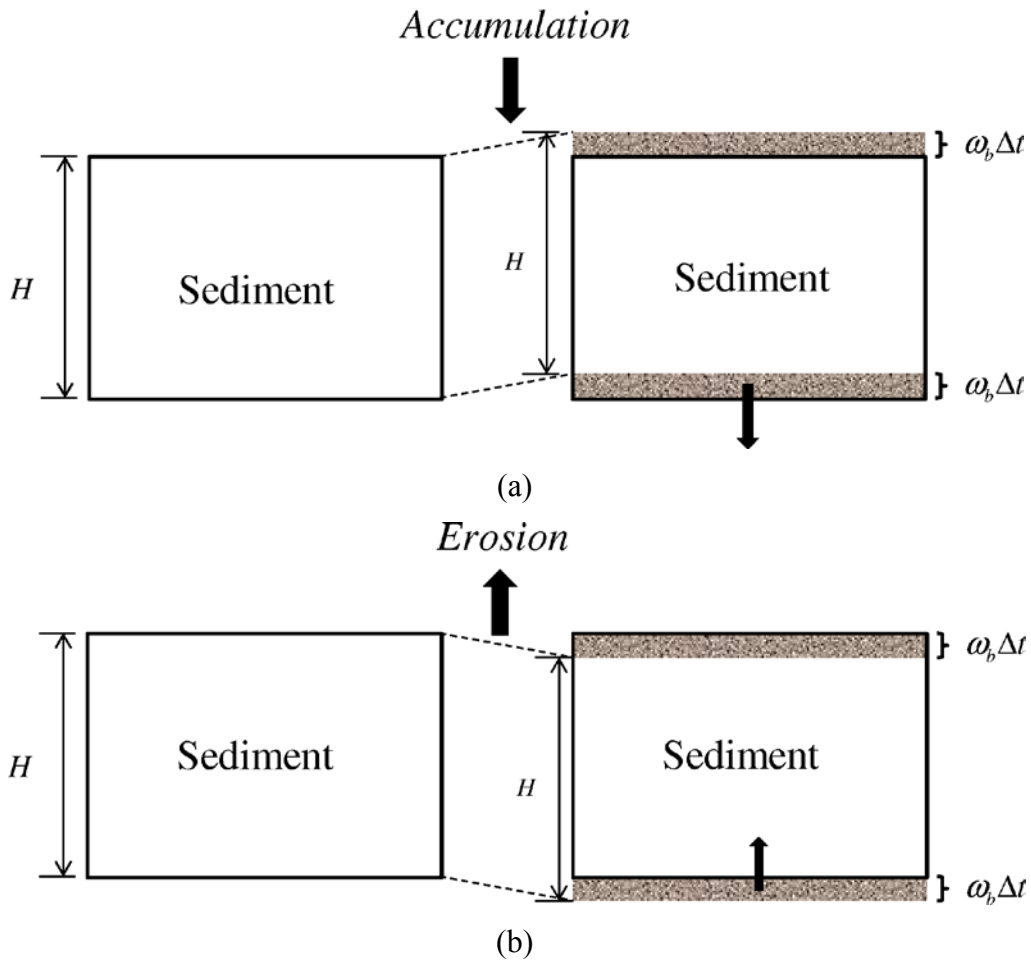

Fig 5.6 Movement of sediment material due to (a) deposition and (b) erosion

Development of governing differential equations for sediment column has been done independently for dissolved and particulate material.

5.4.1 Dissolved matter

For the conservation of mass within the control volume V, the net change of mass should be equivalent to the net mass influx due to advection and diffusion and the mass generation of species due to reactions. Hence, mass conservation equation can be written as;

$$\begin{aligned} &Mass\_change = net\_nass\_diffusion\_flux \\ &+net\_mass\_advectiion\_flux + mass\_source\_gen \end{aligned} \qquad 5.24$$

Taking n as the present time step, the net change of mass during time period of Δt can be written as;

$$Mass\_change = \left(B_{i,j,k}^{n+1} - B_{i,j,k}^{n} \right) \Delta x \Delta y \Delta z_k \phi_{i,j,k} \quad 5.25$$

Net mass advection flux to the control volume V can be written as;

$$Net\_mass\_advection\_flux = -\left(\omega_t B_t \phi_t - \omega_b B_b \phi_b \right) \Delta x \Delta y \Delta t \quad 5.26$$

$$Net\_mass\_advection\_flux = -\left(\omega_{i,j,k+1/2} B_{i,j,k+1/2} \phi_{i,j,k+1/2} - \omega_{i,j,k-1/2} B_{i,j,k-1/2} \phi_{i,j,k-1/2} \right) \Delta x \Delta y \Delta t \quad 5.27$$

Suppose J denotes the diffusion flux influencing a typical dependent variable B in the sediment. The flux $Influx\_z = J_{i,j,k-1/2}$ is entering to the control volume face $\Delta x \Delta y$ while the flux leaving the opposite face is $Efflux\_z = J_{i,j,k+1/2}$ after the time period of Δt. The mass net Influx over the control volume face $\Delta x \Delta y$ can be written as;

$$Net\_mass\_dissfusion\_flux = -\left(flux_t \times \phi_t - flux_b \times \phi_b \right) \Delta x \Delta y \Delta t \quad 5.28$$

$$Net\_mass\_dissfusion\_flux = -\left(J_{i,j,k+/2} \phi_{i,j,k+1/2} - J_{i,j,k-1/2} \phi_{i,j,k-1/2} \right) \Delta x \Delta y \Delta t \quad 5.29$$

Diffusion flux $J_{i,j,k}$ can be expressed by the Fick's law as; $J_{i,j,k} = -K_{i,j,k} \dfrac{\partial B_{i,j,k}}{\partial z}$ where $K_{n,k}$ is the diffusion coefficient in z-direction (m^2/s). Hence;

$$Net\_mass\_dissfusion\_flux = -\begin{bmatrix} \left(-K_{i,j,k+1/2} \dfrac{\partial B_{i,j,k+1/2}}{\partial z} \right) \phi_{i,j,k+1/2} \\ -\left(-K_{i,j,k-1/2} \dfrac{\partial B_{i,j,k-1/2}}{\partial z} \right) \phi_{i,j,k-1/2} \end{bmatrix} \Delta x \Delta y \Delta t \quad 5.30$$

$$Net\_mass\_dissfusion\_flux = \begin{bmatrix} \left(K_{i,j,k+1/2} \dfrac{\partial B_{i,j,k+1/2}}{\partial z} \right) \phi_{i,j,k+1/2} \\ -\left(K_{i,j,k-1/2} \dfrac{\partial B_{i,j,k-1/2}}{\partial z} \right) \phi_{i,j,k-1/2} \end{bmatrix} \Delta x \Delta y \Delta t \quad 5.31$$

Let the rate of generation of chemical species over control volume; $\sum_j R_j$. Then the generation of species over control volume during time period of Δt can be written as,

$$Sourec\_gen = \left[\sum_j R_j \right] \Delta x \Delta y \Delta z_k \phi_{i,j,k} \Delta t \quad 5.32$$

Equations **5.25**, **5.27**, **5.31** and **5.32** can be combined to make the mass conservation over the control volume as;

$$\left(B_{i,\mathrm{j},k}^{n+1}-B_{i,\mathrm{j},k}^{n}\right)\Delta x\Delta y\Delta z_k\phi_{i,\mathrm{j},k}=-\left(\omega_{i,\mathrm{j},k+1/2}B_{i,\mathrm{j},k+1/2}\phi_{i,\mathrm{j},k+1/2}-\omega_{i,\mathrm{j},k-1/2}B_{i,\mathrm{j},k-1/2}\phi_{i,\mathrm{j},k-1/2}\right)\Delta x\Delta y\Delta t$$
$$+\left[\left(K_{i,\mathrm{j},k+1/2}\frac{\partial B_{i,\mathrm{j},k+1/2}}{\partial z}\right)\phi_{i,\mathrm{j},k+1/2}-\left(K_{i,\mathrm{j},k-1/2}\frac{\partial B_{i,\mathrm{j},k-1/2}}{\partial z}\right)\phi_{i,\mathrm{j},k-1/2}\right]\Delta x\Delta y\Delta t \qquad 5.33$$
$$+\left[\sum_j R_j\right]\Delta x\Delta y\Delta z\phi_{i,\mathrm{j},k}\Delta t$$

$$\frac{\left(B_{i,\mathrm{j},k}^{n+1}-B_{i,\mathrm{j},k}^{n}\right)}{\Delta t}\phi_{i,\mathrm{j},k}=-\frac{\left(\omega_{i,\mathrm{j},k+1/2}B_{i,\mathrm{j},k+1/2}\phi_{i,\mathrm{j},k+1/2}-\omega_{i,\mathrm{j},k-1/2}B_{i,\mathrm{j},k-1/2}\phi_{i,\mathrm{j},k-1/2}\right)}{\Delta z_k}$$
$$+\frac{\left[\left(K_{i,\mathrm{j},k+1/2}\frac{\partial B_{i,\mathrm{j},k+1/2}}{\partial z}\right)\phi_{i,\mathrm{j},k+1/2}-\left(K_{i,\mathrm{j},k-1/2}\frac{\partial B_{i,\mathrm{j},k-1/2}}{\partial z}\right)\phi_{i,\mathrm{j},k-1/2}\right]}{\Delta z_k}+\left[\sum_j R_j\right]\phi_{i,\mathrm{j},k} \qquad 5.34$$

$$\frac{\partial B_{i,\mathrm{j},k}}{\partial t}\times\phi_{i,\mathrm{j},k}=-\omega_{i,\mathrm{j}}\frac{\partial\left(B_{i,\mathrm{j},k}\times\phi_{i,\mathrm{j},k}\right)}{\partial z}+\frac{\partial}{\partial z}\left[K_{i,\mathrm{j},k}\times\phi_{i,\mathrm{j},k}\times\frac{\partial B_{i,\mathrm{j},k}}{\partial z}\right]+\left[\sum_j R_j\right]\phi_{i,\mathrm{j},k} \qquad 5.35$$

$$\frac{\partial B_{i,\mathrm{j},k}}{\partial t}\times\phi_{i,\mathrm{j},k}-\frac{\partial}{\partial z}\left[K_{i,\mathrm{j},k}\times\phi_{i,\mathrm{j},k}\times\frac{\partial B_{i,\mathrm{j},k}}{\partial z}\right]+\omega_{i,\mathrm{j}}\frac{\partial\left(B_{i,\mathrm{j},k}\times\phi_{i,\mathrm{j},k}\right)}{\partial z}=\left[\sum_j R_j\right]\phi_{i,\mathrm{j},k} \qquad 5.36$$

Partitioning of the dissolved nutrients have been considered in the model due to the effects of sorption and desorption. As shown in the

Fig 5.7 nutrients especially phosphorus can have two phases: within the pore water and attached to sediment.

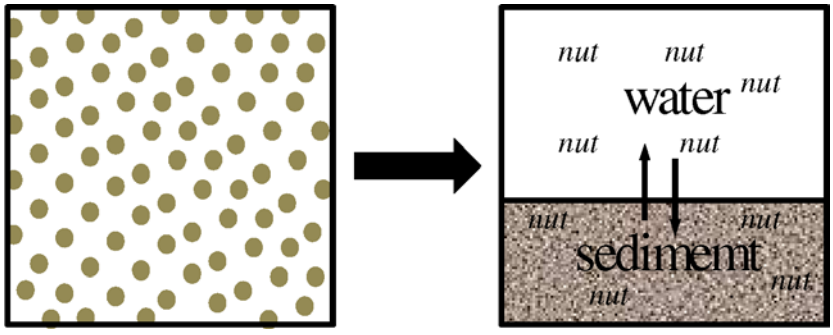

Fig 5.7 Sorption and desorption

Considering the dissolved and particulate fraction of the nutrient B , the diffusion coefficient can be written as; $K_{n,k} = \left(f_p D_p + f_d D_d \right)_{i,\mathrm{j},k}$ where f_p : Particulate fraction, f_d : Dissolve fraction, D_p : Diffusion coefficient for particulate phase mixing and D_d : Diffusion coefficient for dissolved phase mixing. The particulate and dissolved fractions have been computed according to the following equations **5.37** and **5.38** (Di Toro, 2001) except for dissolved oxygen and nitrate which have $f_d = 1$.

$$f_{d_{i,j,k}} = \frac{1}{1 + m_{i,j,k}\pi_{i,j,k} \Big/ \phi_{i,j,k}} \tag{5.37}$$

$$f_{p_{i,j,k}} = \frac{m_{i,j,k}\pi_{i,j,k} \Big/ \phi_{i,j,k}}{1 + m_{i,j,k}\pi_{i,j,k} \Big/ \phi_{i,j,k}} \tag{5.38}$$

$m_{i,j,k}$ is the concentration of solids or mass of solids per unit bulk volume and has been computed as;

$$m_{i,j,k} = Bsilt^n_{i,j,k} + BpocL^n_{i,j,k} + BpocR^n_{i,j,k} + Bpsi^n_{i,j,k} \tag{5.39}$$

$\pi_{i,j,k}$ depends on each state variable and computed through a developed method for a multi-layer model referring two layer model approach (Di Toro, 2001) and (Ji, 2008). Ammonia always has $\pi_{i,j,k} = 1$ while it has been computed for phosphorous, silica and sulfur as;

$$\text{if } B_{dox}(i,j,k) \le B_{dox}\_criti\_nut$$

$$\pi_{nut} = \pi_{po4\_anaerobic\_nut} \tag{5.40}$$

$$\text{else if } C_{dox}(i,j,1) \ge C_{dox}\_criti\_nut$$

$$\pi_{nut} = \pi_{po4\_anaerobic} \times \Delta\pi_{po4} \tag{5.41}$$

$$\text{else if } C_{dox}(i,j,1) \le C_{dox}\_criti\_nut$$

$$\pi_{nut} = \pi_{po4\_anaerobic\_nut} \times \left(\Delta\pi_{nut} \right)^{\frac{C_{dox}(i,j,1)}{C_{dox}\_criti\_\mathrm{nut}}} \tag{5.42}$$

Hence, governing differential equation for any dissolved material in the sediment can be written as;

$$\frac{\partial B_{i,\mathrm{j},k}}{\partial t}\times\phi_{i,\mathrm{j},k}+\omega_{i,\mathrm{j}}\frac{\partial\left(B_{i,\mathrm{j},k}\times\phi_{i,\mathrm{j},k}\right)}{\partial z}=\frac{\partial}{\partial z}\left[\left(f_pD_p+f_dD_d\right)_{i,\mathrm{j},k}\times\phi_{i,\mathrm{j},k}\times\frac{\partial B_{i,\mathrm{j},k}}{\partial z}\right]+\left[\sum_j R_j\right]\phi_{i,\mathrm{j},k} \qquad 5.43$$

For the convenience split operator is used to decompose the equation **5.43**.

Only the advection and diffusion;

$$\frac{\partial B_{i,\mathrm{j},k}}{\partial t}\times\phi_{i,\mathrm{j},k}+\omega_{i,\mathrm{j}}\frac{\partial\left(B_{i,\mathrm{j},k}\times\phi_{i,\mathrm{j},k}\right)}{\partial z}=\frac{\partial}{\partial z}\left[\left(f_pD_p+f_dD_d\right)_{i,\mathrm{j},k}\times\phi_{i,\mathrm{j},k}\times\frac{\partial B_{i,\mathrm{j},k}}{\partial z}\right] \qquad 5.44$$

Only source terms;

$$\frac{\partial B_{i,j,k}}{\partial t}=\sum_j R_j \qquad 5.45$$

Finite difference method with the fourth order Runge-Kutta method which gives the approximation of solutions of ordinary differential equations through explicit approach is used to obtain the solution for the source term equation **5.45**. This approach has been explained in detail under pelagic model (0).

5.4.1.1 Discretization of advection and diffusion equation

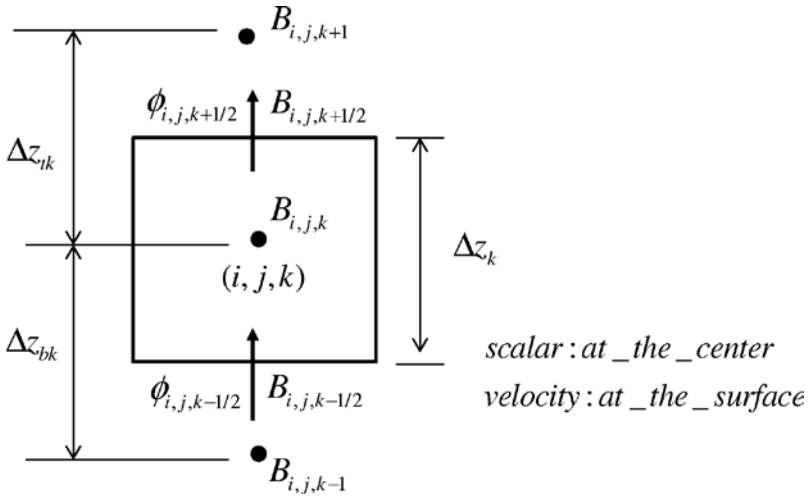

Fig 5.8 2D Control volume

As shown in the **Fig 5.8** scalars have been defined at the centre of the control volume while flux and porosities have been defined at the surface of the control volume. Consider only the advection and diffusion equation **5.44** and develop the discretized form. This has been done in three steps.

1. Consider only the time dependency term

$$\frac{\partial B_{i,j,k}}{\partial t} \times \phi_{i,j,k} = \left(\frac{B_{i,j,k}^{n+1} - B_{i,j,k}^{n}}{\Delta t} \right) \phi_{i,j,k} \qquad 5.46$$

2. Consider only the advection term

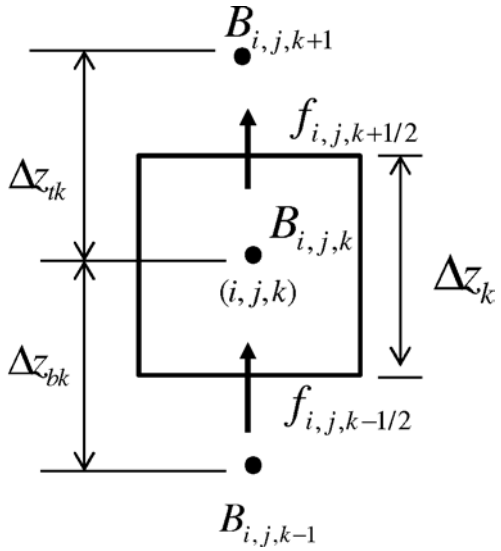

Fig 5.9 Advection term at CV faces

$$\omega_{i,j} \frac{\partial \left(B_{i,j,k} \times \phi_{i,j,k} \right)}{\partial z} = \omega_{i,j} \frac{\left(f_{i,j,k+1/2} - f_{i,j,k-1/2} \right)}{\Delta z_k} \qquad 5.47$$

where,

$$f_{i,j,k+1/2} = B_{i,j,k+1/2} \phi_{i,j,k+1/2} \qquad 5.48$$

$$f_{i,j,k-1/2} = B_{i,j,k-1/2} \phi_{i,j,k-1/2} \qquad 5.49$$

Evaluating the concentrations implicitly and the porosities, sediment layer thickness and burial rate explicitly;

$$\omega_{i,j}\frac{\partial\left(B_{i,j,k}\times\phi_{i,j,k}\right)}{\partial z}=\frac{\omega_{i,j}^{n}}{\Delta z_{k}^{n}}\left(B_{i,j,k+1/2}^{n+1}\phi_{i,j,k+1/2}^{n}-B_{i,j,k-1/2}^{n+1}\phi_{i,j,k-1/2}^{n}\right) \tag{5.50}$$

Use the first order upwind scheme (**Fig 5.10**) to evaluate the surface concentrations.

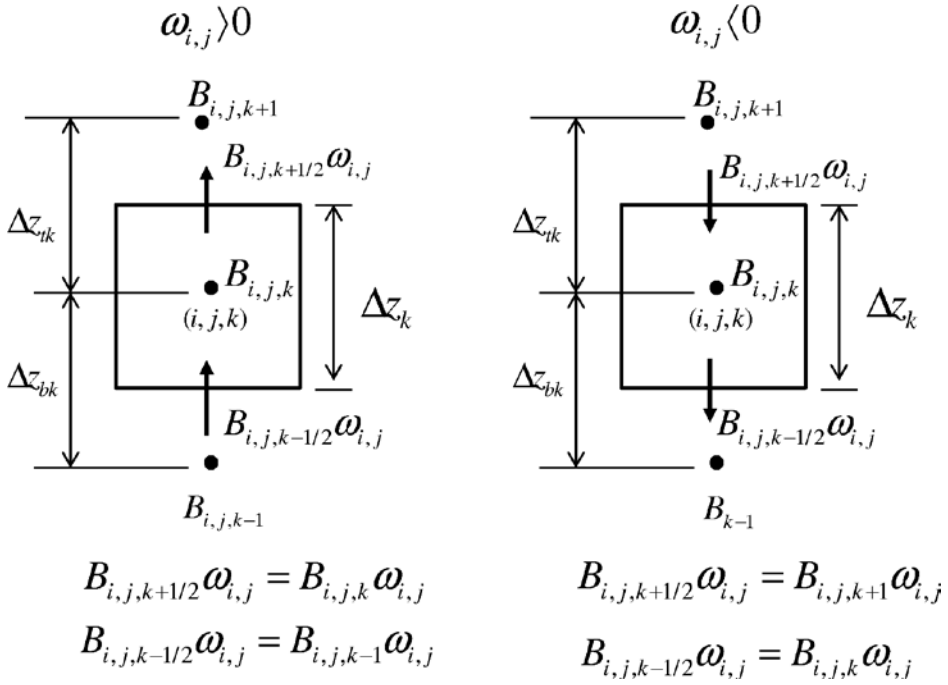

Fig 5.10 Upwind scheme approach

$$B_{i,j,k+1/2}^{n+1}=B_{i,j,k}^{n+1}\ \text{if}\ \omega_{i,j}^{n}\rangle 0 \tag{5.51}$$

$$B_{i,j,k+1/2}^{n+1}=B_{i,j,k+1}^{n+1}\ \text{if}\ \omega_{i,j}^{n}\langle 0 \tag{5.52}$$

$$B_{i,j,k-1/2}^{n+1}=B_{i,j,k-1}^{n+1}\ \text{if}\ \omega_{i,j}^{n}\rangle 0 \tag{5.53}$$

$$B_{i,j,k-1/2}^{m+1}=B_{i,j,k}^{m+1}\ \text{if}\ \omega_{i,j}^{n}\langle 0 \tag{5.54}$$

Define a new operator $[\![A,B]\!]$ to denote the greater of A and B. Then the upwind scheme implies (Patankar, 1980);

$$\omega_{i,j}^{n}B_{i,j,k+1/2}^{n+1}=B_{i,j,k}^{n+1}[\![\omega_{i,j}^{n},0]\!]-B_{i,j,k+1}^{n+1}[\![-\omega_{i,j}^{n},0]\!] \tag{5.55}$$

$$\omega_{i,j}^{n}B_{i,j,k-1/2}^{n+1}=B_{i,j,k-1}^{n+1}[\![\omega_{i,j}^{n},0]\!]-B_{i,j,k}^{n+1}[\![-\omega_{i,j}^{n},0]\!] \tag{5.56}$$

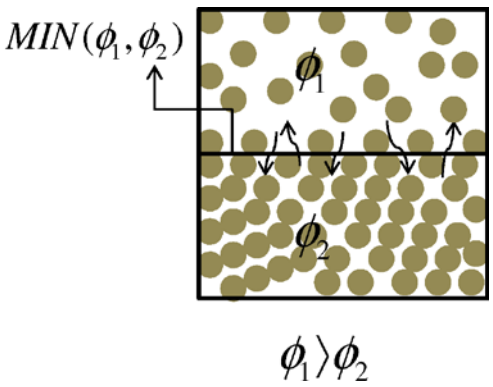

Fig 5.11 Porosity between two adjacent layers in sediment

Porosity effect or the movement of material between two adjacent sediment layers is decided by the minimum porosity between the two layers as shown in the **Fig 5.11**. Hence, evaluating the control volume face porosities as the minimum between adjacent layer porosities;

$$\phi^n_{i,j,k+1/2} = MIN\left(\phi^n_{i,j,k+1}, \phi^n_{i,j,k}\right) \tag{5.57}$$

$$\phi^n_{i,j,k-1/2} = MIN\left(\phi^n_{i,j,k}, \phi^n_{i,j,k-1}\right) \tag{5.58}$$

Then the advection term can be written as;

$$\omega_{i,j}\frac{\partial\left(B_{i,j,k}\times\phi_{i,j,k}\right)}{\partial z} = \frac{1}{\Delta z^n_k}\begin{bmatrix}\left(B^{n+1}_{i,j,k}\left[\!\left[\omega^n_{i,j},0\right]\!\right] - B^{n+1}_{i,j,k+1}\left[\!\left[-\omega^n_{i,j},0\right]\!\right]\right)MIN\left(\phi^n_{i,j,k+1},\phi^n_{i,j,k}\right)\\ -\left(B^{n+1}_{i,j,k-1}\left[\!\left[\omega^n_{i,j},0\right]\!\right] - B^{n+1}_{i,j,k}\left[\!\left[-\omega^n_{i,j},0\right]\!\right]\right)MIN\left(\phi^n_{i,j,k},\phi^n_{i,j,k-1}\right)\end{bmatrix} \tag{5.59}$$

3. Consider only the diffusion term

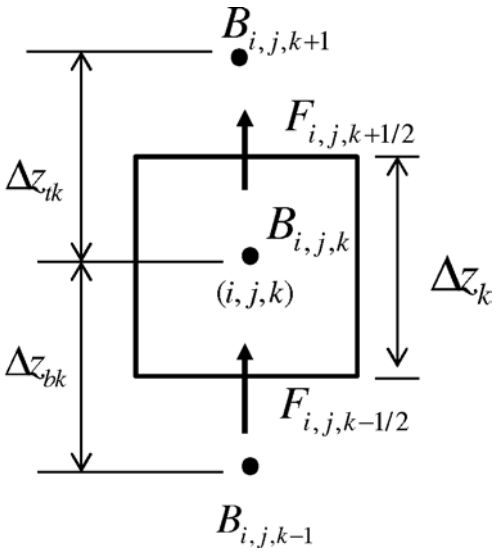

Fig 5.12 Diffusion term at CV faces

$$\frac{\partial}{\partial z}\left[\left(f_p D_p + f_d D_d\right)_{i,j,k} \times \phi_{i,j,k} \times \frac{\partial B_{i,j,k}}{\partial z}\right] = \frac{\partial}{\partial z}\left[K_{i,j,k} \times \phi_{i,j,k} \times \frac{\partial B_{i,j,k}}{\partial z}\right] \tag{5.60}$$

$$\frac{\partial}{\partial z}\left[\left(f_p D_p + f_d D_d\right)_{i,j,k} \times \phi_{i,j,k} \times \frac{\partial B_{i,j,k}}{\partial z}\right] = \frac{\left(F_{i,j,k+1/2} - F_{i,j,k-1/2}\right)}{\Delta z_k} \tag{5.61}$$

where,

$$F_{i,j,k+1/2} = \left(K_{i,j,k+1/2} \frac{\partial B_{i,j,k+1/2}}{\partial z}\right) \phi_{i,j,k+1/2} \tag{5.62}$$

$$F_{i,j,k-1/2} = \left(K_{i,j,k-1/2} \frac{\partial B_{i,j,k-1/2}}{\partial z}\right) \phi_{i,j,k-1/2} \tag{5.63}$$

$$\frac{\partial}{\partial z}\left[\left(f_p D_p + f_d D_d\right)_{i,j,k} \times \phi_{i,j,k} \times \frac{\partial B_{i,j,k}}{\partial z}\right] = \frac{1}{\Delta z_k}\left[\begin{array}{l}\left(K_{i,j,k+1/2} \frac{\partial B_{i,j,k+1/2}}{\partial z}\right) \phi_{i,j,k+1/2} \\ -\left(K_{i,j,k-1/2} \frac{\partial B_{i,j,k-1/2}}{\partial z}\right) \phi_{i,j,k-1/2}\end{array}\right] \tag{5.64}$$

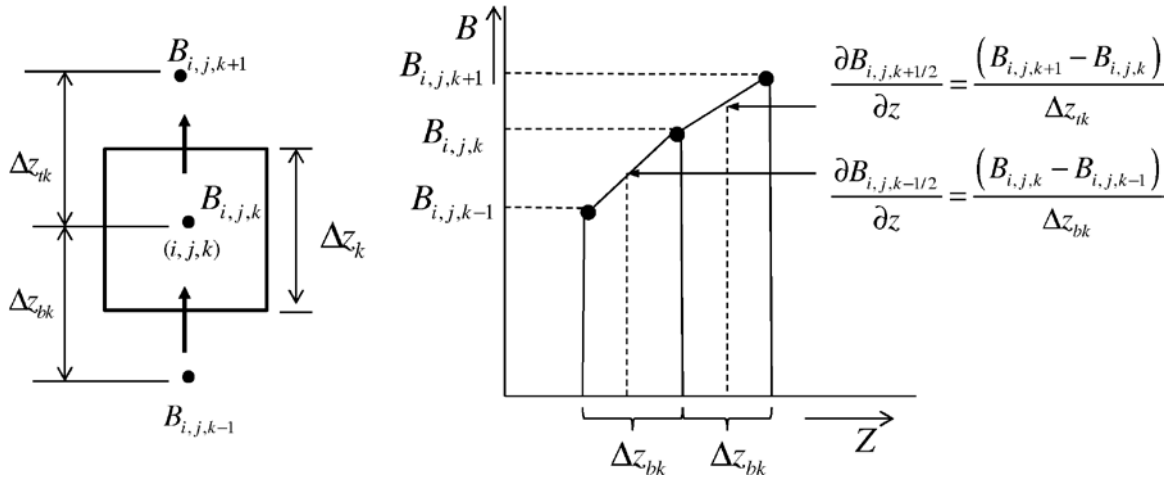

Fig 5.13 Piecewise-linear profile assumption in vertical direction

Evaluating the concentrations implicitly from the piecewise-linear profile: assumes linear distribution between two grid points (

Fig 5.13) and sediment layer thickness explicitly;

$$\frac{\partial B_{i,j,k+1/2}}{\partial z} = \frac{\left(B^{n+1}_{i,j,k+1} - B^{n+1}_{i,j,k}\right)}{\Delta z^{n}_{tk}} \tag{5.65}$$

$$\frac{\partial B_{i,j,k-1/2}}{\partial z} = \frac{\left(B^{n+1}_{i,j,k} - B^{n+1}_{i,j,k-1}\right)}{\Delta z^{n}_{bk}} \qquad 5.66$$

where, $\Delta z^{n}_{tk} = \dfrac{\Delta z^{n}_{k} + \Delta z^{n}_{k+1}}{2}$ and $\Delta z^{n}_{bk} = \dfrac{\Delta z^{n}_{k} + \Delta z^{n}_{k-1}}{2}$

Evaluating the boundary porosities explicitly and as the minimum between adjacent layer porosities (equations **5.57**, **5.58**);

$$\frac{\partial}{\partial z}\left[\left(f_p D_p + f_d D_d\right)_{i,j,k} \times \phi_{i,j,k} \times \frac{\partial B_{i,j,k}}{\partial z}\right] = \frac{1}{\Delta z^{n}_{k}}\left[\begin{array}{l}\left(K^{n}_{i,j,k+1/2}\dfrac{\left(B^{n+1}_{i,j,k+1} - B^{n+1}_{i,j,k}\right)}{\Delta z^{n}_{tk}}\right) MIN\left(\phi^{n}_{i,j,k+1}, \phi^{n}_{i,j,k}\right) \\ -\left(K^{n}_{i,j,k-1/2}\dfrac{\left(B^{n+1}_{i,j,k} - B^{n+1}_{i,j,k-1}\right)}{\Delta z^{n}_{bk}}\right) MIN\left(\phi^{n}_{i,j,k}, \phi^{n}_{i,j,k-1}\right)\end{array}\right] \qquad 5.67$$

Substituting equations **5.46**, **5.59** and **5.67** in equation **5.44;**

$$\begin{aligned}\left[\frac{B^{n+1}_{i,j,k} - B^{n}_{i,j,k}}{\Delta t}\right]\phi^{n}_{i,j,k} &= -\frac{1}{\Delta z^{n}_{k}}\left[\begin{array}{l}\left(B^{n+1}_{i,j,k}\left[\!\left[\omega^{n}_{i,j}, 0\right]\!\right] - B^{n+1}_{i,j,k+1}\left[\!\left[-\omega^{n}_{i,j}, 0\right]\!\right]\right) MIN\left(\phi^{n}_{i,j,k+1}, \phi^{n}_{i,j,k}\right) \\ -\left(B^{n+1}_{i,j,k-1}\left[\!\left[\omega^{n}_{i,j}, 0\right]\!\right] - B^{n+1}_{i,j,k}\left[\!\left[-\omega^{n}_{i,j}, 0\right]\!\right]\right) MIN\left(\phi^{n}_{i,j,k}, \phi^{n}_{i,j,k-1}\right)\end{array}\right] \\ &+ \frac{\left(f_p D_p + f_d D_d\right)^{n}_{i,j,k+1/2}}{\Delta z^{n}_{k}\Delta z^{n}_{tk}}\left[\left(B^{n+1}_{i,j,k+1} - B^{n+1}_{i,j,k}\right) MIN\left(\phi^{n}_{i,j,k+1}, \phi^{n}_{i,j,k}\right)\right] \\ &- \frac{\left(f_p D_p + f_d D_d\right)^{n}_{i,j,k-1/2}}{\Delta z^{n}_{k}\Delta z^{n}_{bk}}\left[\left(B^{n+1}_{i,j,k} - B^{n+1}_{i,j,k-1}\right) MIN\left(\phi^{n}_{i,j,k}, \phi^{n}_{i,j,k-1}\right)\right]\end{aligned} \qquad 5.68$$

$$\begin{aligned}\left[\frac{B^{n+1}_{i,j,k} - B^{n}_{i,j,k}}{\Delta t}\right] &= -\frac{1}{\Delta z^{n}_{k}}\left[\begin{array}{l}\left(B^{n+1}_{i,j,k}\left[\!\left[\omega^{n}_{i,j}, 0\right]\!\right] - B^{n+1}_{i,j,k+1}\left[\!\left[-\omega^{n}_{i,j}, 0\right]\!\right]\right)\dfrac{MIN\left(\phi^{n}_{i,j,k+1}, \phi^{n}_{i,j,k}\right)}{\phi^{n}_{i,j,k}} \\ -\left(B^{n+1}_{i,j,k-1}\left[\!\left[\omega^{n}_{i,j}, 0\right]\!\right] - B^{n+1}_{i,j,k}\left[\!\left[-\omega^{n}_{i,j}, 0\right]\!\right]\right)\dfrac{MIN\left(\phi^{n}_{i,j,k}, \phi^{n}_{i,j,k-1}\right)}{\phi^{n}_{i,j,k}}\end{array}\right] \\ &+ \frac{\left(f_p D_p + f_d D_d\right)^{n}_{i,j,k+1/2}}{\Delta z^{n}_{k}\Delta z^{n}_{tk}}\left[\left(B^{n+1}_{i,j,k+1} - B^{n+1}_{i,j,k}\right)\frac{MIN\left(\phi^{n}_{i,j,k+1}, \phi^{n}_{i,j,k}\right)}{\phi^{n}_{i,j,k}}\right] \\ &- \frac{\left(f_p D_p + f_d D_d\right)^{n}_{i,j,k-1/2}}{\Delta z^{n}_{k}\Delta z^{n}_{bk}}\left[\left(B^{n+1}_{i,j,k} - B^{n+1}_{i,j,k-1}\right)\frac{MIN\left(\phi^{n}_{i,j,k}, \phi^{n}_{i,j,k-1}\right)}{\phi^{n}_{i,j,k}}\right]\end{aligned} \qquad 5.69$$

$$\left[-\frac{\left(f_pD_p+f_dD_d\right)^n_{i,j,k-1/2}}{\Delta z^n_k\Delta z^n_{bk}}\times\frac{MIN\left(\phi^n_{i,j,k},\phi^n_{i,j,k-1}\right)}{\phi^n_{i,j,k}}-\frac{\left[\!\left[\omega^n_{i,j},0\right]\!\right]}{\Delta z^n_k}\frac{MIN\left(\phi^n_{i,j,k},\phi^n_{i,j,k-1}\right)}{\phi^n_{i,j,k}}\right]B^{n+1}_{i,j,k-1}$$

$$+\left[\begin{array}{l}\dfrac{1}{\Delta t}+\dfrac{1}{\Delta z^n_k}\left[\left[\!\left[\omega^n_{i,j},0\right]\!\right]\dfrac{MIN\left(\phi^n_{i,j,k+1},\phi^n_{i,j,k}\right)}{\phi^n_{i,j,k}}+\left[\!\left[-\omega^n_{i,j},0\right]\!\right]\dfrac{MIN\left(\phi^n_{i,j,k},\phi^n_{i,j,k-1}\right)}{\phi^n_{i,j,k}}\right]\\ +\dfrac{\left(f_pD_p+f_dD_d\right)^n_{i,j,k+1/2}}{\Delta z^n_k\Delta z^n_{tk}}\dfrac{MIN\left(\phi^n_{i,j,k+1},\phi^n_{i,j,k}\right)}{\phi^n_{i,j,k}}+\dfrac{\left(f_pD_p+f_dD_d\right)^n_{i,j,k-1/2}}{\Delta z^n_k\Delta z^n_{bk}}\dfrac{MIN\left(\phi^n_{i,j,k},\phi^n_{i,j,k-1}\right)}{\phi^n_{i,j,k}}\end{array}\right]B^{n+1}_{i,j,k}$$

$$+\left[-\frac{\left[\!\left[-\omega^n_{i,j},0\right]\!\right]}{\Delta z^n_k}\frac{MIN\left(\phi^n_{i,j,k+1},\phi^n_{i,j,k}\right)}{\phi^n_{i,j,k}}-\frac{\left(f_pD_p+f_dD_d\right)^n_{i,j,k+1/2}}{\Delta z^n_k\Delta z^n_{tk}}\frac{MIN\left(\phi^n_{i,j,k+1},\phi^n_{i,j,k}\right)}{\phi^n_{i,j,k}}\right]B^{n+1}_{i,j,k+1}=\frac{B^n_{i,j,k}}{\Delta t} \qquad 5.70$$

$$\left[-\left(\frac{\left(f_pD_p+f_dD_d\right)^n_{i,j,k-1/2}}{\Delta z^n_k\Delta z^n_{bk}}+\frac{\left[\!\left[\omega^n_{i,j},0\right]\!\right]}{\Delta z^n_k}\right)\frac{MIN\left(\phi^n_{i,j,k},\phi^n_{i,j,k-1}\right)}{\phi^n_{i,j,k}}\right]B^{n+1}_{i,j,k-1}$$

$$+\left[\begin{array}{l}\dfrac{1}{\Delta t}+\left[\left(\dfrac{\left[\!\left[\omega^n_{i,j},0\right]\!\right]}{\Delta z^n_k}+\dfrac{\left(f_pD_p+f_dD_d\right)^n_{i,j,k+1/2}}{\Delta z^n_k\Delta z^n_{tk}}\right)\dfrac{MIN\left(\phi^n_{i,j,k+1},\phi^n_{i,j,k}\right)}{\phi^n_{i,j,k}}\right]\\ +\left(\dfrac{\left[\!\left[-\omega^n_{i,j},0\right]\!\right]}{\Delta z^n_k}+\dfrac{\left(f_pD_p+f_dD_d\right)^n_{i,j,k-1/2}}{\Delta z^n_k\Delta z^n_{bk}}\right)\dfrac{MIN\left(\phi^n_{i,j,k},\phi^n_{i,j,k-1}\right)}{\phi^n_{i,j,k}}\end{array}\right]B^{n+1}_{i,j,k}$$

$$+\left[-\left(\frac{\left[\!\left[-\omega^n_{i,j},0\right]\!\right]}{\Delta z^n_k}+\frac{\left(f_pD_p+f_dD_d\right)^n_{i,j,k+1/2}}{\Delta z^n_k\Delta z^n_{tk}}\right)\frac{MIN\left(\phi^n_{i,j,k+1},\phi^n_{i,j,k}\right)}{\phi^n_{i,j,k}}\right]B^{n+1}_{i,j,k+1}=\frac{B^n_{i,j,k}}{\Delta t} \qquad 5.71$$

This can be written as, $a_k.B^{n+1}_{i,\mathrm{j},k-1}+b_k.B^{n+1}_{i,\mathrm{j},k}+c_k.B^{n+1}_{i,\mathrm{j},k+1}=d_k$ where a_k, b_k and c_k are the implicit coefficients and d_k is the explicit coefficient which is renewed after the consideration of the boundary flux discretization.

$$a_k=\left[-\left(\frac{\left(f_pD_p+f_dD_d\right)^n_{i,j,k-1/2}}{\Delta z^n_k\Delta z^n_{bk}}+\frac{\left[\!\left[\omega^n_{i,j},0\right]\!\right]}{\Delta z^n_k}\right)\frac{MIN\left(\phi^n_{i,j,k},\phi^n_{i,j,k-1}\right)}{\phi^n_{i,j,k}}\right] \qquad 5.72$$

$$b_k = \left[\begin{array}{l} \dfrac{1}{\Delta t} + \left[\left(\dfrac{\left[\!\left[\omega_{i,j}^n, 0 \right]\!\right]}{\Delta z_k^n} + \dfrac{\left(f_p D_p + f_d D_d \right)_{i,j,k+1/2}^n}{\Delta z_k^n \Delta z_{tk}^n} \right) \dfrac{MIN\left(\phi_{i,j,k+1}^n, \phi_{i,j,k}^n \right)}{\phi_{i,j,k}^n} \right] \\ + \left(\dfrac{\left[\!\left[-\omega_{i,j}^n, 0 \right]\!\right]}{\Delta z_k^n} + \dfrac{\left(f_p D_p + f_d D_d \right)_{i,j,k-1/2}^n}{\Delta z_k^n \Delta z_{bk}^n} \right) \dfrac{MIN\left(\phi_{i,j,k}^n, \phi_{i,j,k-1}^n \right)}{\phi_{i,j,k}^n} \end{array} \right] \quad 5.73$$

$$c_k = \left[-\left(\frac{\left[\!\left[-\omega_{i,j}^n, 0 \right]\!\right]}{\Delta z_k^n} + \frac{\left(f_p D_p + f_d D_d \right)_{i,j,k+1/2}^n}{\Delta z_k^n \Delta z_{tk}^n} \right) \frac{MIN\left(\phi_{i,j,k+1}^n, \phi_{i,j,k}^n \right)}{\phi_{i,j,k}^n} \right] \quad 5.74$$

$$d_k = \frac{B_{i,j,k}^n}{\Delta t} \quad 5.75$$

5.4.2 Particulate matter

Similar to dissolved matter, for the conservation of mass within the control volume V, the net change of mass should be equivalent to the net mass influx due to advection and diffusion and the mass generation of species due to reactions. Hence, mass conservation equation can be written as;

$$\begin{aligned} &Mass\_change = net\_nass\_diffusion\_flux + net\_mass\_advectiion\_flux \\ &+mass\_source\_gen \end{aligned} \quad 5.76$$

n refers to the present time step and the net change of mass during time period of Δt can be written as;

$$Mass\_change = \left(B_{i,j,k}^{n+1} - B_{i,j,k}^n \right) \Delta x \Delta y \Delta z_k \left(1 - \phi_{i,j,k} \right) \quad 5.77$$

ω is positive upwards and the considerations of ω is same as in dissolved matter derivation. The net mass advection flux to the control volume V can be written as;

$$Net\_mass\_advection\_flux = -\left[\omega_t B_t \left(1 - \phi_t \right) - \omega_b B_b \left(1 - \phi_b \right) \right] \Delta x \Delta y \Delta t \quad 5.78$$

$$Net\_mass\_advection\_flux = -\left[\begin{array}{l} \omega_{i,j,k+1/2} B_{i,j,k+1/2} \left(1 - \phi_{i,j,k+1/2} \right) \\ -\omega_{i,j,k-1/2} B_{i,j,k-1/2} \left(1 - \phi_{i,j,k-1/2} \right) \end{array} \right] \Delta x \Delta y \Delta t \quad 5.79$$

Suppose J denotes the diffusion flux influencing a typical dependent variable B in the sediment. The flux $Influx\_z = J_{i,j,k-1/2}$ is entering to the control volume face $\Delta x\Delta y$ while the flux leaving the opposite face is $Efflux\_z = J_{i,j,k+1/2}$ after the time period of Δt. The mass net Influx over the control volume face $\Delta x\Delta y$ can be written as;

$$Net\_\text{mass}\_dissfusion\_flux = -\left[flux_t\left(1-\phi_t\right) - flux_b\left(1-\phi_b\right)\right]\Delta x\Delta y\Delta t \qquad 5.80$$

$$Net\_\text{mass}\_dissfusion\_flux = -\left[J_{i,j,k+/2}\left(1-\phi_{i,j,k+1/2}\right) - J_{i,j,k-1/2}\left(1-\phi_{i,j,k-1/2}\right)\right]\Delta x\Delta y\Delta t \qquad 5.81$$

Diffusion flux $J_{i,j,k}$ can be expressed by the Fick's law as, $J_{i,j,k} = -K_{i,j,k}\dfrac{\partial B_{i,j,k}}{\partial z}$ where $K_{i,j,k}$ is the diffusion coefficient in z-direction (m^2/s) (Ji, 2008).

$$Net\_\text{mass}\_dissfusion\_flux = -\begin{bmatrix}\left(-K_{i,j,k+1/2}\dfrac{\partial B_{i,j,k+1/2}}{\partial z}\right)\left(1-\phi_{i,j,k+1/2}\right)\\ -\left(-K_{i,j,k-1/2}\dfrac{\partial B_{i,j,k-1/2}}{\partial z}\right)\left(1-\phi_{i,j,k-1/2}\right)\end{bmatrix}\Delta x\Delta y\Delta t \qquad 5.82$$

$$Net\_\text{mass}\_dissfusion\_flux = \begin{bmatrix}\left(K_{i,j,k+1/2}\dfrac{\partial B_{i,j,k+1/2}}{\partial z}\right)\left(1-\phi_{i,j,k+1/2}\right)\\ -\left(K_{i,j,k-1/2}\dfrac{\partial B_{i,j,k-1/2}}{\partial z}\right)\left(1-\phi_{i,j,k-1/2}\right)\end{bmatrix}\Delta x\Delta y\Delta t \qquad 5.83$$

Let the rate of generation of chemical species over control volume is $\sum_j R_j$. Then the generation of species over control volume during time period of Δt can be written as;

$$Sourec\_gen = \left[\sum_j R_j\right]\Delta x\Delta y\Delta z_k\left(1-\phi_{i,j,k}\right)\Delta t \qquad 5.84$$

Equations **5.77**, **5.79**, **5.83** and **5.84** combines to make the mass conservation over the control volume;

$$\left(B_{i,j,k}^{n+1}-B_{i,j,k}^{n}\right)\Delta x\Delta y\Delta z_k\left(1-\phi_{i,j,k}\right)=-\begin{bmatrix}\omega_{i,j,k+1/2}B_{i,j,k+1/2}\left(1-\phi_{i,j,k+1/2}\right)\\-\omega_{i,j,k-1/2}B_{i,j,k-1/2}\left(1-\phi_{i,j,k-1/2}\right)\end{bmatrix}\Delta x\Delta y\Delta t$$
$$+\begin{bmatrix}\left(K_{i,j,k+1/2}\dfrac{\partial B_{i,j,k+1/2}}{\partial z}\right)\left(1-\phi_{i,j,k+1/2}\right)\\-\left(K_{i,j,k-1/2}\dfrac{\partial B_{i,j,k-1/2}}{\partial z}\right)\left(1-\phi_{i,j,k-1/2}\right)\end{bmatrix}\Delta x\Delta y\Delta t+\left[\sum_j R_j\right]\Delta x\Delta y\Delta z_k\left(1-\phi_{i,j,k}\right)\Delta t \quad 5.85$$

$$\frac{\left(B_{i,j,k}^{n+1}-B_{i,j,k}^{n}\right)}{\Delta t}\left(1-\phi_{i,j,k}\right)=-\begin{bmatrix}\omega_{i,j,k+1/2}B_{i,j,k+1/2}\left(1-\phi_{i,j,k+1/2}\right)\\-\omega_{i,j,k-1/2}B_{i,j,k-1/2}\left(1-\phi_{i,j,k-1/2}\right)\end{bmatrix}\frac{1}{\Delta z_k}$$
$$+\begin{bmatrix}\left(K_{i,j,k+1/2}\dfrac{\partial B_{i,j,k+1/2}}{\partial z}\right)\left(1-\phi_{i,j,k+1/2}\right)\\-\left(K_{i,j,k-1/2}\dfrac{\partial B_{i,j,k-1/2}}{\partial z}\right)\left(1-\phi_{i,j,k-1/2}\right)\end{bmatrix}\frac{1}{\Delta z_k}+\left[\sum_j R_j\right]\left(1-\phi_{i,j,k}\right) \quad 5.86$$

$$\frac{\partial B_{i,j,k}}{\partial t}\times\left(1-\phi_{i,j,k}\right)=-\omega_{i,j}\frac{\partial\left(B_{i,j,k}\times\left(1-\phi_{i,j,k}\right)\right)}{\partial z}+\frac{\partial}{\partial z}\left[K_{i,j,k}\times\left(1-\phi_{i,j,k}\right)\times\frac{\partial B_{i,j,k}}{\partial z}\right]$$
$$+\left[\sum_j R_j\right]\left(1-\phi_{i,j,k}\right) \quad 5.87$$

In general, governing differential equation for any particulate material in the sediment can be written as;

$$\frac{\partial B_{i,j,k}}{\partial t}\times\left(1-\phi_{i,j,k}\right)-\frac{\partial}{\partial z}\left[K_{i,j,k}\times\left(1-\phi_{i,j,k}\right)\times\frac{\partial B_{i,j,k}}{\partial z}\right]+\omega_{i,j}\frac{\partial\left(B_{i,j,k}\times\left(1-\phi_{i,j,k}\right)\right)}{\partial z}=\left[\sum_j R_j\right]\left(1-\phi_{i,j,k}\right) \quad 5.88$$

Using the split operator the equation **5.88** divides into two for the convenience.
Only the advection and diffusion;

$$\frac{\partial B_{i,j,k}}{\partial t}\times\left(1-\phi_{i,j,k}\right)=\frac{\partial}{\partial z}\left[K_{i,j,k}\times\left(1-\phi_{i,j,k}\right)\times\frac{\partial B_{i,j,k}}{\partial z}\right]-\omega_{i,j}\frac{\partial\left(B_{i,j,k}\times\left(1-\phi_{i,j,k}\right)\right)}{\partial z} \quad 5.89$$

Only source terms;

$$\frac{\partial B_{i,j,k}}{\partial t}=\sum_j R_j \quad 5.90$$

Finite difference method with the fourth order Runge-Kutta method which gives the approximation of solutions of ordinary differential equations through explicit approach is used to obtain the solution for the source term equation **5.45**. This approach has been explained in detail under pelagic model.

5.4.2.1 Discretization of advection and diffusion equation

As shown in the **Fig 5.8** scalars have been defined at the centre of the control volume while flux and porosities have been defined at the surface of the control volume. Consider only the advection and diffusion equation **5.89** and develop the discretized form. This has been done in three steps.

1. Consider only the time dependency;

$$\frac{\partial B_{i,j,k}}{\partial t}\times\left(1-\phi_{i,j,k}\right)=\left(\frac{B_{i,j,k}^{n+1}-B_{i,j,k}^{n}}{\Delta t}\right)\left(1-\phi_{i,j,k}\right) \qquad 5.91$$

2. Consider only the advection term;

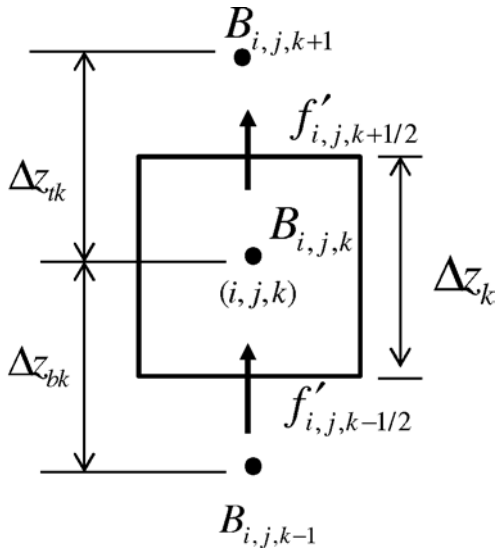

Fig 5.14 Advection term at CV faces

$$\omega_{i,j}\frac{\partial\left(B_{i,j,k}\times\phi_{i,j,k}\right)}{\partial z}=\omega_{i,j}\frac{\left(f'_{i,j,k+1/2}-f'_{i,j,k-1/2}\right)}{\Delta z_k} \qquad 5.92$$

where,

$$f'_{i,j,k+1/2} = B_{i,j,k+1/2}\left(1-\phi_{i,j,k+1/2}\right) \tag{5.93}$$

$$f'_{i,j,k-1/2} = B_{i,j,k-1/2}\left(1-\phi_{i,j,k-1/2}\right) \tag{5.94}$$

Evaluating the concentrations implicitly and sediment layer thickness and porosities explicitly;

$$\omega_{i,j}\frac{\partial\left(B_{i,j,k}\times\phi_{i,j,k}\right)}{\partial z} = \frac{\omega^n_{i,j}}{\Delta z^n_{i,j}}\left[B^{n+1}_{i,j,k+1/2}\left(1-\phi^n_{i,j,k+1/2}\right) - B^{n+1}_{i,j,k-1/2}\left(1-\phi^n_{i,j,k-1/2}\right)\right] \tag{5.95}$$

Same to the dissolved matter equations using the first order upwind scheme to evaluate the surface concentrations (equations **5.51**, **5.52**, **5.53**, **5.54**) and adopting the operator $[\![A,B]\!]$ (equations **5.55**, **5.56**) and evaluate the boundary porosities as the minimum between adjacent layer porosities (equations **5.57**, **5.58**) the advection term can be written as;

$$\omega_{i,j}\frac{\partial\left(B_{i,j,k}\times\phi_{i,j,k}\right)}{\partial z} = \frac{1}{\Delta z^n_k}\begin{bmatrix}\left(B^{n+1}_{i,j,k}[\![\omega^n_{i,j},0]\!] - B^{n+1}_{i,j,k+1}[\![-\omega^n_{i,j},0]\!]\right)\left(1-MIN\left(\phi^n_{i,j,k+1},\phi^n_{i,j,k}\right)\right)\\ -\left(B^{n+1}_{i,j,k-1}[\![\omega^n_{i,j},0]\!] - B^{n+1}_{i,j,k}[\![-\omega^n_{i,j},0]\!]\right)\left(1-MIN\left(\phi^n_{i,j,k},\phi^n_{i,j,k-1}\right)\right)\end{bmatrix} \tag{5.96}$$

3. Consider only the diffusion term;

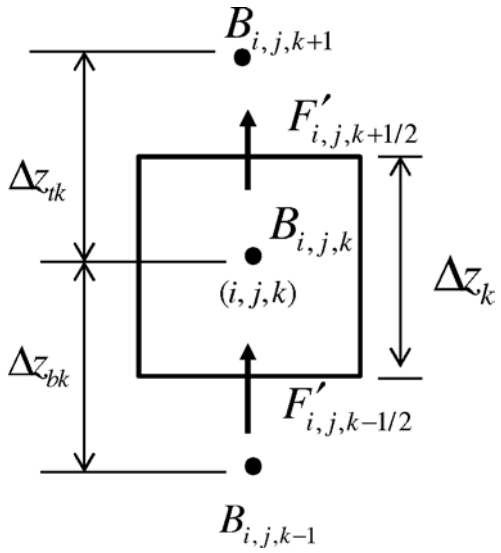

Fig 5.15 Diffusion term at CV faces

$$\frac{\partial}{\partial z}\left[K_{i,j,k}\times\left(1-\phi_{i,j,k}\right)\times\frac{\partial B_{i,j,k}}{\partial z}\right]=\frac{\left(F'_{i,j,k+1/2}-F'_{i,j,k-1/2}\right)}{\Delta z_k} \tag{5.97}$$

where,

$$F'_{i,j,k+1/2}=\left(K_{i,j,k+1/2}\frac{\partial B_{i,j,k+1/2}}{\partial z}\right)\left(1-\phi_{i,j,k+1/2}\right) \tag{5.98}$$

$$F'_{i,j,k-1/2}=\left(K_{i,j,k-1/2}\frac{\partial B_{i,j,k-1/2}}{\partial z}\right)\left(1-\phi_{i,j,k-1/2}\right) \tag{5.99}$$

The diffusion term can be written as;

$$\frac{\partial}{\partial z}\left[K_{i,j,k}\times\left(1-\phi_{i,j,k}\right)\times\frac{\partial B_{i,j,k}}{\partial z}\right]=\frac{1}{\Delta z_k}\begin{bmatrix}\left(K_{i,j,k+1/2}\frac{\partial B_{i,j,k+1/2}}{\partial z}\right)\left(1-\phi_{i,j,k+1/2}\right)\\-\left(K_{i,j,k-1/2}\frac{\partial B_{i,j,k-1/2}}{\partial z}\right)\left(1-\phi_{i,j,k-1/2}\right)\end{bmatrix} \tag{5.100}$$

Same to the dissolved matter equations evaluating the concentrations implicitly from the piecewise-linear profile and sediment layer thickness explicitly (equations **5.65**, **5.66**) and evaluate the boundary porosities as the minimum between adjacent layer porosities (equations **5.57**, **5.58**) the diffusion term can be written as;

$$\frac{\partial}{\partial z}\left[K_{i,j,k}\times\left(1-\phi_{i,j,k}\right)\times\frac{\partial B_{i,j,k}}{\partial z}\right]=\frac{1}{\Delta z_k^n}\begin{bmatrix}\left(K^n_{i,j,k+1/2}\frac{\left(B^{n+1}_{i,j,k+1}-B^{n+1}_{i,j,k}\right)}{\Delta z^n_{tk}}\right)\left(1-MIN\left(\phi^n_{i,j,k+1},\phi^n_{i,j,k}\right)\right)\\-\left(K^n_{i,j,k-1/2}\frac{\left(B^{n+1}_{i,j,k}-B^{n+1}_{i,j,k-1}\right)}{\Delta z^m_{bk}}\right)\left(1-MIN\left(\phi^n_{i,j,k},\phi^n_{i,j,k-1}\right)\right)\end{bmatrix} \tag{5.101}$$

Substituting equations **5.91**, **5.96**, **5.101**, in equation **5.89**;

$$\begin{aligned}\left[\frac{B^{n+1}_{i,j,k}-B^n_{i,j,k}}{\Delta t}\right]\left(1-\phi^n_{i,j,k}\right)=&-\frac{1}{\Delta z^n_k}\begin{bmatrix}\left(B^{n+1}_{i,j,k}\left[\!\left[\omega^n_{i,j},0\right]\!\right]-B^{n+1}_{i,j,k+1}\left[\!\left[-\omega^n_{i,j},0\right]\!\right]\right)\\\times\left(1-MIN\left(\phi^n_{i,j,k+1},\phi^n_{i,j,k}\right)\right)\\-\left(B^{n+1}_{i,j,k-1}\left[\!\left[\omega^n_{i,j},0\right]\!\right]-B^{n+1}_{i,j,k}\left[\!\left[-\omega^n_{i,j},0\right]\!\right]\right)\\\times\left(1-MIN\left(\phi^n_{i,j,k},\phi^n_{i,j,k-1}\right)\right)\end{bmatrix}\\&+\frac{K^n_{i,j,k+1/2}}{\Delta z^n_k\Delta z^m_{tk}}\left[\left(B^{n+1}_{i,j,k+1}-B^{n+1}_{i,j,k}\right)\left(1-MIN\left(\phi^n_{i,j,k+1},\phi^n_{i,j,k}\right)\right)\right]\\&-\frac{K^n_{i,j,k-1/2}}{\Delta z^n_k\Delta z^n_{bk}}\left[\left(B^{n+1}_{i,j,k}-B^{n+1}_{i,j,k-1}\right)\left(1-MIN\left(\phi^n_{i,j,k},\phi^n_{i,j,k-1}\right)\right)\right]\end{aligned} \tag{5.102}$$

$$\left[\frac{B_{i,j,k}^{n+1}-B_{i,j,k}^{n}}{\Delta t}\right]=-\frac{1}{\Delta z_k^n}\left[\begin{array}{l}\left(B_{i,j,k}^{n+1}\left[\!\left[\omega_{i,j}^{n},0\right]\!\right]-B_{i,j,k+1}^{n+1}\left[\!\left[-\omega_{i,j}^{n},0\right]\!\right]\right)\left(\frac{1-MIN\left(\phi_{i,j,k+1}^{n},\phi_{i,j,k}^{n}\right)}{\left(1-\phi_{i,j,k}^{n}\right)}\right)\\-\left(B_{i,j,k-1}^{n+1}\left[\!\left[\omega_{i,j}^{n},0\right]\!\right]-B_{i,j,k}^{n+1}\left[\!\left[-\omega_{i,j}^{n},0\right]\!\right]\right)\left(\frac{1-MIN\left(\phi_{i,j,k}^{n},\phi_{i,j,k-1}^{n}\right)}{\left(1-\phi_{i,j,k}^{n}\right)}\right)\end{array}\right]$$
$$+\frac{K_{i,j,k+1/2}^{n}}{\Delta z_k^n\Delta z_{tk}^m}\left[\left(B_{i,j,k+1}^{n+1}-B_{i,j,k}^{n+1}\right)\frac{\left(1-MIN\left(\phi_{i,j,k+1,}^{n}\phi_{i,j,k}^{n}\right)\right)}{\left(1-\phi_{i,j,k}^{n}\right)}\right] \qquad 5.103$$
$$-\frac{K_{i,j,k-1/2}^{n}}{\Delta z_k^n\Delta z_{bk}^n}\left[\left(B_{i,j,k}^{n+1}-B_{i,j,k-1}^{n+1}\right)\frac{\left(1-MIN\left(\phi_{i,j,k,}^{n}\phi_{i,j,k-1}^{n}\right)\right)}{\left(1-\phi_{i,j,k}^{n}\right)}\right]$$

$$\left[-\frac{K_{n,k-1/2}^{n}}{\Delta z_k^n\Delta z_{bk}^n}\times\left(\frac{1-MIN\left(\phi_{\mathrm{n},k}^{n},\phi_{\mathrm{n},k-1}^{n}\right)}{1-\phi_{\mathrm{n},k}^{n}}\right)-\frac{\left[\!\left[\omega_{i,j}^{n},0\right]\!\right]}{\Delta z_k^n}\left(\frac{1-MIN\left(\phi_{\mathrm{n},k}^{n},\phi_{\mathrm{n},k-1}^{n}\right)}{1-\phi_{\mathrm{n},k}^{n}}\right)\right]B_{n,k-1}^{n+1}$$
$$+\left[\begin{array}{l}\frac{1}{\Delta t}+\frac{1}{\Delta z_k^n}\left[\left[\!\left[\omega_{i,j}^{n},0\right]\!\right]\left(\frac{1-MIN\left(\phi_{i,j,k+1}^{n},\phi_{i,j,k}^{n}\right)}{1-\phi_{i,j,k}^{n}}\right)+\left[\!\left[-\omega_{i,j}^{n},0\right]\!\right]\left(\frac{1-MIN\left(\phi_{i,j,k}^{n},\phi_{i,j,k-1}^{n}\right)}{1-\phi_{i,j,k}^{n}}\right)\right]\\+\frac{K_{i,j,k+1/2}^{n}}{\Delta z_k^n\Delta z_{tk}^n}\left(\frac{1-MIN\left(\phi_{i,j,k+1,}^{n}\phi_{i,j,k}^{n}\right)}{1-\phi_{i,j,k}^{n}}\right)+\frac{K_{i,j,k-1/2}^{n}}{\Delta z_k^n\Delta z_{bk}^n}\left(\frac{1-MIN\left(\phi_{i,j,k,}^{n}\phi_{i,j,k-1}^{n}\right)}{1-\phi_{i,j,k}^{n}}\right)\end{array}\right]B_{i,j,k}^{n+1} \qquad 5.104$$
$$+\left[-\frac{\left[\!\left[-\omega_{i,j}^{n},0\right]\!\right]}{\Delta z_k^n}\left(\frac{1-MIN\left(\phi_{i,j,k+1}^{n},\phi_{i,j,k}^{n}\right)}{1-\phi_{i,j,k}^{n}}\right)-\frac{K_{i,j,k+1/2}^{n}}{\Delta z_k^n\Delta z_{tk}^n}\left(\frac{1-MIN\left(\phi_{i,j,k+1,}^{n}\phi_{i,j,k}^{n}\right)}{1-\phi_{i,j,k}^{n}}\right)\right]B_{i,j,k+1}^{n+1}=\frac{B_{i,j,k}^{n}}{\Delta t}$$

$$\left[-\left(\frac{K_{n,k-1/2}^{n}}{\Delta z_k^n\Delta z_{bk}^n}+\frac{\left[\!\left[\omega_{i,j}^{n},0\right]\!\right]}{\Delta z_k^n}\right)\left(\frac{1-MIN\left(\phi_{\mathrm{n},k}^{n},\phi_{\mathrm{n},k-1}^{n}\right)}{1-\phi_{\mathrm{n},k}^{n}}\right)\right]B_{n,k-1}^{n+1}$$
$$+\left[\begin{array}{l}\frac{1}{\Delta t}+\left(\frac{K_{i,j,k+1/2}^{n}}{\Delta z_k^n\Delta z_{tk}^n}+\frac{\left[\!\left[\omega_{i,j}^{n},0\right]\!\right]}{\Delta z_k^n}\right)\left(\frac{1-MIN\left(\phi_{i,j,k+1,}^{n}\phi_{i,j,k}^{n}\right)}{1-\phi_{i,j,k}^{n}}\right)\\+\left(\frac{K_{i,j,k-1/2}^{n}}{\Delta z_k^n\Delta z_{bk}^n}+\frac{\left[\!\left[-\omega_{i,j}^{n},0\right]\!\right]}{\Delta z_k^n}\right)\left(\frac{1-MIN\left(\phi_{i,j,k,}^{n}\phi_{i,j,k-1}^{n}\right)}{1-\phi_{i,j,k}^{n}}\right)\end{array}\right]B_{i,j,k}^{n+1} \qquad 5.105$$
$$+\left[-\left(\frac{K_{i,j,k+1/2}^{n}}{\Delta z_k^n\Delta z_{tk}^n}+\frac{\left[\!\left[-\omega_{i,j}^{n},0\right]\!\right]}{\Delta z_k^n}\right)\left(\frac{1-MIN\left(\phi_{i,j,k+1,}^{n}\phi_{i,j,k}^{n}\right)}{1-\phi_{i,j,k}^{n}}\right)\right]B_{i,j,k+1}^{n+1}=\frac{B_{i,j,k}^{n}}{\Delta t}$$

This can be written as, $a_k.B_{i,\mathrm{j},k-1}^{n+1}+b_k.B_{i,\mathrm{j},k}^{n+1}+c_k.B_{i,\mathrm{j},k+1}^{n+1}=d_k$ where a_k, b_k and c_k are the implicit coefficients and d_k is the explicit coefficient which is renewed after the consideration of the

boundary flux discretization. Same as in dissolved matter computation, solution for the discretized equation is obtained by adopting the Tri Diagonal Matrix Algorithm(TDMA) (Patankar, 1980).

$$a_k = \left[-\left(\frac{K^n_{n,k-1/2}}{\Delta z^n_k \Delta z^n_{bk}} + \frac{[\![\omega^n_{i,j}, 0]\!]}{\Delta z^n_k} \right) \left(\frac{1 - MIN\left(\phi^n_{\mathrm{n},k}, \phi^n_{\mathrm{n},k-1} \right)}{1 - \phi^n_{\mathrm{n},k}} \right) \right] \tag{5.106}$$

$$b_k = \left[\begin{array}{l} \frac{1}{\Delta t} + \left(\frac{K^n_{i,j,k+1/2}}{\Delta z^n_k \Delta z^n_{tk}} + \frac{[\![\omega^n_{i,j}, 0]\!]}{\Delta z^n_k} \right) \left(\frac{1 - MIN\left(\phi^n_{i,j,k+1}, \phi^n_{i,j,k} \right)}{1 - \phi^n_{i,j,k}} \right) \\ + \left(\frac{K^n_{i,j,k-1/2}}{\Delta z^n_k \Delta z^n_{bk}} + \frac{[\![-\omega^n_{i,j}, 0]\!]}{\Delta z^n_k} \right) \left(\frac{1 - MIN\left(\phi^n_{i,j,k}, \phi^n_{i,j,k-1} \right)}{1 - \phi^n_{i,j,k}} \right) \end{array} \right] \tag{5.107}$$

$$c_k = \left[-\left(\frac{K^n_{i,j,k+1/2}}{\Delta z^n_k \Delta z^n_{tk}} + \frac{[\![-\omega^n_{i,j}, 0]\!]}{\Delta z^n_k} \right) \left(\frac{1 - MIN\left(\phi^n_{i,j,k+1}, \phi^n_{i,j,k} \right)}{1 - \phi^n_{i,j,k}} \right) \right] \tag{5.108}$$

$$d_k = \frac{B^n_{i,j,k}}{\Delta t} \tag{5.109}$$

5.4.3 Surface and bottom boundary conditions

Boundary fluxes have been considered and analyzed separately under Chapter 6 and applied to governing differential equation at the surface and bottom boundaries. Hence both dissolved and particulate matter advection and diffusion equations have been reconsidered and new coefficients for the equation of $a_k.B^{n+1}_{i,\mathrm{j},k-1} + b_k.B^{n+1}_{i,\mathrm{j},k} + c_k.B^{n+1}_{i,\mathrm{j},k+1} = d_k$ have been computed after discretization.

5.4.3.1 Dissolved matter

5.4.3.1.1 Surface boundary conditions

The governing differential equation for a dissolved matter is written as;

$$\frac{\partial B_{i,\mathrm{j},k}}{\partial t} \times \phi_{i,\mathrm{j},k} + \omega_{i,\mathrm{j}} \frac{\partial \left(B_{i,\mathrm{j},k} \times \phi_{i,\mathrm{j},k} \right)}{\partial z} = \frac{\partial}{\partial z} \left[\left(f_p D_p + f_d D_d \right)_{i,\mathrm{j},k} \times \phi_{i,\mathrm{j},k} \times \frac{\partial B_{i,\mathrm{j},k}}{\partial z} \right] \tag{5.110}$$

Since $\left(f_p D_p + f_d D_d\right)_{i,\mathrm{j},k} = K_{i,\mathrm{j},k}$;

$$\frac{\partial B_{i,\mathrm{j},k}}{\partial t} \times \phi_{i,\mathrm{j},k} + \omega_{i,\mathrm{j}} \frac{\partial \left(B_{i,\mathrm{j},k} \times \phi_{i,\mathrm{j},k}\right)}{\partial z} = \frac{\partial}{\partial z}\left[K_{i,\mathrm{j},k} \times \phi_{i,\mathrm{j},k} \times \frac{\partial B_{i,\mathrm{j},k}}{\partial z}\right] \tag{5.111}$$

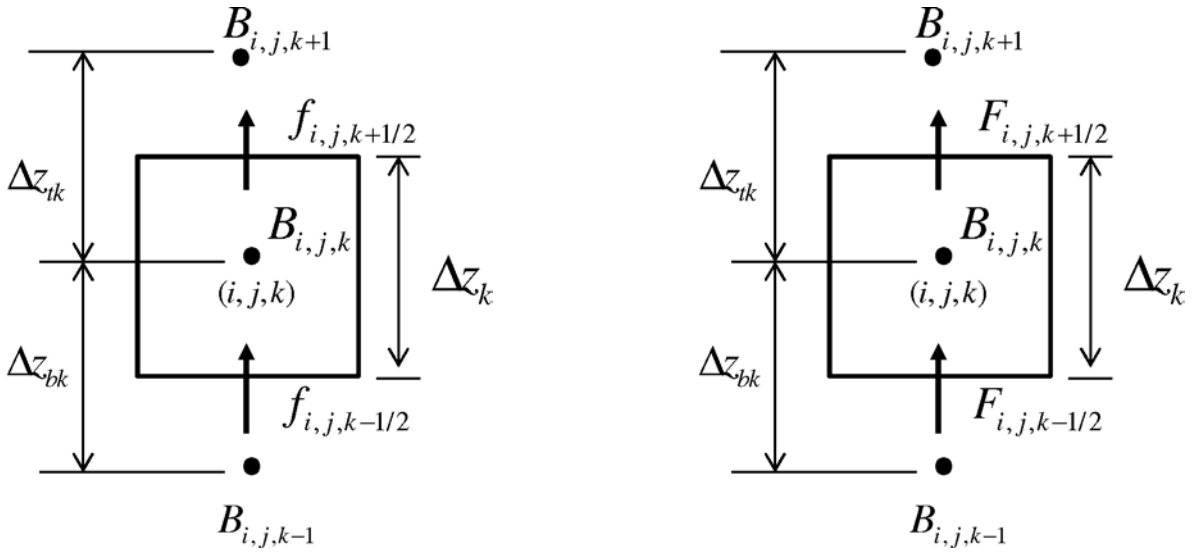

Fig 5.16 Advection term and diffusion term at CV faces

The governing differential equation is rewritten as;

$$\frac{\partial B_{i,\mathrm{j},k}}{\partial t} \times \phi_{i,\mathrm{j},k} + \omega_{i,j} \frac{\left(f_{i,j,k+1/2} - f_{i,j,k-1/2}\right)}{\Delta z_k} = \frac{\left(F_{i,j,k+1/2} - F_{i,j,k-1/2}\right)}{\Delta z_k} \tag{5.112}$$

$$\frac{\partial B_{i,\mathrm{j},k}}{\partial t} \times \phi_{i,\mathrm{j},k} + \frac{\left(\omega_{i,j} f_{i,j,k+1/2} - \omega_{i,j} f_{i,j,k-1/2}\right)}{\Delta z_k} = \frac{\left(F_{i,j,k+1/2} - F_{i,j,k-1/2}\right)}{\Delta z_k} \tag{5.113}$$

where,

$$f_{i,j,k+1/2} = B_{i,j,k+1/2} \phi_{i,j,k+1/2} \tag{5.114}$$

$$f_{i,j,k-1/2} = B_{i,j,k-1/2} \phi_{i,j,k-1/2} \tag{5.115}$$

$$F_{i,j,k+1/2} = \left(K_{i,j,k+1/2} \frac{\partial B_{i,j,k+1/2}}{\partial z}\right) \phi_{i,j,k+1/2} \tag{5.116}$$

$$F_{i,j,k-1/2} = \left(K_{i,j,k-1/2} \frac{\partial B_{i,j,k-1/2}}{\partial z} \right) \phi_{i,j,k-1/2} \qquad 5.117$$

The terms $\omega_{i,j} f_{i,j,k+1/2}$ and $F_{i,j,k+1/2}$ in the equation **5.113** are replaced as $F_{adv,s}$ and $F_{dif,s}$ which have been computed as sediment-water interface flux under the section **6.2** giving $F_{adv,s} = flux\_s2w_{i,j}^{n}$ and $F_{dif,s} = -\left(Diffusion\_flux\_s2w_{i,j}^{n} \right)$.

1. Consider only the time dependency term

$$\frac{\partial B_{i,j,k}}{\partial t} \times \phi_{i,j,k} = \left(\frac{B_{i,j,k}^{n+1} - B_{i,j,k}^{n}}{\Delta t} \right) \phi_{i,j,k} \qquad 5.118$$

2. Consider only the advection term

Evaluating the concentrations implicitly and the porosities, sediment layer thickness and burial rate explicitly;

$$\frac{\left(\omega_{i,j} f_{i,j,k+1/2} - \omega_{i,j} f_{i,j,k-1/2} \right)}{\Delta z_k} = \frac{\omega_{i,j}^{n} B_{i,j,k+1/2}^{n+1} \phi_{i,j,k+1/2}^{n}}{\Delta z_k^{n}} - \frac{\omega_{i,j}^{n} B_{i,j,k-1/2}^{n+1} \phi_{i,j,k-1/2}^{n}}{\Delta z_k^{n}} \qquad 5.119$$

$$\frac{\left(\omega_{i,j} f_{i,j,k+1/2} - \omega_{i,j} f_{i,j,k-1/2} \right)}{\Delta z_k} = \frac{F_{adv,s}}{\Delta z_k^{n}} - \frac{\omega_{i,j}^{n} B_{i,j,k-1/2}^{n+1} \phi_{i,j,k-1/2}^{n}}{\Delta z_k^{n}} \qquad 5.120$$

$F_{adv,s} = flux\_s2w_{i,j}^{n}$ is computed as advection boundary flux of dissolved matter at the sediment-water interface under the section **6.2.1.2**.

Using the first order upwind scheme to evaluate the surface concentrations;

$$B_{i,j,k-1/2}^{n+1} = B_{i,j,k-1}^{n+1} \text{ if } \omega_{i,j}^{n} \rangle 0 \qquad 5.121$$

$$B_{i,j,k-1/2}^{m+1} = B_{i,j,k}^{m+1} \text{ if } \omega_{i,j}^{n} \langle 0 \qquad 5.122$$

Define a new operator $[\![A, B]\!]$ to denote the greater of A and B. Then the upwind scheme implies (Patankar, 1980);

$$\omega_{i,j}^{n} B_{i,j,k-1/2}^{n+1} = B_{i,j,k-1}^{n+1} [\![\omega_{i,j}^{n}, 0]\!] - B_{i,j,k}^{n+1} [\![-\omega_{i,j}^{n}, 0]\!] \qquad 5.123$$

Evaluating the control volume face porosities as the minimum between adjacent layer porosities;

$$\phi^n_{i,j,k-1/2} = MIN\left(\phi^n_{i,j,k}, \phi^n_{i,j,k-1}\right) \quad 5.124$$

Then the advection term can be written as;

$$\frac{\left(\omega_{i,j} f_{i,j,k+1/2} - \omega_{i,j} f_{i,j,k-1/2}\right)}{\Delta z_k} = \frac{1}{\Delta z^n_k}\left[F_{adv,s} - \left(B^{n+1}_{i,j,k-1}\left[\!\left[\omega^n_{i,j}, 0\right]\!\right] - B^{n+1}_{i,j,k}\left[\!\left[-\omega^n_{i,j}, 0\right]\!\right]\right) MIN\left(\phi^n_{i,j,k}, \phi^n_{i,j,k-1}\right)\right] \quad 5.125$$

3. Consider only the diffusion term

$$\frac{\left(F_{i,j,k+1/2} - F_{i,j,k-1/2}\right)}{\Delta z_k} = \frac{\left(K_{i,j,k+1/2}\dfrac{\partial B_{i,j,k+1/2}}{\partial z}\right)\phi_{i,j,k+1/2}}{\Delta z_k} - \frac{\left(K_{i,j,k-1/2}\dfrac{\partial B_{i,j,k-1/2}}{\partial z}\right)\phi_{i,j,k-1/2}}{\Delta z_k} \quad 5.126$$

$$\frac{\left(F_{i,j,k+1/2} - F_{i,j,k-1/2}\right)}{\Delta z_k} = \frac{F_{dif,s}}{\Delta z_k} - \frac{\left(K_{i,j,k-1/2}\dfrac{\partial B_{i,j,k-1/2}}{\partial z}\right)\phi_{i,j,k-1/2}}{\Delta z_k} \quad 5.127$$

$F_{dif,s} = -\left(Diffusion\_flux\_s2w^n_{i,j}\right)$ is computed as diffusion boundary flux of dissolved matter at the sediment-water interface under the section **6.2.1.1**.

Evaluating the concentrations implicitly from the piecewise-linear profile and sediment layer thickness explicitly;

$$\frac{\partial B_{i,j,k+1/2}}{\partial z} = \frac{\left(B^{n+1}_{i,j,k+1} - B^{n+1}_{i,j,k}\right)}{\Delta z^n_{tk}} \quad 5.128$$

Since $B_{i,\mathrm{j},\mathrm{k}+1} = B_{i,\mathrm{j},\mathrm{k}}$ at the surface

$$\frac{\partial B_{i,j,k+1/2}}{\partial z} = 0 \quad 5.129$$

$$\frac{\partial B_{i,j,k-1/2}}{\partial z} = \frac{\left(B^{n+1}_{i,j,k} - B^{n+1}_{i,j,k-1}\right)}{\Delta z^n_{bk}} \quad 5.130$$

where, $\Delta z^n_{bk} = \dfrac{\Delta z^n_k + \Delta z^n_{k-1}}{2}$

Evaluating the boundary porosities explicitly and as the minimum between adjacent layer porosities (equations **5.57**, **5.58**);

$$\frac{\left(F_{i,j,k+1/2}-F_{i,j,k-1/2}\right)}{\Delta z_k}=\frac{1}{\Delta z_k^n}\left[F_{dif,s}-\left(K_{i,j,k-1/2}^n\frac{\left(B_{i,j,k}^{n+1}-B_{i,j,k-1}^{n+1}\right)}{\Delta z_{bk}^n}\right)MIN\left(\phi_{i,j,k}^n,\phi_{i,j,k-1}^n\right)\right] \qquad 5.131$$

Substituting equations **5.118**, **5.125** and **5.131**, in equation **5.113** and substituting $K_{i,\mathrm{j},k}=\left(f_pD_p+f_dD_d\right)_{i,\mathrm{j},k}$;

$$\left[\frac{B_{i,j,k}^{n+1}-B_{i,j,k}^n}{\Delta t}\right]\phi_{i,j,k}^n=-\frac{1}{\Delta z_k^n}\left[F_{adv,s}-\left(B_{i,j,k-1}^{n+1}\left[\!\left[\omega_{i,j}^n,0\right]\!\right]-B_{i,j,k}^{n+1}\left[\!\left[-\omega_{i,j}^n,0\right]\!\right]\right)MIN\left(\phi_{i,j,k}^n,\phi_{i,j,k-1}^n\right)\right]$$
$$+\frac{F_{dif,s}}{\Delta z_k^n}-\frac{\left(f_pD_p+f_dD_d\right)_{i,j,k-1/2}^n}{\Delta z_k^n\Delta z_{bk}^n}\left[\left(B_{i,j,k}^{n+1}-B_{i,j,k-1}^{n+1}\right)MIN\left(\phi_{i,j,k}^n,\phi_{i,j,k-1}^n\right)\right] \qquad 5.132$$

$$\left[\frac{B_{i,j,k}^{n+1}-B_{i,j,k}^n}{\Delta t}\right]=-\frac{1}{\Delta z_k^n}\left[\frac{F_{adv,s}}{\phi_{i,j,k}^n}-\left(B_{i,j,k-1}^{n+1}\left[\!\left[\omega_{i,j}^n,0\right]\!\right]-B_{i,j,k}^{n+1}\left[\!\left[-\omega_{i,j}^n,0\right]\!\right]\right)\frac{MIN\left(\phi_{i,j,k}^n,\phi_{i,j,k-1}^n\right)}{\phi_{i,j,k}^n}\right]$$
$$+\frac{F_{dif,s}}{\Delta z_k^n\phi_{i,j,k}^n}-\frac{\left(f_pD_p+f_dD_d\right)_{i,j,k-1/2}^n}{\Delta z_k^n\Delta z_{bk}^n}\left[\left(B_{i,j,k}^{n+1}-B_{i,j,k-1}^{n+1}\right)\frac{MIN\left(\phi_{i,j,k}^n,\phi_{i,j,k-1}^n\right)}{\phi_{i,j,k}^n}\right] \qquad 5.133$$

$$\left[-\frac{\left(f_pD_p+f_dD_d\right)_{i,j,k-1/2}^n}{\Delta z_k^n\Delta z_{bk}^n}\frac{MIN\left(\phi_{i,j,k}^n,\phi_{i,j,k-1}^n\right)}{\phi_{i,j,k}^n}-\frac{\left[\!\left[\omega_{i,j}^n,0\right]\!\right]}{\Delta z_k^n}\frac{MIN\left(\phi_{i,j,k}^n,\phi_{i,j,k-1}^n\right)}{\phi_{i,j,k}^n}\right]B_{i,j,k-1}^{n+1}$$
$$+\left[\frac{1}{\Delta t}+\frac{1}{\Delta z_k^n}\left[\left[\!\left[-\omega_{i,j}^n,0\right]\!\right]\frac{MIN\left(\phi_{i,j,k}^n,\phi_{i,j,k-1}^n\right)}{\phi_{i,j,k}^n}\right]+\frac{\left(f_pD_p+f_dD_d\right)_{i,j,k-1/2}^n}{\Delta z_k^n\Delta z_{bk}^n}\frac{MIN\left(\phi_{i,j,k}^n,\phi_{i,j,k-1}^n\right)}{\phi_{i,j,k}^n}\right]B_{i,j,k}^{n+1} \qquad 5.134$$
$$+\left[0\right]B_{i,j,k+1}^{n+1}=\frac{B_{i,j,k}^n}{\Delta t}+\frac{F_{dif,s}}{\Delta z_k^n\phi_{i,j,k}^n}-\frac{F_{adv,s}}{\Delta z_k^n\phi_{i,j,k}^n}$$

$$\left[-\left(\frac{\left(f_pD_p+f_dD_d\right)_{i,j,k-1/2}^n}{\Delta z_k^n\Delta z_{bk}^n}+\frac{\left[\!\left[\omega_{i,j}^n,0\right]\!\right]}{\Delta z_k^n}\right)\frac{MIN\left(\phi_{i,j,k}^n,\phi_{i,j,k-1}^n\right)}{\phi_{i,j,k}^n}\right]B_{i,j,k-1}^{n+1}$$
$$+\left[\frac{1}{\Delta t}+\left(\frac{\left[\!\left[-\omega_{i,j}^n,0\right]\!\right]}{\Delta z_k^n}+\frac{\left(f_pD_p+f_dD_d\right)_{i,j,k-1/2}^n}{\Delta z_k^n\Delta z_{bk}^n}\right)\frac{MIN\left(\phi_{i,j,k}^n,\phi_{i,j,k-1}^n\right)}{\phi_{i,j,k}^n}\right]B_{i,j,k}^{n+1} \qquad 5.135$$
$$+\left[0\right]B_{i,j,k+1}^{n+1}=\frac{B_{i,j,k}^n}{\Delta t}+\frac{F_{dif,s}}{\Delta z_k^n\phi_{i,j,k}^n}-\frac{F_{adv,s}}{\Delta z_k^n\phi_{i,j,k}^n}$$

This can be written as, $a_k.B^{n+1}_{i,j,k-1}+b_k.B^{n+1}_{i,j,k}+c_k.B^{n+1}_{i,j,k+1}=d_k$ where a_k, b_k and c_k are the implicit coefficients and d_k is the explicit coefficient.

$$a_k=\left[-\left(\frac{\left(f_pD_p+f_dD_d\right)^n_{i,j,k-1/2}}{\Delta z^n_k\Delta z^n_{bk}}+\frac{[\![\omega^n_{i,j},0]\!]}{\Delta z^n_k}\right)\frac{MIN\left(\phi^n_{i,j,k},\phi^n_{i,j,k-1}\right)}{\phi^n_{i,j,k}}\right] \quad 5.136$$

$$b_k=\left[\frac{1}{\Delta t}+\left(\frac{[\![-\omega^n_{i,j},0]\!]}{\Delta z^n_k}+\frac{\left(f_pD_p+f_dD_d\right)^n_{i,j,k-1/2}}{\Delta z^n_k\Delta z^n_{bk}}\right)\frac{MIN\left(\phi^n_{i,j,k},\phi^n_{i,j,k-1}\right)}{\phi^n_{i,j,k}}\right] \quad 5.137$$

$$c_k=0 \quad 5.138$$

$$d_k=\frac{B^n_{i,j,k}}{\Delta t}+\frac{F_{dif,s}}{\Delta z^n_k\phi^n_{i,j,k}}-\frac{F_{adv,s}}{\Delta z^n_k\phi^n_{i,j,k}} \quad 5.139$$

5.4.3.1.2 Bottom boundary conditions

The governing differential equation for a dissolved matter is written as;

$$\frac{\partial B_{i,j,k}}{\partial t}\times\phi_{i,j,k}+\omega_{i,j}\frac{\partial\left(B_{i,j,k}\times\phi_{i,j,k}\right)}{\partial z}=\frac{\partial}{\partial z}\left[\left(f_pD_p+f_dD_d\right)_{i,j,k}\times\phi_{i,j,k}\times\frac{\partial B_{i,j,k}}{\partial z}\right] \quad 5.140$$

Since $\left(f_pD_p+f_dD_d\right)_{i,j,k}=K_{i,j,k}$;

$$\frac{\partial B_{i,j,k}}{\partial t}\times\phi_{i,j,k}+\omega_{i,j}\frac{\partial\left(B_{i,j,k}\times\phi_{i,j,k}\right)}{\partial z}=\frac{\partial}{\partial z}\left[K_{i,j,k}\times\phi_{i,j,k}\times\frac{\partial B_{i,j,k}}{\partial z}\right] \quad 5.141$$

The governing differential equation is rewritten as;

$$\frac{\partial B_{i,j,k}}{\partial t}\times\phi_{i,j,k}+\omega_{i,j}\frac{\left(f_{i,j,k+1/2}-f_{i,j,k-1/2}\right)}{\Delta z_k}=\frac{\left(F_{i,j,k+1/2}-F_{i,j,k-1/2}\right)}{\Delta z_k} \quad 5.142$$

$$\frac{\partial B_{i,j,k}}{\partial t}\times\phi_{i,j,k}+\frac{\left(\omega_{i,j}f_{i,j,k+1/2}-\omega_{i,j}f_{i,j,k-1/2}\right)}{\Delta z_k}=\frac{\left(F_{i,j,k+1/2}-F_{i,j,k-1/2}\right)}{\Delta z_k} \quad 5.143$$

where,

$$f_{i,j,k+1/2} = B_{i,j,k+1/2}\phi_{i,j,k+1/2} \quad 5.144$$

$$f_{i,j,k-1/2} = B_{i,j,k-1/2}\phi_{i,j,k-1/2} \quad 5.145$$

$$F_{i,j,k+1/2} = \left(K_{i,j,k+1/2} \frac{\partial B_{i,j,k+1/2}}{\partial z} \right) \phi_{i,j,k+1/2} \quad 5.146$$

$$F_{i,j,k-1/2} = \left(K_{i,j,k-1/2} \frac{\partial B_{i,j,k-1/2}}{\partial z} \right) \phi_{i,j,k-1/2} \quad 5.147$$

The term $\omega_{i,j} f_{i,j,k-1/2}$ in the equation **5.143** is replaced as $F_{adv,b}$ which has been computed as the sediment-bed interface flux under the section **6.3** giving $F_{adv,b} = flux\_b2s^n_{i,j}$. Assume no diffusion at the bottom boundary and hence $F_{dif,b} = 0$.

1. Consider only the time dependency term

$$\frac{\partial B_{i,j,k}}{\partial t} \times \phi_{i,j,k} = \left(\frac{B^{n+1}_{i,j,k} - B^n_{i,j,k}}{\Delta t} \right) \phi_{i,j,k} \quad 5.148$$

2. Consider only the advection term

Evaluating the concentrations implicitly and the porosities, sediment layer thickness and burial rate explicitly;

$$\frac{\left(\omega_{i,j} f_{i,j,k+1/2} - \omega_{i,j} f_{i,j,k-1/2} \right)}{\Delta z_k} = \frac{\omega^n_{i,j} B^{n+1}_{i,j,k+1/2} \phi^n_{i,j,k+1/2}}{\Delta z^n_k} - \frac{\omega^n_{i,j} B^{n+1}_{i,j,k-1/2} \phi^n_{i,j,k-1/2}}{\Delta z^n_k} \quad 5.149$$

$$\frac{\left(\omega_{i,j} f_{i,j,k+1/2} - \omega_{i,j} f_{i,j,k-1/2} \right)}{\Delta z_k} = \frac{\omega^n_{i,j} B^{n+1}_{i,j,k+1/2} \phi^n_{i,j,k+1/2}}{\Delta z^n_k} - \frac{F_{adv,b}}{\Delta z^n_k} \quad 5.150$$

The term $\omega_{i,j} f_{i,j,k-1/2}$ in the equation **5.143** is replaced as $F_{adv,b} = flux\_b2s^n_{i,j}$ which has been computed as the sediment-bed interface flux under the section **6.3.2.1**.

Using the first order upwind scheme to evaluate the surface concentrations;

$$B^{n+1}_{i,j,k+1/2} = B^{n+1}_{i,j,k} \text{ if } \omega^n_{i,j} \rangle 0 \quad 5.151$$

$$B^{n+1}_{i,j,k+1/2} = B^{n+1}_{i,j,k+1} \text{ if } \omega^n_{i,j} \langle 0 \quad 5.152$$

Define a new operator $[\![A,B]\!]$ to denote the greater of A and B. Then the upwind scheme implies (Patankar, 1980);

$$\omega^n_{i,j}B^{n+1}_{i,j,k+1/2} = B^{n+1}_{i,j,k}[\![\omega^n_{i,j},0]\!] - B^{n+1}_{i,j,k+1}[\![-\omega^n_{i,j},0]\!] \quad 5.153$$

Evaluating the control volume face porosities as the minimum between adjacent layer porosities;

$$\phi^n_{i,j,k+1/2} = MIN\left(\phi^n_{i,j,k+1},\phi^n_{i,j,k}\right) \quad 5.154$$

Then the advection term can be written as;

$$\frac{\left(\omega_{i,j}f_{i,j,k+1/2}-\omega_{i,j}f_{i,j,k-1/2}\right)}{\Delta z_k} = \frac{1}{\Delta z^n_k}\left[\begin{array}{l}\left(B^{n+1}_{i,j,k}[\![\omega^n_{i,j},0]\!] - B^{n+1}_{i,j,k+1}[\![-\omega^n_{i,j},0]\!]\right)MIN\left(\phi^n_{i,j,k+1},\phi^n_{i,j,k}\right)\\ -F_{adv,b}\end{array}\right] \quad 5.155$$

3. Consider only the diffusion term

$$\frac{\left(F_{i,j,k+1/2}-F_{i,j,k-1/2}\right)}{\Delta z_k} = \frac{\left(K_{i,j,k+1/2}\dfrac{\partial B_{i,j,k+1/2}}{\partial z}\right)\phi_{i,j,k+1/2}}{\Delta z_k} - \frac{\left(K_{i,j,k-1/2}\dfrac{\partial B_{i,j,k-1/2}}{\partial z}\right)\phi_{i,j,k-1/2}}{\Delta z_k} \quad 5.156$$

$$\frac{\left(F_{i,j,k+1/2}-F_{i,j,k-1/2}\right)}{\Delta z_k} = \frac{\left(K_{i,j,k+1/2}\dfrac{\partial B_{i,j,k+1/2}}{\partial z}\right)\phi_{i,j,k+1/2}}{\Delta z_k} - \frac{F_{dif,b}}{\Delta z_k} \quad 5.157$$

Assume no diffusion at the bottom boundary and hence $F_{dif,b} = 0$.

Evaluating the concentrations implicitly from the piecewise-linear profile and sediment layer thickness explicitly;

$$\frac{\partial B_{i,j,k+1/2}}{\partial z} = \frac{\left(B^{n+1}_{i,j,k+1}-B^{n+1}_{i,j,k}\right)}{\Delta z^n_{tk}} \quad 5.158$$

where, $\Delta z^n_{tk} = \dfrac{\Delta z^n_k + \Delta z^n_{k+1}}{2}$

Evaluating the boundary porosities explicitly and as the minimum between adjacent layer porosities (equations **5.57**, **5.58**);

$$\frac{\left(F_{i,j,k+1/2}-F_{i,j,k-1/2}\right)}{\Delta z_k} = \frac{1}{\Delta z^n_k}\left[\left(K^n_{i,j,k+1/2}\frac{\left(B^{n+1}_{i,j,k+1}-B^{n+1}_{i,j,k}\right)}{\Delta z^n_{tk}}\right)MIN\left(\phi^n_{i,j,k+1},\phi^n_{i,j,k}\right)\right] \quad 5.159$$

Substituting equations **5.148**, **5.155** and **5.159** in equation **5.143** and substituting $K_{i,j,k} = \left(f_p D_p + f_d D_d\right)_{i,j,k}$;

$$\left[\frac{B^{n+1}_{i,j,k} - B^{n}_{i,j,k}}{\Delta t}\right]\phi^{n}_{i,j,k} = -\frac{1}{\Delta z^{n}_{k}}\left[\left(B^{n+1}_{i,j,k}\left[\!\left[\omega^{n}_{i,j},0\right]\!\right] - B^{n+1}_{i,j,k+1}\left[\!\left[-\omega^{n}_{i,j},0\right]\!\right]\right)MIN\left(\phi^{n}_{i,j,k+1},\phi^{n}_{i,j,k}\right) - F_{adv,b}\right]$$
$$+\frac{\left(f_p D_p + f_d D_d\right)^{n}_{i,j,k+1/2}}{\Delta z^{n}_{k}\Delta z^{n}_{tk}}\left[\left(B^{n+1}_{i,j,k+1} - B^{n+1}_{i,j,k}\right)MIN\left(\phi^{n}_{i,j,k+1},\phi^{n}_{i,j,k}\right)\right] \qquad 5.160$$

$$\left[\frac{B^{n+1}_{i,j,k} - B^{n}_{i,j,k}}{\Delta t}\right] = -\frac{1}{\Delta z^{n}_{k}}\left[\left(B^{n+1}_{i,j,k}\left[\!\left[\omega^{n}_{i,j},0\right]\!\right] - B^{n+1}_{i,j,k+1}\left[\!\left[-\omega^{n}_{i,j},0\right]\!\right]\right)\frac{MIN\left(\phi^{n}_{i,j,k+1},\phi^{n}_{i,j,k}\right)}{\phi^{n}_{i,j,k}}\right]$$
$$+\frac{\left(f_p D_p + f_d D_d\right)^{n}_{i,j,k+1/2}}{\Delta z^{n}_{k}\Delta z^{n}_{tk}}\left[\left(B^{n+1}_{i,j,k+1} - B^{n+1}_{i,j,k}\right)\frac{MIN\left(\phi^{n}_{i,j,k+1},\phi^{n}_{i,j,k}\right)}{\phi^{n}_{i,j,k}}\right] + \frac{F_{adv,b}}{\Delta z^{n}_{k}\phi^{n}_{i,j,k}} \qquad 5.161$$

$$\left[0\right]B^{n+1}_{i,j,k-1}$$
$$+\left[\frac{1}{\Delta t} + \frac{1}{\Delta z^{n}_{k}}\left[\left[\!\left[\omega^{n}_{i,j},0\right]\!\right]\frac{MIN\left(\phi^{n}_{i,j,k+1},\phi^{n}_{i,j,k}\right)}{\phi^{n}_{i,j,k}}\right] + \frac{\left(f_p D_p + f_d D_d\right)^{n}_{i,j,k+1/2}}{\Delta z^{n}_{k}\Delta z^{n}_{tk}}\frac{MIN\left(\phi^{n}_{i,j,k+1},\phi^{n}_{i,j,k}\right)}{\phi^{n}_{i,j,k}}\right]B^{n+1}_{i,j,k}$$
$$+\left[-\frac{\left[\!\left[-\omega^{n}_{i,j},0\right]\!\right]}{\Delta z^{n}_{k}}\frac{MIN\left(\phi^{n}_{i,j,k+1},\phi^{n}_{i,j,k}\right)}{\phi^{n}_{i,j,k}} - \frac{\left(f_p D_p + f_d D_d\right)^{n}_{i,j,k+1/2}}{\Delta z^{n}_{k}\Delta z^{n}_{tk}}\frac{MIN\left(\phi^{n}_{i,j,k+1},\phi^{n}_{i,j,k}\right)}{\phi^{n}_{i,j,k}}\right]B^{n+1}_{i,j,k+1} \qquad 5.162$$
$$= \frac{B^{n}_{i,j,k}}{\Delta t} + \frac{F_{adv,b}}{\Delta z^{n}_{k}\phi^{n}_{i,j,k}}$$

$$\left[0\right]B^{n+1}_{i,j,k-1}$$
$$+\left[\frac{1}{\Delta t} + \left[\left(\frac{\left[\!\left[\omega^{n}_{i,j},0\right]\!\right]}{\Delta z^{n}_{k}} + \frac{\left(f_p D_p + f_d D_d\right)^{n}_{i,j,k+1/2}}{\Delta z^{n}_{k}\Delta z^{n}_{tk}}\right)\frac{MIN\left(\phi^{n}_{i,j,k+1},\phi^{n}_{i,j,k}\right)}{\phi^{n}_{i,j,k}}\right]\right]B^{n+1}_{i,j,k}$$
$$+\left[-\left(\frac{\left[\!\left[-\omega^{n}_{i,j},0\right]\!\right]}{\Delta z^{n}_{k}} + \frac{\left(f_p D_p + f_d D_d\right)^{n}_{i,j,k+1/2}}{\Delta z^{n}_{k}\Delta z^{n}_{tk}}\right)\frac{MIN\left(\phi^{n}_{i,j,k+1},\phi^{n}_{i,j,k}\right)}{\phi^{n}_{i,j,k}}\right]B^{n+1}_{i,j,k+1} \qquad 5.163$$
$$= \frac{B^{n}_{i,j,k}}{\Delta t} + \frac{F_{adv,b}}{\Delta z^{n}_{k}\phi^{n}_{i,j,k}}$$

This can be written as, $a_k.B^{n+1}_{i,j,k-1} + b_k.B^{n+1}_{i,j,k} + c_k.B^{n+1}_{i,j,k+1} = d_k$ where a_k, b_k and c_k are the implicit coefficients and d_k is the explicit coefficient.

$$a_k = 0 \tag{5.164}$$

$$b_k = \left[\frac{1}{\Delta t} + \left[\left(\frac{\left[\left[\omega_{i,j}^n, 0 \right]\right]}{\Delta z_k^n} + \frac{\left(f_p D_p + f_d D_d \right)_{i,j,k+1/2}^n}{\Delta z_k^n \Delta z_{tk}^n} \right) \frac{MIN\left(\phi_{i,j,k+1}^n, \phi_{i,j,k}^n \right)}{\phi_{i,j,k}^n} \right] \right] \tag{5.165}$$

$$c_k = \left[-\left(\frac{\left[\left[-\omega_{i,j}^n, 0 \right]\right]}{\Delta z_k^n} + \frac{\left(f_p D_p + f_d D_d \right)_{i,j,k+1/2}^n}{\Delta z_k^n \Delta z_{tk}^n} \right) \frac{MIN\left(\phi_{i,j,k+1}^n, \phi_{i,j,k}^n \right)}{\phi_{i,j,k}^n} \right] \tag{5.166}$$

$$d_k = \frac{B_{i,j,k}^n}{\Delta t} + \frac{F_{adv,b}}{\Delta z_k^n \phi_{i,j,k}^n} \tag{5.167}$$

These simultaneous equations are solved using a Tri Diagonal Matrix Algorithm described in the sub-section **5.4.4**.

5.4.3.2 Particulate matter

5.4.3.2.1 Surface boundary conditions

The governing differential equation for a particulate matter is written as;

$$\frac{\partial B_{i,j,k}}{\partial t}\left(1-\phi_{i,j,k}\right) + \omega_{i,j} \frac{\partial \left(B_{i,j,k}\left(1-\phi_{i,j,k}\right)\right)}{\partial z} = \frac{\partial}{\partial z}\left[K_{i,j,k}\left(1-\phi_{i,j,k}\right)\frac{\partial B_{i,j,k}}{\partial z} \right] \tag{5.168}$$

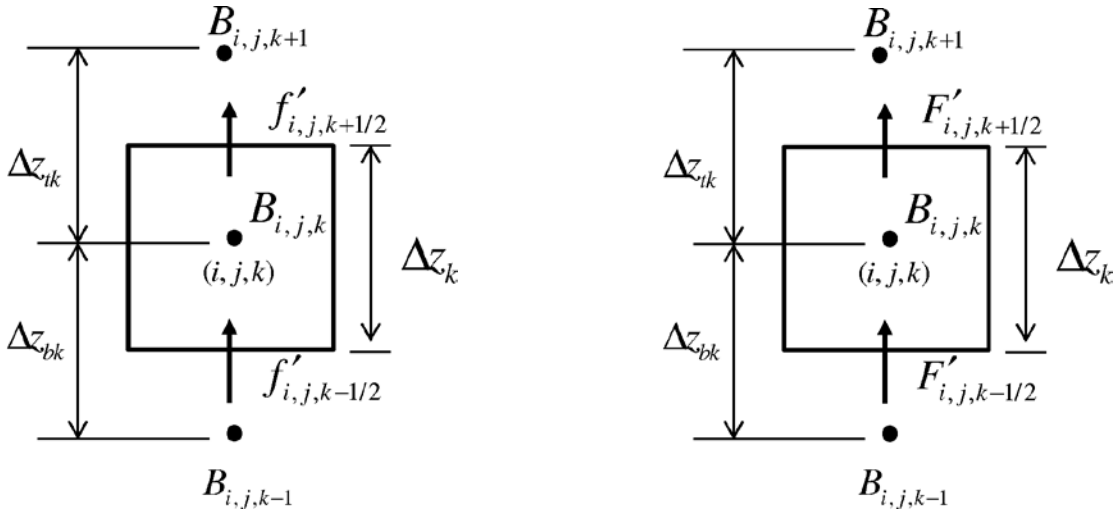

Fig 5.17 Advection term and diffusion term at CV faces

The governing differential equation is rewritten as;

$$\frac{\partial B_{i,j,k}}{\partial t}\left(1-\phi_{i,j,k}\right)+\omega_{i,j}\frac{\left(f'_{i,j,k+1/2}-f'_{i,j,k-1/2}\right)}{\Delta z_k}=\frac{\left(F'_{i,j,k+1/2}-F'_{i,j,k-1/2}\right)}{\Delta z_k} \quad 5.169$$

$$\frac{\partial B_{i,j,k}}{\partial t}\left(1-\phi_{i,j,k}\right)+\frac{\left(\omega_{i,j}f'_{i,j,k+1/2}-\omega_{i,j}f'_{i,j,k-1/2}\right)}{\Delta z_k}=\frac{\left(F'_{i,j,k+1/2}-F'_{i,j,k-1/2}\right)}{\Delta z_k} \quad 5.170$$

where,

$$f'_{i,j,k+1/2}=B_{i,j,k+1/2}\left(1-\phi_{i,j,k+1/2}\right) \quad 5.171$$

$$f'_{i,j,k-1/2}=B_{i,j,k-1/2}\left(1-\phi_{i,j,k-1/2}\right) \quad 5.172$$

$$F'_{i,j,k+1/2}=\left(K_{i,j,k+1/2}\frac{\partial B_{i,j,k+1/2}}{\partial z}\right)\left(1-\phi_{i,j,k+1/2}\right) \quad 5.173$$

$$F'_{i,j,k-1/2}=\left(K_{i,j,k-1/2}\frac{\partial B_{i,j,k-1/2}}{\partial z}\right)\left(1-\phi_{i,j,k-1/2}\right) \quad 5.174$$

It has been assumed that there exists zero diffusion flux at the sediment water interface and hence, $F'_{i,j,k+1/2}=0$. The term $\omega_{i,j}f'_{i,j,k+1/2}$ in the equation **5.170** is replaced as $F'_{adv,s}$ which has been computed as sediment-water interface flux due to particulate matter settling or erosion.

1. Consider only the time dependency term

$$\frac{\partial B_{i,j,k}}{\partial t}\times\phi_{i,j,k}=\left(\frac{B^{n+1}_{i,j,k}-B^{n}_{i,j,k}}{\Delta t}\right)\phi_{i,j,k} \quad 5.175$$

2. Consider only the advection term

Evaluating the concentrations implicitly and the porosities, sediment layer thickness and burial rate explicitly;

$$\frac{\left(\omega_{i,j}f'_{i,j,k+1/2}-\omega_{i,j}f'_{i,j,k-1/2}\right)}{\Delta z_k}=\frac{\omega^{n}_{i,j}B^{n+1}_{i,j,k+1/2}\left(1-\phi^{n}_{i,j,k+1/2}\right)}{\Delta z^{n}_{k}}-\frac{\omega^{n}_{i,j}B^{n+1}_{i,j,k-1/2}\left(1-\phi^{n}_{i,j,k-1/2}\right)}{\Delta z^{n}_{k}} \quad 5.176$$

$$\frac{\left(\omega_{i,j}f'_{i,j,k+1/2}-\omega_{i,j}f'_{i,j,k-1/2}\right)}{\Delta z_k}=\frac{F'_{adv,s}}{\Delta z^{n}_{k}}-\frac{\omega^{n}_{i,j}B^{n+1}_{i,j,k-1/2}\left(1-\phi^{n}_{i,j,k-1/2}\right)}{\Delta z^{n}_{k}} \quad 5.177$$

$F'_{adv,s}$ is computed from the equation **4.122** as the boundary flux due to accumulation or erosion of particulate matter at the sediment-water interface and hence;

$$F'_{adv,s} = -Flux\_b\left(1-\phi_{i,j,k+1/2}\right) \quad 5.178$$

Using the first order upwind scheme to evaluate the surface concentrations;

$$B^{n+1}_{i,j,k-1/2} = B^{n+1}_{i,j,k-1} \text{ if } \omega^n_{i,j} \rangle 0 \quad 5.179$$

$$B^{m+1}_{i,j,k-1/2} = B^{m+1}_{i,j,k} \text{ if } \omega^n_{i,j} \langle 0 \quad 5.180$$

Define a new operator $[\![A,B]\!]$ to denote the greater of A and B. Then the upwind scheme implies (Patankar, 1980);

$$\omega^n_{i,j} B^{n+1}_{i,j,k-1/2} = B^{n+1}_{i,j,k-1}[\![\omega^n_{i,j},0]\!] - B^{n+1}_{i,j,k}[\![-\omega^n_{i,j},0]\!] \quad 5.181$$

Evaluating the control volume face porosities as the minimum between adjacent layer porosities;

$$\phi^n_{i,j,k-1/2} = MIN\left(\phi^n_{i,j,k},\phi^n_{i,j,k-1}\right) \quad 5.182$$

Then the advection term can be written as;

$$\frac{\left(\omega_{i,j}f'_{i,j,k+1/2} - \omega_{i,j}f'_{i,j,k-1/2}\right)}{\Delta z_k} = \frac{1}{\Delta z^n_k}\left[F'_{adv,s} - \left(B^{n+1}_{i,j,k-1}[\![\omega^n_{i,j},0]\!] - B^{n+1}_{i,j,k}[\![-\omega^n_{i,j},0]\!]\right)\left(1-MIN\left(\phi^n_{i,j,k},\phi^n_{i,j,k-1}\right)\right)\right] \quad 5.183$$

3. Consider only the diffusion term

$$\frac{\left(F'_{i,j,k+1/2} - F'_{i,j,k-1/2}\right)}{\Delta z_k} = \frac{\left(K_{i,j,k+1/2}\dfrac{\partial B_{i,j,k+1/2}}{\partial z}\right)\left(1-\phi_{i,j,k+1/2}\right)}{\Delta z_k} - \frac{\left(K_{i,j,k-1/2}\dfrac{\partial B_{i,j,k-1/2}}{\partial z}\right)\left(1-\phi_{i,j,k-1/2}\right)}{\Delta z_k} \quad 5.184$$

$$\frac{\left(F'_{i,j,k+1/2} - F'_{i,j,k-1/2}\right)}{\Delta z_k} = \frac{F'_{dif,s}}{\Delta z_k} - \frac{\left(K_{i,j,k-1/2}\dfrac{\partial B_{i,j,k-1/2}}{\partial z}\right)\left(1-\phi_{i,j,k-1/2}\right)}{\Delta z_k} \quad 5.185$$

Assume no diffusion flux of particulate matter at the sediment water interface and hence, $F'_{dif,s} = 0$.

Evaluating the concentrations implicitly from the piecewise-linear profile and sediment layer thickness explicitly;

$$\frac{\partial B_{i,j,k-1/2}}{\partial z} = \frac{\left(B^{n+1}_{i,j,k} - B^{n+1}_{i,j,k-1}\right)}{\Delta z^{n}_{bk}} \tag{5.186}$$

where, $\Delta z^{n}_{bk} = \dfrac{\Delta z^{n}_{k} + \Delta z^{n}_{k-1}}{2}$

Evaluating the boundary porosities explicitly and as the minimum between adjacent layer porosities (equations **5.57**, **5.58**);

$$\frac{\left(F'_{i,j,k+1/2} - F'_{i,j,k-1/2}\right)}{\Delta z_{k}} = \frac{1}{\Delta z^{n}_{k}}\left[-\left(K^{n}_{i,j,k-1/2}\frac{\left(B^{n+1}_{i,j,k} - B^{n+1}_{i,j,k-1}\right)}{\Delta z^{n}_{bk}}\right)\left(1 - MIN\left(\phi^{n}_{i,j,k}, \phi^{n}_{i,j,k-1}\right)\right)\right] \tag{5.187}$$

Substituting equations **5.175**, **5.183** and **5.187** in equation **5.170;**

$$\left[\frac{B^{n+1}_{i,j,k} - B^{n}_{i,j,k}}{\Delta t}\right]\left(1-\phi^{n}_{i,j,k}\right) = -\frac{1}{\Delta z^{n}_{k}}\left[\begin{array}{l} F'_{adv,s} - \left(B^{n+1}_{i,j,k-1}\left[\!\left[\omega^{n}_{i,j}, 0\right]\!\right] - B^{n+1}_{i,j,k}\left[\!\left[-\omega^{n}_{i,j}, 0\right]\!\right]\right) \\ \left(1 - MIN\left(\phi^{n}_{i,j,k}, \phi^{n}_{i,j,k-1}\right)\right) \end{array}\right]$$
$$+\frac{1}{\Delta z^{n}_{k}}\left[-\left(K^{n}_{i,j,k-1/2}\frac{\left(B^{n+1}_{i,j,k} - B^{n+1}_{i,j,k-1}\right)}{\Delta z^{n}_{bk}}\right)\left(1 - MIN\left(\phi^{n}_{i,j,k}, \phi^{n}_{i,j,k-1}\right)\right)\right] \tag{5.188}$$

$$\left[\frac{B^{n+1}_{i,j,k} - B^{n}_{i,j,k}}{\Delta t}\right] = -\frac{1}{\Delta z^{n}_{k}}\left[\frac{F'_{adv,s}}{\left(1-\phi^{n}_{i,j,k}\right)} - \left(B^{n+1}_{i,j,k-1}\left[\!\left[\omega^{n}_{i,j}, 0\right]\!\right] - B^{n+1}_{i,j,k}\left[\!\left[-\omega^{n}_{i,j}, 0\right]\!\right]\right)\frac{\left(1 - MIN\left(\phi^{n}_{i,j,k}, \phi^{n}_{i,j,k-1}\right)\right)}{\left(1-\phi^{n}_{i,j,k}\right)}\right]$$
$$-\frac{K^{n}_{i,j,k-1/2}}{\Delta z^{n}_{k}\Delta z^{n}_{bk}}\left[\left(B^{n+1}_{i,j,k} - B^{n+1}_{i,j,k-1}\right)\frac{\left(1 - MIN\left(\phi^{n}_{i,j,k}, \phi^{n}_{i,j,k-1}\right)\right)}{\left(1-\phi^{n}_{i,j,k}\right)}\right] \tag{5.189}$$

$$\left[-\frac{K^{n}_{i,j,k-1/2}}{\Delta z^{n}_{k}\Delta z^{n}_{bk}}\frac{\left(1 - MIN\left(\phi^{n}_{i,j,k}, \phi^{n}_{i,j,k-1}\right)\right)}{\left(1-\phi^{n}_{i,j,k}\right)} - \frac{\left[\!\left[\omega^{n}_{i,j}, 0\right]\!\right]}{\Delta z^{n}_{k}}\frac{\left(1 - MIN\left(\phi^{n}_{i,j,k}, \phi^{n}_{i,j,k-1}\right)\right)}{\left(1-\phi^{n}_{i,j,k}\right)}\right]B^{n+1}_{i,j,k-1}$$
$$+\left[\frac{1}{\Delta t} + \frac{1}{\Delta z^{n}_{k}}\left[\!\left[-\omega^{n}_{i,j}, 0\right]\!\right]\frac{MIN\left(\phi^{n}_{i,j,k}, \phi^{n}_{i,j,k-1}\right)}{\phi^{n}_{i,j,k}}\right] + \frac{K^{n}_{i,j,k-1/2}}{\Delta z^{n}_{k}\Delta z^{n}_{bk}}\frac{\left(1 - MIN\left(\phi^{n}_{i,j,k}, \phi^{n}_{i,j,k-1}\right)\right)}{\left(1-\phi^{n}_{i,j,k}\right)}\right]B^{n+1}_{i,j,k} \tag{5.190}$$
$$+\left[0\right]B^{n+1}_{i,j,k+1} = \frac{B^{n}_{i,j,k}}{\Delta t} - \frac{F'_{adv,s}}{\Delta z^{n}_{k}\left(1-\phi^{n}_{i,j,k}\right)}$$

$$\left[-\left(\frac{K^n_{i,j,k-1/2}}{\Delta z^n_k \Delta z^n_{bk}}+\frac{[\![\omega^n_{i,j},0]\!]}{\Delta z^n_k}\right)\frac{\left(1-MIN\left(\phi^n_{i,j,k},\phi^n_{i,j,k-1}\right)\right)}{\left(1-\phi^n_{i,j,k}\right)}\right]B^{n+1}_{i,j,k-1}$$

$$+\left[\frac{1}{\Delta t}+\left(\frac{[\![-\omega^n_{i,j},0]\!]}{\Delta z^n_k}+\frac{K^n_{i,j,k-1/2}}{\Delta z^n_k \Delta z^n_{bk}}\right)\frac{\left(1-MIN\left(\phi^n_{i,j,k},\phi^n_{i,j,k-1}\right)\right)}{\left(1-\phi^n_{i,j,k}\right)}\right]B^{n+1}_{i,j,k} \qquad 5.191$$

$$+[0]B^{n+1}_{i,j,k+1}=\frac{B^n_{i,j,k}}{\Delta t}-\frac{F'_{adv,s}}{\Delta z^n_k\left(1-\phi^n_{i,j,k}\right)}$$

This can be written as, $a_k.B^{n+1}_{i,\mathrm{j},k-1}+b_k.B^{n+1}_{i,\mathrm{j},k}+c_k.B^{n+1}_{i,\mathrm{j},k+1}=d_k$ where a_k, b_k and c_k are the implicit coefficients and d_k is the explicit coefficient.

$$a_k=\left[-\left(\frac{K^n_{i,j,k-1/2}}{\Delta z^n_k \Delta z^n_{bk}}+\frac{[\![\omega^n_{i,j},0]\!]}{\Delta z^n_k}\right)\frac{\left(1-MIN\left(\phi^n_{i,j,k},\phi^n_{i,j,k-1}\right)\right)}{\left(1-\phi^n_{i,j,k}\right)}\right] \qquad 5.192$$

$$b_k=\left[\frac{1}{\Delta t}+\left(\frac{[\![-\omega^n_{i,j},0]\!]}{\Delta z^n_k}+\frac{K^n_{i,j,k-1/2}}{\Delta z^n_k \Delta z^n_{bk}}\right)\frac{\left(1-MIN\left(\phi^n_{i,j,k},\phi^n_{i,j,k-1}\right)\right)}{\left(1-\phi^n_{i,j,k}\right)}\right] \qquad 5.193$$

$$c_k=0 \qquad 5.194$$

$$d_k=\frac{B^n_{i,j,k}}{\Delta t}-\frac{F'_{adv,s}}{\Delta z^n_k\left(1-\phi^n_{i,j,k}\right)} \qquad 5.195$$

5.4.3.2.2 Bottom boundary conditions

The governing differential equation for a particulate matter is written as;

$$\frac{\partial B_{i,j,k}}{\partial t}\left(1-\phi_{i,j,k}\right)+\omega_{i,j}\frac{\partial\left(B_{i,j,k}\left(1-\phi_{i,j,k}\right)\right)}{\partial z}=\frac{\partial}{\partial z}\left[K_{i,j,k}\left(1-\phi_{i,j,k}\right)\frac{\partial B_{i,j,k}}{\partial z}\right] \qquad 5.196$$

The governing differential equation is rewritten as;

$$\frac{\partial B_{i,\mathrm{j},k}}{\partial t}\left(1-\phi_{i,j,k}\right)+\omega_{i,j}\frac{\left(f'_{i,j,k+1/2}-f'_{i,j,k-1/2}\right)}{\Delta z_k}=\frac{\left(F'_{i,j,k+1/2}-F'_{i,j,k-1/2}\right)}{\Delta z_k} \qquad 5.197$$

$$\frac{\partial B_{i,\mathrm{j},k}}{\partial t}\left(1-\phi_{i,j,k}\right)+\frac{\left(\omega_{i,j}f'_{i,j,k+1/2}-\omega_{i,j}f'_{i,j,k-1/2}\right)}{\Delta z_k}=\frac{\left(F'_{i,j,k+1/2}-F'_{i,j,k-1/2}\right)}{\Delta z_k} \qquad 5.198$$

where,

$$f'_{i,j,k+1/2} = B_{i,j,k+1/2}\left(1-\phi_{i,j,k+1/2}\right) \quad 5.199$$

$$f'_{i,j,k-1/2} = B_{i,j,k-1/2}\left(1-\phi_{i,j,k-1/2}\right) \quad 5.200$$

$$F'_{i,j,k+1/2} = \left(K_{i,j,k+1/2}\frac{\partial B_{i,j,k+1/2}}{\partial z}\right)\left(1-\phi_{i,j,k+1/2}\right) \quad 5.201$$

$$F'_{i,j,k-1/2} = \left(K_{i,j,k-1/2}\frac{\partial B_{i,j,k-1/2}}{\partial z}\right)\left(1-\phi_{i,j,k-1/2}\right) \quad 5.202$$

The term $\omega_{i,j}f'_{i,j,k-1/2}$ in the equation **5.143** is replaced as $F_{adv,b}$ which has been computed as the sediment-bed interface flux under the section **6.3** giving $F_{adv,b} = flux\_b2s^n_{i,j}$. Assume no diffusion at the bottom boundary and hence $F'_{dif,b} = 0$.

1. Consider only the time dependency term

$$\frac{\partial B_{i,j,k}}{\partial t}\times\phi_{i,j,k} = \left(\frac{B^{n+1}_{i,j,k}-B^n_{i,j,k}}{\Delta t}\right)\phi_{i,j,k} \quad 5.203$$

2. Consider only the advection term

Evaluating the concentrations implicitly and the porosities, sediment layer thickness and burial rate explicitly;

$$\frac{\left(\omega_{i,j}f'_{i,j,k+1/2}-\omega_{i,j}f'_{i,j,k-1/2}\right)}{\Delta z_k} = \frac{\omega^n_{i,j}B^{n+1}_{i,j,k+1/2}\left(1-\phi^n_{i,j,k+1/2}\right)}{\Delta z^n_k} - \frac{\omega^n_{i,j}B^{n+1}_{i,j,k-1/2}\left(1-\phi^n_{i,j,k-1/2}\right)}{\Delta z^n_k} \quad 5.204$$

$$\frac{\left(\omega_{i,j}f'_{i,j,k+1/2}-\omega_{i,j}f'_{i,j,k-1/2}\right)}{\Delta z_k} = \frac{\omega^n_{i,j}B^{n+1}_{i,j,k+1/2}\left(1-\phi^n_{i,j,k+1/2}\right)}{\Delta z^n_k} - \frac{F'_{adv,b}}{\Delta z^n_k} \quad 5.205$$

The term $\omega_{i,j}f_{i,j,k-1/2}$ in the equation **5.198** is replaced as $F'_{adv,b}$ which has been computed as the sediment-bed interface flux under the section **6.3.2.1**.

Using the first order upwind scheme to evaluate the surface concentrations;

$$B^{n+1}_{i,j,k+1/2} = B^{n+1}_{i,j,k} \text{ if } \omega^n_{i,j} \rangle 0 \quad 5.206$$

$$B^{n+1}_{i,j,k+1/2} = B^{n+1}_{i,j,k+1} \text{ if } \omega^n_{i,j} \langle 0 \tag{5.207}$$

Define a new operator $[\![A,B]\!]$ to denote the greater of A and B. Then the upwind scheme implies (Patankar, 1980);

$$\omega^n_{i,j} B^{n+1}_{i,j,k+1/2} = B^{n+1}_{i,j,k} [\![\omega^n_{i,j}, 0]\!] - B^{n+1}_{i,j,k+1} [\![-\omega^n_{i,j}, 0]\!] \tag{5.208}$$

Evaluating the control volume face porosities as the minimum between adjacent layer porosities;

$$\phi^n_{i,j,k+1/2} = MIN\left(\phi^n_{i,j,k+1}, \phi^n_{i,j,k}\right) \tag{5.209}$$

Then the advection term can be written as;

$$\frac{\left(\omega_{i,j} f'_{i,j,k+1/2} - \omega_{i,j} f'_{i,j,k-1/2}\right)}{\Delta z_k} = \frac{1}{\Delta z^n_k} \begin{bmatrix} \left(B^{n+1}_{i,j,k} [\![\omega^n_{i,j}, 0]\!] - B^{n+1}_{i,j,k+1} [\![-\omega^n_{i,j}, 0]\!]\right) \\ \left(1 - MIN\left(\phi^n_{i,j,k+1}, \phi^n_{i,j,k}\right)\right) - F'_{adv,b} \end{bmatrix} \tag{5.210}$$

3. Consider only the diffusion term

$$\frac{\left(F'_{i,j,k+1/2} - F'_{i,j,k-1/2}\right)}{\Delta z_k} = \frac{\left(K_{i,j,k+1/2} \dfrac{\partial B_{i,j,k+1/2}}{\partial z}\right)\left(1 - \phi_{i,j,k+1/2}\right)}{\Delta z_k} - \frac{\left(K_{i,j,k-1/2} \dfrac{\partial B_{i,j,k-1/2}}{\partial z}\right)\left(1 - \phi_{i,j,k-1/2}\right)}{\Delta z_k} \tag{5.211}$$

$$\frac{\left(F'_{i,j,k+1/2} - F'_{i,j,k-1/2}\right)}{\Delta z_k} = \frac{\left(K_{i,j,k+1/2} \dfrac{\partial B_{i,j,k+1/2}}{\partial z}\right)\left(1 - \phi_{i,j,k+1/2}\right)}{\Delta z_k} - \frac{F'_{dif,b}}{\Delta z_k} \tag{5.212}$$

Assume no diffusion at the bottom boundary and hence $F'_{dif,b} = 0$.

Evaluating the concentrations implicitly from the piecewise-linear profile and sediment layer thickness explicitly;

$$\frac{\partial B_{i,j,k+1/2}}{\partial z} = \frac{\left(B^{n+1}_{i,j,k+1} - B^{n+1}_{i,j,k}\right)}{\Delta z^n_{tk}} \tag{5.213}$$

where, $\Delta z^n_{tk} = \dfrac{\Delta z^n_k + \Delta z^n_{k+1}}{2}$

Evaluating the boundary porosities explicitly and as the minimum between adjacent layer porosities (equations **5.57**, **5.58**);

$$\frac{\left(F'_{i,j,k+1/2}-F'_{i,j,k-1/2}\right)}{\Delta z_k}=\frac{1}{\Delta z_k^n}\left[\left(K^n_{i,j,k+1/2}\frac{\left(B^{n+1}_{i,j,k+1}-B^{n+1}_{i,j,k}\right)}{\Delta z^n_{tk}}\right)\left(1-MIN\left(\phi^n_{i,j,k+1},\phi^n_{i,j,k}\right)\right)\right] \qquad 5.214$$

Substituting equations **5.203**, **5.210** and **5.214** in equation **5.198;**

$$\begin{aligned}\left[\frac{B^{n+1}_{i,j,k}-B^n_{i,j,k}}{\Delta t}\right]\left(1-\phi^n_{i,j,k}\right)&=-\frac{1}{\Delta z_k^n}\left[\begin{array}{l}\left(B^{n+1}_{i,j,k}\left[\!\left[\omega^n_{i,j},0\right]\!\right]-B^{n+1}_{i,j,k+1}\left[\!\left[-\omega^n_{i,j},0\right]\!\right]\right)\\ \left(1-MIN\left(\phi^n_{i,j,k+1},\phi^n_{i,j,k}\right)\right)-F'_{adv,b}\end{array}\right]\\ &+\frac{1}{\Delta z_k^n}\left[\left(K^n_{i,j,k+1/2}\frac{\left(B^{n+1}_{i,j,k+1}-B^{n+1}_{i,j,k}\right)}{\Delta z^n_{tk}}\right)\left(1-MIN\left(\phi^n_{i,j,k+1},\phi^n_{i,j,k}\right)\right)\right]\end{aligned} \qquad 5.215$$

$$\begin{aligned}\left[\frac{B^{n+1}_{i,j,k}-B^n_{i,j,k}}{\Delta t}\right]&=-\frac{1}{\Delta z_k^n}\left[\left(B^{n+1}_{i,j,k}\left[\!\left[\omega^n_{i,j},0\right]\!\right]-B^{n+1}_{i,j,k+1}\left[\!\left[-\omega^n_{i,j},0\right]\!\right]\right)\frac{\left(1-MIN\left(\phi^n_{i,j,k+1},\phi^n_{i,j,k}\right)\right)}{\left(1-\phi^n_{i,j,k}\right)}\right]\\ &+\frac{F'_{adv,b}}{\left(1-\phi^n_{i,j,k}\right)\Delta z^n_k}+\frac{1}{\Delta z_k^n}\left[\left(K^n_{i,j,k+1/2}\frac{\left(B^{n+1}_{i,j,k+1}-B^{n+1}_{i,j,k}\right)}{\Delta z^n_{tk}}\right)\frac{\left(1-MIN\left(\phi^n_{i,j,k+1},\phi^n_{i,j,k}\right)\right)}{\left(1-\phi^n_{i,j,k}\right)}\right]\end{aligned} \qquad 5.216$$

$$\begin{aligned}&[0]B^{n+1}_{i,j,k-1}\\ &+\left[\frac{1}{\Delta t}+\frac{1}{\Delta z_k^n}\left[\left[\!\left[\omega^n_{i,j},0\right]\!\right]\frac{\left(1-MIN\left(\phi^n_{i,j,k+1},\phi^n_{i,j,k}\right)\right)}{\left(1-\phi^n_{i,j,k}\right)}\right]+\frac{K^n_{i,j,k+1/2}}{\Delta z^n_k\Delta z^n_{tk}}\frac{\left(1-MIN\left(\phi^n_{i,j,k+1},\phi^n_{i,j,k}\right)\right)}{\left(1-\phi^n_{i,j,k}\right)}\right]B^{n+1}_{i,j,k}\\ &+\left[-\frac{\left[\!\left[-\omega^n_{i,j},0\right]\!\right]}{\Delta z^n_k}\frac{\left(1-MIN\left(\phi^n_{i,j,k+1},\phi^n_{i,j,k}\right)\right)}{\left(1-\phi^n_{i,j,k}\right)}-\frac{K^n_{i,j,k+1/2}}{\Delta z^n_k\Delta z^n_{tk}}\frac{\left(1-MIN\left(\phi^n_{i,j,k+1},\phi^n_{i,j,k}\right)\right)}{\left(1-\phi^n_{i,j,k}\right)}\right]B^{n+1}_{i,j,k+1}\\ &=\frac{B^n_{i,j,k}}{\Delta t}+\frac{F'_{adv,b}}{\left(1-\phi^n_{i,j,k}\right)\Delta z^n_k}\end{aligned} \qquad 5.217$$

$$\begin{aligned}&[0]B^{n+1}_{i,j,k-1}\\ &+\left[\frac{1}{\Delta t}+\left[\left(\frac{\left[\!\left[\omega^n_{i,j},0\right]\!\right]}{\Delta z^n_k}+\frac{K^n_{i,j,k+1/2}}{\Delta z^n_k\Delta z^n_{tk}}\right)\frac{\left(1-MIN\left(\phi^n_{i,j,k+1},\phi^n_{i,j,k}\right)\right)}{\left(1-\phi^n_{i,j,k}\right)}\right]\right]B^{n+1}_{i,j,k}\\ &+\left[-\left(\frac{\left[\!\left[-\omega^n_{i,j},0\right]\!\right]}{\Delta z^n_k}+\frac{K^n_{i,j,k+1/2}}{\Delta z^n_k\Delta z^n_{tk}}\right)\frac{\left(1-MIN\left(\phi^n_{i,j,k+1},\phi^n_{i,j,k}\right)\right)}{\left(1-\phi^n_{i,j,k}\right)}\right]B^{n+1}_{i,j,k+1}=\frac{B^n_{i,j,k}}{\Delta t}+\frac{F'_{adv,b}}{\left(1-\phi^n_{i,j,k}\right)\Delta z^n_k}\end{aligned} \qquad 5.218$$

This can be written as, $a_k.B^{n+1}_{i,j,k-1} + b_k.B^{n+1}_{i,j,k} + c_k.B^{n+1}_{i,j,k+1} = d_k$ where a_k, b_k and c_k are the implicit coefficients and d_k is the explicit coefficient.

$$a_k = 0 \tag{5.219}$$

$$b_k = \left[\frac{1}{\Delta t} + \left[\left(\frac{[\![\omega^n_{i,j}, 0]\!]}{\Delta z^n_k} + \frac{K^n_{i,j,k+1/2}}{\Delta z^n_k \Delta z^n_{tk}} \right) \frac{\left(1 - MIN\left(\phi^n_{i,j,k+1}, \phi^n_{i,j,k}\right)\right)}{\left(1 - \phi^n_{i,j,k}\right)} \right] \right] \tag{5.220}$$

$$c_k = \left[-\left(\frac{[\![-\omega^n_{i,j}, 0]\!]}{\Delta z^n_k} + \frac{K^n_{i,j,k+1/2}}{\Delta z^n_k \Delta z^n_{tk}} \right) \frac{\left(1 - MIN\left(\phi^n_{i,j,k+1}, \phi^n_{i,j,k}\right)\right)}{\left(1 - \phi^n_{i,j,k}\right)} \right] \tag{5.221}$$

$$d_k = \frac{B^n_{i,j,k}}{\Delta t} + \frac{F'_{adv,b}}{\left(1 - \phi^n_{i,j,k}\right) \Delta z^n_k} \tag{5.222}$$

These simultaneous equations are solved using a Tri Diagonal Matrix Algorithm described in the sub-section **5.4.4**.

5.4.4 Solution for the discretized equations

Solution for the discretized equation is obtained by adopting the Tri Diagonal Matrix Algorithm(TDMA) (Patankar, 1980).

$$a_k.B^{n+1}_{i,j,k-1} + b_k.B^{n+1}_{i,j,k} + c_k.B^{n+1}_{i,j,k+1} = d_k \tag{5.223}$$

After setting $a_{-kbe} = 0$ and $c_0 = 0$, $B^{n+1}_{i,j,-kbe-1}$ and $B^{n+1}_{i,j,1}$ do not have any meaningful role to play. When $k = -kbe$,

$$b_{-kbe}.B^{n+1}_{i,j,-kbe} + c_{-kbe}.B^{n+1}_{i,j,-kbe+1} = d_{-kbe} \tag{5.224}$$

$$B^{n+1}_{i,j,-kbe} = \frac{d_{-kbe} - c_{-kbe}.B^{n+1}_{i,j,-kbe+1}}{b_{-kbe}} \tag{5.225}$$

This means $B^{n+1}_{i,j,-kbe}$ is known in terms of $B^{n+1}_{i,j,-kbe+1}$. This can be continued until $B^{n+1}_{i,j,0}$ is expressed in terms of $B^{n+1}_{i,j,1}$

$$B^{n+1}_{i,j,0} = \frac{d_0 - c_0.B^{n+1}_{i,j,1}}{b_0} \tag{5.226}$$

But since $B_{i,j,1}^{n+1}$ has no meaningful existence, $B_{i,j,0}^{n+1}$ is obtained at this stage.

$$B_{i,j,0}^{n+1} = \frac{d_0}{b_0} \tag{5.227}$$

This enables us to begin the "back-substitution" process in which $B_{i,j,-1}^{n+1}$ in form of $B_{i,j,0}^{n+1}$, $B_{i,j,-2}^{n+1}$ in form of $B_{i,j,-1}^{n+1}$, ..., $B_{i,j,-kbe+1}^{n+1}$ in form of $B_{i,j,-kbe+2}^{n+1}$ and $B_{i,j,-kbe}^{n+1}$ in form of $B_{i,j,-kbe+1}^{n+1}$. In the forward substitution we seek a relation, $B_{i,j,k}^{n+1} = P_k B_{i,j,k+1}^{n+1} + Q_k$ We obtain,

$$B_{i,j,k-1}^{n+1} = P_{k-1} B_{i,j,k}^{n+1} + Q_{k-1} \tag{5.228}$$

Substituting the value of $B_{i,j,k-1}^{n+1}$ in equation $a_k.B_{i,j,k-1}^{n+1} + b_k.B_{i,j,k}^{n+1} + c_k.B_{i,j,k+1}^{n+1} = d_k$

$$a_k\left(P_{k-1}B_{i,j,k}^{n+1} + Q_{k-1}\right). + b_k.B_{i,j,k}^{n+1} + c_k.B_{i,j,k+1}^{n+1} = d_k \tag{5.229}$$

$$\left(a_k P_{k-1} + b_k\right) B_{i,j,k}^{n+1} + a_k Q_{k-1} + c_k.B_{i,j,k+1}^{n+1} = d_k \tag{5.230}$$

$$\left(a_k P_{k-1} + b_k\right) B_{i,j,k}^{n+1} = \left(-c_k\right) B_{i,j,k+1}^{n+1} + \left(d_k - a_k Q_{k-1}\right) \tag{5.231}$$

$$B_{i,j,k}^{n+1} = \left(\frac{-c_k}{a_k P_{k-1} + b_k}\right) B_{i,j,k+1}^{n+1} + \left(\frac{d_k - a_k Q_{k-1}}{a_k P_{k-1} + b_k}\right) \tag{5.232}$$

If we write the equation **5.232** in the form of $B_{i,j,k}^{n+1} = P_k B_{i,j,k+1}^{n+1} + Q_k$,then $P_k = \left(\frac{-c_k}{a_k P_{k-1} + b_k}\right)$ and $Q_k = \left(\frac{d_k - a_k Q_{k-1}}{a_k P_{k-1} + b_k}\right)$. Then the solution has been obtained through following steps.

Step_1: Calculate P and Q when $k = -kbe$

when $k = -kbe$, $a_{-kbe} = 0$ and hence,

$P_{-kbe} = \left(\frac{-c_{-kbe}}{b_{-kbe}}\right)$ and $Q_{-kbe} = \left(\frac{d_{-kbe}}{b_{-kbe}}\right)$

Step_2: Use recurrence relations to obtain Calculate P_k and Q_k when $k = \left(-kbe+1\right), \left(-kbe+2\right), ...-1, 0$

$P_k = \left(\frac{-c_k}{a_k P_{k-1} + b_k}\right)$ and $Q_k = \left(\frac{d_k - a_k Q_{k-1}}{a_k P_{k-1} + b_k}\right)$

Step_3: Calculate $B_{i,j,0}^{n+1}$ when $k=0$

When $k=0$, $c_0=0$ and that leads to $B_{i,j,1}^{n+1}=0$

From $B_{i,j,0}^{n+1}=P_0B_{i,j,1}^{n+1}+Q_0$

$B_{i,j,0}^{n+1}=Q_0$

Now we are in a position to start back substitution

Step_4: Calculate $B_{i,j,k}^{n+1}$ when $k=-1,-2,.....,\left(-kbe+1\right),-kbe$

Use the equation $B_{i,j,k-1}^{n+1}=P_{k-1}B_{i,j,k}^{n+1}+Q_{k-1}$ and calculate $B_{i,j,-1}^{n+1},B_{i,j,-2}^{n+1},.....,B_{i,j,-\mathrm{kbe}+1}^{n+1},B_{i,j,-kbe}^{n+1}$

5.4.5 Source terms

Similar to the pelagic model (refer section **4.1.4**) finite difference method with the fourth order Runge-Kutta method which gives the approximation of solutions of ordinary differential equations through explicit approach is used to obtain the solution for the source term equations **5.45** and **5.90**.

5.4.5.1 Kinetic equations for source terms in benthic model

The kinetic equations for source terms in benthic model are adopted refering (Ji, 2008) and (Di Toro, 2001).

Particulate Organic Carbon Labile

$$\frac{dB_{pocL}(i,j,k)}{dt}=-R_{B_{pocL}}\_\mathrm{dec\_oxic}(i,j,k)-R_{B_{pocL}}\_\mathrm{dec\_anoxic\_}no3(i,j,k)$$
$$-R_{B_{pocL}}\_\mathrm{dec\_anoxic\_}so4(i,j,k) \qquad 5.233$$

Oxic carbon diagenesis rate for labile POC

$$R_{B_{pocL},BpocL}\_\mathrm{dec}(i,j,k)=k_{B_{pocL},BpocL}\_\mathrm{dec}\times\theta_{B_{pocL}}^{(tempt(i,j,1-20)}\times B_{pocL}(i,j,k) \qquad 5.234$$

Since oxic decomposition rate is controlled by the availability of oxygen:

$$R_{B_{pocL},CpocL}\_\mathrm{dec\_oxic}(i,j,k)=k_{B_{pocL},\mathrm{B}\,pocL}\_\mathrm{dec\_oxic}\times\theta_{B_{pocL}}^{(tempt(i,j,1)-20)}\times\left[\frac{B_{dox}(i,j,k)}{K_{O_2,\mathrm{B}\,poc}+B_{dox}(i,j,k)}\right] \qquad 5.235$$
$$\times B_{pocL}(i,j,k)$$

Anoxic carbon diagenesis rate for labile POC or denitrification

Rate of nitrification $R_{B_{NO3},BpocL}\_\text{denit}(i,j,k)$ follows 1st order reaction rate constant $k_{B_{NO3},BpocL}\_\text{denit}$:

$$R_{B_{NO3},BpocL}\_\text{denit}(n,k) = k_{B_{NO3},BpocL}\_\text{denit}\left[B_{NO3}(i,j,k)\right] \quad 5.236$$

Since anoxic decomposition rate by the use of nitrate is controlled by the availability of oxygen and pock and temperature coefficient also applicable for the $R_{B_{NO3},BpocL}\_\text{denit}(i,j,k)$(temperature of the sediment has been considered as the temperature of the bottom layer of the water column):

$$R_{B_{NO3},BpocL}\_\text{denit}(i,j,k) = k_{B_{no3},BpocL}\_\text{denit}\times\theta_{B_{no3}}^{(tempt(i,j,1)-20)} \times MIN\left[\frac{K_{O_2,Bpoc}}{K_{O_2,Bpoc}+B_{dox}(i,j,k)}, \frac{B_{pocL}(i,j,k)}{K_{dec,Bpoc}+B_{pocL}(i,j,k)}\right]\times B_{no3}(i,j,k) \quad 5.237$$

$$R_{B_{pocL}}\_\text{dec\_anoxic\_no3}(i,j,k) = R_{B_{NO3},CpocL}\_\text{denit}(i,j,k)\times \text{rCN\_denit} \quad 5.238$$

Anoxic carbon diagenesis rate for labile POC or sulfate as electron acceptor

Since anoxic decomposition rate by the use of sulfate is controlled by the availability of oxygen and nitrate (Sulfate is abundant and has not considered as a limiting factor):

$$R_{B_{pocL}}\_\text{dec\_anoxic\_so4}(i,j,k) = k_{B_{pocL}}\_\text{dec\_anoxic\_so4}\times\theta_{B_{pocL}\_anoxic\_\_so4}^{(tempt(i,j,1)-20)} \times MIN\left[\frac{K_{O_2,Bpoc}}{K_{O_2,Bpoc}+B_{dox}(i,j,k)}, \frac{K_{Bno3,\text{denit}}}{K_{Bno3,\text{denit}}+B_{no3}(i,j,k)}\right]\times B_{pocL}(i,j,k) \quad 5.239$$

Particulate Organic Carbon Refractory

$$\frac{dB_{pocR}(i,j,k)}{dt} = -R_{B_{pocR}}\_\text{dec\_oxic}(i,j,k) - R_{B_{pocR}}\_\text{dec\_anoxic\_}no3(i,j,k) - R_{B_{pocR}}\_\text{dec\_anoxic\_}so4(i,j,k) \quad 5.240$$

Oxic carbon diagenesis rate for refractory POC

$$R_{B_{pocR}}\_\text{dec}(i,j,k) = k_{B_{pocR}}\_\text{dec}\times\theta_{B_{pocR}}^{(tempt(i,j,1)-20)}\times B_{pocR}(i,j,k)$$

Since oxic decomposition rate is controlled by the availability of oxygen:

$$R_{B_{pocR}}\_\text{dec\_oxic}(i,j,k) = k_{B_{pocR}}\_\text{dec\_oxic}\times\theta_{B_{pocR}}^{(tempt(i,j,1)-20)}\times\left[\frac{B_{dox}(i,j,k)}{K_{O_2,Bpoc}+B_{dox}(i,j,k)}\right]\times B_{pocR}(i,j,k) \quad 5.241$$

Anoxic carbon diagenesis rate for refractory POC or denitrification

Since anoxic decomposition rate by the use of nitrate is controlled by the availability of oxygen and pock and temperature coefficient also applicable for the $R_{B_{NO3},BpocR}\_\text{denit}(i,j,k)$ (temperature of the sediment has been considered as the temperature of the bottom layer of the water column):

$$R_{B_{NO3},BpocR}\_\text{denit}(i,j,k) = k_{B_{no3},BpocR}\_\text{denit} \times \theta_{B_{no3}}^{(tempt(i,j,1)-20)} \times MIN\left[\frac{K_{O_2,Bpoc}}{K_{O_2,Bpoc}+B_{dox}(i,j,k)}, \frac{B_{pocR}(i,j,k)}{K_{dec,Bpoc}+B_{pocR}(i,j,k)}\right] \times B_{no3}(i,j,k) \quad 5.242$$

$$R_{B_{pocR}}\_\text{dec\_anoxic\_no3}(i,j,k) = R_{B_{NO3},BpocR}\_\text{denit}(i,j,k) \times \text{rCN\_denit} \quad 5.243$$

Anoxic carbon diagenesis rate for refractory POC or sulfate as electron acceptor

Since anoxic decomposition rate by the use of sulfate is controlled by the availability of oxygen and nitrate (Sulfate is abundant and has not considered as a limiting factor):

$$R_{B_{pocR}}\_\text{dec\_anoxic\_so4}(i,j,k) = k_{B_{pocR}}\_\text{dec\_anoxic\_so4} \times \theta_{B_{pocR}\_anoxic\_so4}^{(tempt(i,j,1)-20)} \times MIN\left[\frac{K_{O_2,Bpoc}}{K_{O_2,Bpoc}+B_{dox}(i,j,k)}, \frac{K_{Bno3,\text{denit}}}{K_{Bno3,\text{denit}}+B_{no3}(i,j,k)}\right] \times B_{pocR}(i,j,k) \quad 5.244$$

Particulate Organic Carbon Inert

$$\frac{dB_{pocI}(i,j,k)}{dt} = -R_{B_{pocI}}\_\text{dec\_oxic}(i,j,k) - R_{B_{pocI}}\_\text{dec\_anoxic\_}no3(i,j,k) - R_{B_{pocI}}\_\text{dec\_anoxic\_}so4(i,j,k) \quad 5.245$$

Oxic carbon diagenesis rate for refractory POC

$$R_{B_{pocI}}\_\text{dec}(i,j,k) = k_{B_{pocI}}\_\text{dec} \times \theta_{B_{pocI}}^{(tempt(i,j,1)-20)} \times B_{pocI}(i,j,k)$$

Since oxic decomposition rate is controlled by the availability of oxygen:

$$R_{B_{pocI}}\_\text{dec\_oxic}(i,j,k) = k_{B_{pocI}}\_\text{dec\_oxic} \times \theta_{B_{pocI}}^{(tempt(i,j,1)-20)} \times \left[\frac{B_{dox}(i,j,k)}{K_{O_2,Bpoc}+B_{dox}(i,j,k)}\right] \times B_{pocI}(i,j,k) \quad 5.246$$

Anoxic carbon diagenesis rate for refractory POC or denitrification

Since anoxic decomposition rate by the use of nitrate is controlled by the availability of oxygen and pocI and temperature coefficient also applicable for the $R_{B_{NO3},CpocI}\_\text{denit}(i,j,k)$

(temperature of the sediment has been considered as the temperature of the bottom layer of the water column):

$$R_{B_{NO3},BpocI}\_\text{denit}(i,j,k) = k_{B_{no3},BpocI}\_\text{denit} \times \theta_{B_{no3}}^{(tempt(i,j,1)-20)} \times MIN\left[\frac{K_{O_2,Bpoc}}{K_{O_2,Bpoc}+B_{dox}(i,j,k)}, \frac{B_{pocI}(i,j,k)}{K_{dec,Cpoc}+B_{pocI}(i,j,k)}\right] \times B_{no3}(i,j,k) \quad 5.247$$

$$R_{B_{pocI}}\_\text{dec\_anoxic\_no3}(i,j,k) = R_{B_{NO3},BpocI}\_\text{denit}(i,j,k) \times \text{rCN\_denit} \quad 5.248$$

Anoxic carbon diagenesis rate for refractory POC or sulfate as electron acceptor

Since anoxic decomposition rate by the use of sulfate is controlled by the availability of oxygen and nitrate (Sulfate is abundant and has not considered as a limiting factor):

$$R_{B_{pocI}}\_\text{dec\_anoxic\_so4}(i,j,k) = k_{B_{pocI}}\_\text{dec\_anoxic\_so4} \times \theta_{B_{pocI}\_anoxic\_so4}^{(tempt(i,j,1)-20)} \times MIN\left[\frac{K_{O_2,Bpoc}}{K_{O_2,Bpoc}+B_{dox}(i,j,k)}, \frac{K_{Bno3,\text{denit}}}{K_{Bno3,\text{denit}}+B_{no3}(i,j,k)}\right] \times B_{pocI}(i,j,k) \quad 5.249$$

Phosphorous

$$\frac{dB_{PO_4}(i,j,k)}{dt} = \left\{\begin{array}{l}\sum_{q=1}^{2} R_{B_{poc,q}}\_\text{dec\_oxic}(i,j,k) \\ +\sum_{q=1}^{2} R_{B_{poc,q}}\_\text{dec\_anoxic\_no3}(i,j,k) \\ +\sum_{q=1}^{2} R_{B_{poc,q}}\_\text{dec\_anoxic\_so4}(i,j,k)\end{array}\right\} \times \text{rPC\_dec} \quad 5.250$$

Ammonia

$$\frac{dB_{NH_4}(i,j,k)}{dt} = \left\{\begin{array}{l}\sum_{q=1}^{2} R_{B_{poc,q}}\_\text{dec\_oxic}(i,j,k) \\ +\sum_{q=1}^{2} R_{B_{poc,q}}\_\text{dec\_anoxic\_no3}(i,j,k) \\ +\sum_{q=1}^{2} R_{B_{poc,q}}\_\text{dec\_anoxic\_so4}(i,j,k)\end{array}\right\} \times \text{rNC\_dec} - R_{B_{NH_4}}\_\text{nit}(i,j,k) \quad 5.251$$

Rate of Nitrification flux

Rate of nitrification $R_{B_{NH_4}}\_\text{nit}(i,j,k)$ follows 1st order reaction rate constant $k_{B_{NH_4}}\_\text{nit}$ $R_{B_{NH_4}}\_\text{nit}(i,j,k)$ decreases as the ammonia concentration increases $R_{B_{NH_4}}\_\text{nit}(i,j,k)$ follows

Monod kinetics with respect to $B_{NH_4}(i,j,k)$:

$$R_{B_{NH_4}}\_\text{nit}(i,j,k) = k_{B_{NH_4}}\_\text{nit}\left[B_{NH_4}(i,j,k)\right]\left[\frac{K_{M,B_{NH_4}}}{K_{M,B_{NH_4}} + B_{NH_4}(i,j,k)}\right] \quad 5.252$$

$R_{B_{NH_4}}\_\text{nit}(i,j,k)$ decreases with decreasing oxygen concentration $R_{B_{NH_4}}\_\text{nit}(i,j,k)$ follows Michaelis-Menton expression:

$$R_{B_{NH_4}}\_\text{nit}(i,j,k) = k_{B_{NH_4}}\_\text{nit}\left[B_{NH_4}(i,j,k)\right]\left[\frac{K_{M,B_{NH_4}}}{K_{M,B_{NH_4}} + B_{NH_4}(i,j,k)}\right]\left[\frac{B_{dox}(i,j,k)}{K_{O_2,B_{NH_4}} + B_{dox}(i,j,k)}\right] \quad 5.253$$

Temperature coefficient also applicable to $R_{B_{NH_4}}\_\text{nit}(i,j,k)$ and temperature of the sediment has been considered as the temperature of the bottom layer of the water column.

$$R_{B_{NH_4}}\_\text{nit}(i,j,k) = k_{B_{NH_4}}\_\text{nit}\times\theta_{B_{NH_4}}^{(tempt(i,j,1)-20)}\left[B_{NH_4}(i,j,k)\right]\left[\frac{K_{M,B_{NH_4}}\theta_{K_{M,B_{NH_4}}}^{(tempt(i,j,k)-20)}}{K_{M,B_{NH_4}}\theta_{K_{M,B_{NH_4}}}^{(tempt(i,j,k)-20)} + B_{NH_4}(i,j,k)}\right]\left[\frac{B_{dox}(i,j,k)}{K_{O_2,B_{NH_4}} + B_{dox}(i,j,k)}\right] \quad 5.254$$

Nitrate

$$\frac{dB_{NO3}(i,j,k)}{dt} = R_{B_{NH_4}}\_\text{nit}(i,j,k) - \left\{\sum_q^2 R_{B_{NO3},BpocR}\_\text{denit}(i,j,k)\right\} \quad 5.255$$

Particulate Silica

$$\frac{dB_{PSi}(i,j,k)}{dt} = -R_{B_{Si}}\_\text{pro}(i,j,k)\times\text{rSi\_PSi} \quad 5.256$$

Dissolved silica production rate or Particulate silica dissolution rate

Rate of silica production $R_{B_{Si}}\_\text{pro}(i,j,k)$ follows 1st order reaction rate constant $k_{B_{Si}}\_\text{pro}$, $R_{B_{Si}}\_\text{pro}(i,j,k)$ is proportional to the silica solubility deficit $\left[B_{Si,sat} - B_{Si}(i,j,k)\right]$, $R_{B_{Si}}\_\text{pro}(i,j,k)$ is proportional to the particulate biogenic silica concentration, and $R_{B_{Si}}\_\text{pro}(i,j,k)$ follows the temperature coefficient (temperature of the sediment has been considered as the temperature of the bottom layer of the water column):

$$R_{B_{Si}}\_\text{pro}(i,j,k) = k_{B_{Si}}\theta_{B_{Si}}^{(tempt(i,j,1)-20)}\left[B_{PSi}(i,j,k)\right]\left[B_{Si,sat} - B_{Si}(i,j,k)\right] \quad 5.257$$

$R_{B_{Si}}$ _pro(i,j,k) follows Michaelis-Menton expression:

$$R_{B_{Si}}\text{\_pro}(i,j,k) = k_{B_{Si}}\theta_{B_{Si}}^{(tempt(i,j,k)-20)}\left[\frac{B_{PSi}(i,j,k)}{B_{PSi}(i,j,k)+K_{M,C_{PSi}}}\right]\left[B_{Si,sat}-B_{Si}(i,j,k)\right] \quad 5.258$$

Dissolved Silica

$$\frac{dB_{Si}(i,j,k)}{dt} = R_{B_{Si}}\text{\_pro}(i,j,k) \quad 5.259$$

Sulfide

$$\frac{dB_{H_2S}(i,j,k)}{dt} = \left\{\sum_{q=1}^{2} R_{B_{poc,q}}\text{\_dec\_anoxic\_so}4(i,j,k)\right\}\times \text{rCS\_dec} - R_{B_{H_2S}}\text{\_oxi}(i,j,k) \quad 5.260$$

Sulfide oxidation rate

Rate of sulfide oxidation $R_{B_{H_2S}}$ _oxi(i,j,k) follows 1st order reaction rate constant $k_{B_{H_2S}}$ _oxi and $R_{B_{H_2S}}$ _oxi(i,j,k) depends on the concentration of oxygen:

$$R_{B_{H_2S}}\text{\_oxi}(i,j,k) = k_{B_{H_2S}}\text{\_oxi}\left[\frac{B_{dox}(i,j,k)}{K_{M,B_{H_2S},O_2}}\right]\frac{1}{\text{rCS\_oxi}}$$

Temperature coefficient also applicable for $R_{B_{H_2S}}$ _oxi(i,j,k) and temperature of the sediment has been considered as the temperature of the bottom layer of the water column.

$$R_{B_{H_2S}}\text{\_oxi}(i,j,k) = k_{B_{H_2S}}\text{\_oxi}\times\theta_{B_{H_2S}}^{(tempt(i,j,1)-20)}\left[\frac{B_{dox}(i,j,k)}{K_{M,B_{H_2S},O_2}}\right]\frac{1}{\text{rOS\_oxi}} \quad 5.261$$

Dissolved Oxygen

$$\frac{dB_{dox}(i,j,k)}{dx} = -\left\{\sum_{q=1}^{2} R_{B_{poc,q}}\text{\_dec\_oxic}(i,j,k)\right\}\times\text{rOC\_dec} - R_{B_{NH_4}}\text{\_nit}(i,j,k)\times\text{rON\_nit} - R_{B_{H_2S}}\text{\_oxi}(i,j,k)\times\text{rOS\_oxi} \quad 5.262$$

5.5 Evaluation of the burial rate

Assume that the accumulation or erosion occurs within the top layer of the sediment. Burial rate has defined as upward positive. Depositional or erosion flux which has been computed in equation **4.122** under pelagic model (4.1.3) has been considered the flux at the bottom of the water column is downward direction . Burial rate is defined as;

$$\omega_{i,j} = -\frac{\left[Flux\_ss_{i,j} \times 10^{-3} + \left(Flux\_poc_{i,j} + Flux\_psi_{i,j} + Flux\_phy_{i,j} \right) \times 10^{-6} \right]}{\rho_{bulk}} \qquad 5.263$$

where bulk density is computed as the total mass of material within the control volume including the mass of water divided by the bulk volume.

$$\rho_{bulk} = \frac{m_s + m_{poc} + m_{psi} + m_w}{V_b} \qquad 5.264$$

Since the concentrations of state variables are defined as the mass of material of corresponding state variable in unit bulk volume;

$$\rho_{bulk} = \frac{Bss_{i,j,0} \times 10^{-3} V_b + \left(Bpoc_{i,j,0} V_b + Bpsi_{i,j,0} V_b \right) \times 10^{-6} + \phi_{i,j,0} V_b \rho_w}{V_b} \qquad 5.265$$

$$\rho_{bulk} = Bss_{i,j,0} \times 10^{-3} + \left(Bpoc_{i,j,0} + Bpsi_{i,j,0} \right) \times 10^{-6} + \phi_{i,j,0} \rho_w \qquad 5.266$$

Then the burial rate is computed as shown in the equation **5.267** and this has been computed explicitly in the model.

$$\omega_{i,j} = -\frac{\left[Flux\_ss_{i,j} \times 10^{-3} + \left(Flux\_poc_{i,j} + Flux\_psi_{i,j} + Flux\_phy_{i,j} \right) \times 10^{-6} \right]}{Bss_{i,j,0} \times 10^{-3} + \left(Bpoc_{i,j,0} + Bpsi_{i,j,0} \right) \times 10^{-6} + \phi_{i,j,0} \rho_w} \qquad 5.267$$

6. BOUNDARY FLUX ANALYSIS AND BENTHIC-PELAGIC MODEL COUPLING

Three types of boundary fluxes are discussed in this chapter in particular the flux at the surface of the water column, flux at the water-sediment interface and the flux at the bottom of the sediment column. It has been considered no flux at the surface of the water column for all the state variables except for the dissolved oxygen,. At the bottom of a water body or the sediment water interface, dissolved nutrients and dissolved oxygen constantly exchange between the sediment bed and the overlying water through a process of diffusion which is largely controlled by the difference in the concentrations between the sediment bed and the overlying water. Moreover, the diffusion flux from sediment to water is controlled not only by the concentration difference of nutrients but also by the oxygen concentration at the bottom of the water column. It has been assumed that zero diffusion flux for the particulate matter at the sediment-water interface. Advection flux due to burial effect also creates the exchange of flux through the sediment-water interface for both dissolved and particulate matter. It has been assumed that zero diffusion flux for all the state variables at the bottom of the sediment column while advection flux is considered for both dissolved and particulate matter due to burial effect.

6.1 Dissolved oxygen flux at the water surface

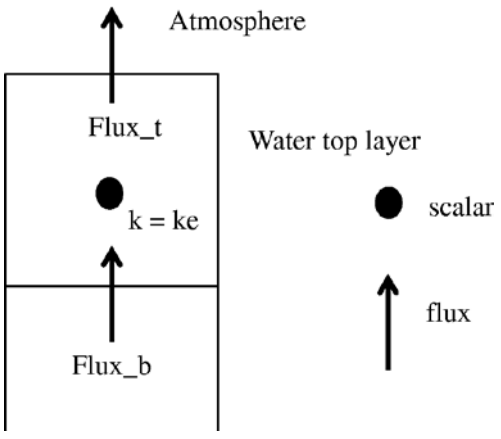

Fig 6.1 2D Control volume at water surface layer

Flux through the surface diffusive boundary is applicable only for the dissolved oxygen state variable which is affected by reaeration due to the difference in concentrations of oxygen in the atmosphere and in the surface layer of water column, while there is no diffusive boundary flux for all other parameters. This has treated implicitly in the following derivation. Consider the vertical diffusion term $\frac{\partial}{\partial z}\left[K_z \frac{\partial C_{i,\mathrm{j},k}}{\partial z}\right]$ described in the equation **4.11**.

$$\frac{\partial}{\partial z}\left\{K_v \frac{\partial C_{DOX_{i,j,k}}}{\partial z}\right\} = \frac{1}{\Delta z}\left\{\left[-K_v \frac{\Delta C_{DOX_{i,j,k}}}{\Delta z}\right]_t - \left[-K_v \frac{\Delta C_{DOX_{i,j,k}}}{\Delta z}\right]_b\right\} \tag{6.1}$$

According to the Fick's law, rate of dissolved matter transfer due to diffusion is inversely proportional to the gradient of dissolved matter concentration and $Flux = -K_v \frac{\partial C}{\partial z}$.

$$\frac{\partial}{\partial z}\left\{K_v \frac{\partial C_{DOX_{i,j,k}}}{\partial z}\right\} = \frac{1}{\Delta z}\left(Flux\_t - flux\_b\right) \tag{6.2}$$

According to (Ji, 2008) rate of reaeration is proportional to the DO deficit.

$$Flux_t = -K_{reaeration}\left(C_{sat} - C_{DOX_{i,j,ke}}^{n+1}\right) \tag{6.3}$$

$$\left[-K_v \frac{\Delta C_{DOX_{i,j,k}}}{\Delta z}\right]_t = \frac{1}{D^{n+1}}\left[-K_v \frac{\Delta C_{DOX_{i,j,k}}}{\Delta \sigma}\right]_t = -K_{reaeration}\left(C_{sat} - C_{DOX_{i,j,ke}}^{n+1}\right) \tag{6.4}$$

$$\frac{1}{D^{n+1}}\frac{\partial}{\partial \sigma}\left[K_v \frac{\partial C_{DOX_{i,j,k}}}{\partial \sigma}\right]_t = \frac{1}{D^{n+1}}\frac{1}{\Delta \sigma}\left[K_v \frac{\Delta C_{DOX_{i,j,ke}}}{\Delta \sigma}\right]_t \tag{6.5}$$

$$\frac{1}{D^{n+1}}\frac{\partial}{\partial \sigma}\left[K_v \frac{\partial C_{DOX_{i,j,k}}}{\partial \sigma}\right]_t = \frac{1}{D^{n+1}}\frac{1}{\Delta \sigma}\left[D^{n+1} \times K_{reaeration}\left(C_{sat} - C_{DOX_{i,j,ke}}^{n+1}\right)\right] \tag{6.6}$$

$$\frac{1}{D^{n+1}}\frac{\partial}{\partial \sigma}\left[K_v \frac{\partial C_{DOX_{i,j,k}}}{\partial \sigma}\right]_t = \frac{1}{\Delta \sigma}\left[K_{reaeration}\left(C_{sat} - C_{DOX_{i,j,ke}}^{n+1}\right)\right] \tag{6.7}$$

$$\frac{1}{D^{n+1}}\frac{\partial}{\partial \sigma}\left[K_v \frac{\partial C_{DOX_{i,j,k}}}{\partial \sigma}\right]_t = \frac{1}{\Delta \sigma}\left[K_{reaeration}\left(C_{sat} - C_{DOX_{i,j,ke}}^{n+1}\right)\right] \tag{6.8}$$

Bottom diffusion flux for dissolved oxygen can be written as;

$$Flux_b = \left[-K_v \frac{\Delta C_{DOX_{i,j,k}}}{\Delta z} \right]_b \tag{6.9}$$

$$\left[-K_v \frac{\Delta C_{DOX_{i,j,k}}}{\Delta z} \right]_b = \frac{1}{D^{n+1}} \frac{\partial}{\partial \sigma} \left[-K_v \frac{\partial C_{DOX_{i,j,k}}}{\partial \sigma} \right]_b = \frac{1}{\Delta \sigma} \left[-K_v \frac{\Delta C_{DOX_{i,j,ke-1}}}{D^{n+1} \Delta \sigma} \right]_b \tag{6.10}$$

$$\frac{1}{D^{n+1}} \frac{\partial}{\partial \sigma} \left[K_v \frac{\partial C_{DOX_{i,j,k}}}{\partial \sigma} \right]_b = \frac{1}{\Delta \sigma} \left[K_v \frac{\Delta C_{DOX_{i,j,k}}}{D^{n+1} \Delta \sigma} \right]_b \tag{6.11}$$

According to the equation **4.13** diffusion term in sigma coordinate is $\frac{1}{D} \frac{\partial}{\partial \sigma} \left(K_v \frac{\partial C_{i,j,k}}{\partial \sigma} \right)$.

Hence;

$$\frac{1}{D^{n+1}} \frac{\partial}{\partial \sigma} \left\{ K_v \frac{\partial C_{DOX_{i,j,k}}}{\partial \sigma} \right\} = \frac{1}{D^{n+1}} \frac{\partial}{\partial \sigma} \left[K_v \frac{\partial C_{DOX_{i,j,k}}}{\partial \sigma} \right]_t - \frac{1}{D^{n+1}} \frac{\partial}{\partial \sigma} \left[K_v \frac{\partial C_{DOX_{i,j,k}}}{\partial \sigma} \right]_b \tag{6.12}$$

$$\frac{1}{D^{n+1}} \frac{\partial}{\partial \sigma} \left\{ K_v \frac{\partial C_{DOX_{i,j,k}}}{\partial \sigma} \right\} = \frac{1}{\Delta \sigma} \left[K_{reaeration} \left(C_{sat} - C_{DOX_{i,j,ke}}^{n+1} \right) \right] - \frac{1}{\Delta \sigma} \left[K_v \frac{\Delta C_{DOX_{i,j,k}}}{D^{n+1} \Delta \sigma} \right]_b \tag{6.13}$$

Diffusion term for dissolved oxygen in sigma coordinates $\frac{1}{D} \frac{\partial}{\partial \sigma} \left(K_v \frac{\partial C_{i,j,k}}{\partial \sigma} \right)$ is revised by using the term defined in the equation **6.13**. For the convenience in the model the term $\frac{1}{\Delta \sigma} \left[K_{reaeration} \left(C_{sat} - C_{DOX_{i,j,ke}}^{n+1} \right) \right]$ is added to the source term and computed explicitly.

6.2 Flux at sediment-water interface

It has been considered that only diffusion flux is applied for dissolved matter and depositional or erosion flux is applied for particulate matter at the sediment-water interface. Flux of dissolved matter at sediment-water interface is computed under this section while particulate matter flux has at sediment-water interface has been computed under section **4.1.3**.

6.2.1 Dissolved matter

6.2.1.1 Diffusion flux at the surface boundary

According to the equation **5.36** diffusion term is $-\frac{\partial}{\partial z}\left[K_{i,\mathrm{j},k}\times\phi_{i,\mathrm{j},k}\times\frac{\partial B_{i,\mathrm{j},k}}{\partial z}\right]$ and hence diffusion flux from sediment to water is computed as;

$$Diffusion\_flux\_s2w=\left[-K_{i,j,k+1/2}\frac{\partial B_{i,j,k+1/2}}{\partial z}\phi^{n}_{i,\mathrm{j},k+1/2}\right]\times flag1\_0 \qquad 6.14$$

where, $flag1\_0=1$ only when $k=0$.

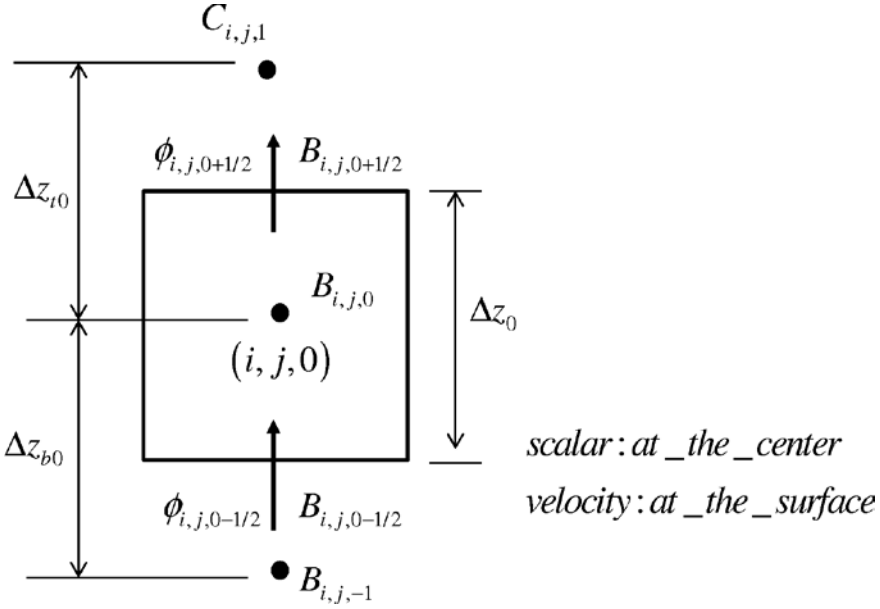

Fig 6.2 2D Control volume at sediment-water interface

Boundary flux has been considered as shown in the **Fig 6.3**.

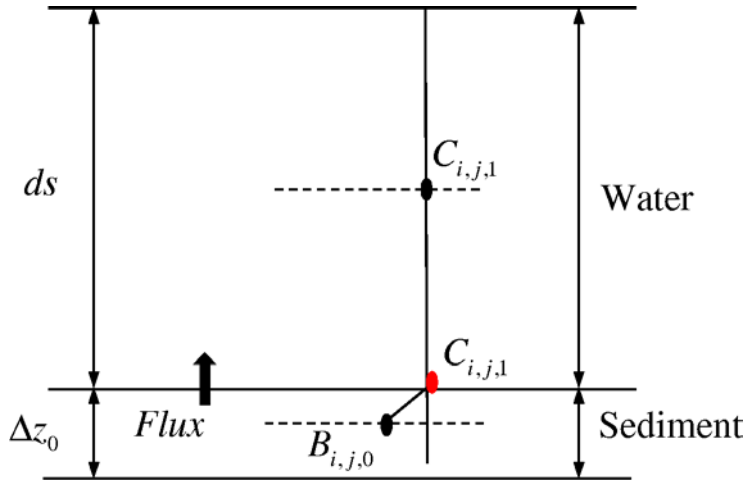

Fig 6.3 Boundary flux at sediment-water interface

Diffusion flux from sediment to water is written as;

$$Diffusion\_flux\_s2w_{i,j}^{n} = \left[-K_{i,j,0+1/2}^{n} \frac{C_{i,j,1}^{n+1} - B_{i,j,0}^{n+1}}{\frac{\Delta z_0^n}{2}} \phi_{i,\mathrm{j},0+1/2}^{n} \right] \times flag1\_0 \qquad 6.15$$

Evaluate the control volume face porosities explicitly and as the minimum between adjacent layer porosities. $\phi_{i,j,0+1/2}^{n} = MIN\left(\phi_{i,j,1}^{n}, \phi_{i,j,0}^{n}\right)$

$$Diffusion\_flux\_s2w_{i,j}^{n} = \left[-K_{i,j,0+1/2}^{n} \frac{C_{i,j,1}^{n+1} - B_{i,j,0}^{n+1}}{\frac{\Delta z_0^n}{2}} MIN\left(\phi_{i,j,1}^{n}, \phi_{i,j,0}^{n}\right) \right] \times flag1\_0 \qquad 6.16$$

Assume, $\phi_{i,j,1}^{m} = 1$

$$Diffusion\_flux\_s2w_{i,j}^{n} = \left[-K_{i,j,0+1/2}^{n} \frac{C_{i,j,1}^{n+1} - B_{i,j,0}^{n+1}}{\frac{\Delta z_0^n}{2}} MIN\left(1, \phi_{i,j,0}^{n}\right) \right] \times flag1\_0 \qquad 6.17$$

$$Diffusion\_flux\_s2w_{i,j}^{n} = \left[-K_{i,j,0+1/2}^{n} \frac{C_{i,j,1}^{n+1} - B_{i,j,0}^{n+1}}{\frac{\Delta z_0^n}{2}} \phi_{i,j,0}^{n} \right] \times flag1\_0 \qquad 6.18$$

since $K_{i,j,0+1/2}^{n} = \left(f_p D_p + f_d D_d\right)_{i,j,0+1/2}^{n}$

$$Diffusion\_flux\_s2w_{i,j}^{n} = \left[-\left(f_p D_p + f_d D_d\right)_{i,j,0+1/2}^{n} \frac{C_{i,j,1}^{n+1} - B_{i,j,0}^{n+1}}{\frac{\Delta z_0^n}{2}} \phi_{i,j,0}^{n} \right] \times flag1\_0 \qquad 6.19$$

6.2.1.2 Advection Flux at the surface boundary

According to the equation **5.36** advection term is $\omega_{i,\mathrm{j}} \frac{\partial\left(B_{i,\mathrm{j},k} \times \phi_{i,\mathrm{j},k}\right)}{\partial z}$ and hence advection flux from sediment to water is computed as;

$$flux\_s2w_{i,j}^{n} = \left[\omega_{i,j}^{n} B_{i,j,k+1/2}^{n+1} \phi_{i,\mathrm{j},k+1/2}^{n} \right] \times flag1\_0 \qquad 6.20$$

where, $flag1\_0 = 1$ only when $k = 0$. From the upwind scheme;

$\omega_{i,j}^{n} B_{i,j,k+1/2}^{n+1} = B_{i,j,k}^{n+1} [\![\omega_{i,j}^{n}, 0]\!] - B_{i,j,k+1}^{n+1} [\![-\omega_{i,j}^{n}, 0]\!]$ and hence;

$$flux\_s2w_{i,j}^{n} = \left[B_{i,j,k}^{n+1} [\![\omega_{i,j}^{n}, 0]\!] - B_{i,j,k+1}^{n+1} [\![-\omega_{i,j}^{n}, 0]\!] \right] \phi_{i,\mathrm{j},k+1/2}^{n} \times flag1\_0 \qquad 6.21$$

since $B_{i,j,k+1}^{n+1} \times flag1\_0 = C_{i,j,1}^{n+1}$

$$flux\_s2w_{i,j}^{n} = \left[B_{i,j,k}^{n+1} [\![\omega_{i,j}^{n}, 0]\!] - C_{i,j,1}^{n+1} [\![-\omega_{i,j}^{n}, 0]\!] \right] \phi_{i,\mathrm{j},k+1/2}^{n} \times flag1\_0 \qquad 6.22$$

Evaluate the control volume face porosities explicitly and as the minimum between adjacent layer porosities $\phi_{i,j,k+1/2}^{n} = MIN\left(\phi_{i,j,k+1}^{n}, \phi_{i,j,k}^{n}\right)$.

$$flux\_s2w_{i,j}^{n} = \left[B_{i,j,k}^{n+1} [\![\omega_{i,j}^{n}, 0]\!] - C_{i,j,1}^{n+1} [\![-\omega_{i,j}^{n}, 0]\!] \right] MIN\left(\phi_{i,j,k+1}^{n}, \phi_{i,j,k}^{n}\right) \times flag1\_0 \qquad 6.23$$

Assume, $\phi_{\mathrm{n},k+1}^{m} \times flag1\_0 = 1$

$$flux\_s2w_{i,j}^{n} = \left[B_{i,j,k}^{n+1} [\![\omega_{i,j}^{n}, 0]\!] - C_{i,j,1}^{n+1} [\![-\omega_{i,j}^{n}, 0]\!] \right] MIN\left(1, \phi_{i,j,k}^{n}\right) \times flag1\_0 \qquad 6.24$$

$$flux\_s2w_{i,j}^{n} = \left[B_{i,j,k}^{n+1} [\![\omega_{i,j}^{n}, 0]\!] - C_{i,j,1}^{n+1} [\![-\omega_{i,j}^{n}, 0]\!] \right] \phi_{i,j,k}^{n} \times flag1\_0 \qquad 6.25$$

6.3 Flux at the bottom of the sediment

It has been considered that only advection flux is applied for both dissolved matter and particulate matter at the sediment-bed interface while diffusion flux has been assumed zero.

6.3.1 Dissolved matter

6.3.1.1 Advection flux at the bottom boundary

According to the equation **5.36** advection term is $\omega_{i,\mathrm{j}} \frac{\partial \left(B_{i,\mathrm{j},k} \times \phi_{i,\mathrm{j},k} \right)}{\partial z}$ and hence advection flux from bed to bottom sediment is computed as;

$$flux\_b2s_{i,j}^{n} = \left[\omega_{i,j}^{n} B_{i,j,k-1/2}^{n+1} \phi_{i,\mathrm{j},k-1/2}^{n} \right] \times flag1\_(-kbe) \qquad 6.26$$

where, $flag1\_(-\text{kbe}) = 1$ only when $k = -kbe$. From the upwind scheme;

$\omega^n_{i,j} B^{n+1}_{i,j,k-1/2} = B^{n+1}_{i,j,k-1} [\![\omega^n_{i,j}, 0]\!] - B^{n+1}_{i,j,k} [\![-\omega^n_{i,j}, 0]\!]$ and hence;

$$flux\_b2s^n_{i,j} = \left[B^{n+1}_{i,j,k-1} [\![\omega^n_{i,j}, 0]\!] - B^{n+1}_{i,j,k} [\![-\omega^n_{i,j}, 0]\!] \right] \phi^n_{i,\text{j},k-1/2} \times flag1\_(-kbe) \quad 6.27$$

Assume, $B^{n+1}_{i,j,k-1} \times flag1\_(-\text{kbe}) = B^{n+1}_{i,j,k} \times flag1\_(-\text{kbe})$ and hence;

$$flux\_b2s^n_{i,j} = \left[[\![\omega^n_{i,j}, 0]\!] - [\![-\omega^n_{i,j}, 0]\!] \right] B^{n+1}_{i,j,k} \phi^n_{i,\text{j},k-1/2} \times flag1\_(-kbe) \quad 6.28$$

Evaluate the control volume face porosities explicitly and as the minimum between adjacent layer porosities $\phi^n_{i,j,k-1/2} = MIN\left(\phi^n_{i,j,k}, \phi^n_{i,j,k-1}\right)$.

$$flux\_b2s^n_{i,j} = \left[[\![\omega^n_{i,j}, 0]\!] - [\![-\omega^n_{i,j}, 0]\!] \right] B^{n+1}_{i,j,k} \times MIN\left(\phi^n_{i,j,k}, \phi^n_{i,j,k-1}\right) \times flag1\_(-kbe) \quad 6.29$$

Assume, $\phi^m_{\text{n},k-1} \times flag1\_(-\text{kbe}) = \phi^m_{\text{n},k} \times flag1\_(-\text{kbe})$ and hence;

$$flux\_b2s^n_{i,j} = \left[[\![\omega^n_{i,j}, 0]\!] - [\![-\omega^n_{i,j}, 0]\!] \right] B^{n+1}_{i,j,k} \phi^n_{i,j,k} \times flag1\_(-kbe) \quad 6.30$$

6.3.2 Particulate matter

6.3.2.1 Advection flux at the bottom boundary

According to the equation **5.88** advection term is $\omega_{i,j} \dfrac{\partial\left(B_{i,j,k} \times \left(1 - \phi_{i,j,k}\right)\right)}{\partial z}$ and hence advection flux from bed to bottom sediment is computed as;

$$flux\_b2s^n_{i,j} = \left[\omega^n_{i,j} B^{n+1}_{i,j,k-1/2} \left(1 - \phi^n_{i,\text{j},k-1/2}\right) \right] \times flag1\_(-kbe) \quad 6.31$$

where, $flag1\_(-\text{kbe}) = 1$ only when $k = -kbe$. From the upwind scheme;

$\omega^n_{i,j} B^{n+1}_{i,j,k-1/2} = B^{n+1}_{i,j,k-1} [\![\omega^n_{i,j}, 0]\!] - B^{n+1}_{i,j,k} [\![-\omega^n_{i,j}, 0]\!]$ and hence;

$$flux\_b2s^n_{i,j} = \left[B^{n+1}_{i,j,k-1} [\![\omega^n_{i,j}, 0]\!] - B^{n+1}_{i,j,k} [\![-\omega^n_{i,j}, 0]\!] \right] \left(1 - \phi^n_{i,\text{j},k-1/2}\right) \times flag1\_(-kbe) \quad 6.32$$

Assume, $B^{n+1}_{i,j,k-1} \times flag1\_(-\text{kbe}) = B^{n+1}_{i,j,k} \times flag1\_(-\text{kbe})$ and hence;

$$flux\_b2s_{i,j}^{n} = \left[\left[\omega_{i,j}^{n},0\right]-\left[\left[-\omega_{i,j}^{n},0\right]\right]B_{i,j,k}^{n+1}\left(1-\phi_{i,\mathrm{j},k-1/2}^{n}\right)\times flag1\_(-kbe)\right. \quad 6.33$$

Evaluate the control volume face porosities explicitly and as the minimum between adjacent layer porosities $\phi_{i,j,k-1/2}^{n} = MIN\left(\phi_{i,j,k}^{n},\phi_{i,j,k-1}^{n}\right)$.

$$flux\_b2s_{i,j}^{n} = \left[\left[\omega_{i,j}^{n},0\right]-\left[\left[-\omega_{i,j}^{n},0\right]\right]B_{i,j,k}^{n+1}\left(1-MIN\left(\phi_{i,j,k}^{n},\phi_{i,j,k-1}^{n}\right)\right)\times flag1\_(-kbe)\right. \quad 6.34$$

Assume, $\phi_{\mathrm{n},k-1}^{m}\times flag1\_(-\mathrm{kbe}) = \phi_{\mathrm{n},k}^{m}\times flag1\_(-\mathrm{kbe})$ and hence;

$$flux\_b2s_{i,j}^{n} = \left[\left[\omega_{i,j}^{n},0\right]-\left[\left[-\omega_{i,j}^{n},0\right]\right]B_{i,j,k}^{n+1}\left(1-\phi_{i,j,k}^{n}\right)\times flag1\_(-kbe)\right. \quad 6.35$$

6.4 Benthic-pelagic model coupling and bottom boundary treatment

Benthic-pelagic models have been coupled through the interaction layer flux. All the flux terms for the interaction layer and the bottom boundary which have been computed under sections **6.2** and **6.3** are compute explicitly and the explicit coefficients in advection diffusion equations have been corrected. Water surface boundary flux has been treated as discussed under section **6.1**.

6.4.1 Boundary flux treatment in pelagic model

6.4.1.1 Dissolved matter

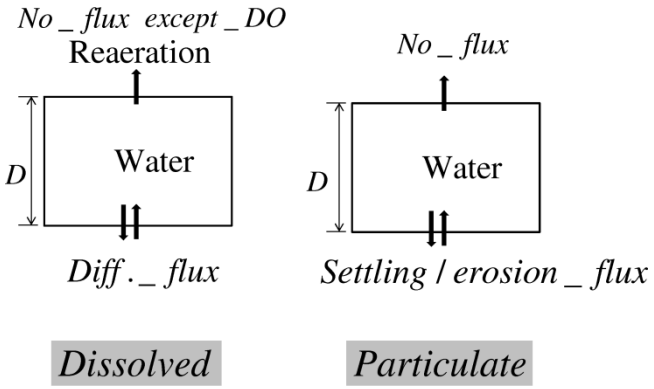

Fig 6.4 Boundary flux in water surface and bottom boundaries

Consider the vertical diffusion term $\frac{\partial}{\partial z}\left[K_z \frac{\partial C_{i,j,k}}{\partial z}\right]$ described in the equation **4.11**.

$$\frac{\partial}{\partial z}\left(K_z \frac{\partial C}{\partial z}\right) \simeq \frac{1}{\Delta z}\left[\left(K_z \frac{\partial C}{\partial z}\right)_t - \left(K_z \frac{\partial C}{\partial z}\right)_b\right] \qquad 6.36$$

During the advection diffusion computation through discretized equations, $\left(K_z \frac{\partial C_s}{\partial z}\right)_b$ has been considered as zero at k=1. But for dissolved oxygen and dissolved nutrients it is not zero and hence it has to be computed and corrected the explicit tem in the advection diffusion equation in pelagic model. Since it is confirmed that there is no significant difference this correction flux term has been computed explicitly and added to the source term of each state variable in water.

At $k = 1$, at the bottom of the water column receives flux from the sediment or leave the flux from the water to the sediment due to vertical advection and diffusion. Vertical diffusion term in sigma-coordinates is written as;

$$\frac{1}{D^{n+1}}\frac{\partial}{\partial \sigma}\left(K_v \frac{\partial C}{\partial \sigma}\right) \simeq \frac{1}{D^{n+1}}\frac{1}{\Delta \sigma}\left[\left(K_v \frac{\partial C}{\partial \sigma}\right)_t - \left(K_v \frac{\partial C}{\partial \sigma}\right)_b\right] \qquad 6.37$$

Then bottom flux has to be corrected with the term;

$$flux\_correction7 = -\frac{1}{D^{n+1}}\frac{1}{\Delta \sigma}\left(K_v \frac{\partial C}{\partial \sigma}\right)_b \times flag1\_1 \qquad 6.38$$

where, $flag1\_1 = 1$ only when $k = 1$.

According to the Flick's law of diffusion, $\left(K_z \frac{\partial C}{\partial z}\right)_b = -(Influx\_s2w)$ Where influx to water from sediment has been computed from the interface flux equation **6.19** as, $Influx\_s2w_{i,j}^n = Diffusion\_flux\_s2w_{i,j}^n$. According to the sigma-coordinate transformation, $\left(K_z \frac{\partial C}{\partial z}\right)_b = \frac{1}{D^{n+1}}\left(K_v \frac{\partial C}{\partial \sigma}\right)_b$ and hence;

$$\left(K_v \frac{\partial C}{\partial \sigma}\right)_b = -D^{n+1}(Influx\_s2w) \qquad 6.39$$

Then the flux is corrected as;

$$flux\_correction7 = -\frac{1}{D^{n+1}}\frac{1}{\Delta\sigma}\left(-D^{n+1}(Influx\_s2w_{i,j}^{n})\right)\times flag1\_1 \qquad 6.40$$

$$flux\_correction7 = \frac{1}{\Delta\sigma}Influx\_s2w_{i,j}^{n}\times flag1\_1 \qquad 6.41$$

6.4.1.2 Particulate matter

Similar to the dissolved matter in at $k=1$, at the bottom of the water column receives flux from the sediment or leave the flux from the water to the sediment due to vertical advection. Hence correction term of flux at the bottom of the water column is calculated in a same manner as in dissolved matter and computed the correction term as;

$$flux\_correction8 = \frac{1}{\Delta\sigma}Influx\_s2w_{i,j}^{n}\times flag1\_1 \qquad 6.42$$

where in sediment $Influx\_s2w_{i,j}^{n} = \left[flux\_s2w_{i,j}^{n}\right]$ gives from the equation. Even though the above boundary flux should be computed implicitly, for the convenience this term has been added to the source term of each state variable of particulate matter and computed explicitly in the pelagic model.

6.4.2 Boundary flux treatment in benthic model

6.4.2.1 Dissolved matter

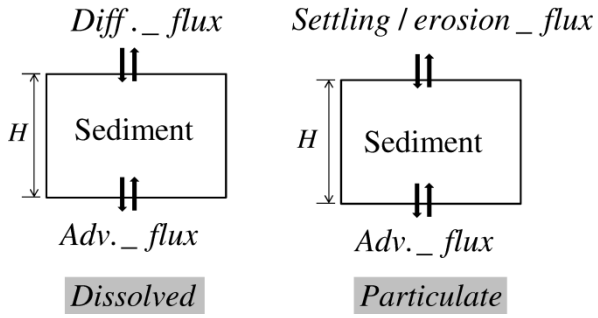

Fig 6.5 Boundary flux in sediment surface and bottom boundaries

According to the solution of advection and diffusion equation fluxes at boundaries have been considered and modified the coefficients of general equation. According to the governing equation **5.34** the diffusion flux correction to the explicit coefficient is;

$$flux\_correction1_{i,j}^{n} = \frac{\left(K_{i,j,k+1/2} \frac{\partial B_{i,j,k+1/2}}{\partial z} \right) \phi_{i,j,k+1/2}^{n}}{\Delta z_k^n \phi_{i,j,k}^n} \times flag1\_0$$ where, $flag1\_0 = 1$ only when $k = 0$. Since equation **6.14** gives,

$$Diffusion\_flux\_s2w_{i,j}^{n} = \left[-K_{n,k+1/2} \frac{\partial B_{n,k+1/2}}{\partial z} \phi_{i,j,k+1/2}^{n} \right] \times flag1\_0$$

$F_{dif,s}$ in equation **5.139** is replaced by;

$$F_{dif,s} = \left(-Diffusion\_flux\_s2w_{i,j}^{n} \right) \qquad 6.43$$

At $k = -kbe$, the bottom of the sediment column makes advection flux with the bed sediment and this has been considered in the discretized form of the advection diffusion computation and modified the coefficients of general equation.

Since equation **6.30** gives,

$$flux\_b2s_{i,j}^{n} = \left[\omega_{i,j}^{n} B_{i,j,k-1/2}^{n+1} \phi_{i,\mathrm{j},k-1/2}^{n} \right] \times flag1\_(-kbe)$$

$F_{adv,s}$ in equation **5.167** is replaced by;

$$F_{adv,s} = flux\_b2s_{i,j}^{n} \qquad 6.44$$

6.4.2.2 Particulate matter

Method of treatment for the boundary flux of particular matter has been done in a same procedure as in dissolved matter. According to the solution of advection and diffusion equation fluxes at boundaries have been considered and modified the coefficients of general equation.

Particulate matters settle in the water column and accumulate or erode across the surface of the sediment and this flux has been considered in the advection diffusion equation of the sediment and modified the coefficients of general equation. The net settling flux, $Flux\_b$ in water for each state variable C is computed from equation **4.122** under section **4.1.3**. Hence

$F'_{adv,s}$ in the equation **5.195** is replaced by;

$$F'_{adv,s} = -Flux\_b\left(1-\phi_{i,j,k+1/2}\right) \qquad 6.45$$

At $k=-kbe$, the bottom of the sediment column makes advection flux with the bed sediment and this has been considered in the discretized form of the advection diffusion computation and modified the coefficients of general equation.

Since equation **6.35** gives,

$$flux\_b2s^{n}_{i,j} = \left[\omega^{n}_{i,j} B^{n+1}_{i,j,k-1/2}\left(1-\phi^{n}_{i,\mathrm{j},k-1/2}\right)\right]\times flag1\_(-kbe)$$

$F'_{adv,b}$ in equation **5.222** is replaced by;

$$F'_{adv,b} = flux\_b2s^{n}_{i,j} \qquad 6.46$$

7. RESULTS AND DISCUSSION

7.1 Water quality

Model results of water quality have been validated with the collected data (Koibuchi et al., 2000) for the period of March 1999 to April 2000 at three locations CLH, KSB and TLH (**Fig 2.6**). Even though the simulation is started from March 1999, since it is confirmed that the initial conditions affect the results during one year period of simulation, simulation has been continued until a reasonable steady state is obtained. Validation of water quality is done with the comparison of vertical distributions of water state variables.

7.1.1 Salinity and temperature

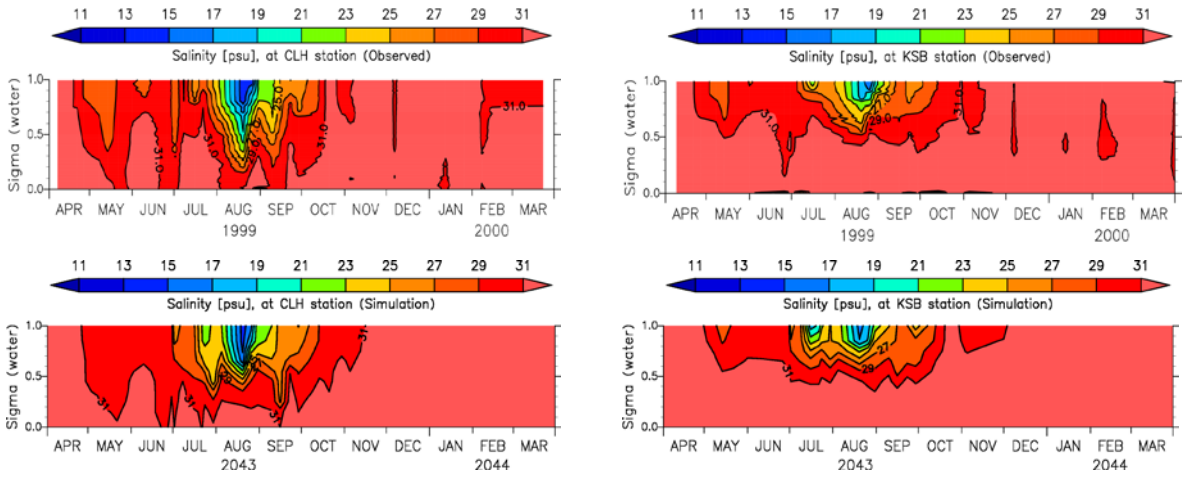

(a) (b)

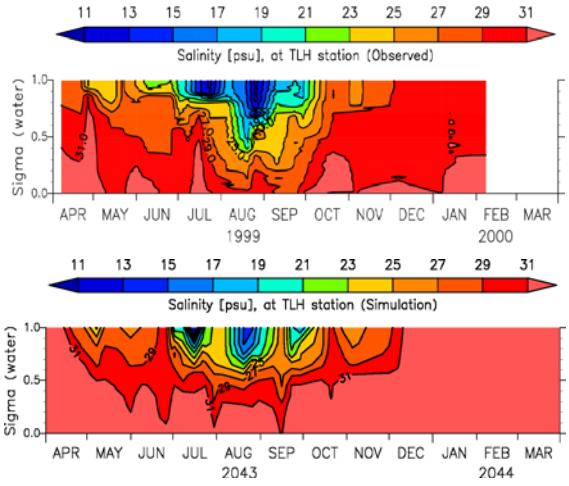

(c)

Fig 7.1 Observed and simulated salinity at (a) CLH, (b) KSB and (c) TLH

Water quality is highly affected by the salinity and temperature. The kinetic rates of nutrient transformations are significantly influenced by temperature as their transformation rates increase with increasing temperature. All the kinetic equations of the model are linked with temperature having a temperature coefficient. Moreover, algal growth is also controlled by the temperature as growth rate increases with temperature to an optimum level which depends on the type of algae. Water stratification is controlled by both salinity and temperature which affect the mixing of water column. Penetration of light which controls by the light extinction coefficient is related with salinity of the water column. Hence, the reproducibility of temperature and salinity are important state variables in a water quality model.

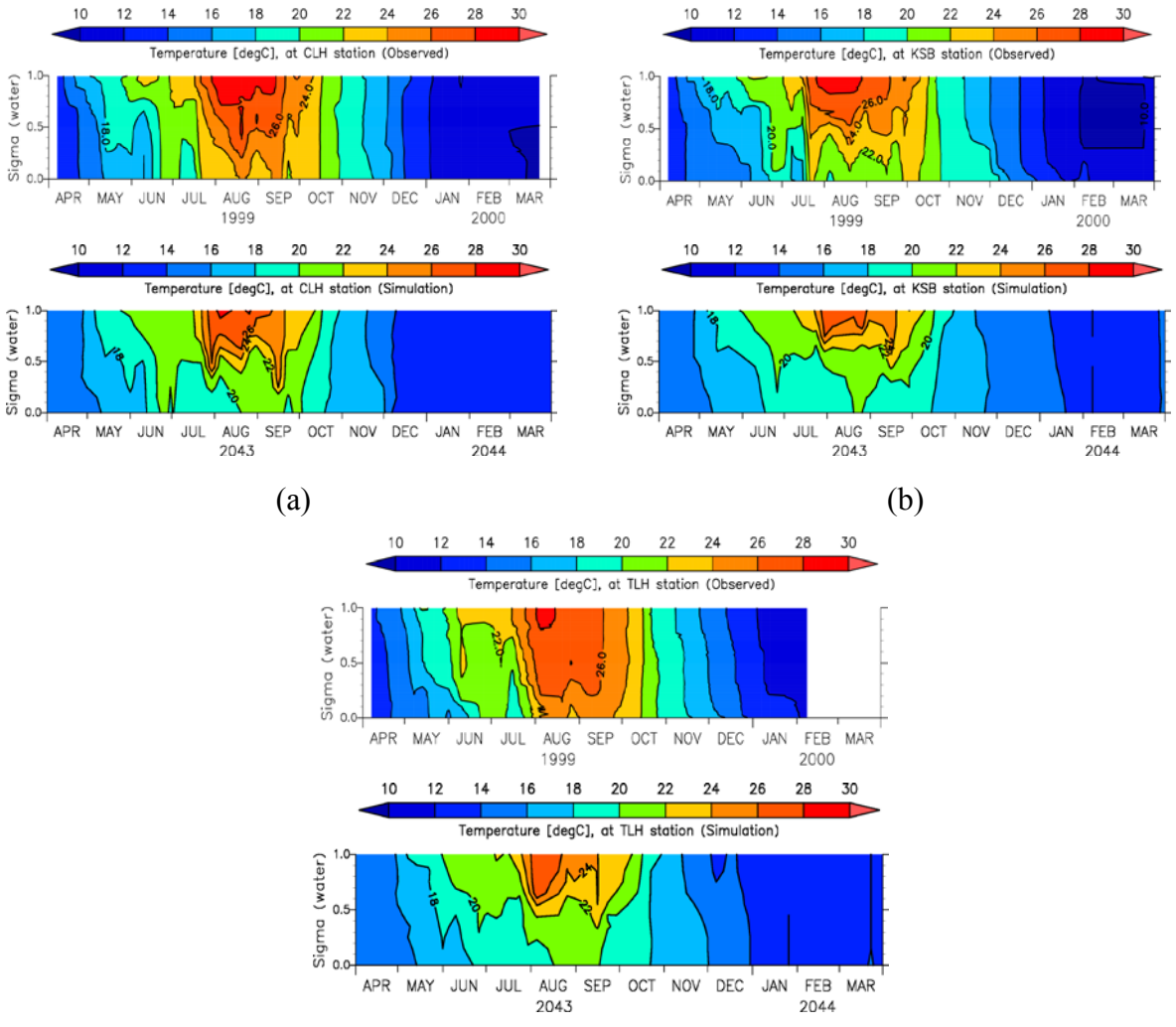

(a) (b)

(c)

Fig 7.2 Observed and simulated temperature at (a) CLH, (b) KSB and (c) TLH

Comparison of observed and simulated variations of salinity and temperature are shown **Fig 7.1** and **Fig 7.2**. Even though there are some discrepancies, seasonal variation of salinity and temperature well reproduce in the model. Surface salinity highly influence by the river inflows especially near the river mouths. Thus, accuracy of the river discharge measurements is important to improve the accuracy of the reproducibility of salinity. Both salinity and temperature has been modeled for uniform initial conditions in space and in depth. The improvement of salinity and temperature models with depth varying initial conditions may improve their reproducibility.

After analyzing the sensitivity of magnification factor of river discharge, available river discharge data has been enhanced by a magnification factor of 2.0. The effect of magnification factor of river discharge on salinity has been discussed under sensitivity analysis.

7.1.2 Chlorophyll_ *a*

Reproducibility of seasonal hypoxia in water column has a strong correlation with the reproducibility of Chl_*a* concentration. Hence the seasonal hypoxia is able to reproduce through the accurate reproduction of Chl_*a*. Three seasonal blooms which have appeared every year in Tokyo Bay in particular spring, summer and winter, reproduce from the model (**Fig 7.3**). The strongest blooming is during spring throughout the water column due to well mixed water while summer blooming is mainly at surface layers of the water column due to the effect of stratification. Even though the winter blooming is not as strong as the spring blooming, the well mixed water column has resulted in blooming throughout the water column. Although the simulated phytoplankton variation has showed some discrepancies quantitatively, model could well reproduce the blooming qualitatively. In order to improve the results, focus should be especially made on the modeling of light extinction coefficient. Light extinction coefficient which has been used in the model is only a function of Chl_*a*, suspended sediment and salinity while it may also have some effect due to particulate organic carbon concentration. Moreover the reproducibility of water temperature and the accuracy of river and sewage boundary conditions have also been responsible for those discrepancies.

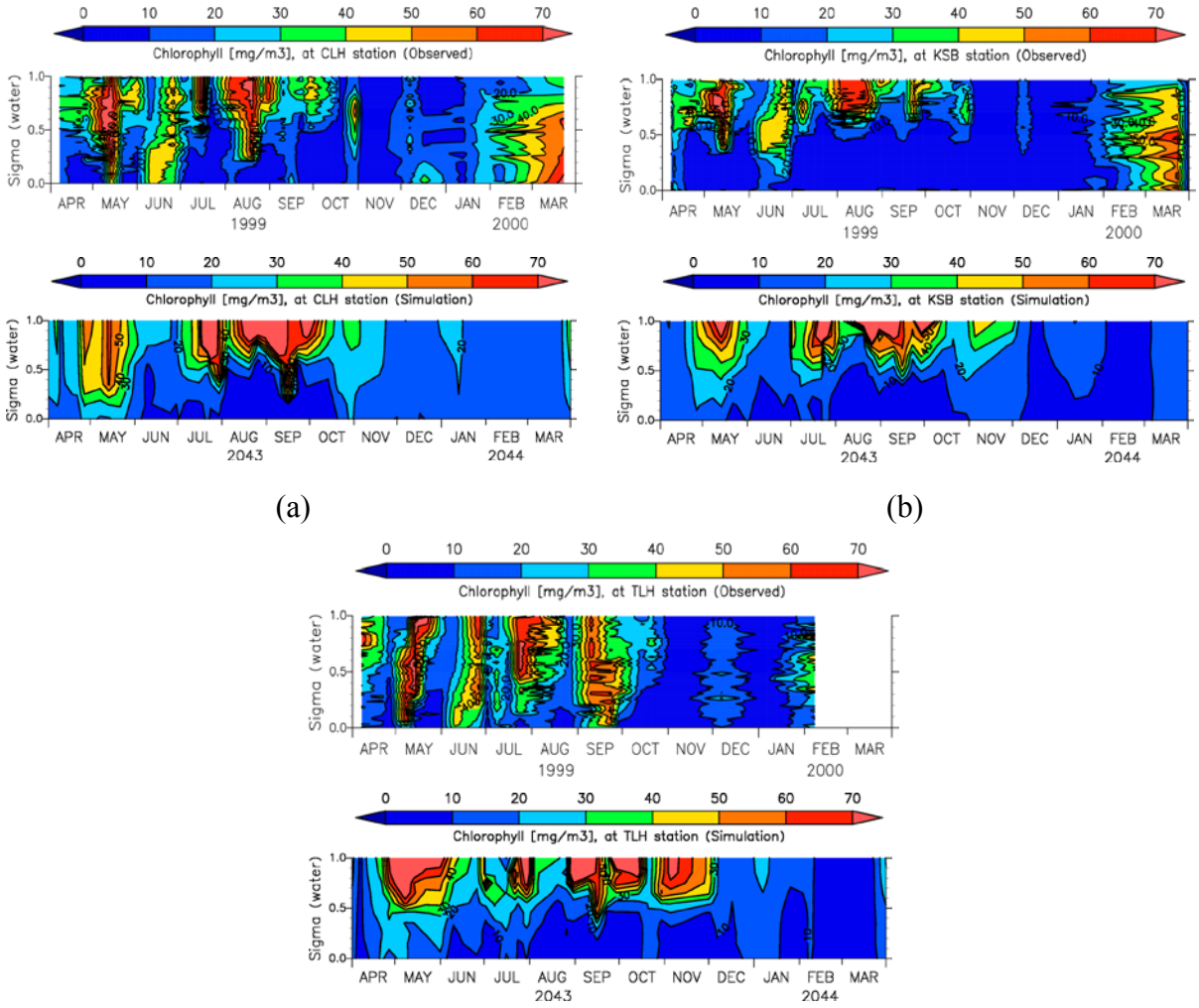

(a) (b)

(c)

Fig 7.3 Observed and simulated Chl_*a* concentration at (a) CLH, (b) KSB and (c) TLH

7.1.3 Dissolved oxygen

Seasonal hypoxia which has been validated for three locations namely CLH, KSB and TLH is shown in the **Fig 7.4** . Hypoxic water which appeared especially during the summer season which corresponded to summer blooming is well reproduced in the model. Even though the hypoxia has well reproduced qualitatively, during the spring and summer seasons, it is somewhat underestimated. Underestimation of settled particulate organic carbon concentration may have resulted in this discrepancy. Improvement of the reproducibility of seasonal hypoxia has been expected through the improvement of chlorophyll model. Moreover, the settling velocity of particulate organic carbon taken as a constant can be modeled considering particulate organic carbon concentration and the effect of turbulence. One of the reasons for the underestimation of dissolved oxygen concentration in water during

the winter is a result of underestimation of Chl_*a* concentration during that period. Overestimation of DO during the spring can be explained by **Fig 7.3** which shows the overestimation of spring bloom. Other than that it is noticed that the saturated dissolved oxygen concentration which has adopted as a constant in the model has some effect on the seasonal dissolved oxygen concentration in the surface layers of water. Comparison of bottom DO variation with computed and measured DO at CLH, KSB and TLH are shown in the **Fig 7.5**. Computed results of bottom DO at all three locations mostly follow the data except during the spring season. The seasonal variations of computed bottom DO at three locations follow a similar pattern as shown in the **Fig 7.6**. Reproducibility of bottom dissolved oxygen at three stations is further discussed with correlation factor which computes between observed and simulated values **Fig 7.7**. Reproducibility at station CLH, KSB and CLH has been shown with 0.55, 0.60 and 0.59 correlation factors respectively.

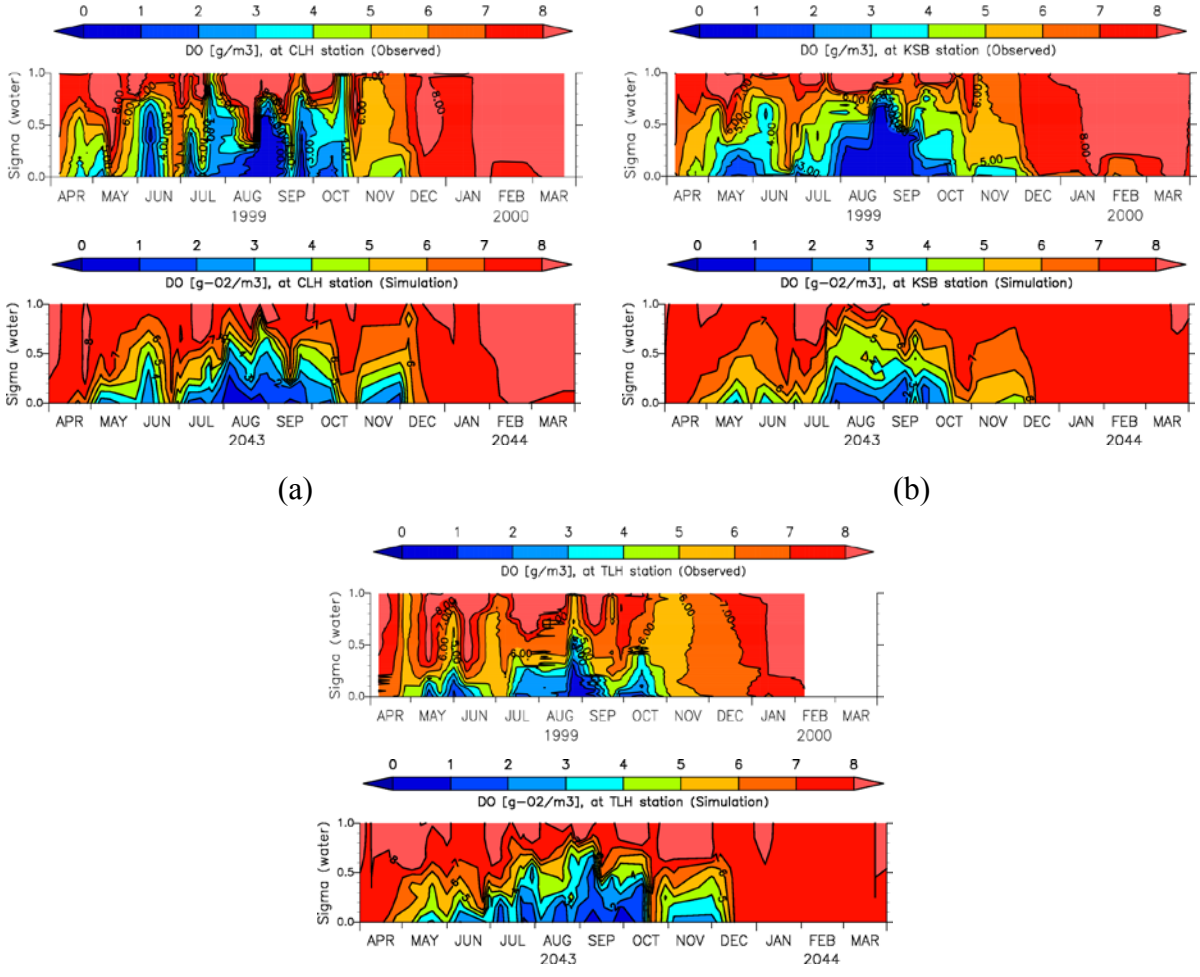

(a) (b)

(c)

Fig 7.4 Observed and simulated DO concentration at (a) CLH, (b) KSB and (c) TLH

(a)

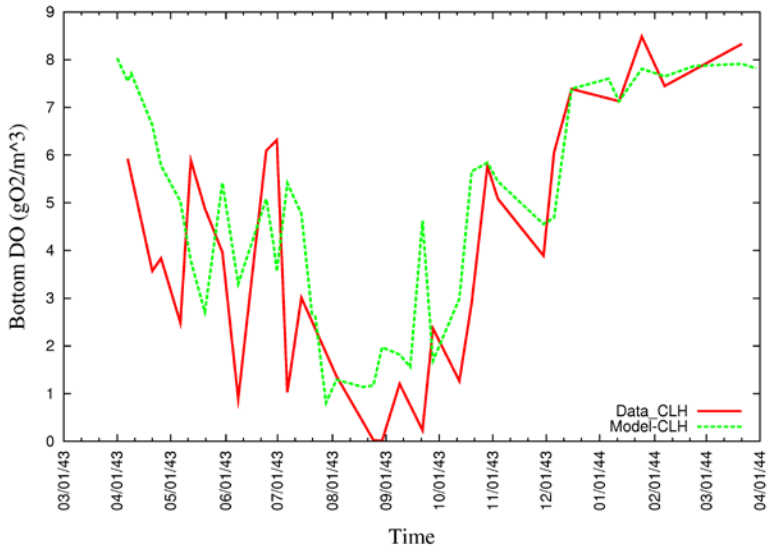

(b)

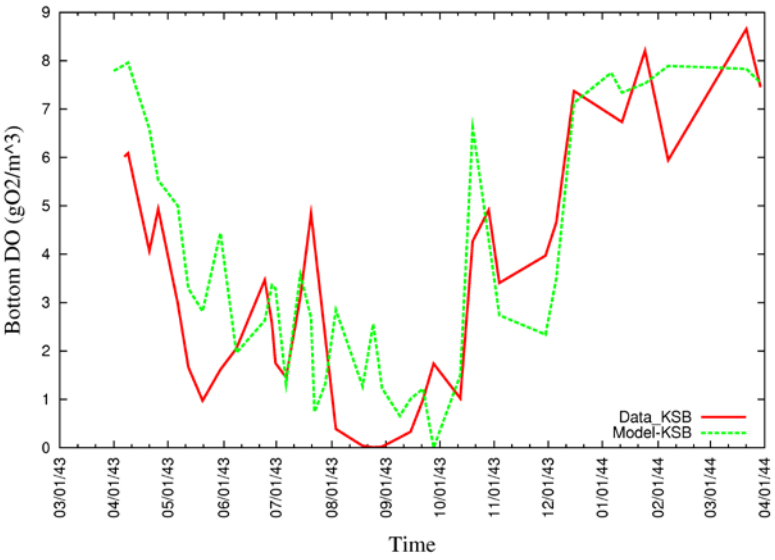

(c)

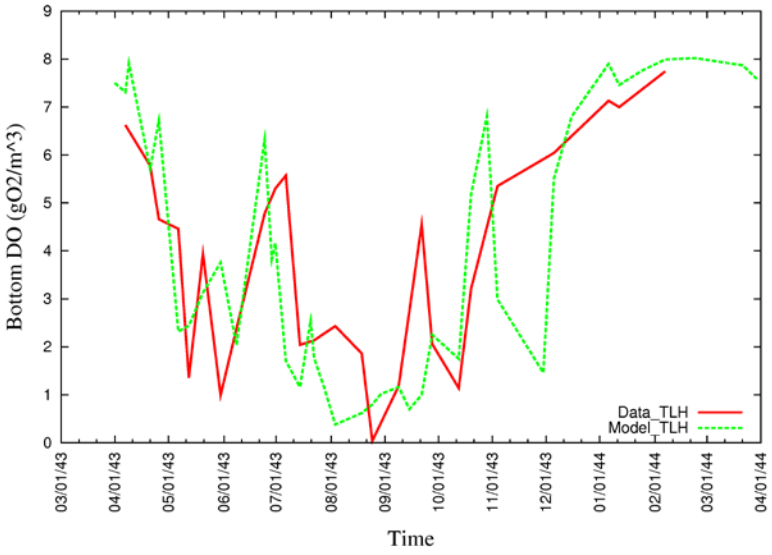

Fig 7.5 Bottom DO comparison with measured and computed at (a) CLH, (b) KSB and (c) TLH

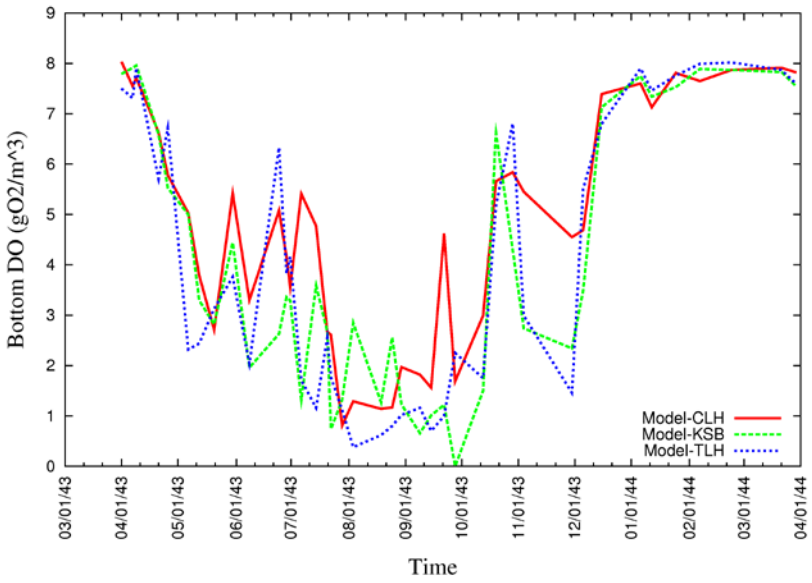

Fig 7.6 Simulate bottom DO at three stations

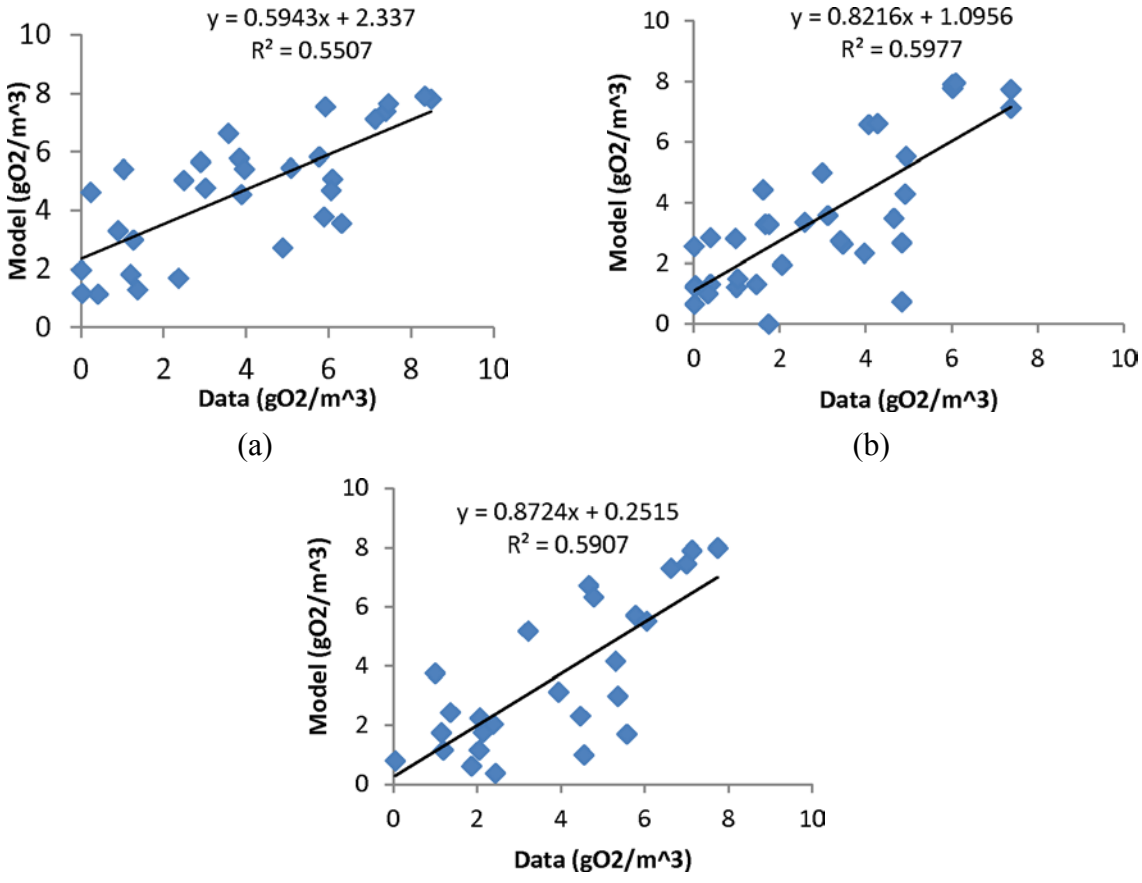

Fig 7.7 Correlation of bottom DO between measured and computed at (a) CLH, (b) KSB and (c) TLH

7.1.4 Phosphate phosphorous

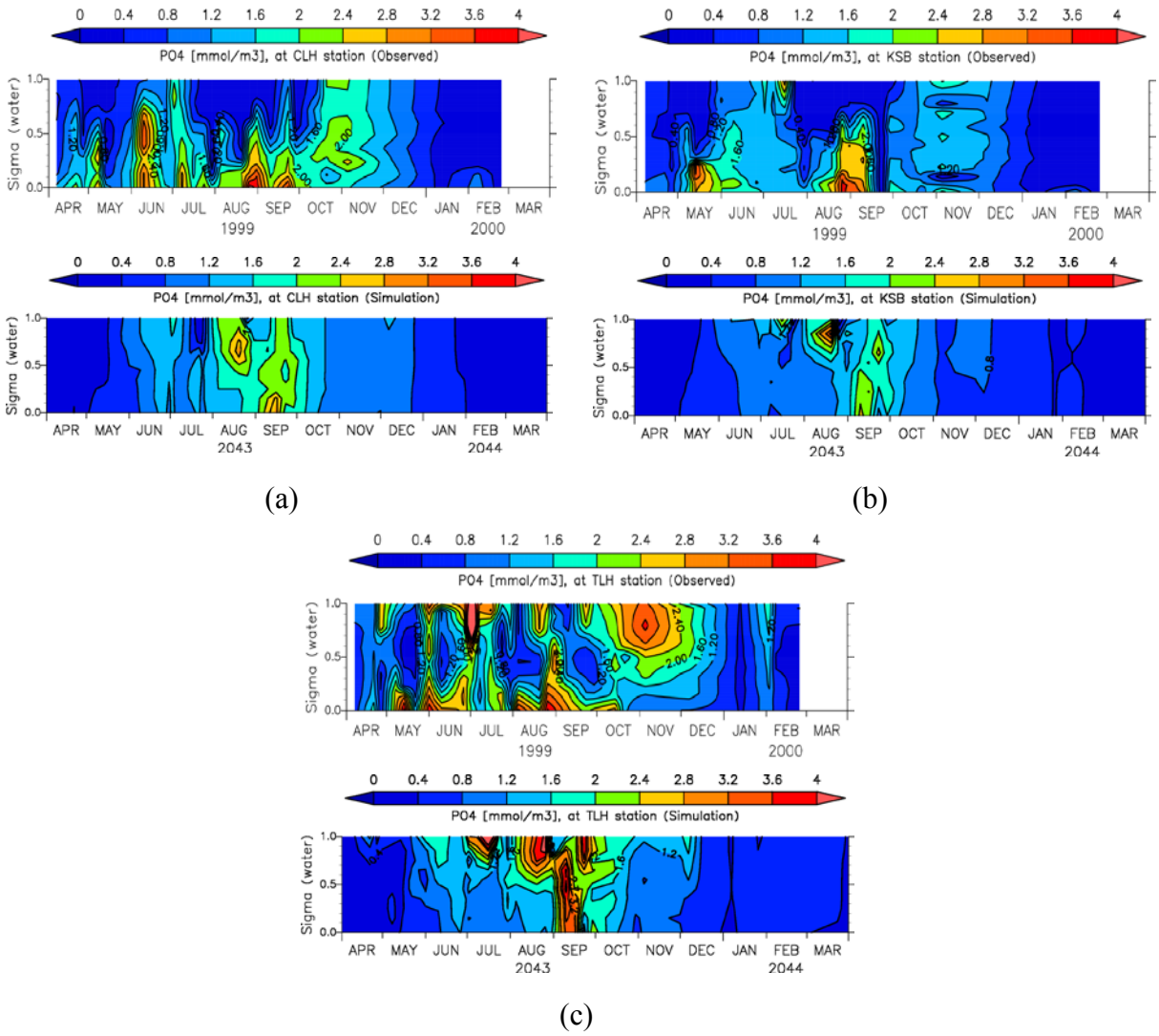

Fig 7.8 Observed and simulated phosphorous concentration at (a) CLH, (b) KSB and (c) TLH

Most of the time phosphorous is the limiting nutrient in Tokyo Bay. Comparison of observed and modeled phosphorous is shown in **Fig 7.8.** Even though the order is followed there are some discrepancies especially at the bottom of the water column. At the bottom, phosphorous flux is added from sediment under anoxic condition which has been underestimated in the model. It is confirmed by sensitivity analysis that phosphorous flux release is mainly controlled by the attached and dissolved fractions of phosphate in the sediment. The critical parameter to model this partitioning is the diffusion coefficient of attached sediment which controls by the benthic animal. This effect is further discussed under

sensitivity analysis. Moreover, the overestimation of bottom DO can result a lower flux release than expected.

Overestimation of surface phosphorous especially during the summer is found to be the overestimation of Chl_*a* concentration during the summer. Metabolism of phytoplankton especially under no light condition, primary production is lower than the metabolism rate which can cause accumulation of nutrients mainly at the surface.

7.1.5 Ammonia nitrogen

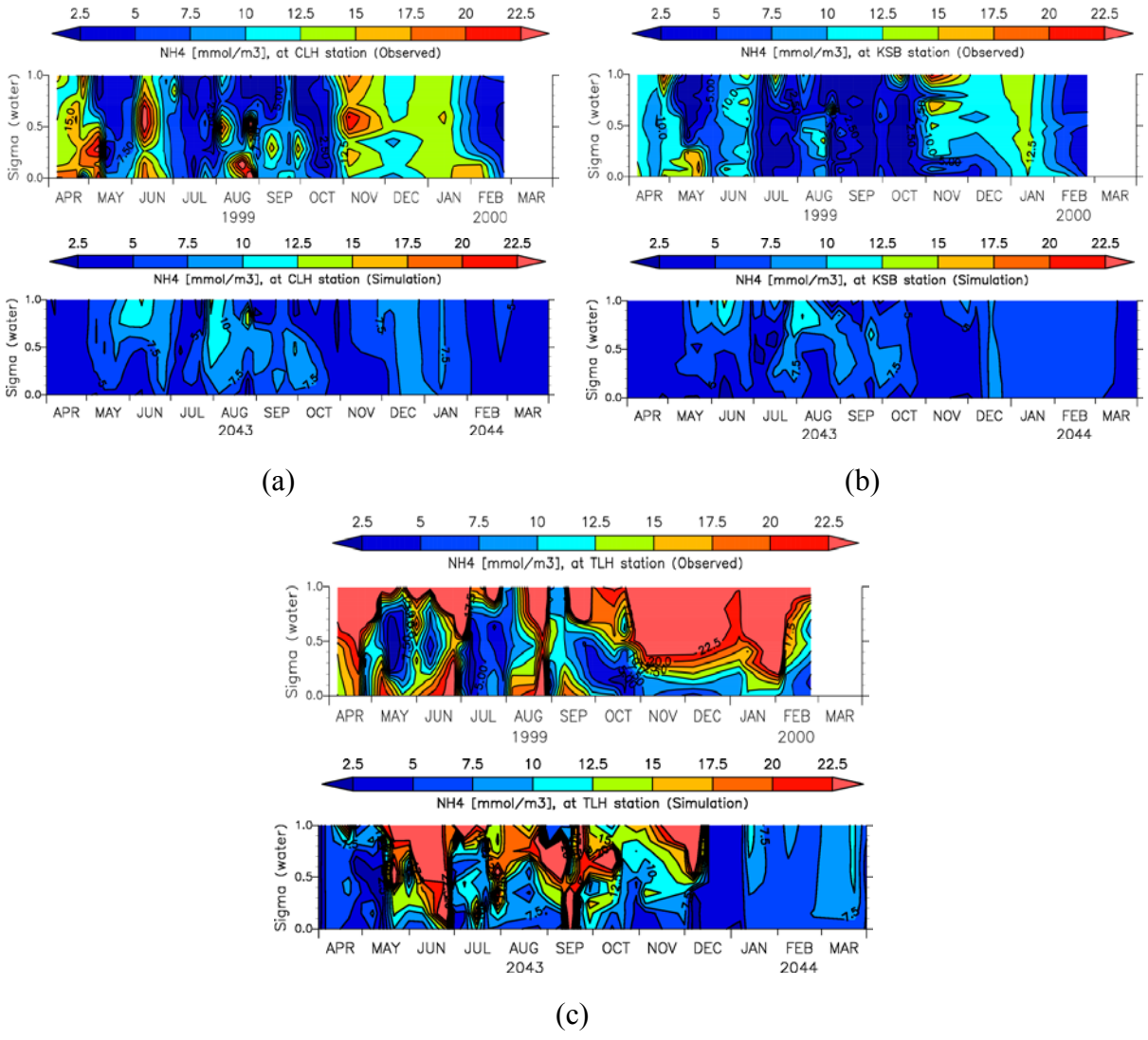

Fig 7.9 Observed and simulated ammonia concentration at (a) CLH, (b) KSB and (c) TLH

Two kinds of nitrogen as ammonia nitrogen and nitrate nitrogen are available in water for algae to grow on. Preference factor has been considered for phytoplankton to grow on as the

ratio of each nitrogen concentration to the total nitrogen concentration. It has been assumed that ammonia nitrogen is preferred five times higher than the nitrate nitrogen.

Comparison of observed and modeled ammonia is shown in **Fig 7.9.** Similar to the phosphorous model the flux release from the sediment to water is underestimated.

7.1.6 Nitrate nitrogen

Comparison of observed and modeled nitrate is shown in **Fig 7.10** and Nitrate-nitrogen well reproduces in the model. The results can be improved through further tuning of the preference factor of ammonia and nitrate on phytoplankton uptake.

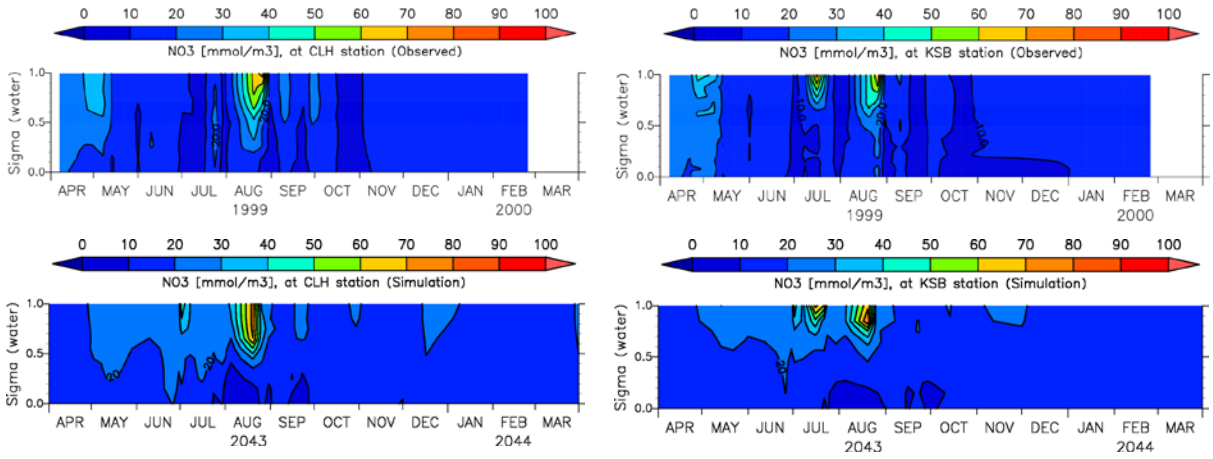

(a) (b)

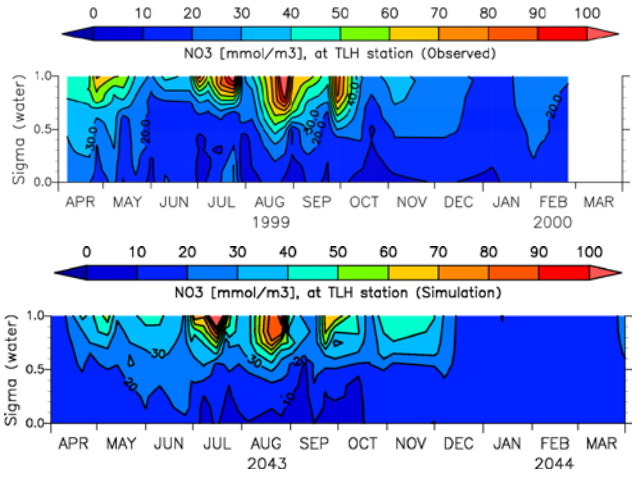

(c)

Fig 7.10 Observed and simulated nitrate concentration at (a) CLH, (b) KSB and (c) TLH

7.1.7 Dissolved silica

Silica is an essential nutrient for diatom growth. Comparison of observed and computed dissolved silica is shown in **Fig 7.11.** In general silica follows a same pattern like phosphorus. Computed dissolved silica is considerably underestimated. It has been assumed that three seasonal blooms are mainly diatoms which might be different during the data collected period. Similar to phosphate bottom flux of dissolved silica is highly affected by the partitioning coefficients of dissolved and attached phase. Hence tuning the model for different partitioning coefficients may improve the bottom concentration.

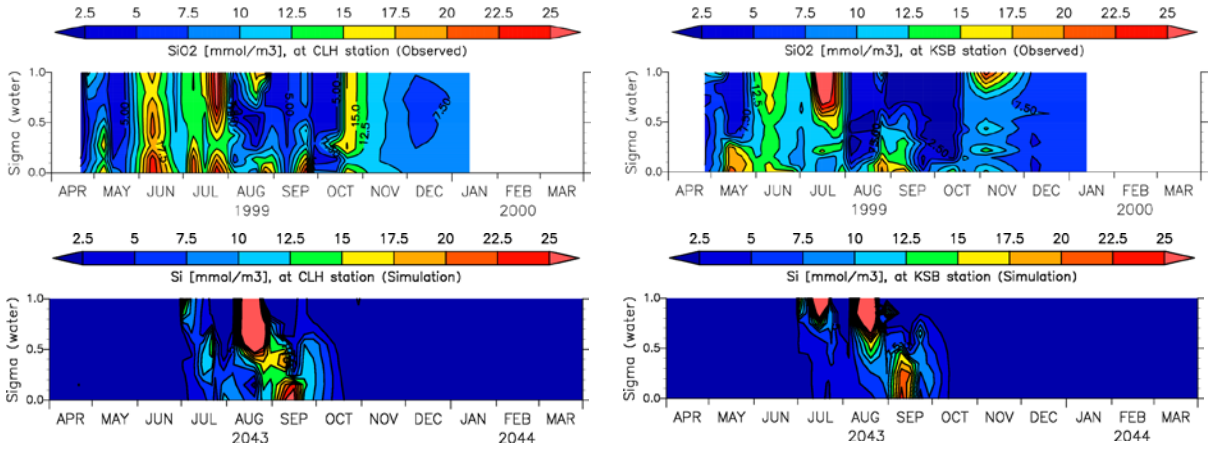

(a) (b)

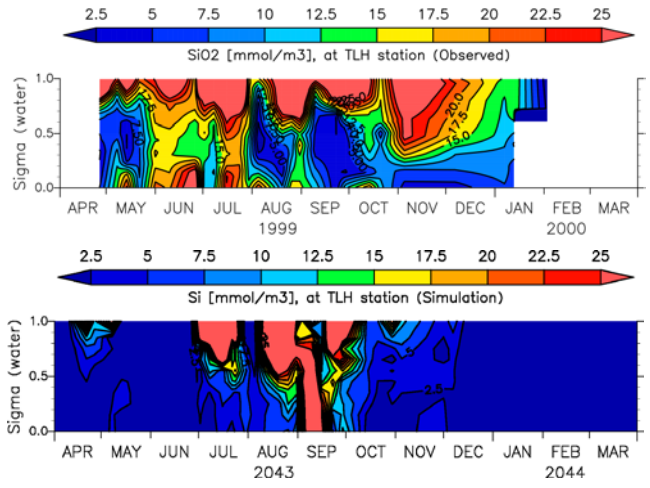

(c)

Fig 7.11 Observed and simulated dissolved silica concentration at (a) CLH, (b) KSB and (c) TLH

7.2 Sediment quality

Model results of sediment quality have been validated with the collected data of Tokyo Bay for the year 2001 (Okada and Furukawa, 2005). Even though the simulation is started from March 1999, since it is confirmed that the initial conditions affect the results during one year period of simulation until the steady state is obtained, reasonable steady state has been assumed after 45 years of simulation and last year results have been used for the validation of the model. Validation of water quality is done with the comparison of spatial distribution of sediment state variables. Spatial distribution of sediment quality parameters such as WC, POCC, TNC and TPC, are validated.

7.2.1 Spatial distributions of sediment quality

7.2.1.1 Particulate organic carbon content

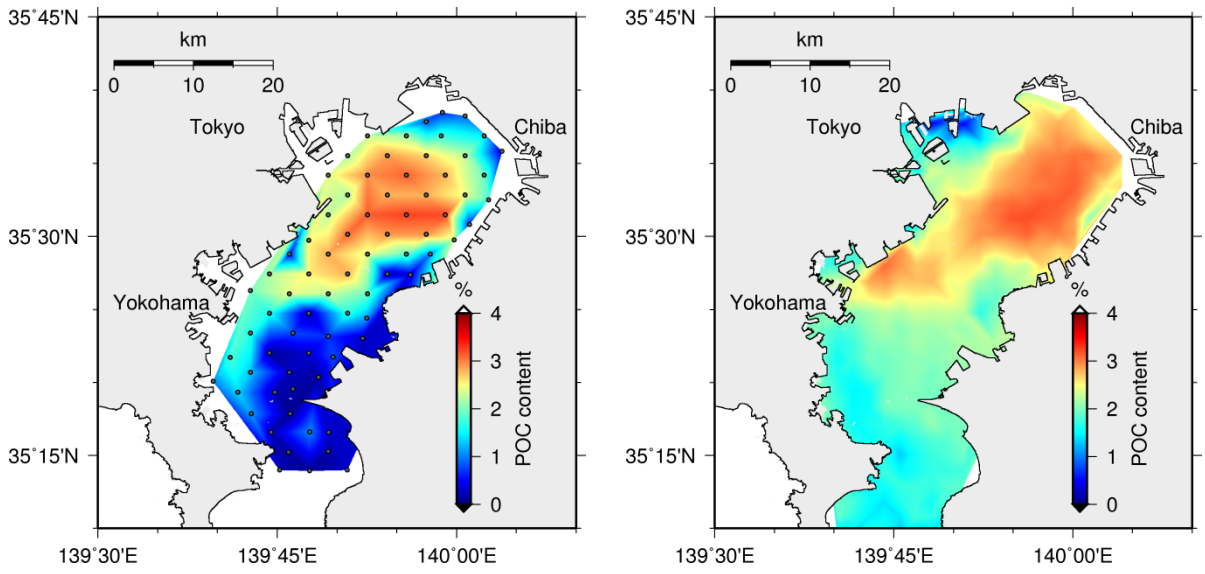

Fig 7.12 Observed (left) and simulated (right) spatial distributions of POCC

The computed spatial distribution of POCC was consistent with the measurements showing high concentration at the central part of the bay (**Fig 7.12**). Over estimation of POCC may be a result of under estimation of accumulated inorganic sediment in the model. Mainly, inorganic sediment enters to the water column at river boundaries which have been considered as uniform during each month of the year and settles down in the water and

accumulates on the surface of the sediment. There is a possibility to change those monthly inorganic sediment concentrations during extreme weather conditions. Other than that, modeling of settling velocity of particulate matter may have an important effect on settled quantities where model has considered constant settling velocity depend on the type of the material.

Fig 7.13 has shown the **s**patial distribution of POCC with 5-year interval of simulation giving the same pattern of variation increasing the POCC at the central part of the bay.

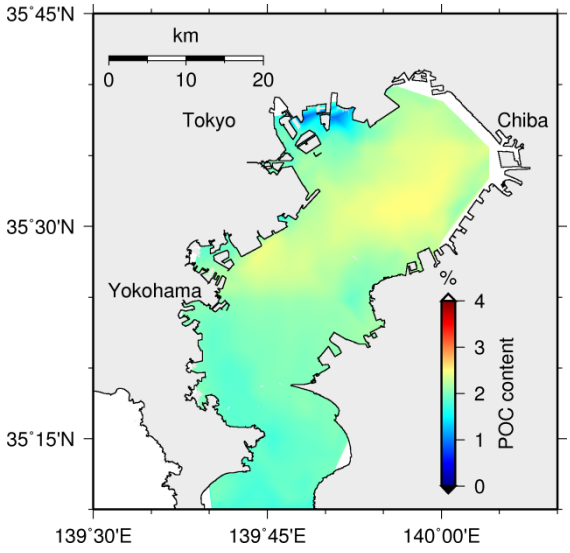

(year-5)

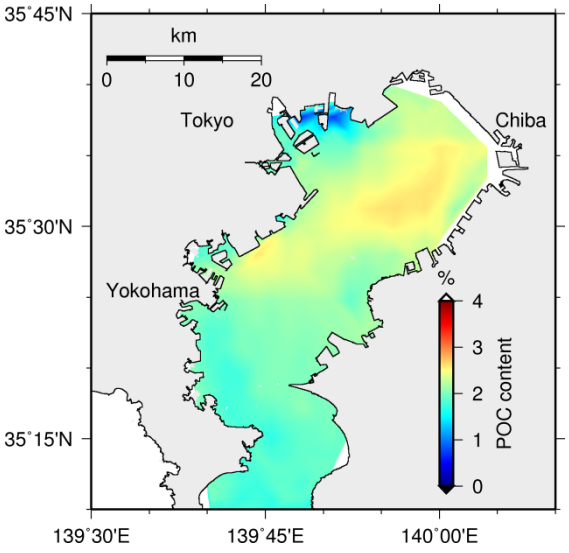

(year-10)

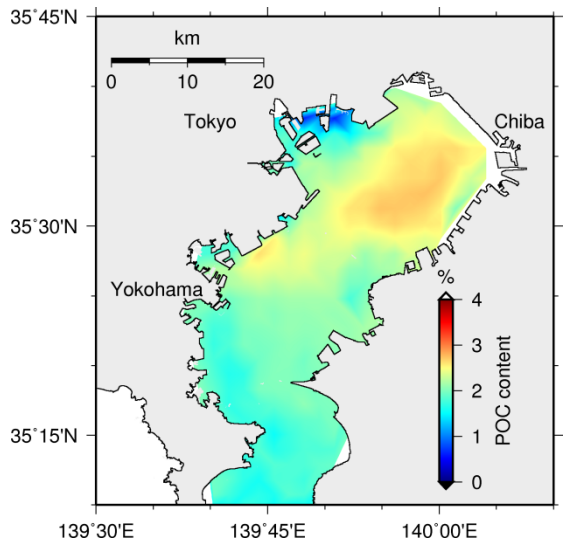

(year-15)

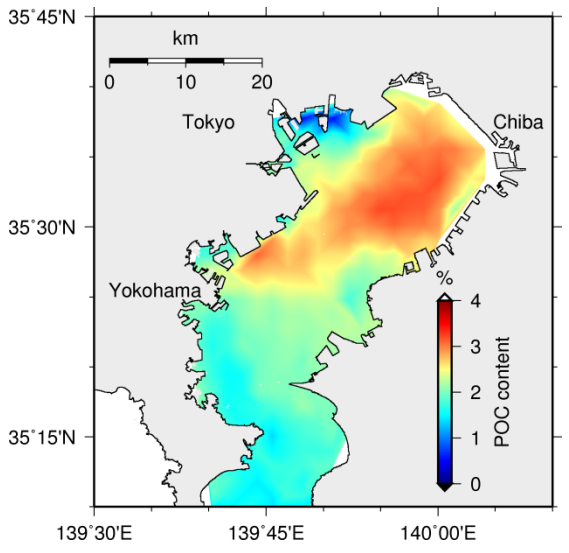

(year-20)

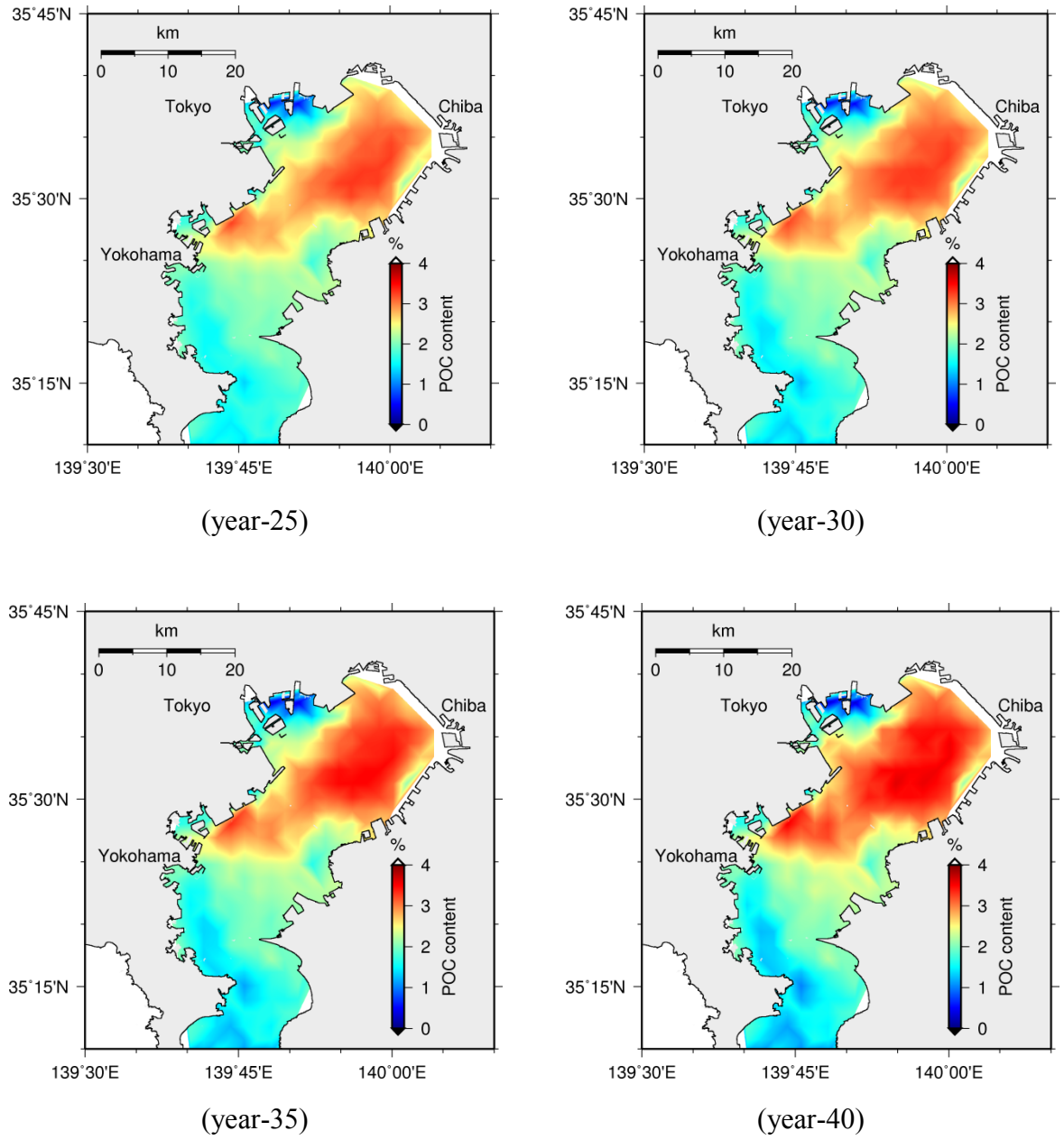

Fig 7.13 Simulated spatial distributions of POCC in every 5_year until model reaching a reasonable steady state

The spatial distribution of settled particulate matter can be explained in detail with the consideration of BSS since settling or erosion is controlled by BSS. Deposition and erosion of particulate matter is modeled based on the BSS and, critical BSS on deposition and critical BSS on erosion. Since the total BSS has been modeled as a vector summation of CBSS and WBSS, effect of each component can be analysed independently.

CBSS gets the highest near the bay mouth while WBSS stress shows the highest near to the coast. Hence, the total BSS shows the lowest at the central part of the bay (**Fig.10**). These results have shown the bottom dynamics are current dominated in the inner part of the bay while it is wave dominated closer to the coast. BSS has a direct correlation with the sediment grain size distribution at the surface of the bed which has been assumed uniform in the model. Even though the spatial distribution of total BSS has showed generally expected variation, results may be further improved if the sediment grain size distribution is considered in the model.

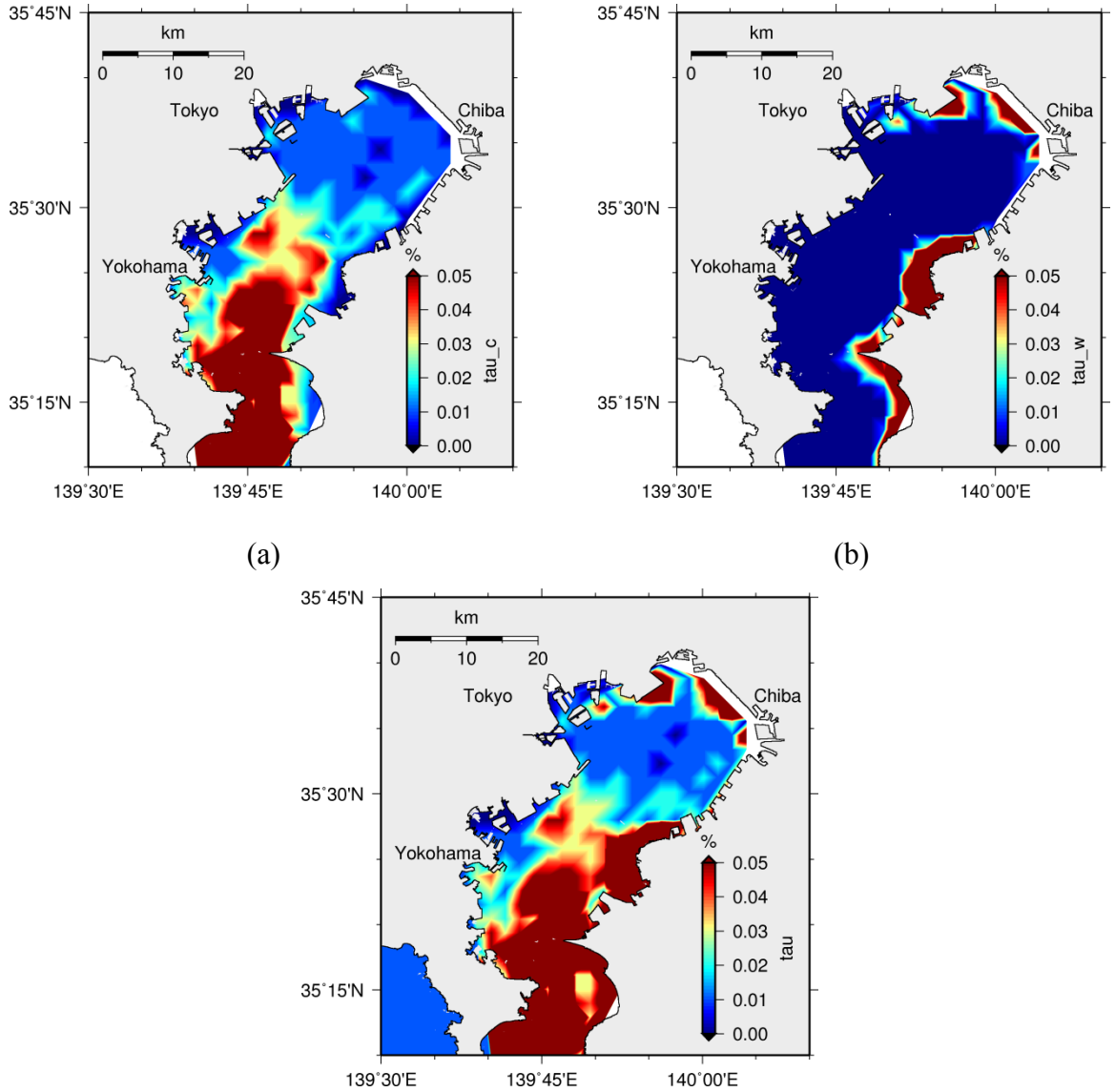

(a) (b)

(c)

Fig 7.14 Spatial distributions of (a) current induced bed shear stress, (b) wave induced bed shear stress and (c) total bed shear stress

In general, towards the bay mouth the sandy bottom with intense CBSS creates erosive effect on sediment. Furthermore, the up-welling areas may also have a high potential to build erosion effect due to high CBSS on sediment. The outer coast with higher bottom sand fraction than the central part of the bay and shallower characteristics can be affected by south-westward wind causing erosive effect on sediment. In contrast, the central part of the bay, with high cohesive sediment, can be considered as the low energy area where exists reduced wave effect with depth and reduced current effect with insufficient CBSS to reach the critical BSS on erosion ensuing the highest deposition within the bay.

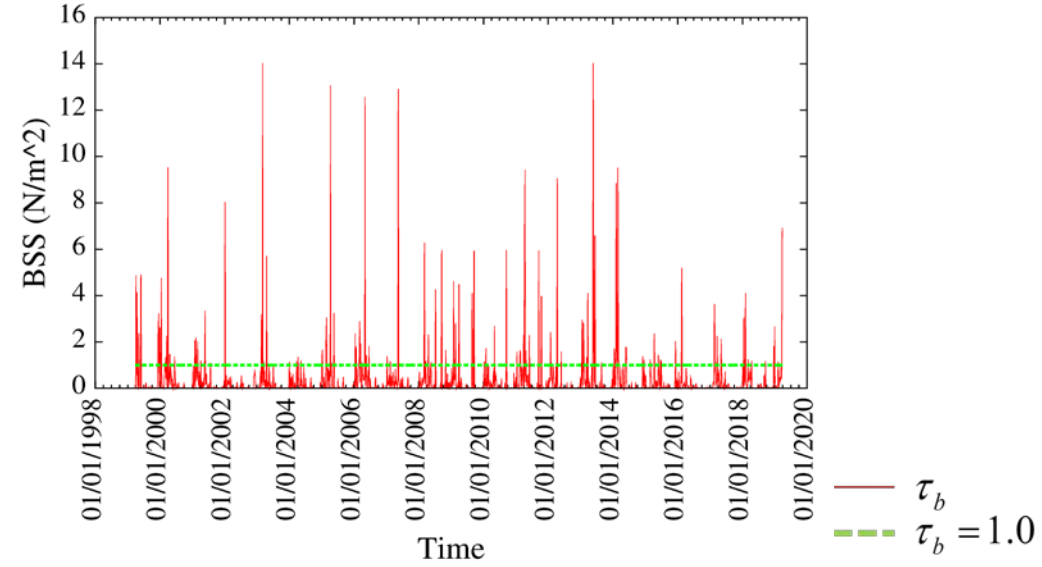

(a)

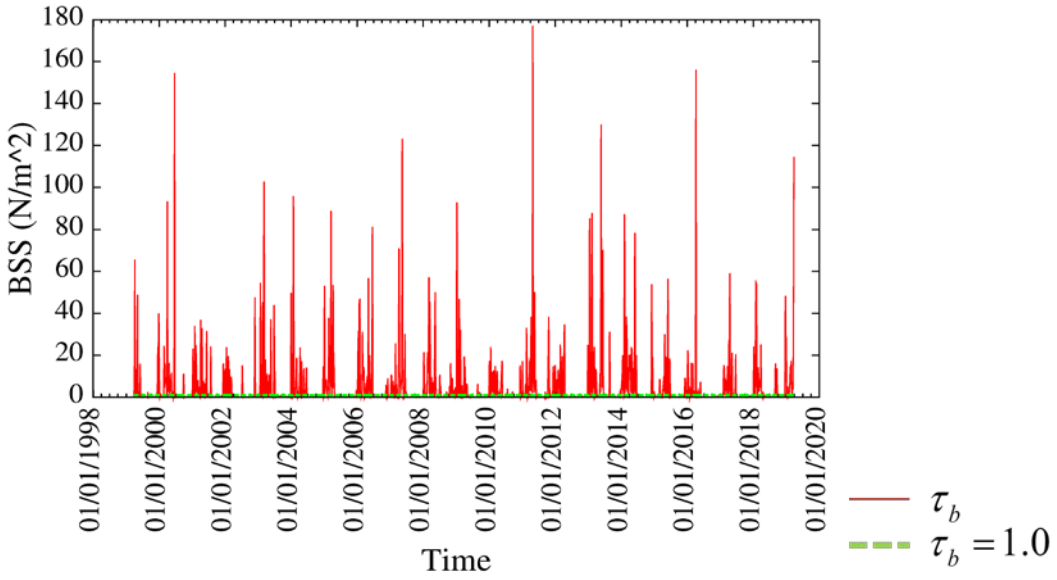

(b)

Fig 7.15 Distributions of BSS during 20-year period (a) at the inner part of the bay (b) at the bay mouth

Effect of BSS on deposition and erosion is further discussed considering the **Fig 7.15**. It shows that the BSS is high near the bay mouth while it is relatively low in the inner part of the bay. If the critical BSS on deposition and critical BSS on erosion are set to $\tau_D = 1.0 N/m^2$ and $\tau_E = 1.0 N/m^2$ respectively, then the particulate organic matter mainly deposits in the inner part of the bay while it mainly erodes at the bay mouth.

7.2.1.2 Water content

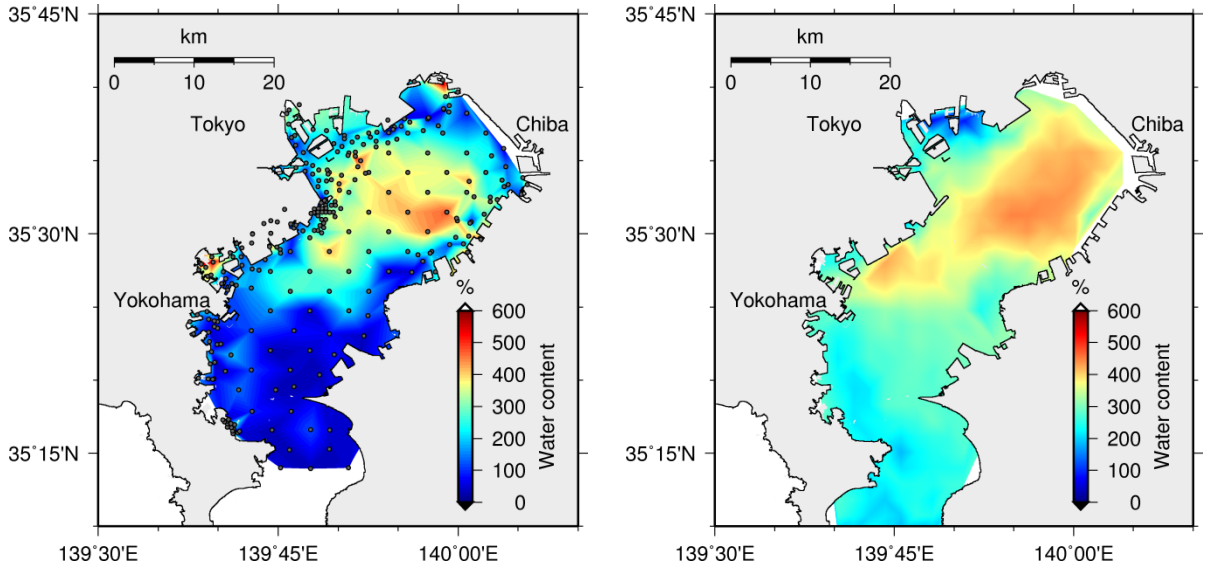

Fig 7.16 Observed (left) and simulated (right) spatial distributions of WC

The computed spatial distribution of WC is consistent with those in measurements showing high concentration at the central part of the bay (**Fig 7.16**). Simulated WC is somewhat overestimated due to the over estimation of POCC. According to the data analysis, it has been revealed that the WC and POCC have a positive correlation, which has been well reproduced in the model.

7.2.1.3 Total phosphorous content and total nitrogen content

Computed spatial distributions of TNC and TPC are consistent with data showing high concentration at the central part of the bay. Even though the Particulate organic carbon (POC) is modeled with three components, particulate organic phosphorus (POP) and particulate

organic nitrogen (PON) have not been modeled. Only inorganic components of phosphorous and nitrogen are modeled with dissolved and attached fractions. Hence, in order to validate the model for spatial distribution of nutrients, POC is converted into PON and POP through the Redfield ratio of C: N: P=106:16:1. After adding inorganic and organic components of PON and POP, TNC and TPC are obtained.

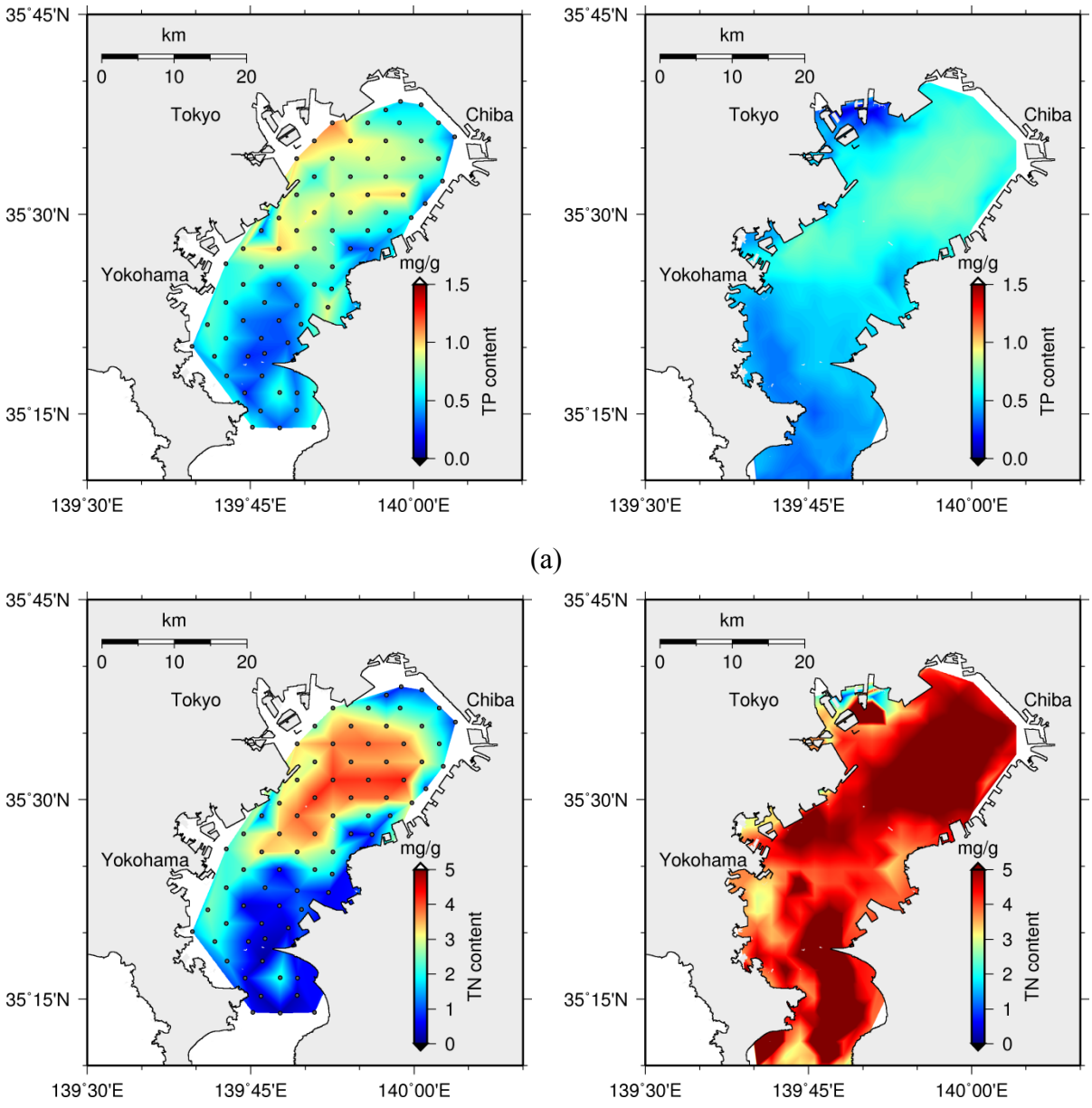

(a)

(b)

Fig 7.17 Observed (left) and simulated (right) spatial distributions of (a) TP content and (b) TN content

Same as the relationship of WC and POCC, TNC and TPC have been showed positive correlations with the WC and those correlations were well reproduced in the model. Even though the TPC followed the data quantitatively, TNC showed large discrepancy with the data. One of the reasons for this discrepancy may be the difference in C: N ratio at the site with Redfield ratio. Other than that, overestimated POCC may have been caused some overestimation of TNC and TPC.

7.2.1.4 Effect of bed formation on water quality

According to the data collected for the Tokyo Bay, it has been observed that similar pattern of spatial distributions between sediment POCC and the dissolved oxygen in bottom water. This similarity suggests that the sediment pollution represented by POCC cause severe DO depletion (anoxia) in Tokyo Bay. Moreover, this confirms the active benthic-pelagic coupling in the inner part of the Tokyo Bay. This phenomenon has well reproduced in the model as shown in the **Fig 7.18**.

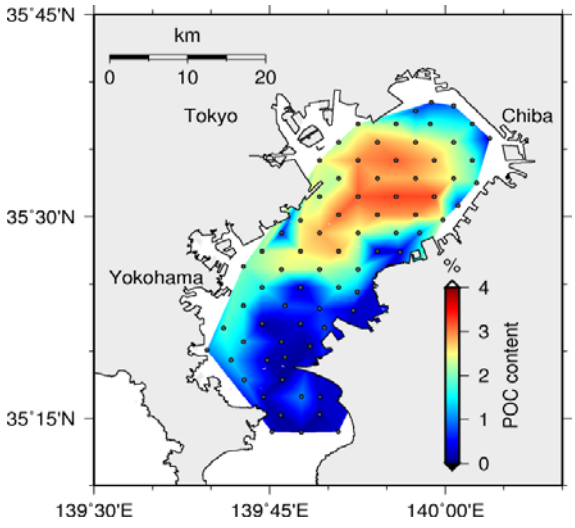

(Okada and Furukawa, 2005)

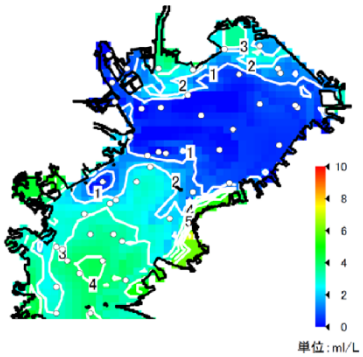

("Prediction of Bottom water hypoxia in Tokyo Bay", Chiba Prefecture., July 24, 2014)

(a)

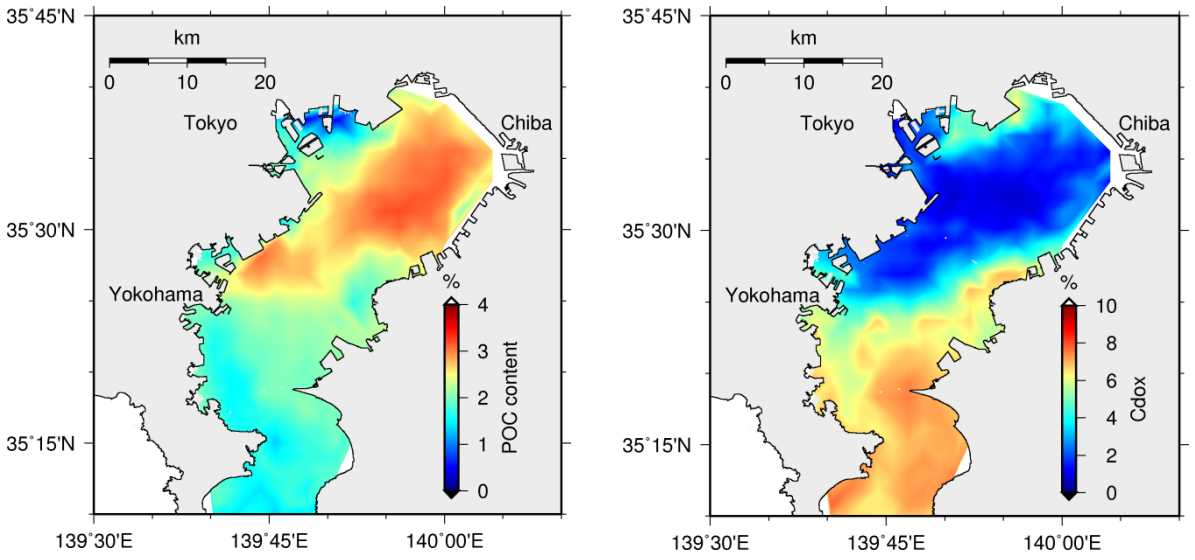

(b)

Fig 7.18 Spatial distributions of POCC in sediment (left) and DO in bottom water (right) (a) data (b) simulated

7.2.2 Vertical distribution of sediment quality

Vertical distributions of sediment quality variation with depth have been shown in the **Fig 7.19**. It is very clear that with the increase of POCC, the thickness of the active sediment layer has been increased and vice versa. It has shown that DO is available only within surface few millimeters of sediment having almost no DO in sediment during the summer. Nutrients of ammonia, phosphate and dissolved silica in pore water which have been drawn show the accumulation of nutrients especially after the spring and summer while they have low concentrations during spring and summer as a result of nutrient release to water column.

Nitrate variation in sediment have shown the availability of nitrate only during the summer which has been resulted by the denitrification flux from water to sediment. Vertical distributions of POCC, WC, TPC and TNC show the large concentration within the surface 5cm while they are uniform below that level. Moreover, POCC, TPC and TNC show positive correlations with WC which has confirmed the relationship proposed by (T Okada and Furukawa, 2005). With the increase of POCC Silt content has been decreased.

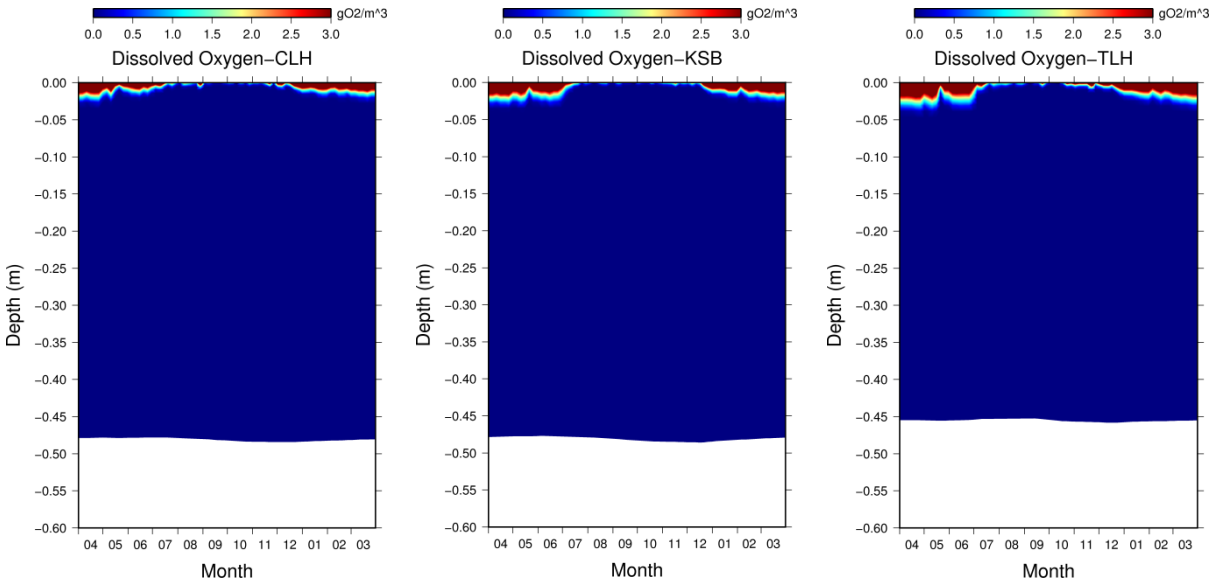
gO2/m^3
0.0 0.5 1.0 1.5 2.0 2.5 3.0
Dissolved Oxygen–CLH
Dissolved Oxygen–KSB
Dissolved Oxygen–TLH
Depth (m)
0.00 −0.05 −0.10 −0.15 −0.20 −0.25 −0.30 −0.35 −0.40 −0.45 −0.50 −0.55 −0.60
04 05 06 07 08 09 10 11 12 01 02 03
Month

(a)

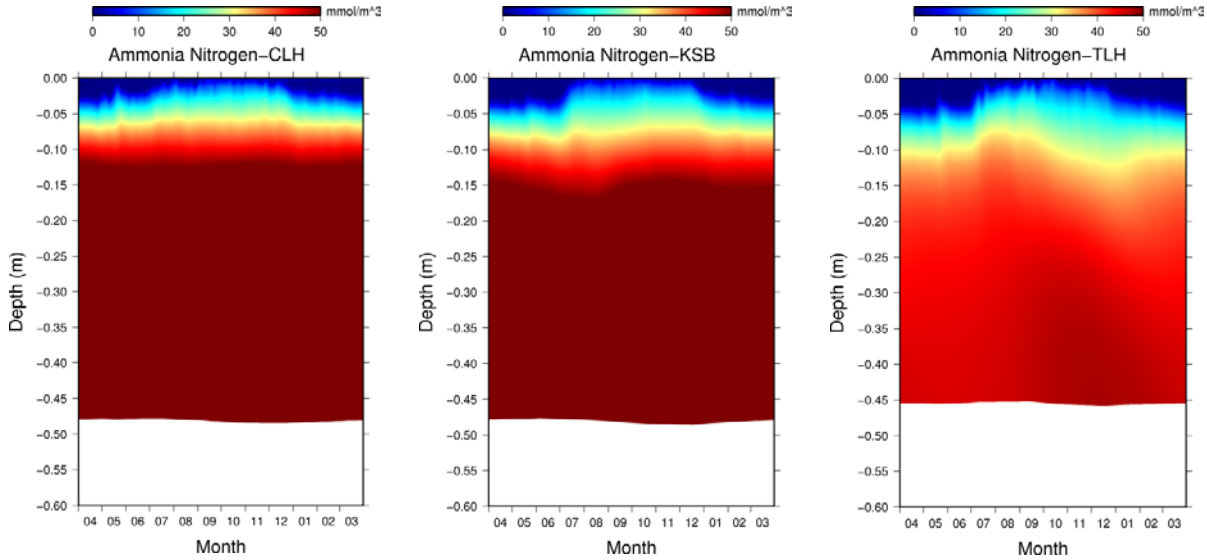
mmol/m^3
0 10 20 30 40 50
Ammonia Nitrogen–CLH
Ammonia Nitrogen–KSB
Ammonia Nitrogen–TLH
Depth (m)
0.00 −0.05 −0.10 −0.15 −0.20 −0.25 −0.30 −0.35 −0.40 −0.45 −0.50 −0.55 −0.60
04 05 06 07 08 09 10 11 12 01 02 03
Month

(b)

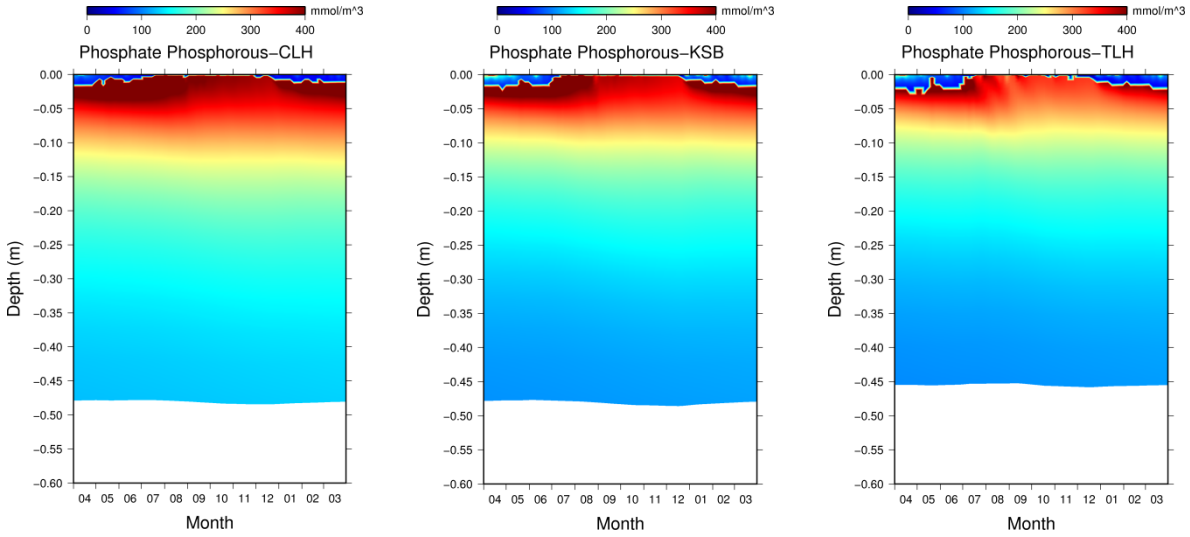
mmol/m^3
0 100 200 300 400
Phosphate Phosphorous–CLH
Phosphate Phosphorous–KSB
Phosphate Phosphorous–TLH
Depth (m)
0.00 −0.05 −0.10 −0.15 −0.20 −0.25 −0.30 −0.35 −0.40 −0.45 −0.50 −0.55 −0.60
04 05 06 07 08 09 10 11 12 01 02 03
Month

(c)

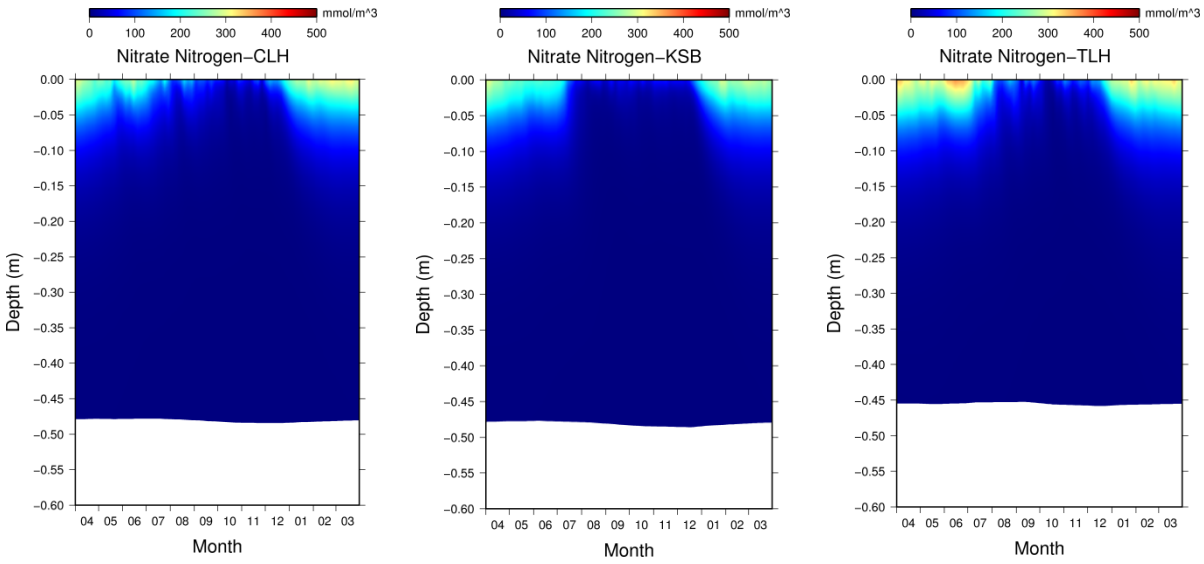
mmol/m^3
0 100 200 300 400 500
Nitrate Nitrogen–CLH
Nitrate Nitrogen–KSB
Nitrate Nitrogen–TLH
Depth (m)
0.00 −0.05 −0.10 −0.15 −0.20 −0.25 −0.30 −0.35 −0.40 −0.45 −0.50 −0.55 −0.60
04 05 06 07 08 09 10 11 12 01 02 03
Month

(d)

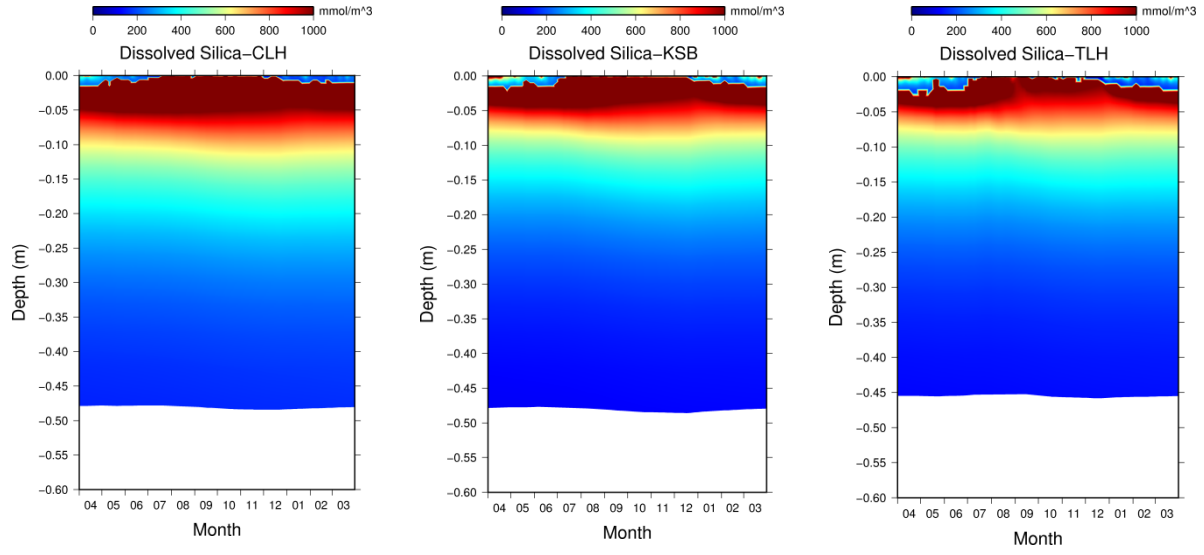
mmol/m^3
0 200 400 600 800 1000
Dissolved Silica–CLH
Dissolved Silica–KSB
Dissolved Silica–TLH
Depth (m)
0.00 −0.05 −0.10 −0.15 −0.20 −0.25 −0.30 −0.35 −0.40 −0.45 −0.50 −0.55 −0.60
04 05 06 07 08 09 10 11 12 01 02 03
Month

(e)

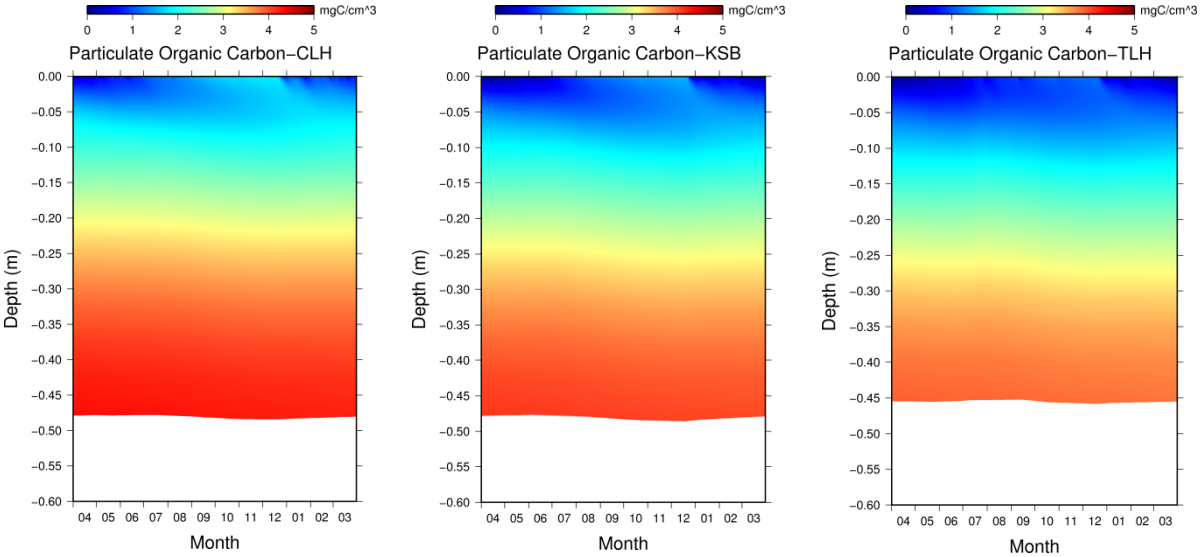
mgC/cm^3
0 1 2 3 4 5
Particulate Organic Carbon–CLH
Particulate Organic Carbon–KSB
Particulate Organic Carbon–TLH
Depth (m)
0.00 −0.05 −0.10 −0.15 −0.20 −0.25 −0.30 −0.35 −0.40 −0.45 −0.50 −0.55 −0.60
04 05 06 07 08 09 10 11 12 01 02 03
Month

(f)

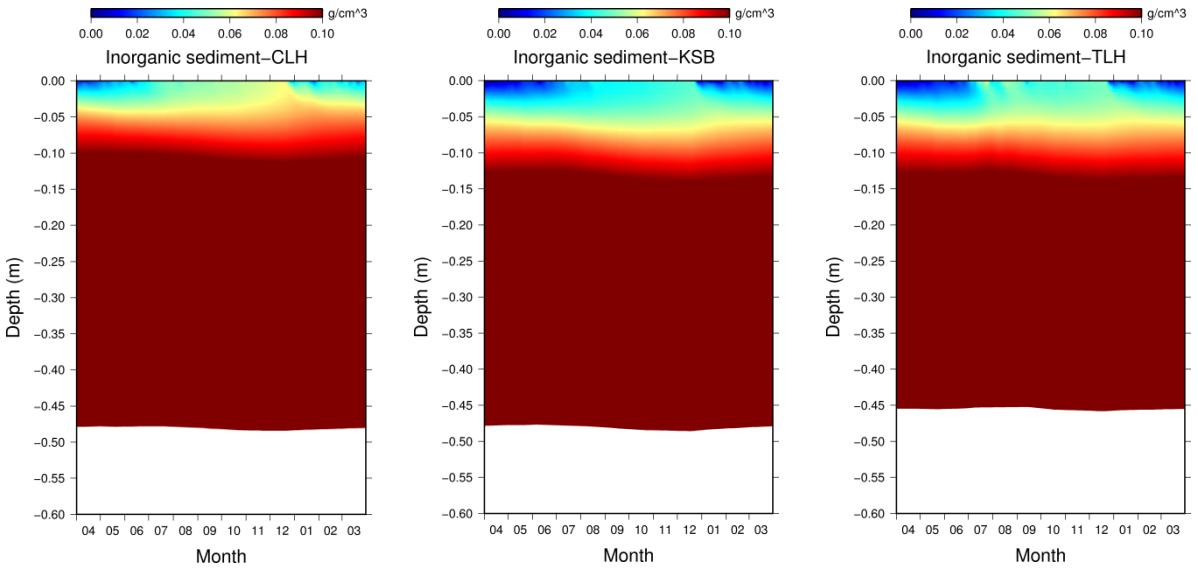
g/cm^3
0.00 0.02 0.04 0.06 0.08 0.10
Inorganic sediment–CLH
Inorganic sediment–KSB
Inorganic sediment–TLH
Depth (m)
0.00 −0.05 −0.10 −0.15 −0.20 −0.25 −0.30 −0.35 −0.40 −0.45 −0.50 −0.55 −0.60
Month
04 05 06 07 08 09 10 11 12 01 02 03

(g)

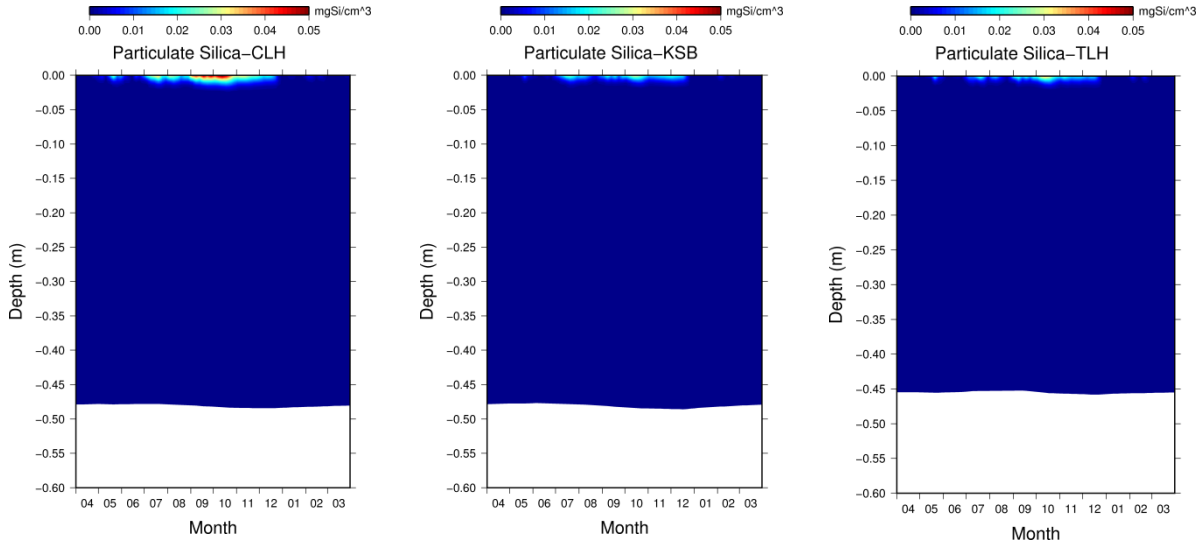
mgSi/cm^3
0.00 0.01 0.02 0.03 0.04 0.05
Particulate Silica–CLH
Particulate Silica–KSB
Particulate Silica–TLH
Depth (m)
0.00 −0.05 −0.10 −0.15 −0.20 −0.25 −0.30 −0.35 −0.40 −0.45 −0.50 −0.55 −0.60
Month
04 05 06 07 08 09 10 11 12 01 02 03

(h)

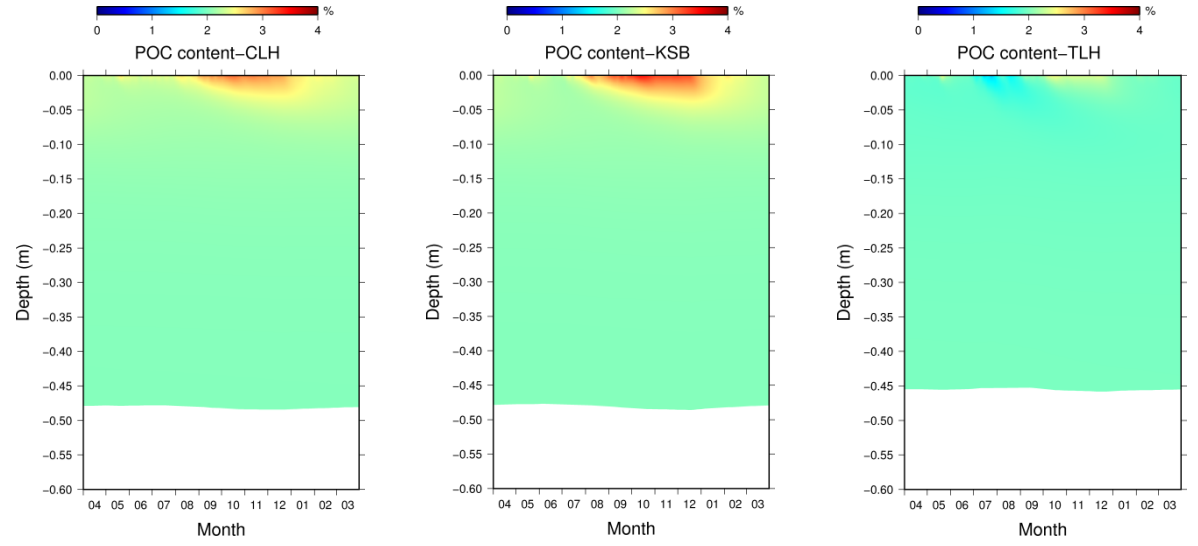
%
0 1 2 3 4
POC content–CLH
POC content–KSB
POC content–TLH
Depth (m)
0.00 −0.05 −0.10 −0.15 −0.20 −0.25 −0.30 −0.35 −0.40 −0.45 −0.50 −0.55 −0.60
Month
04 05 06 07 08 09 10 11 12 01 02 03

(i)

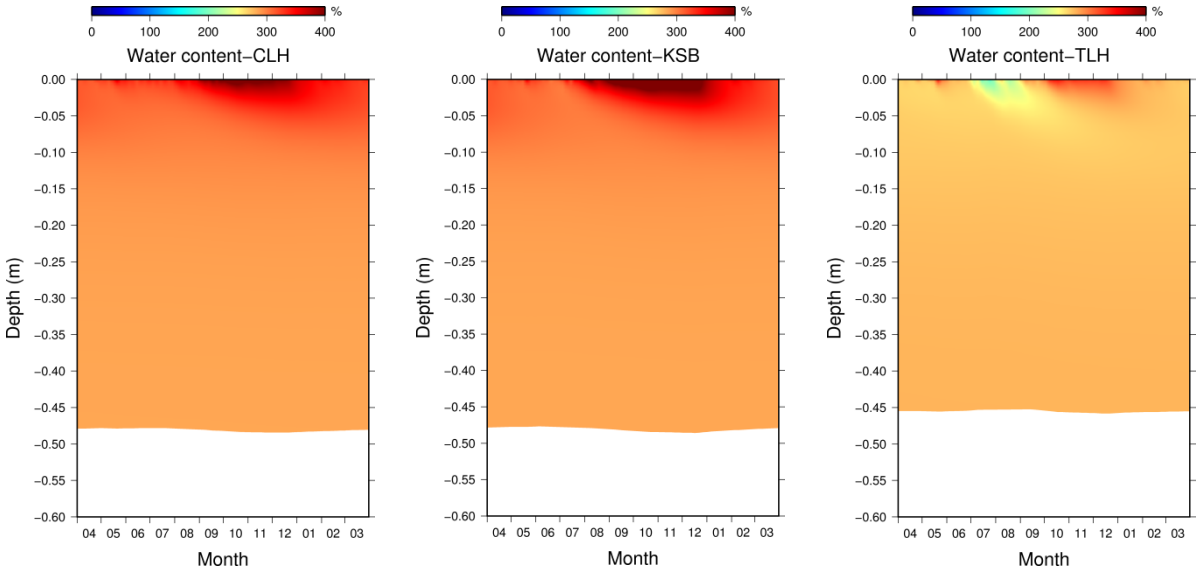
Water content–CLH
Water content–KSB
Water content–TLH
%
0 100 200 300 400
Depth (m)
0.00 −0.05 −0.10 −0.15 −0.20 −0.25 −0.30 −0.35 −0.40 −0.45 −0.50 −0.55 −0.60
Month
04 05 06 07 08 09 10 11 12 01 02 03

(j)

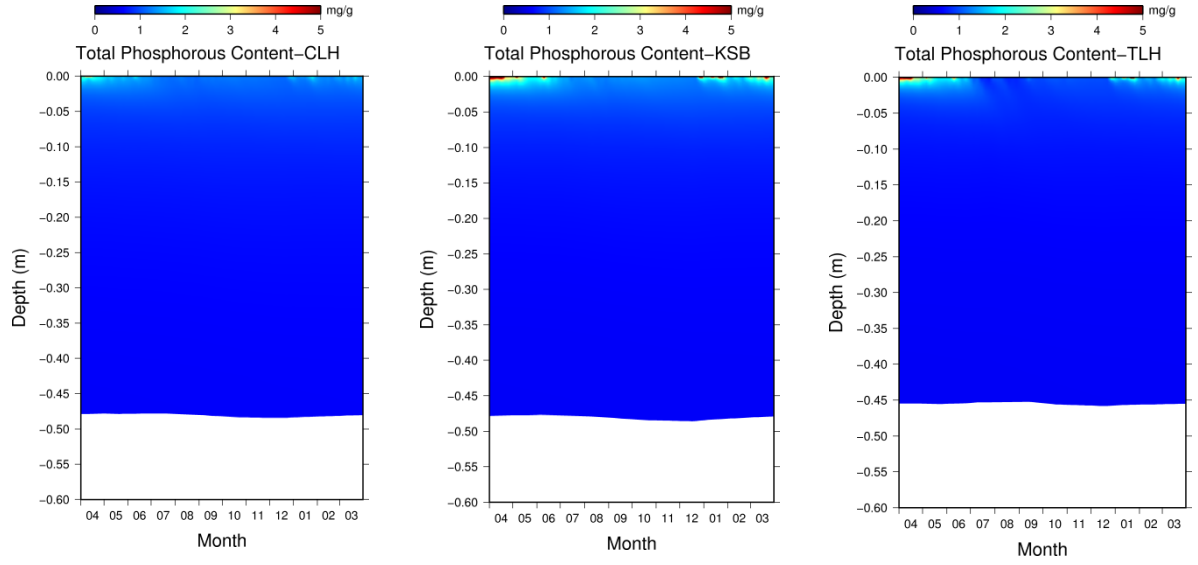
Total Phosphorous Content–CLH
Total Phosphorous Content–KSB
Total Phosphorous Content–TLH
mg/g
0 1 2 3 4 5
Depth (m)
0.00 −0.05 −0.10 −0.15 −0.20 −0.25 −0.30 −0.35 −0.40 −0.45 −0.50 −0.55 −0.60
Month
04 05 06 07 08 09 10 11 12 01 02 03

(k)

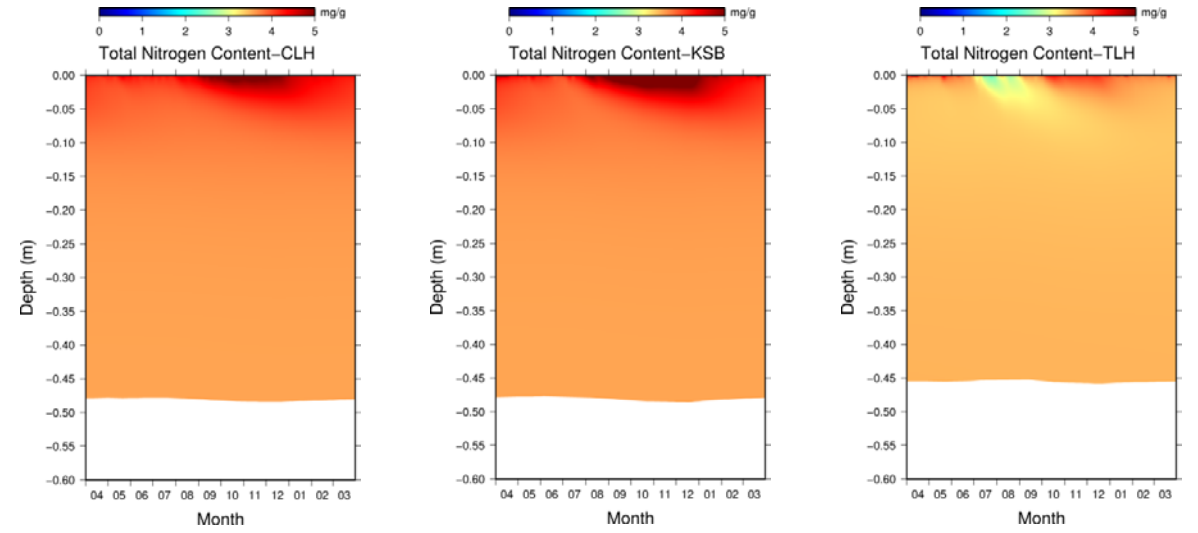
Total Nitrogen Content–CLH
Total Nitrogen Content–KSB
Total Nitrogen Content–TLH
mg/g
0 1 2 3 4 5
Depth (m)
0.00 −0.05 −0.10 −0.15 −0.20 −0.25 −0.30 −0.35 −0.40 −0.45 −0.50 −0.55 −0.60
Month
04 05 06 07 08 09 10 11 12 01 02 03

(l)

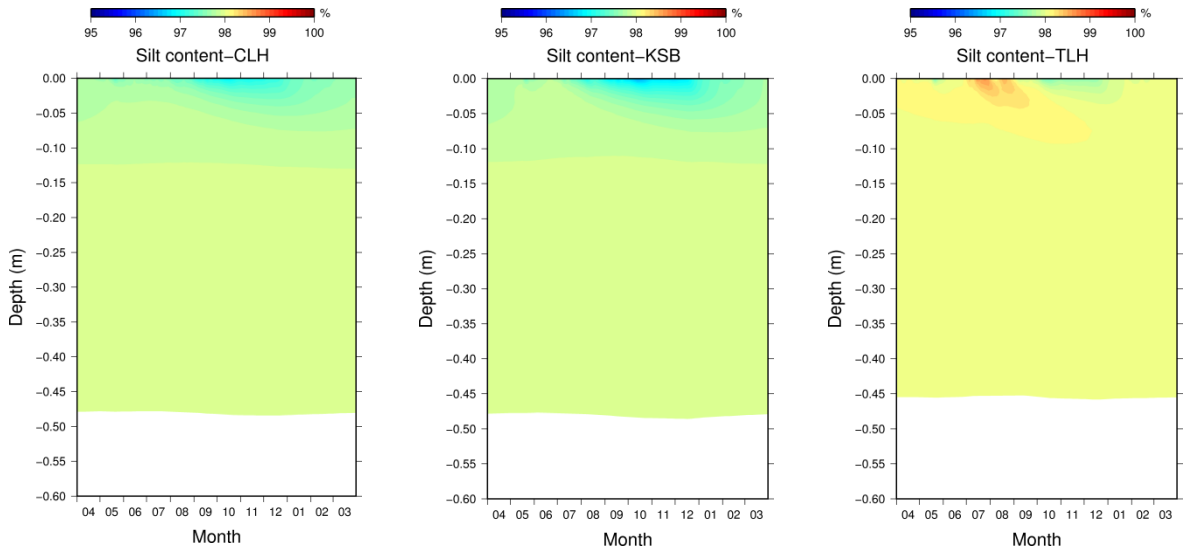

(m)

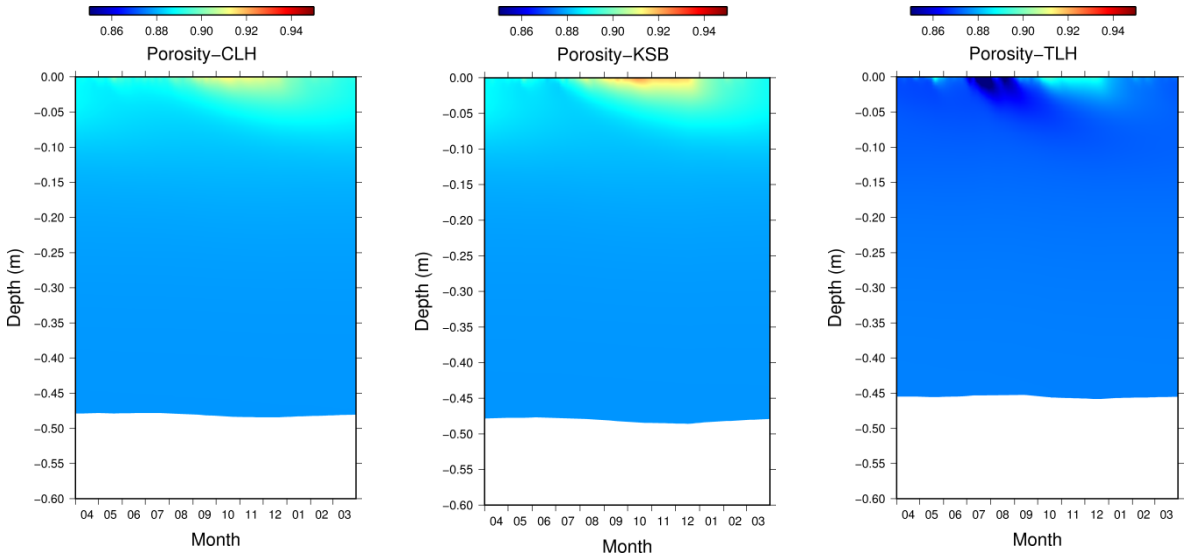

(n)

Fig 7.19 Simulated vertical distributions of (a) DO, (b) ammonia (c) phosphorus (d) nitrate (e) dissolved silica (f) POC (g) Silt (h) particulate silica (i) POCC (j) WC (k) TPC (l) TNC (m) SiltC (n) porosity at CLH, KSB and TLH

Furthermore, the vertical distributions of ammonia, phosphate-phosphorus and nitrate follow the distributions proposed by (Di Toro, 2001) as shown in the **Fig 7.20**, **Fig 7.21** and **Fig 7.22**. Even though the vertical distributions of nutrients are consistent with the proposed distributions qualitatively, their quantitative reproducibility has yet to be analyzed. Since the vertical distributions of nutrients are changing drastically, it gives difficulties to discuss the reproducibility.

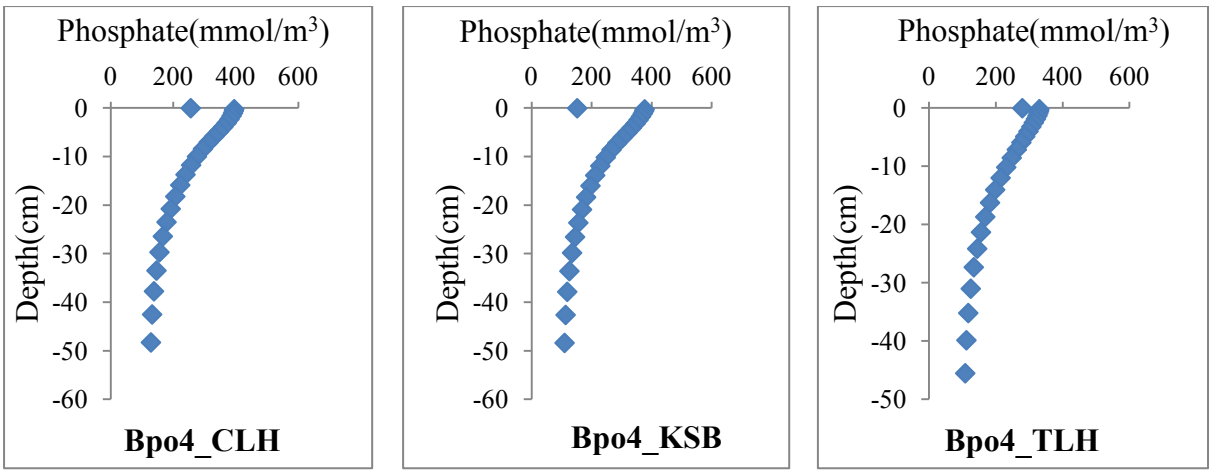

(a) Simulated

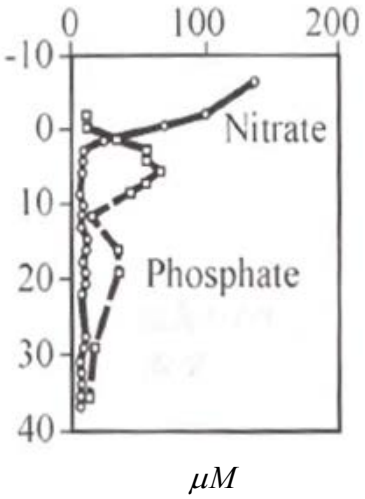

(b) Data (Di Toro, 2001)

Fig 7.20 Vertical distributions of phosphate (a) simulated and (b) data

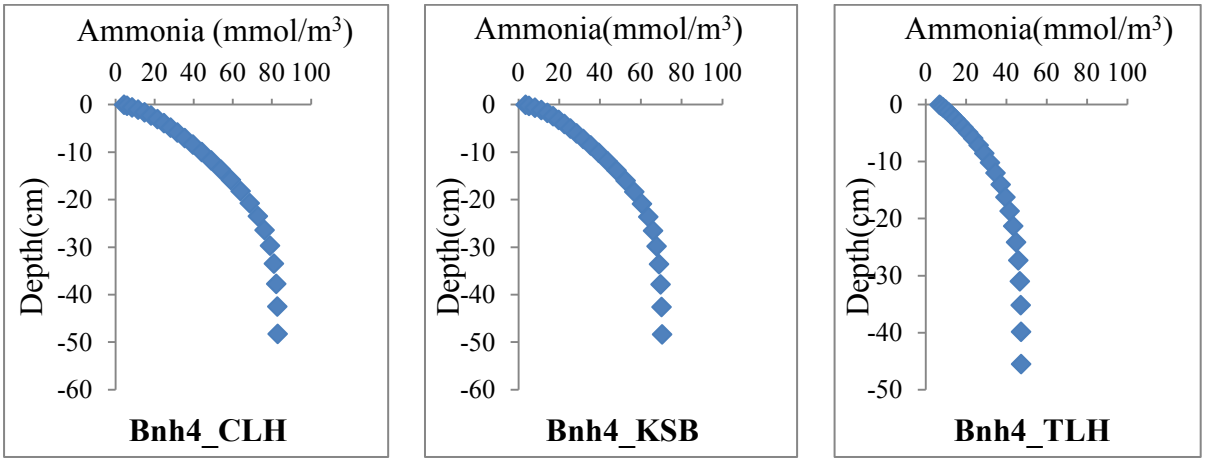

(a) Simulated

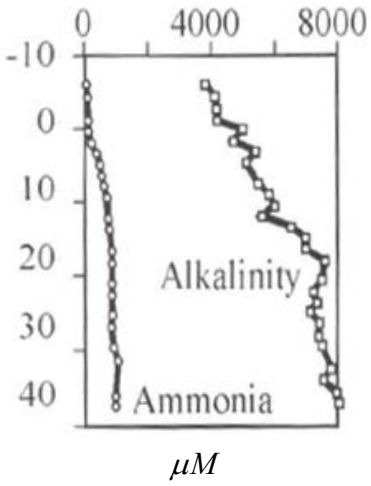

(b) Data (Di Toro, 2001)

Fig 7.21 Vertical distributions of ammonia (a) simulated and (b) data

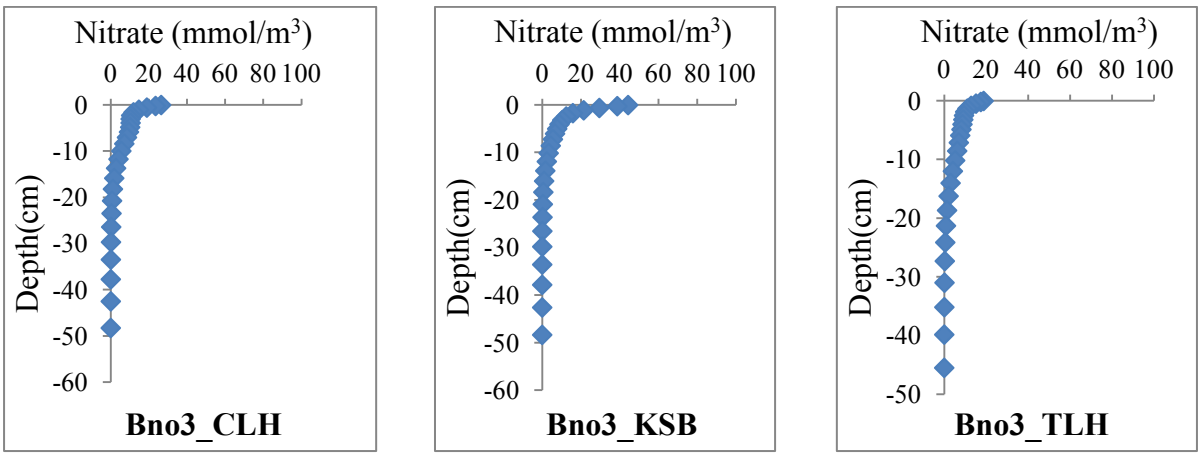

(a) Simulated

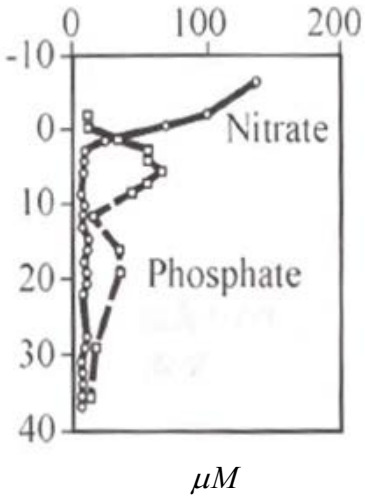

(b) Data (Di Toro, 2001)

Fig 7.22 Vertical distributions of nitrate (a) simulated and (b) data

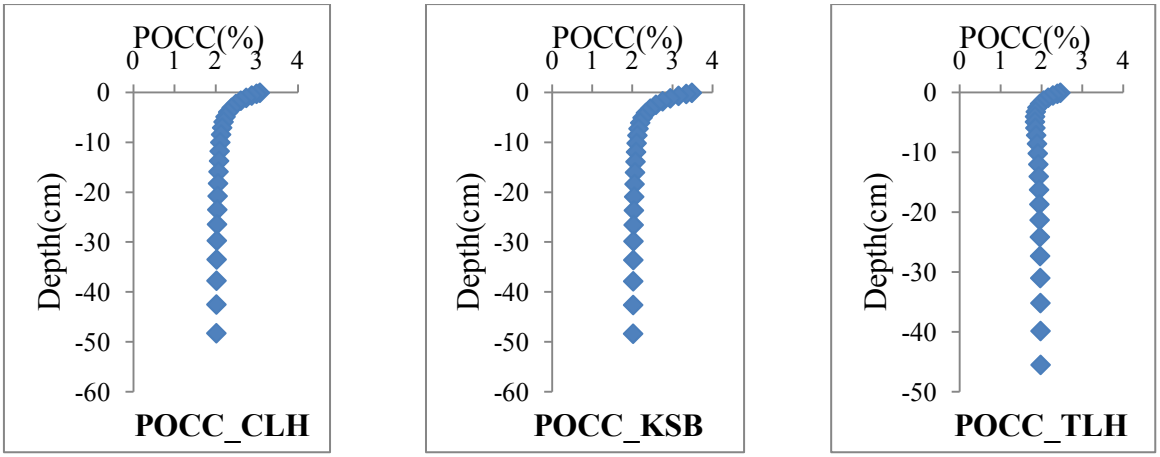

(a) Simulated

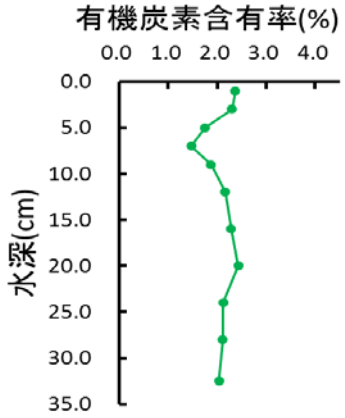

(b) Data (Sano H., 2014)

Fig 7.23 Vertical distributions of POCC (a) simulated and (b) data

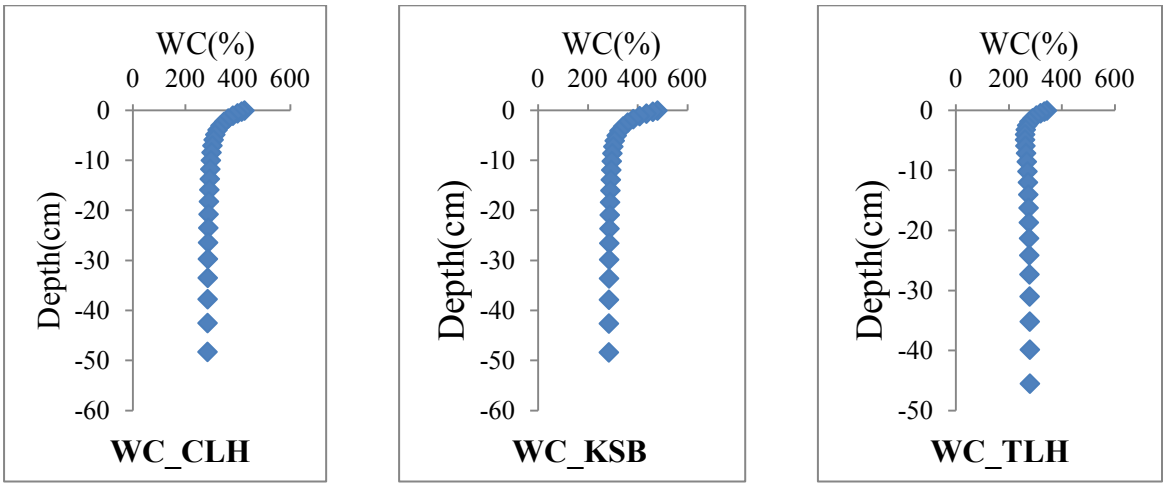

(a) Simulated

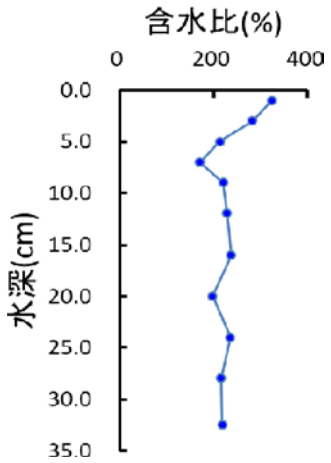

(b) Data (Sano H., 2014)

Fig 7.24 Vertical distributions of WC (a) simulated and (b) data

Vertical distributions of POCC and WC have been proposed by Sano Hiroaki, 2015 analyzing collected data for Tokyo Bay. Simulated model vertical distribution follows those proposed distributions as shown in the figures **Fig 7.23** and **Fig 7.24**.

7.3 Effect of flux on water and sediment quality

Fig 7.25 shows the effect of sediment flux release on both water and sediment quality. Under anoxic conditions phosphorous and ammonia flux will be released from sediment to water increasing the bottom water concentration of corresponding nutrient while decreasing the concentrations on the sediment surface. (This effect of flux on water and sediment quality has been analyzed before the final tuning of the model. Even though it can be expected the same conclusions it is recommended to perform the same analysis for the final tuned model).

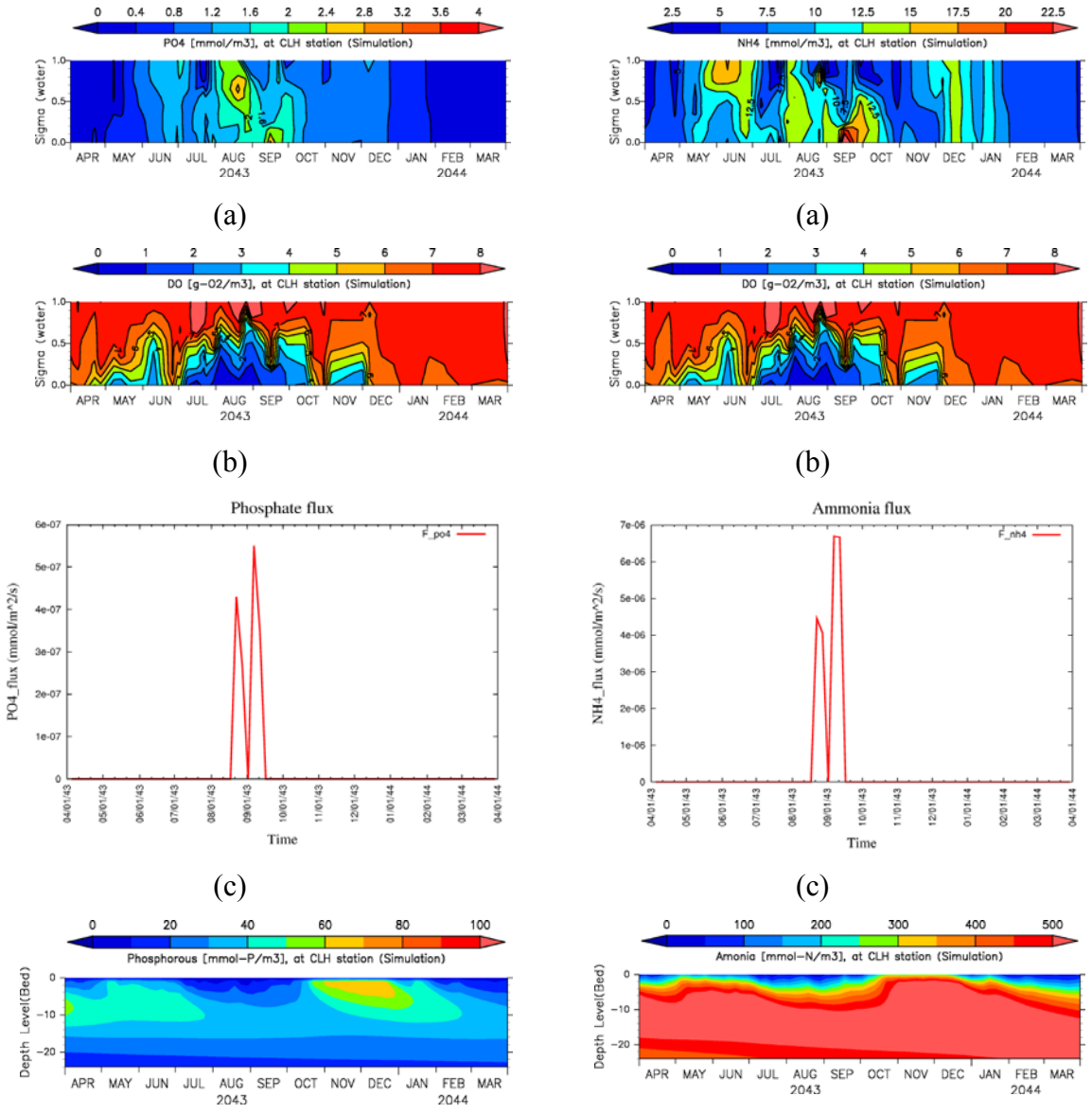

Fig 7.25 Simulated vertical distributions of (a) water nutrient, (b) water DO, (c) nutrient flux and (d) bed nutrient for phosphorous (left) and ammonia (right) at CLH

Nitrate flux is released from water to sediment under anoxic conditions reducing the bottom water concentration and increasing the concentration on surface sediment.

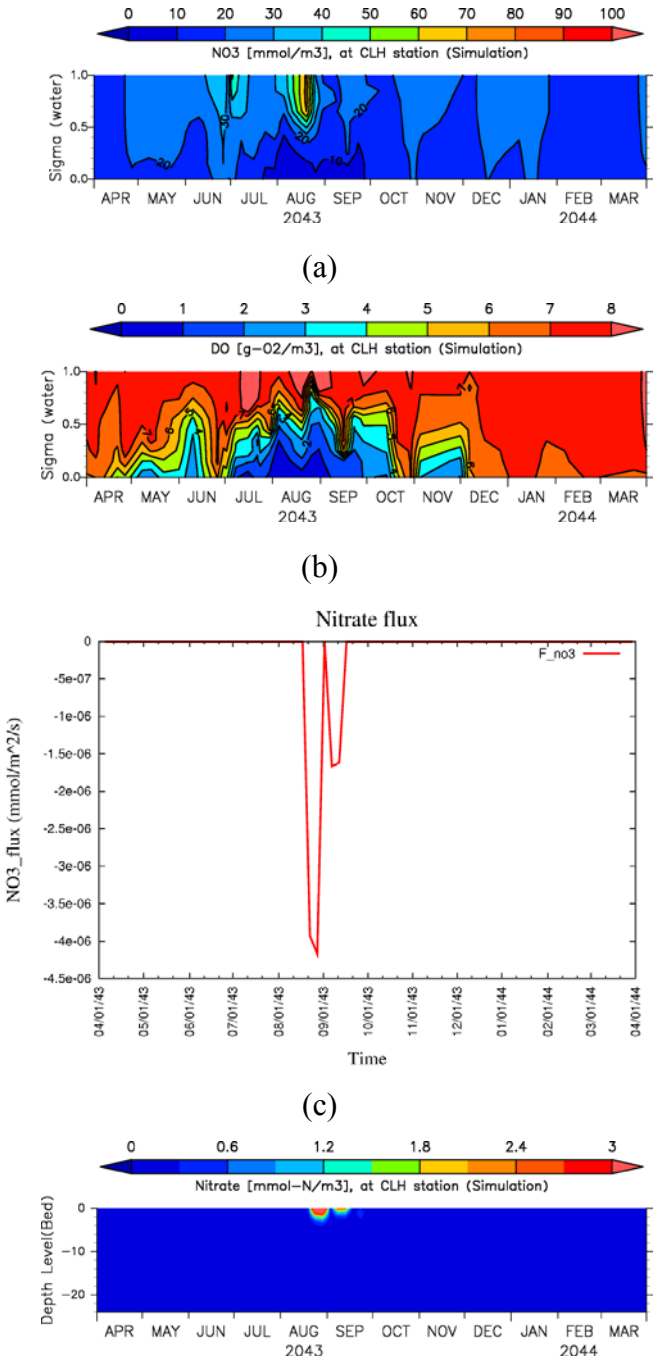

Fig 7.26 Simulated vertical distributions of (a) water nitrate, (b) water DO, (c) nitrate flux and (d) bed nitrate at CLH

According to the **Fig 7.27** SOD which has been defined as DO flux from water to sediment, gets its lowest during the summer when the bottom DO in water column reaches its lowest. This has resulted very low DO concentration in sediment.

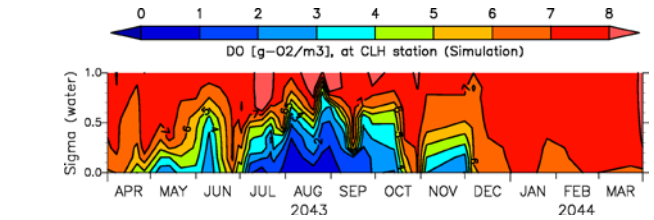

(a)

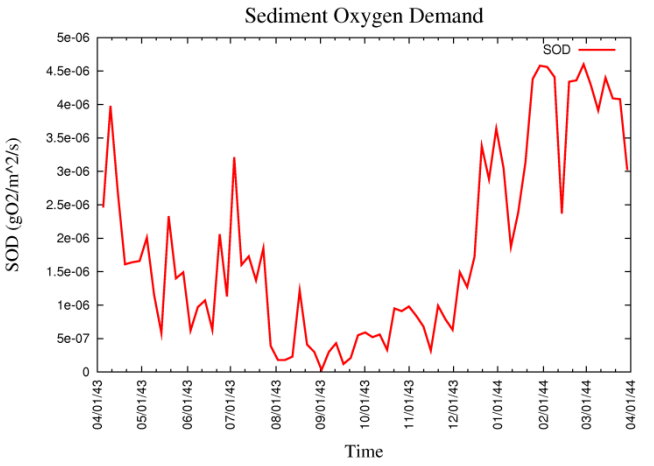

(b)

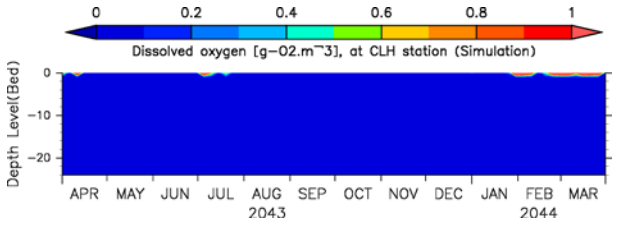

(c)

Fig 7.27 Simulated vertical distributions of (a) water DO, (b) nutrient flux and (c) bed DO at CLH

7.4 Long term water and sediment quality

Fig 7.28 shows the results for the formation of sediment bed during 20-year period, with high POCC at the surface and bottom mud layers. With the increase of surface POCC, silt content is decreasing. These long term simulated results have confirmed the robustness of the model for long term computations of sediment quality. Similarly **Fig 7.29** has confirmed the robustness of the model for long term computations of water quality giving similar yearly variations of DO and chlorophyll within the water column.

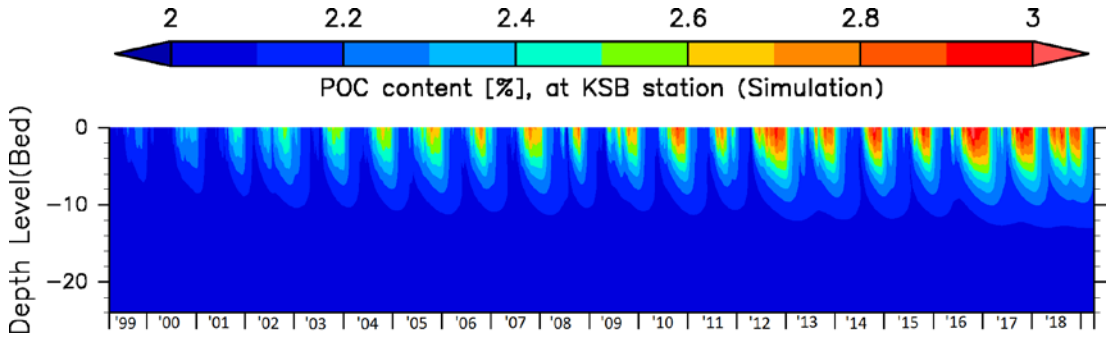

(a)

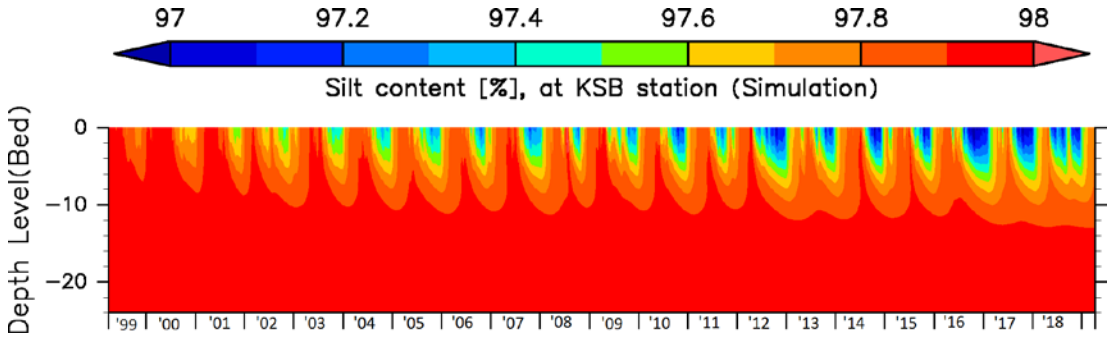

(b)

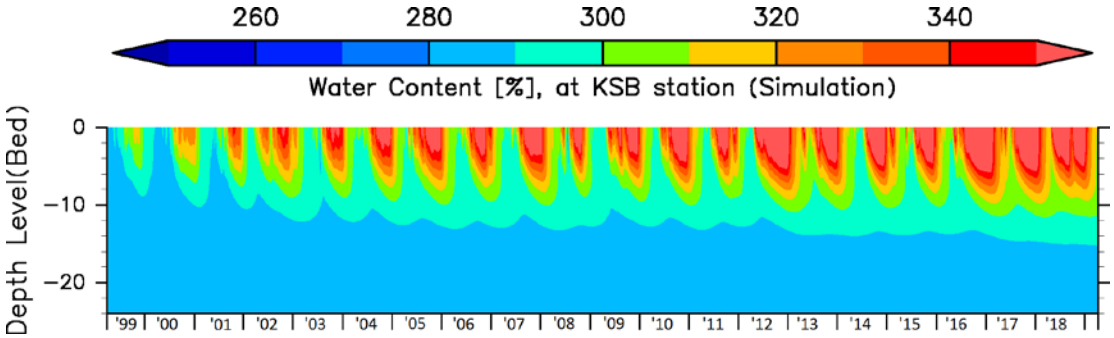

(c)

Fig 7.28 20-year simulated vertical distributions of (a) POCC (b) Silt content and (c) WC in sediment column

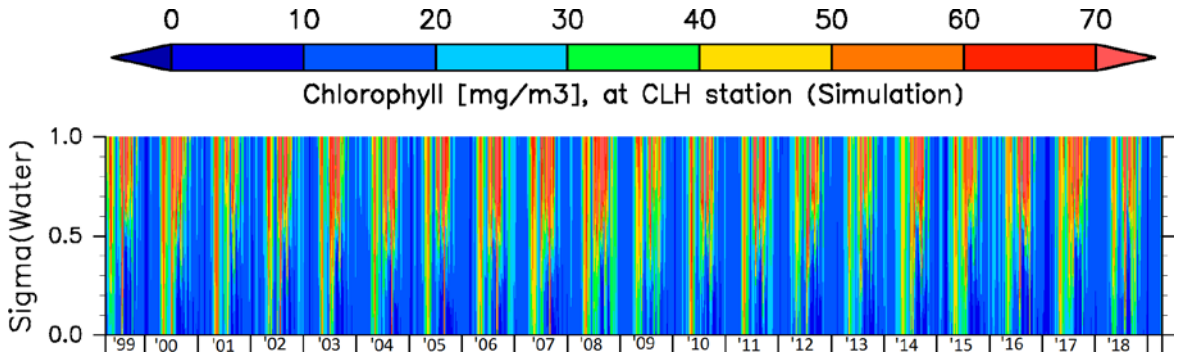

(a)

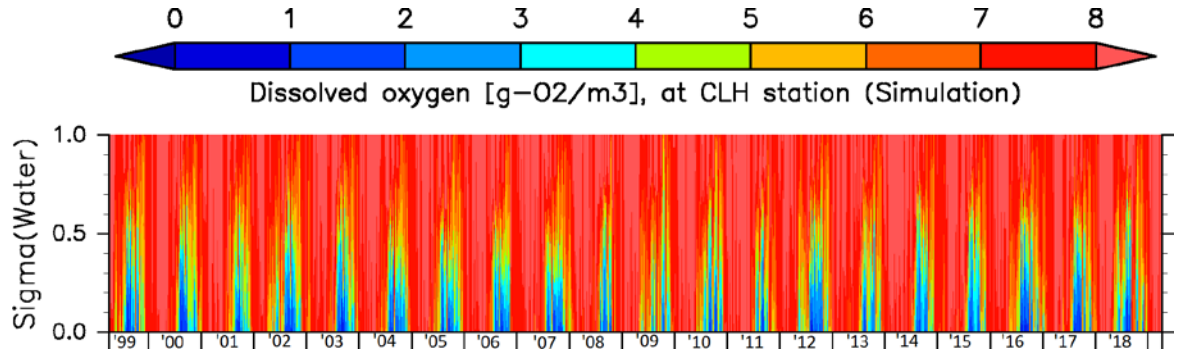

(b)

Fig 7.29 20-year simulated vertical distributions of (a) *Chl_a* (b) DO in water column

During the long term simulation, initial conditions are renewed after each year of simulation. Since it is confirmed that the initial conditions affect the results during one year period of simulation until the steady state is obtained, the simulation is continued until the agreeable reproduction with reasonable steady state is obtained through realistic initial conditions. Analysis of most realistic steady state found to be important to improve the reproducibility of the model.

8. SENSITIVITY ANALYSIS

The consistency of the pelagic model and the benthic model are confirmed independently towards some aspects. After coupling, model is first tuned and examined through the sensitivity analysis of critical parameters and then validated comparing with observed vertical variation in water quality and spatial variation in sediment quality along with the analysis of model robustness.

8.1 Consistency of the pelagic model on settling

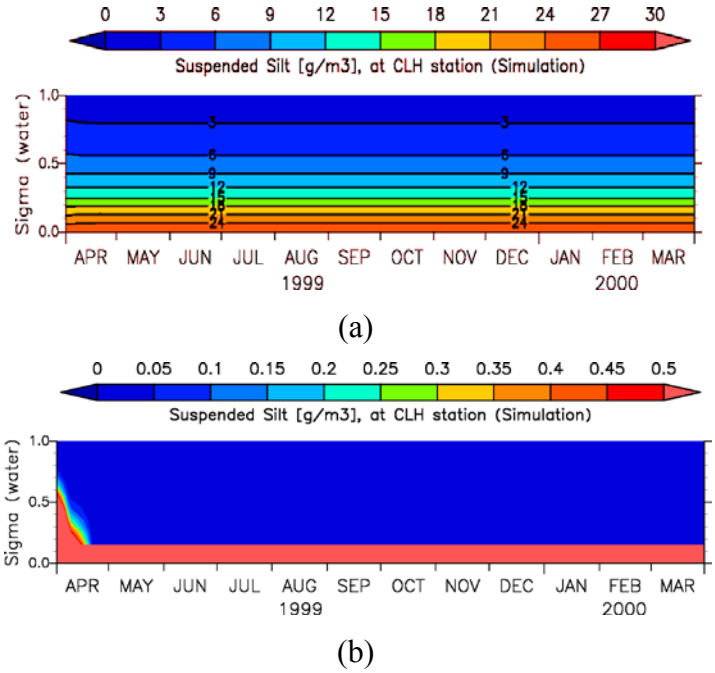

Fig 8.1 Settling of suspended silt (a) with only diffusion (b) no diffusion

In order to confirm the consistency of the pelagic model, settling of suspended silt with constant velocity is analysed under following set conditions.

- Meteorological forces such as wind speed, solar radiation and rainfall are set to zero
- River boundary conditions are changed to zero discharge
- Heat exchange is deactivated
- Tidal effect is deactivated
- Velocity effect deactivated

- For (a) in **Fig 8.1**, diffusion is considered while for (b) diffusion computation is deactivated.
- Settled particulate matter transformation to sediment is held.

It is confirmed that settling model is consistent accumulating silt at the bottom of the water column under the effect of settling velocity while particles have diffusion mixing with top layers if settling undergoes with diffusion.

8.2 Consistency of the benthic model under no flux condition

Model has set to run under no flux of dissolved matter through the sediment water interface while particulate matter settling or erosion at the surface of sediment has been considered, and no flux of both dissolved and particulate matter across the bottom boundary of the sediment. Particulate matter decomposition releases nutrients and they accumulate in the surface layers and penetrate towards the bottom due to advection and diffusion between layers, confirming the consistency of the sediment model as shown in the **Fig 8.2.**

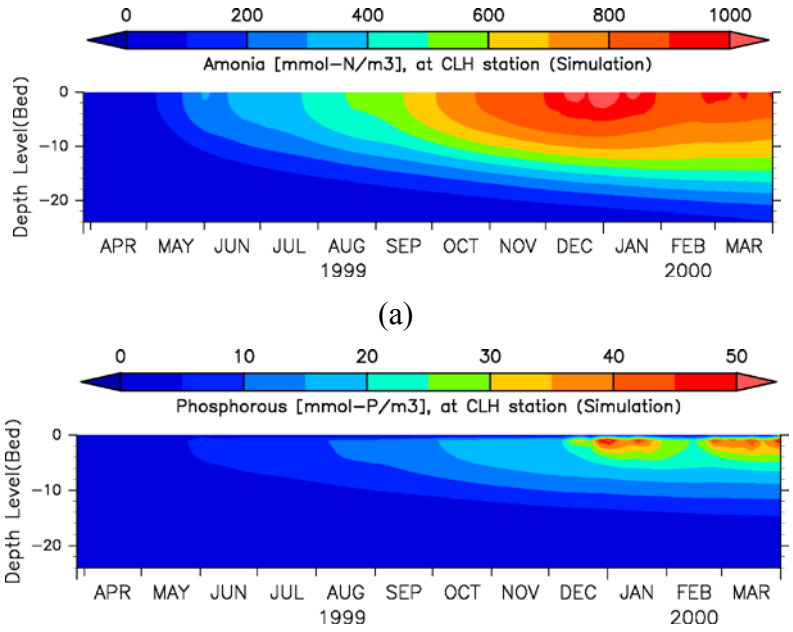

Fig 8.2 Sediment nutrients (a) ammonia and (b) phosphorous

8.3 Consistency of the benthic-pelagic coupled model

After coupling the benthic and pelagic models, the consistency of the coupled model is proved. Suspended silt is settled or eroded on the sediment-water interface. Hence, during a particular time period the cumulative settled mass of the suspended sediment (A) is computed and during the same period, the change of mass of silt within the sediment under no flux condition at the bottom boundary (B) is also computed. It has been proved that (A)=(B) confirming the consistency of the coupled model. **Fig 8.3** shows the accumulation of silt at the bottom of the sediment column during a one year period under no flux condition at the bottom boundary.

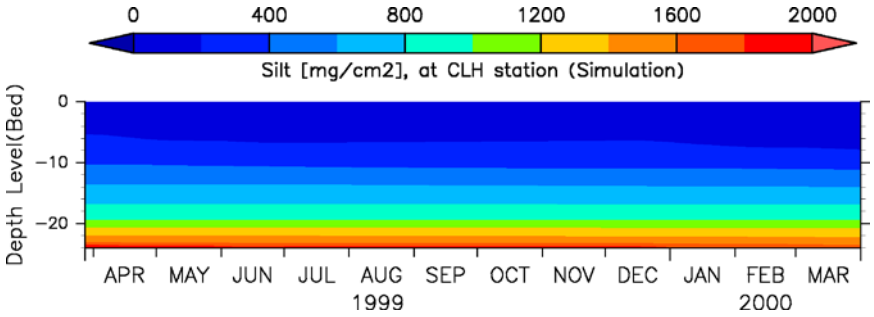

Fig 8.3 Silt accumulation under no flux condition at the bottom boundary

8.4 Sensitivity analysis on discharge magnification factor

Water salinity and temperature are important parameters to model in order to improve the reproducibility of seasonal variations of phytoplankton blooms. Density stratification is largely influenced by the surface salinity and water temperature, and thus on phytoplankton bloom. Quantity of river discharge can strongly influence on surface salinity and temperature while the available data of river discharges may not be accurate. Hence to achieve reasonable reproducibility of salinity and temperature, model has considered a magnification factor to magnify all the river inflows to the bay. Following results show how magnification factor affects surface salinity and temperature.

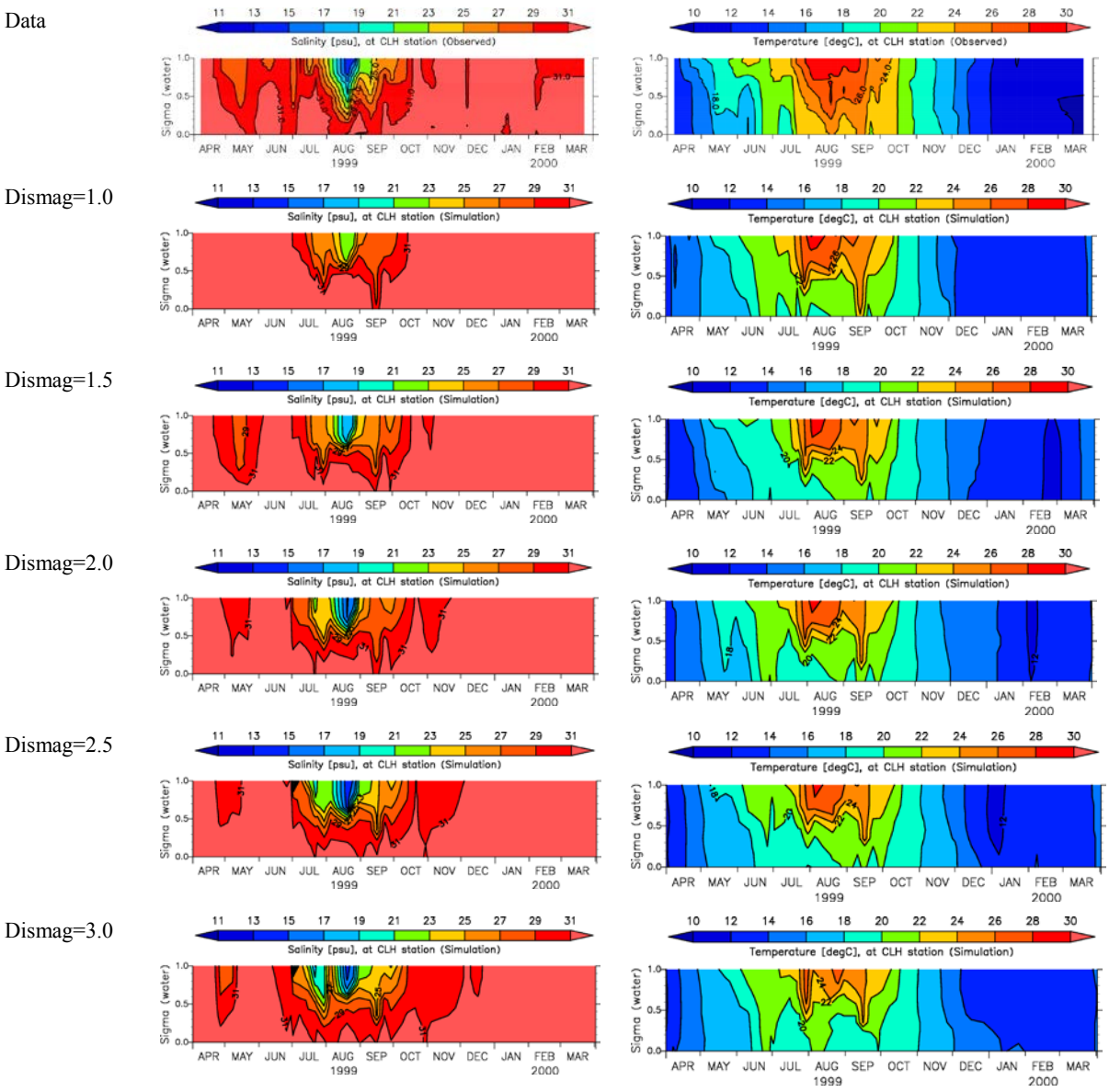

(a) Salinity (b) Temperature

Fig 8.4 Water salinity and temperature at CLH for different discharge magnification factors

The sensitivity analysis at CLH shows with increasing the river discharges both salinity and temperature are decreasing (**Fig 8.4**).In order to reproduce both salinity and temperature $dismag = 2.0$ has to be used.

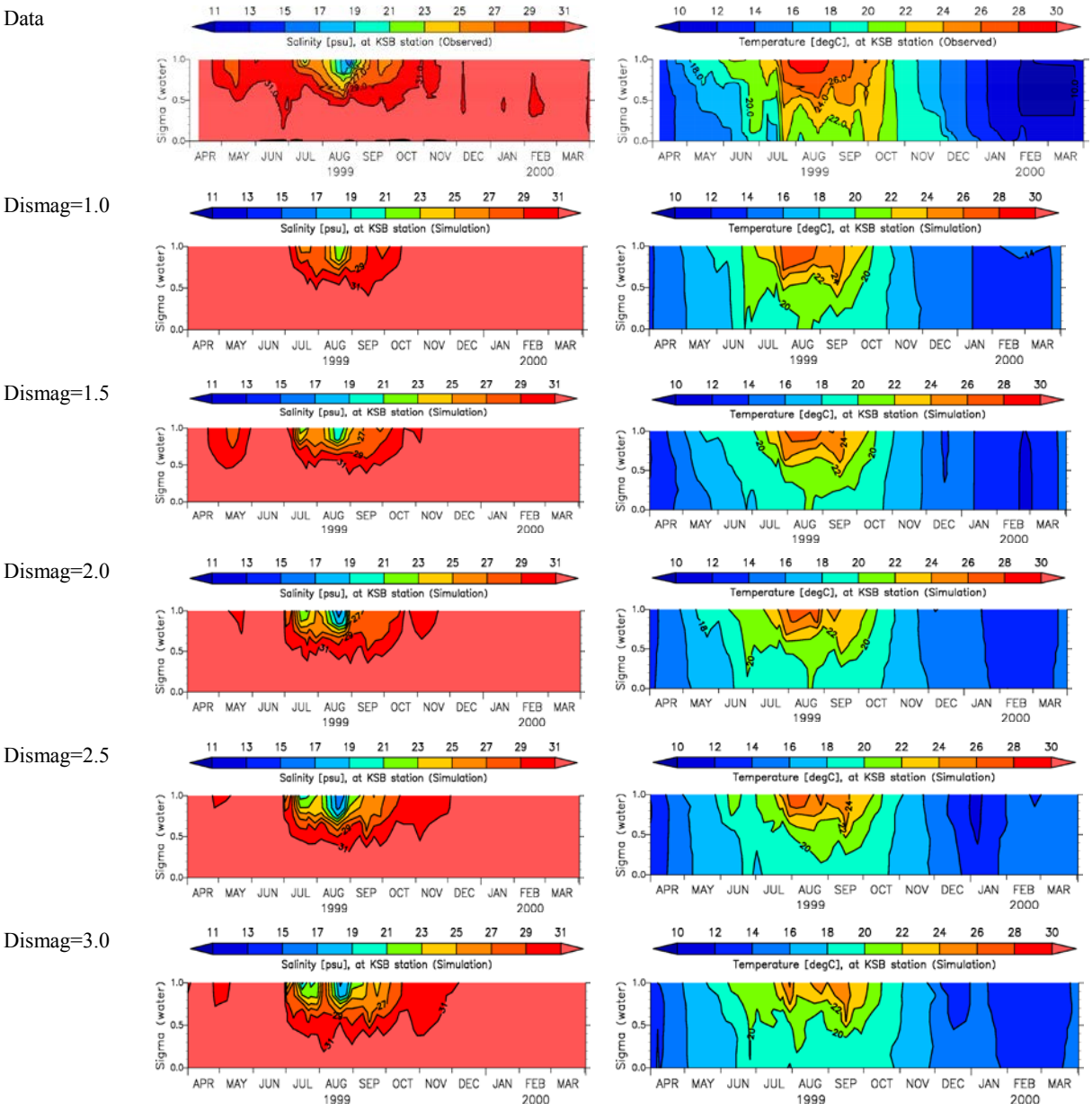

Fig 8.5 Water salinity and temperature at KSB for different discharge magnification factors

The sensitivity analysis at KSB also shows with increasing the river discharges both salinity and temperature is decreasing (**Fig 8.5**). In order to reproduce both salinity and temperature $dismag = 2.0$ has to be used.

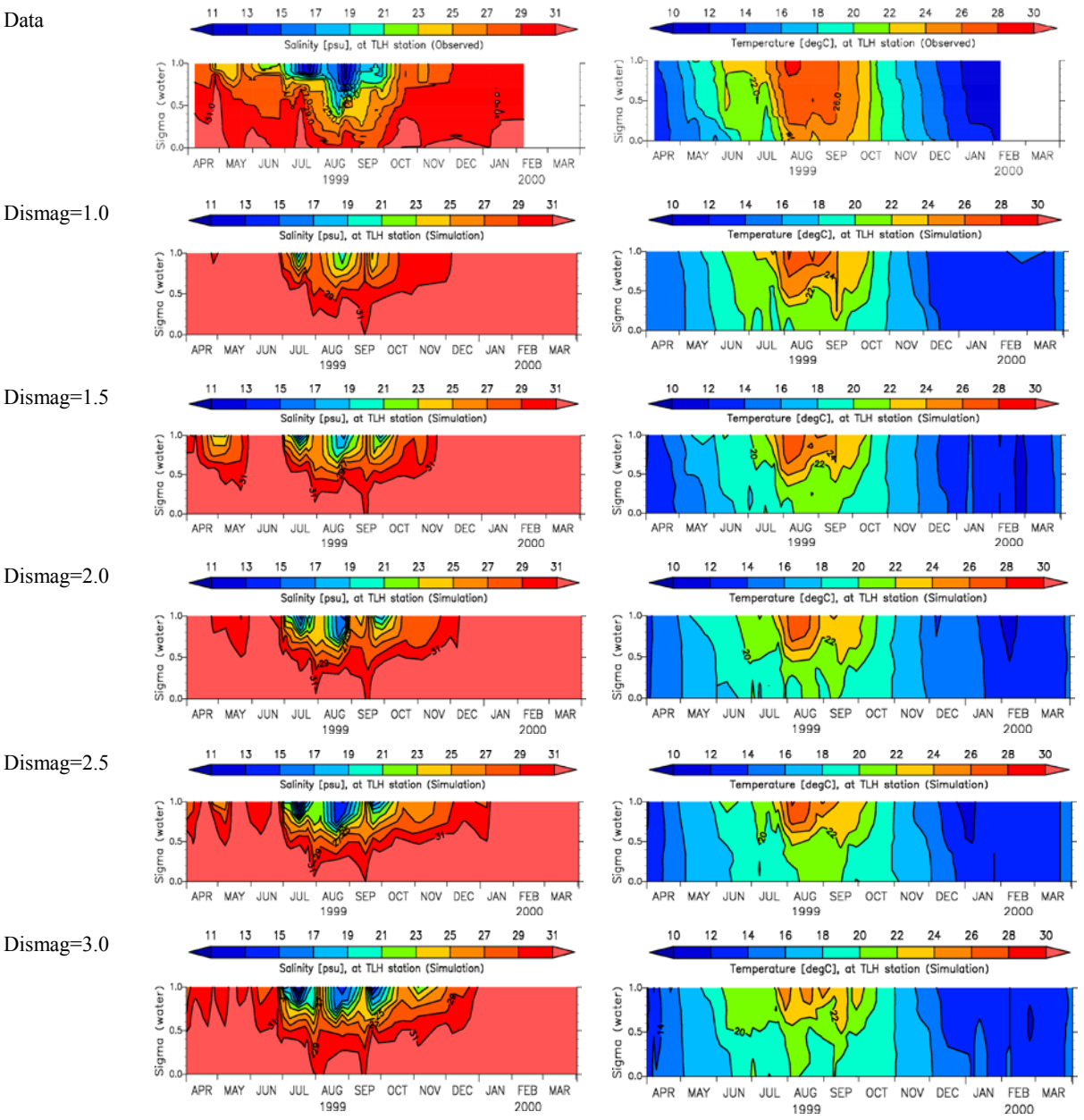

Fig 8.6 Water salinity and temperature at TLH for different discharge magnification factors

The sensitivity analysis at CLH also shows with increasing the river discharges both salinity and temperature is decreasing (**Fig 8.6**). In order to reproduce both salinity and temperature $dismag = 2.0$ has to be used.

Hence, in order to reproduce salinity and temperature at all three stations $dismag = 2.0$ has been used in the model.

8.5 Sensitivity analysis on sediment layers

Sediment model comprised with multi layers where layer thicknesses are changing based on POCC. Confirming the thickness of total effective sediment layer, the number of layers and the initial layer thicknesses are important on estimating sediment flux which is affecting both water and sediment quality. Hence, a sensitivity analysis is made for one year period of computation assuming initial particulate organic carbon is totally refractory to examine the effects of total sediment layer thickness, number of layers within the sediment, individual layer thicknesses and surface layer thickness in sediment on overall results especially, on sediment flux. It has been found that the thickness of the surface layer of sediment has a considerable effect on the sediment flux release while the others have no significant effect.

Fig 8.7 shows the variation of ammonia flux for different surface layer thicknesses in sediment column at one data collected station called Chiba Light House (CLH). It is clear that when the surface layer thickness of the sediment gets smaller flux can easily release to the water column resulting increase in bottom concentration of nutrients in water while reducing surface concentration of nutrients in sediment. (The sensitivity of sediment layers on model results were analysed before the final tuning of the model. Even though it can be expected the same conclusions it is recommended to perform the same analysis for the final tuned model).

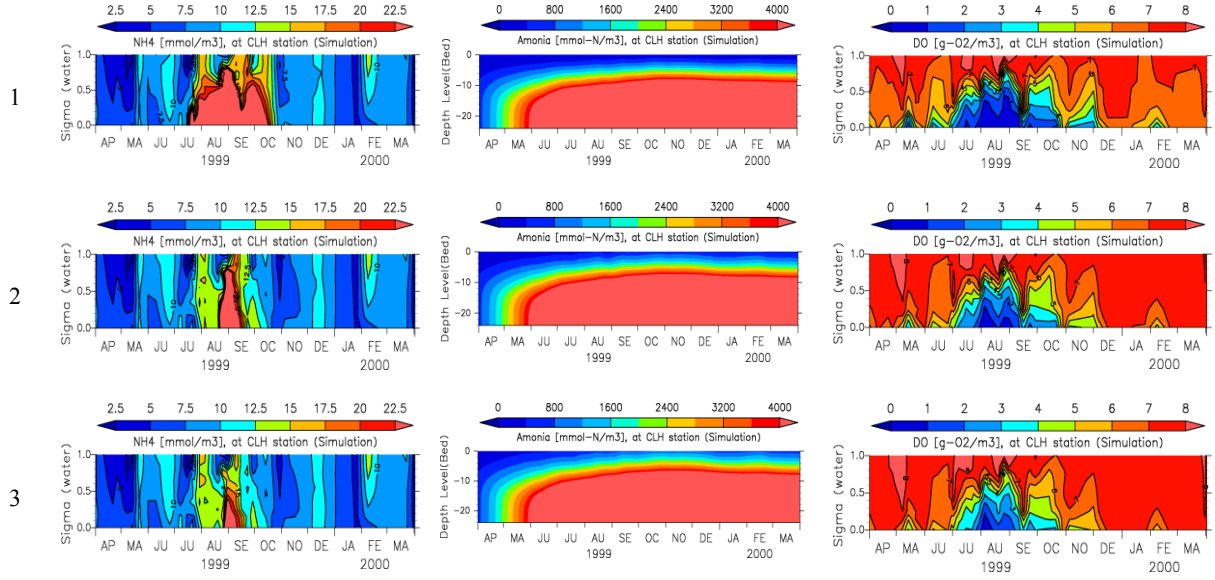

(a) (b) (c)

Fig 8.7 (a) Simulated bottom ammonia variation in water column, (b) surface ammonia variation in sediment column, (c) bottom oxygen variation in water column with (1) 1mm, (2) 3mm and (3) 5mm surface layer thickness in sediment

At the same time, since the oxygen flux to sediment which has been considered as sediment oxygen demand (SOD) has increased **(Fig 8.8)** with the reducing surface layer thickness in sediment, duration of hypoxic or anoxic water has increased ensuing increased duration of flux release.

On the other hand when the thickness of the surface layer of sediment is increased, increased concentrations of nutrients have released flux with larger peak value during a short period. Those sensitivity analysis results have confirmed the consistency of the model (**Fig 8.9)**.

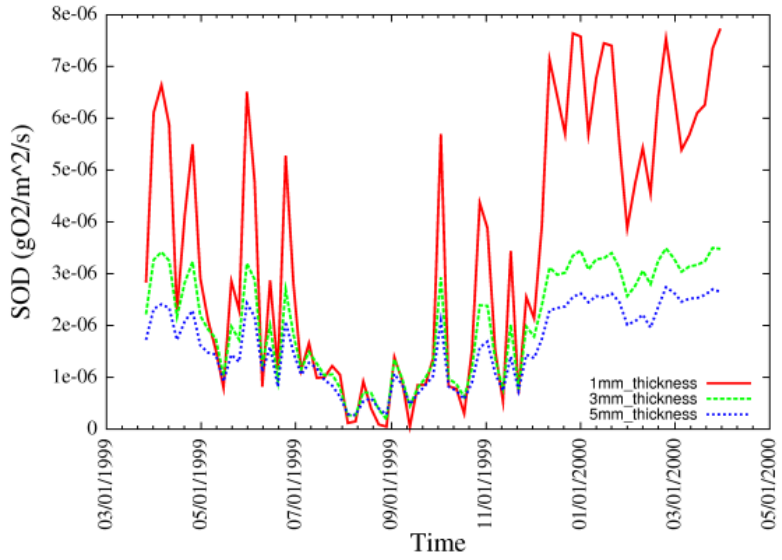

Fig 8.8 Sediment oxygen demand

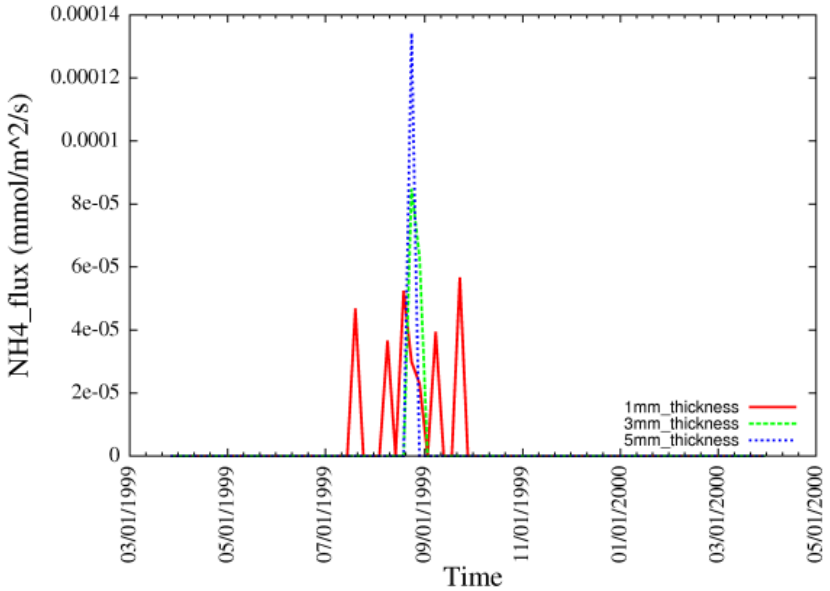

Fig 8.9 Ammonia flux

According to the **Fig 8.10** simulated bottom dissolved oxygen concentration in water column when the surface sediment layer thickness got 1mm, is more realistic with data. Hence, this analysis has been concluded that the multi-layered sediment model with maximum 1mm surface layer thickness gives the most realistic reproducibility of flux release in Tokyo Bay.

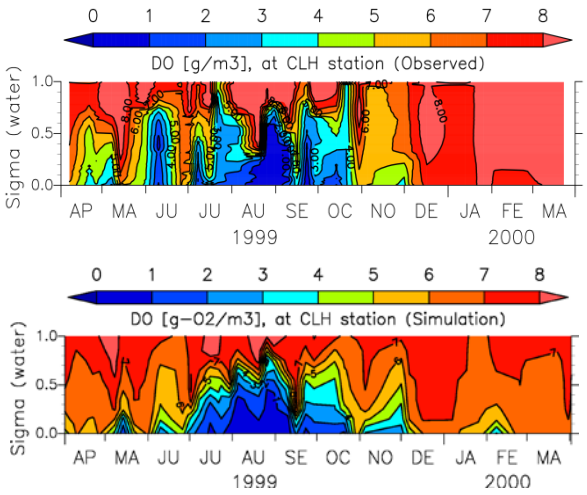

Fig 8.10 Observed and simulated (with 1mm surface layer thickness) dissolved oxygen concentration in water column at CLH

8.6 Sensitivity analysis on sorption and desorption

It has been found that particles which we expect to be stationery in sediment mix at approximately one-tenth the rate of pore water mixing. This movement has been confirmed as the effect of benthic macrofauna in surface layers. Macrofauna, the large animals that inhibit the sediment have a significant effect on flux release due to their metabolic process and/or as a consequence of their behaviour, for example tube building (Di Toro, 2001). Hence this mixing is highly sensitive to their existence. Under anoxic and hypoxic conditions they will decrease drastically while they can reappear when there is sufficient oxygen.

According to the equations **5.37** and **5.38** partitioning of the dissolved nutrients B have been considered as; $K_{n,k} = \left(f_p D_p + f_d D_d\right)_{i,j,k}$ where f_p : Particulate fraction, f_d : Dissolve fraction, D_p : Diffusion coefficient for particulate phase mixing and D_d : Diffusion coefficient for dissolved phase mixing. D_p represents the availability of macrofauna and

hence sensitivity of this parameter on sediment flux release has been analysed in this study (**Fig 8.11**).

It can be concluded that the larger the particulate mixing lower the release of flux. In another way the importance of benthic animal to restore the water quality has been confirmed through this analysis. Thus modeling of benthic animals is essential to reproduce accurate nutrient dynamics in Tokyo Bay. (The sensitivity of diffusion coefficient on flux release has been analysed before the final tuning of the model. Even though it can be expected the same conclusions it is recommended to perform the same analysis for the final tuned model).

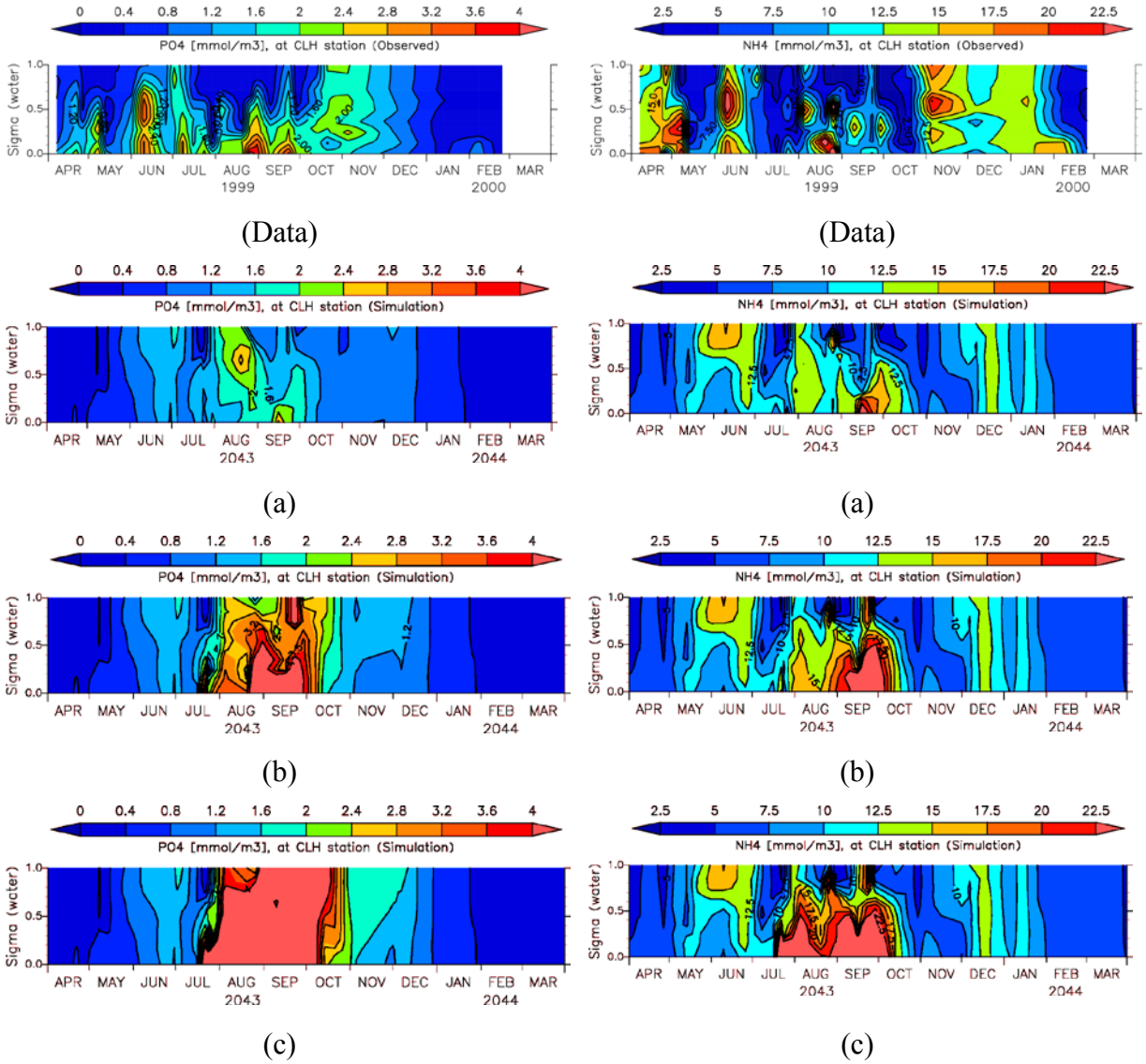

Fig 8.11 Simulated phosphorous and ammonia concentration in water column when (a) $D_p = 1\times10^{-5}$, (b) $D_p = 1\times10^{-6}$ and (c) $D_p = 1\times10^{-7}$ m^2/s

8.7 Sensitivity analysis of critical BSS on deposition and erosion

According to the equation **4.118** POC deposition or erosion is controlled by the BSS and critical bed shear stress on deposition (τ_D) and critical bed shear stress on erosion (τ_E). Hence, sensitivity of τ_D and τ_E on spatial distribution of POCC is analysed at the end of 10-year computation.

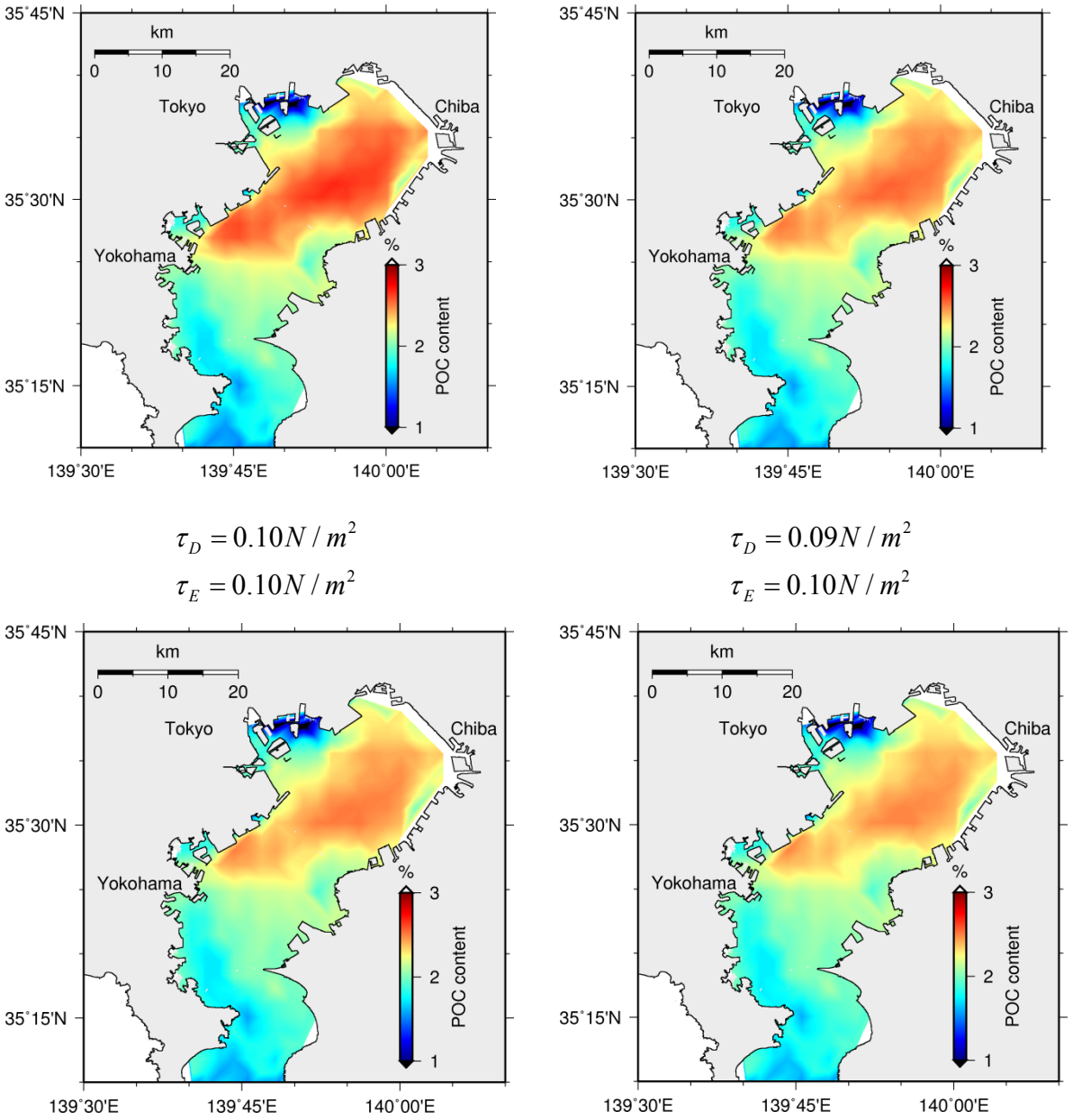

$\tau_D = 0.10N/m^2$, $\tau_E = 0.10N/m^2$

$\tau_D = 0.09N/m^2$, $\tau_E = 0.10N/m^2$

$\tau_D = 0.08N/m^2$, $\tau_E = 0.01N/m^2$

$\tau_D = 0.07N/m^2$, $\tau_E = 0.01N/m^2$

Fig 8.12 Variation of POCC with changing τ_D

Sensitivity of τ_D and τ_E on spatial distribution of POCC is analysed with changing τ_D and keeping τ_E constant. According to the **Fig 8.12** change of τ_D keeping τ_E constant has no significant effect on the spatial distribution of POCC qualitatively while it is reducing with reducing τ_D quantitatively.

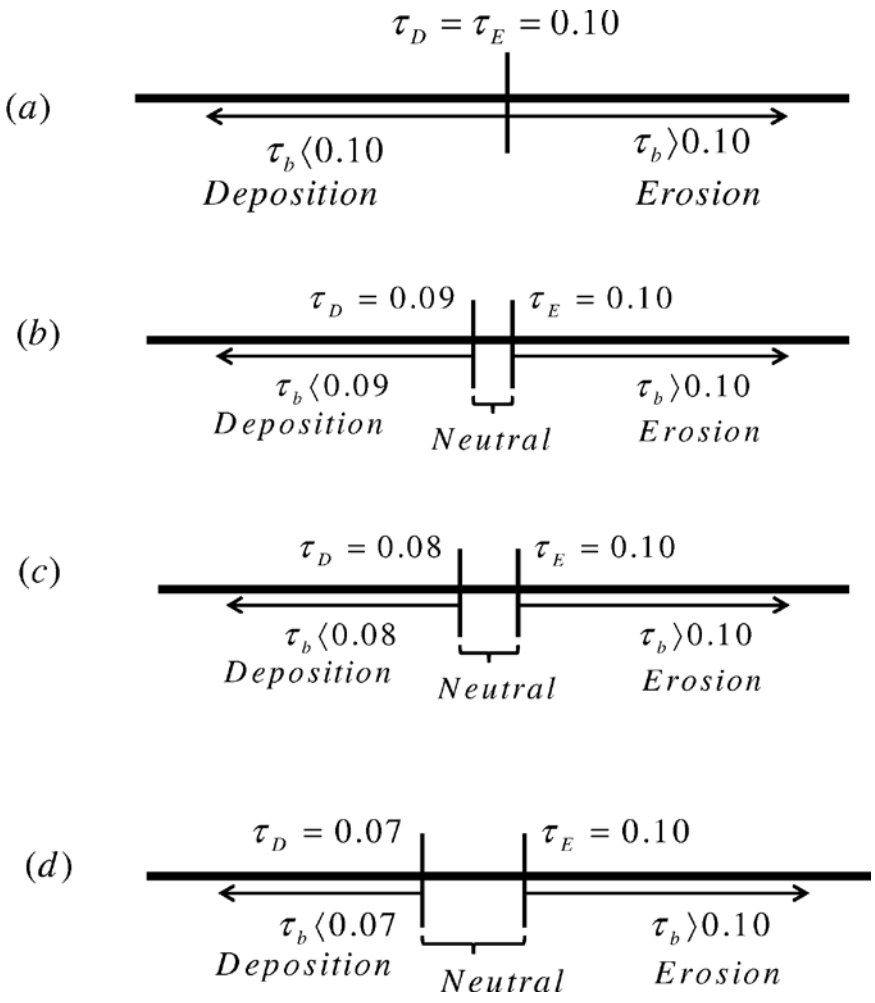

Fig 8.13 Change of neutral zone with change of τ_D

According to the **Fig 8.13**, neutral zone has increased with the decrease of τ_D. When the BSS is less than τ_E but greater than τ_D, sediments suspend in the bottom of the water. Thus, the possibility of sediment stratification at the water-sediment interface increases with the increase of the interval of τ_E and τ_D. At the same time with the decrease of τ_D possibility of particulate matter deposition is reduced causing lower POCC on sediment.

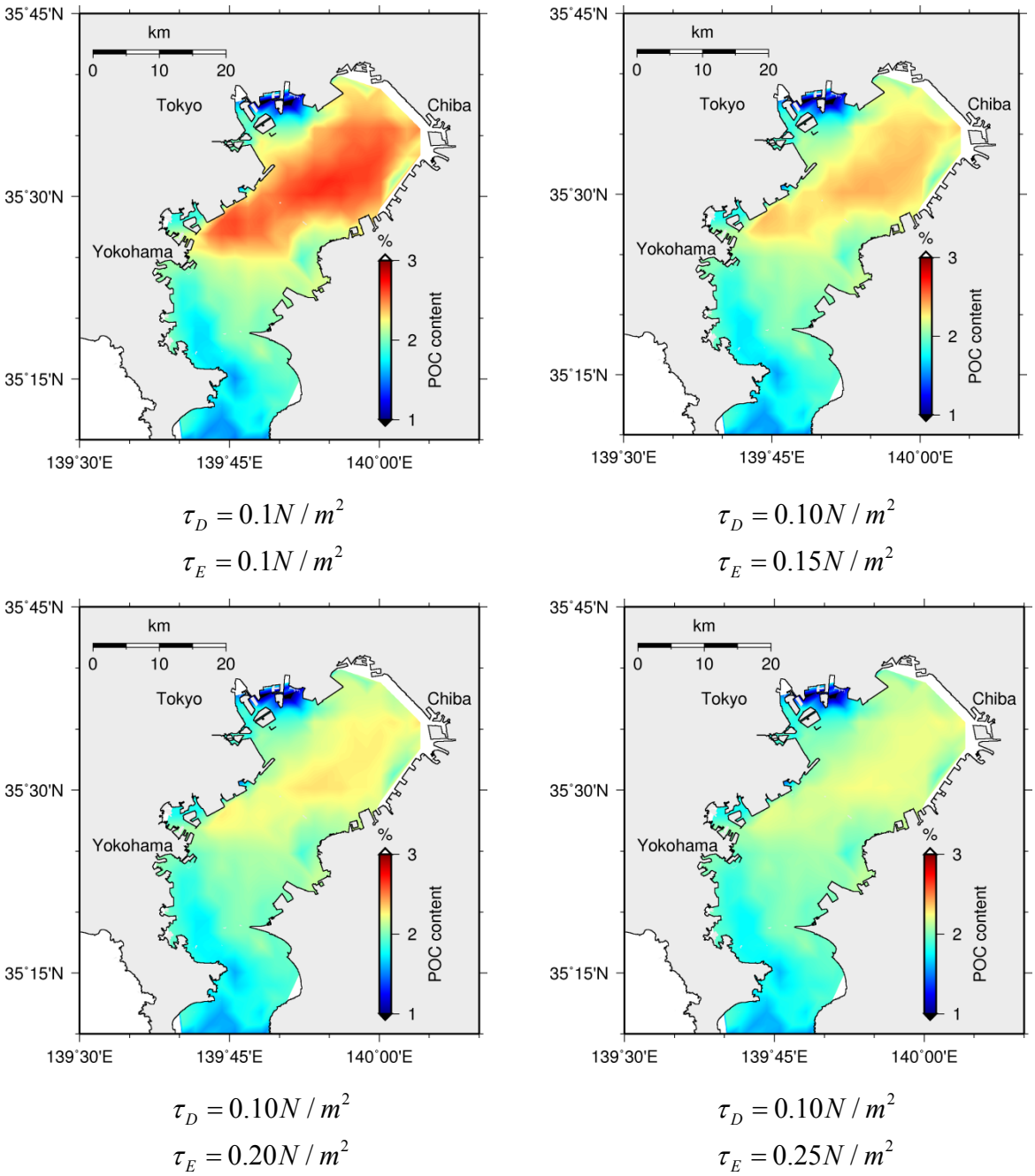

$\tau_D = 0.1N/m^2$ $\tau_E = 0.1N/m^2$

$\tau_D = 0.10N/m^2$ $\tau_E = 0.15N/m^2$

$\tau_D = 0.10N/m^2$ $\tau_E = 0.20N/m^2$

$\tau_D = 0.10N/m^2$ $\tau_E = 0.25N/m^2$

Fig 8.14 Variation of POCC with changing τ_E

Sensitivity of τ_D and τ_E on spatial distribution of POCC is analysed with changing τ_E and keeping τ_D constant. According to the **Fig 8.14** change of τ_E keeping τ_D constant has no significant effect on the spatial distribution of POCC qualitatively while it is reducing with increasing τ_E quantitatively.

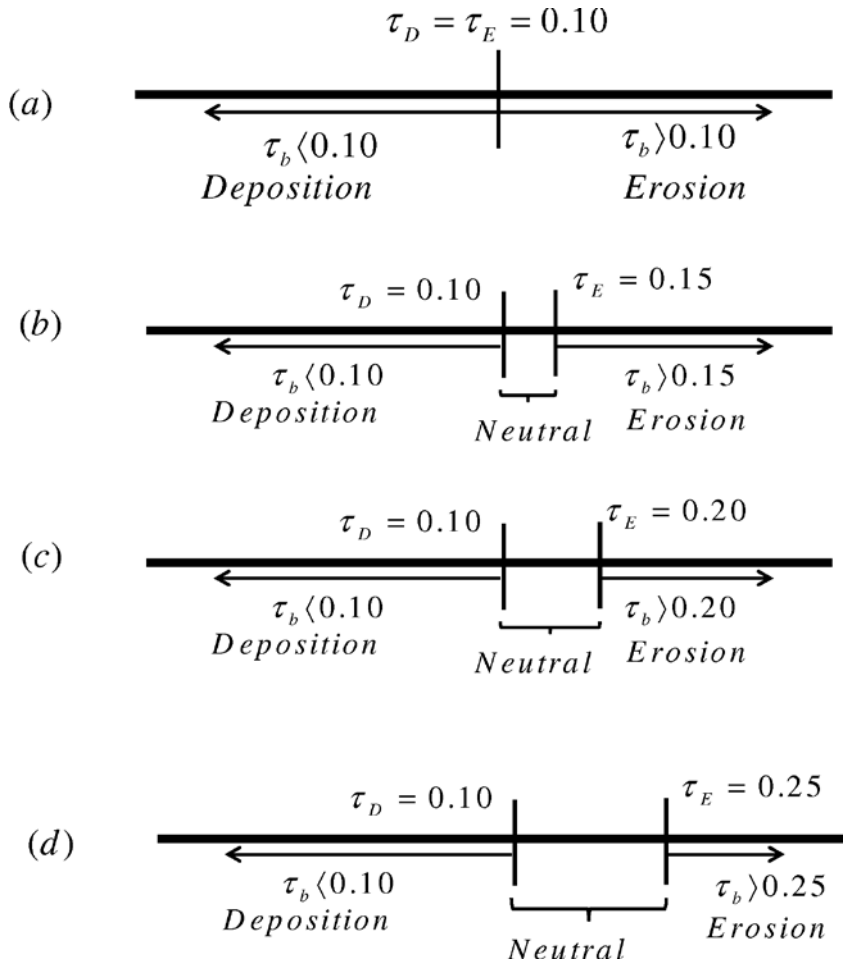

Fig 8.15 Change of neutral zone with the change of τ_E

According to the **Fig 8.15** neutral zone has increased with the increase of τ_E. When the BSS is less than τ_E but greater than τ_D, sediments suspend in the bottom of the water. Thus, the possibility of sediment stratification at the water-sediment interface increases with the increase of the interval of τ_E and τ_D. At the same time with the increase of τ_E possibility of particulate matter erosion is reduced. Even though the accumulation of POCC is expected to increase with decreased erosion it cannot be observed. This can be explained as, though the erosion is reduced particulate matter move out from the bed and suspend in the bottom of the water column and create a barrier to settle particulate organic matter across the bottom of the water column causing reduced particulate matter settling velocity. This has further confirmed that the settling velocity of particulate matter is controlled by its concentration.

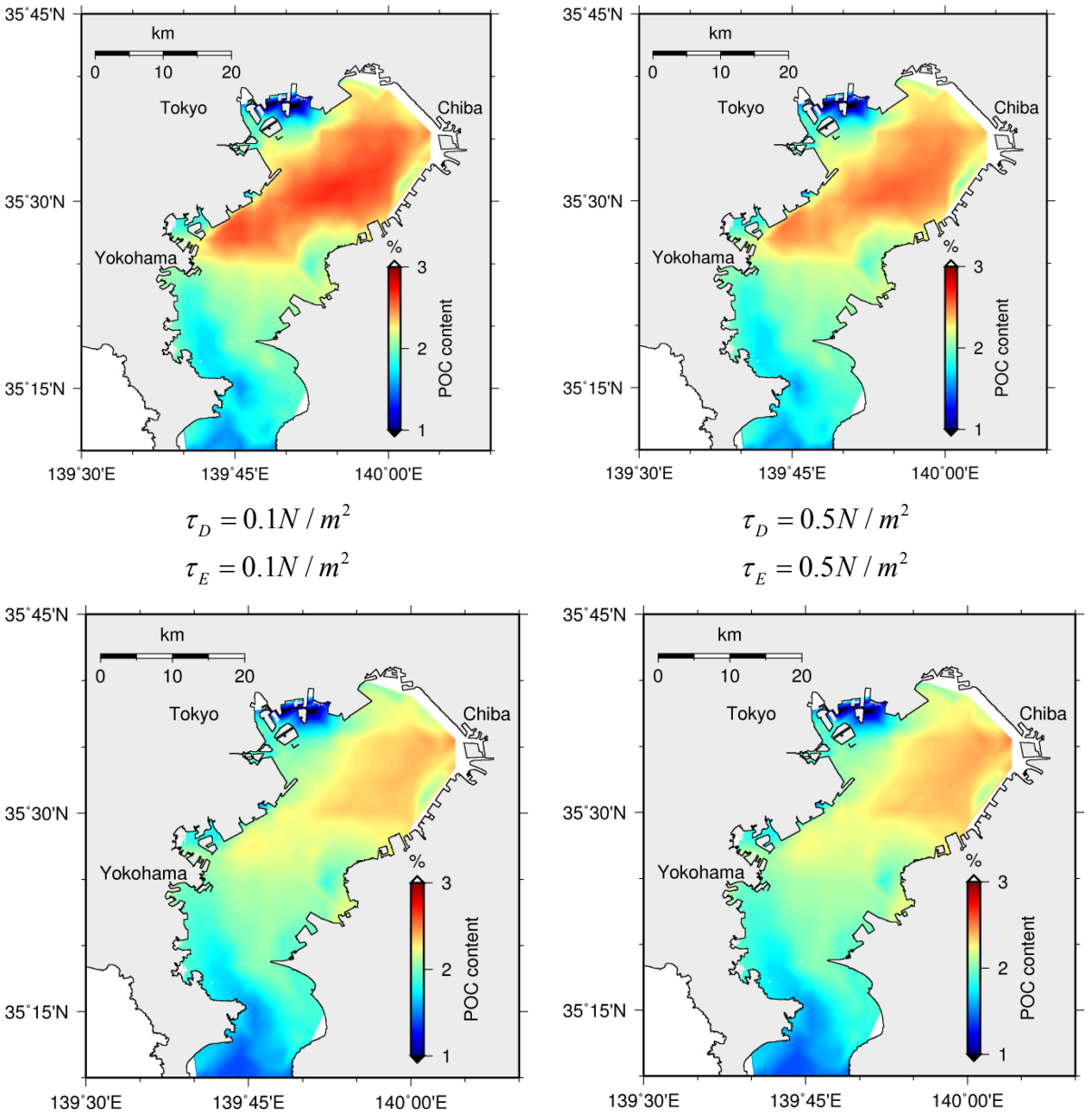

$\tau_D = 0.1N/m^2$ $\tau_E = 0.1N/m^2$

$\tau_D = 0.5N/m^2$ $\tau_E = 0.5N/m^2$

$\tau_D = 0.7N/m^2$ $\tau_E = 0.7N/m^2$

$\tau_D = 1.0N/m^2$ $\tau_E = 1.0N/m^2$

Fig 8.16 Variation of POCC with changing both τ_D and τ_E

Sensitivity of τ_D and τ_E on spatial distribution of POCC is analysed when the τ_D and τ_E are changed with no neutral zone. According to the **Fig 8.16**, change of τ_D and τ_E with no neutral zone makes significant effect on the spatial distribution of POCC. Even though it is expected to have increased POCC with increased τ_D, it has reduced.

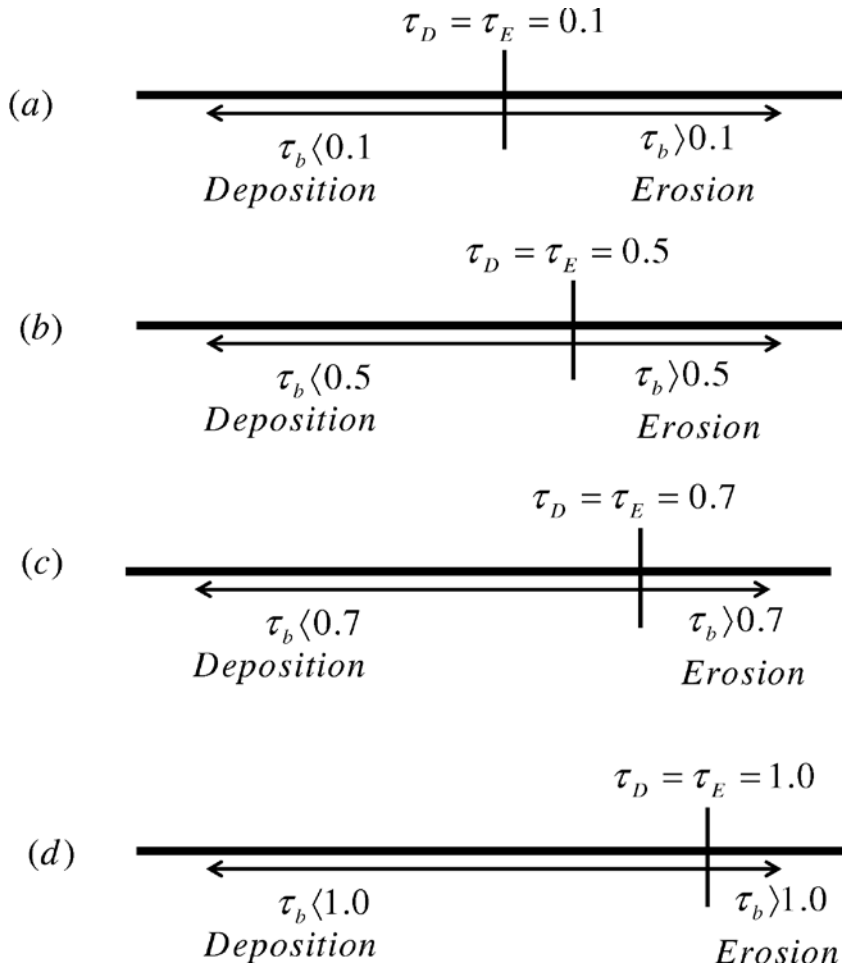

Fig 8.17 Change of possibility for deposition or erosion with change of τ_D and τ_E

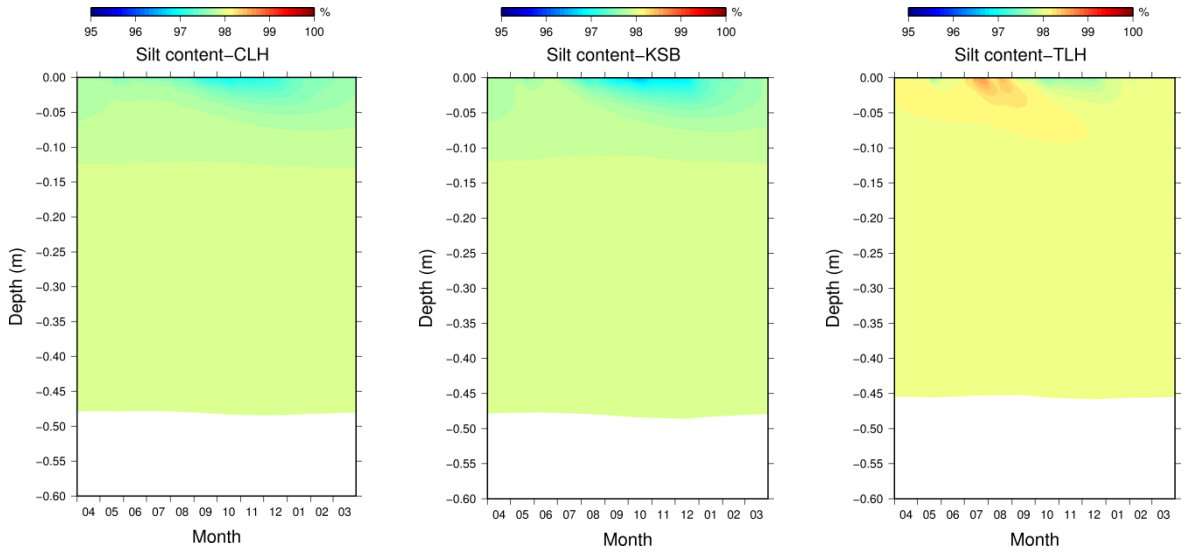

Fig 8.18 vertical distribution of Silt content

As shown in the **Fig 8.17**, either deposition or erosion occurs keeping no neutral zone. With the increase of $\tau_D = \tau_E$, the possibility of erosion increases while the possibility of erosion decreases. Hence POCC should have increased even though it has decreased. This can be further explained by the

Fig 8.18. Silt content is high towards the TLH while relatively low towards CLH and KSB. This may be due to the location of TLH is closer to a main river mouth. Thus, when the possibility of deposition increases POCC become diluted due to the lager component of silt deposition.

Thus, it is concluded that for long term computation of sediment quality, both τ_E and τ_D are very sensitive in the phase of quantitative accumulation of POC changing the spatial distribution of POCC quantitatively at the inner part of the Tokyo Bay. In order to obtain quantitatively accurate spatial distribution of POCC, τ_D and τ_E has to be tuned.

8.8 Sensitivity analysis of particulate organic carbon settling velocity on deposition

Sensitivity of particulate organic carbon settling velocity on spatial distribution of POCC is analyzed. The settling velocity of this model has been set as a constant during the whole model run. But sensitivity analysis results in **Fig 8.19** show that the particulate organic carbon settling velocity can significantly change the spatial distribution of POCC not only quantitatively but also qualitatively and hence it is recommended to model this in future studies.

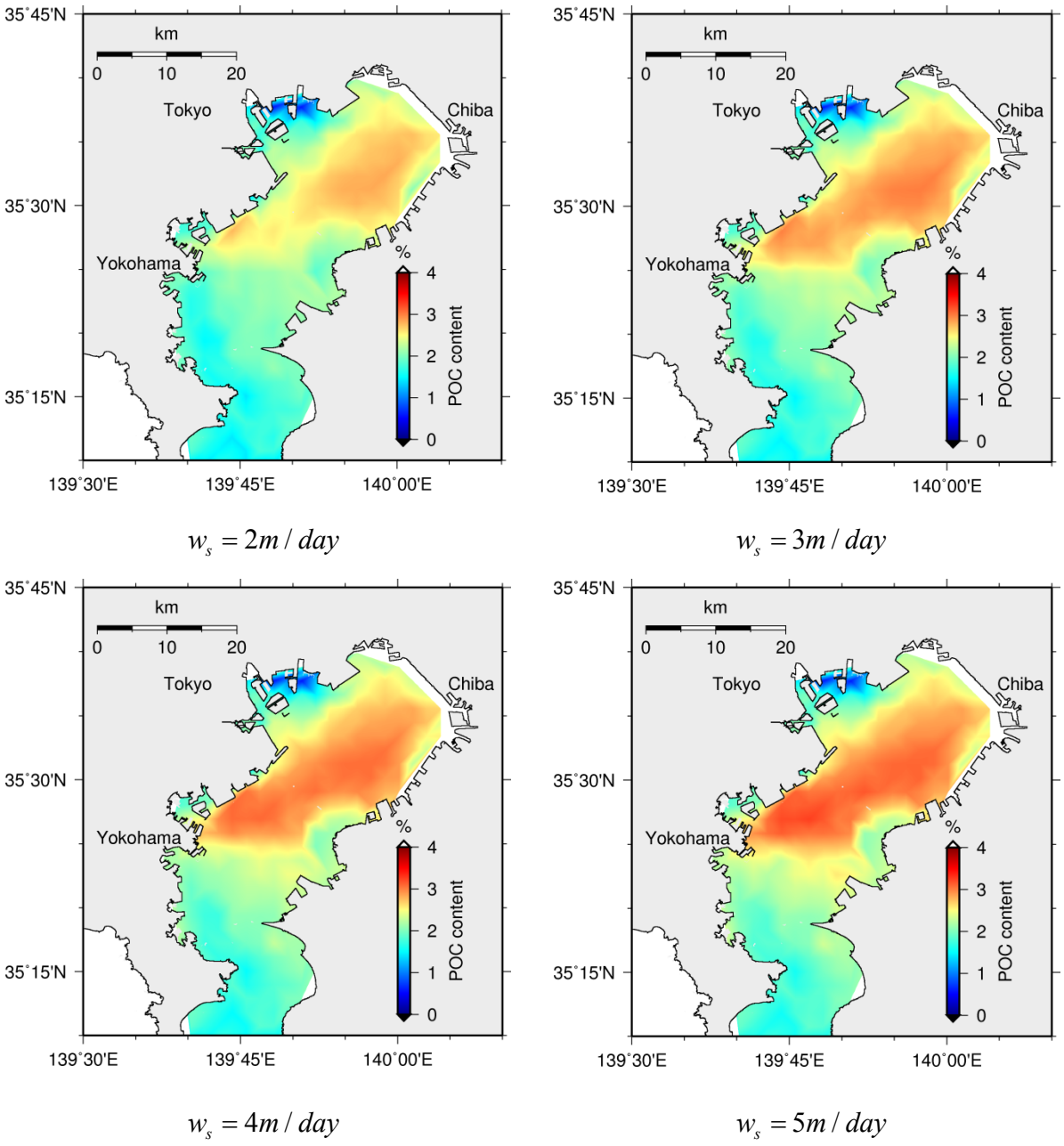

Fig 8.19 Variation of POCC with changing POC settling velocity

9. CONCLUSIONS

A long-term predictive model aiming for reproducing long-term dynamics of water quality and sediment quality in estuaries, including realistic process of sedimentary bed formation have been developed. Long term computation has been performed until the agreeable reproduction of both water and sediment quality with reasonable steady state is obtained through realistic initial conditions in Tokyo Bay.

The pelagic model is based on a multi-layer concept which provides a capability to analyze the vertical profiles of water quality, including salinity, temperature, DO, *Chl_a*, and nutrients such as ammonia, phosphorous, nitrate and silica and three forms of POC. Through the sensitivity analysis, it has been found that the available river discharge data has to be corrected and to obtain the optimum results of salinity and temperature they have to magnify with a magnification factor of 2.0. Computed model results for oxygen, Chlorophyll_*a*, ammonia and phosphorous dynamics of Tokyo Bay are basically consistent with those in measurements. Reproducibility of *Chl_a*, DO and nutrients can further improve through the model tuning. In addition to the above, the robustness of the model for long-term computation of water quality has been confirmed.

The benthic model is also based on a multi-layer concept which provides a capability to analyze the vertical profiles of sediment quality, including the porosity, WC, and POCC. Through the sensitivity analysis, it has been found that adopting the thickness of 1 mm for the surface bed layer gave the most realistic results in terms of nutrient flux release in Tokyo Bay. In addition, it has been confirmed that the existence of benthic animal can decrease the release of nutrient flux to water. Hence modeling of benthic animals is essential to reproduce the accurate nutrient dynamics in Tokyo Bay. Computed vertical distributions of sediment nutrients follow the vertical distributions proposed by reference data analysis while computed vertical distributions of POCC and WC are consistent with those in measurements. Furthermore, it is found that the computed spatial variation in sediment quality, including POCC, WC, TNC and TPC are basically consistent with those in measurements, showing that their highest contents are observed around the central part of the inner bay. At the same time it has been confirmed that the positive correlation of sediment quality such as POCC, TNC and TPC with WC. In order to improve the reproducibility of TNC and TPC, it is essential to model PON and POP in water and sediment. Furthermore, it has been obtained that the similar distribution of POCC in sediment and DO distribution in bottom water confirming the

phenomena of sediment pollution represented by POCC cause severe DO depletion (anoxia) in Tokyo Bay. The robustness of the model for long term computation of sediment quality has also been confirmed.

It has been confirmed that there exists strong correlation between the spatial distribution of BSS and spatial distribution of POCC, and hence accurate modeling of BSS is essential to reproduce the spatial distributions of sediment quality thus bottom water deterioration such as anoxia/hypoxia formation. It is concluded that, with the long term computational results, both τ_E and τ_D are sensitive especially for the quantitative accumulation of POC changing the spatial distribution of POCC quantitatively in the inner part of the Tokyo Bay. Moreover, settling velocity of particulate matter settling has significant effect on the spatial distribution of sediment quality. Hence, further improvements should be made especially in the modeling of settling velocity of particulate materials considering the effect of turbulence.

More considerations on boundary conditions must also be significant to improve the computational results, including the effect of the oceanic waters intruding into the bay and inorganic sediment flux discharged into the bay through rivers. After the validation of long term results, this model can be adopted to predict long term conditions and to propose measures against hypoxia in Tokyo Bay. Moreover, this modeling approach will be useful for considering long-term strategy to improve anoxia and hypoxia in polluted embayments in the world.

REFERENCES

Achiari, H., Sasaki, J., 2007. Numerical analysis of wind-wave climate change and spatial distribution of bottom sediment properties in Sanbanze Shallows of Tokyo Bay. J. Coast. Res. 50, 343–347.

Achiari, H., 2007, Computation of Wave-Current Field in Sanbanze Shallows of Tokyo Bay, PhD Dissertation, Yokohama National University, 102pp.

Attari, M.J., 2012, Numerical Modeling of Water Quality Considering Sediment Biochemical Processes in Tokyo Bay, PhD Dissertation, Yokohama National University, 154pp.

Attari, M.J., Sasaki, J., 2012. An Enhanced Numerical Model for Material Cycling and Dissolved Oxygen Dynamics in Tokyo Bay, Japan.

Attari, M.J., Sasaki, J., others, 2012. Modeling of Light Intensity and Phytoplankton Dynamics in Tokyo Bay Using Monitoring Dataset, in: The Twenty-Second International Offshore and Polar Engineering Conference. International Society of Offshore and Polar Engineers.

Bouman, H.A., Nakane, T., Oka, K., Nakata, K., Kurita, K., Sathyendranath, S., Platt, T., 2010. Environmental controls on phytoplankton production in coastal ecosystems: A case study from Tokyo Bay. Estuar. Coast. Shelf Sci. 87, 63–72.

Di Toro, D.M., 2001. Sediment flux modeling. Wiley-Interscience New York.

Fennel, W., Neumann, T., 2004. Introduction to the Modelling of Marine Ecosystems. Elsevier BV pp. 297.

Fossing H., Berg P., Thamdrup B., Rysgaard S., Sorensen H.M., Nielsen K., 2004, A model set-up for an oxygen and nutrient flux model for Aarhus Bay (Denmark), NERI Technical Report, No.483.Franz, G., Pinto, L., Ascione, I., Mateus, M., Fernandes, R., Leitão, P., Neves, R., 2014. Modelling of cohesive sediment dynamics in tidal estuarine systems: Case study of Tagus estuary, Portugal. Estuar. Coast. Shelf Sci. 151, 34–44.

Fujiwara, T., Yamada, Y., 2002. Inflow of oceanic water into Tokyo Bay and generation of a subsurface hypoxic water mass. J. Geophys. Res. Oceans 107, 13–1.

Gao, G., Falconer, R.A., Lin, B., 2011. Numerical Modelling Sediment-Bacteria Interaction Processes in the Severn Estuary. J. Water Resour. Prot. Vol.3, pp. 22–631.

Goda, Y., 2010. Random Seas and Design of Maritime Structures, 3 edition. ed. World Scientific Publishing Company, New Jersey.

Han, M.-S., Furuya, K., 2000. Size and species-specific primary productivity and community structure of phytoplankton in Tokyo Bay. J. Plankton Res. 22, 1221–1235.

Han, M.-S., Furuya, K., Nemoto, T., 1991. Species-specific productivity of Skeletonema costatum (Bacillariophyceae) in the inner part of Tokyo Bay. Mar. Ecol.-Prog. Ser. - MAR ECOL-PROGR SER 79, 267–273.

Ji, Z.-G., 2008. Hydrodynamics and water quality: modeling rivers, lakes, and estuaries. Wiley. com.

Justić, D., Wang, L., 2014. Assessing temporal and spatial variability of hypoxia over the inner Louisiana–upper Texas shelf: Application of an unstructured-grid three-dimensional coupled hydrodynamic-water quality model. Cont. Shelf Res. 72, 163–179.

Kim, D.-M., Nakada, N., Horiguchi, T., Takada, H., Shiraishi, H., Nakasugi, O., 2004. Numerical simulation of organic chemicals in a marine environment using a coupled 3D hydrodynamic and ecotoxicological model. Mar. Pollut. Bull. 48, 671–678.

Kim, T., Peter Sheng, Y., Park, K., 2010. Modeling water quality and hypoxia dynamics in Upper Charlotte Harbor, Florida, U.S.A. during 2000. Estuar. Coast. Shelf Sci. 90, 250–263.

Koibuchi, Y., Isobe, M., 2007. Phytoplankton bloom mechanism in an area affected by eutrophication: Tokyo Bay in spring 1999. Coast. Eng. J. 49, 461–479.

Koibuchi, Y., Ogura, H., Ando, H., Gomyo, H., Sasaki, J., Isobe, M., 2000. Observation of annual cycle of nutrients in the inner part of Tokyo Bay. Annu. J Coast. Eng JSCE Vol. 47, pp. 1066–1070.

Koibuchi, Y., Sasaki, J., Isobe, M., 2001. Study on budget and circulation of nitrogen and phosphorus in Tokyo Bay. Proc Coast. Eng JSCE Vol. 48, pp. 1076–1080.

Li, K., Zhang, L., Li, Y., Zhang, L., Wang, X., 2015. A three-dimensional water quality model to evaluate the environmental capacity of nitrogen and phosphorus in Jiaozhou Bay, China. Mar. Pollut. Bull. 91, 306–316.

Liu, W.-C., Chan, W.-T., Young, C.-C., 2015. Modeling fecal coliform contamination in a tidal Danshuei River estuarine system. Sci. Total Environ. 502, 632–640.

Lopes, J.F., Silva, C.I., Cardoso, A.C., 2008. Validation of a water quality model for the Ria de Aveiro lagoon, Portugal. Environ. Model. Softw. 23, 479–494.

Massoudieh, A., Bombardelli, F.A., Ginn, T.R., 2010. A biogeochemical model of contaminant fate and transport in river waters and sediments. J. Contam. Hydrol., Frontiers in Reactive Transport: Microbial Dynamics nad Redox Zonation in the Subsurface 112, 103–117.

Missaghi, S., Hondzo, M., 2010. Evaluation and application of a three-dimensional water quality model in a shallow lake with complex morphometry. Ecol. Model. 221, 1512–1525.

Na, E.H., Park, S.S., 2006. A hydrodynamic and water quality modeling study of spatial and temporal patterns of phytoplankton growth in a stratified lake with buoyant incoming flow. Ecol. Model., Ecological Models as Decision Tools in the 21st Century Proceedings of a conference organized by the International Society for Ecological Modelling (ISEM)in Quebec, Canada, August 22--24, 2004 199, 298–314.

Nakane, T., Nakaka, K., Bouman, H., Platt, T., 2008. Environmental control of short-term variation in the plankton community of inner Tokyo Bay, Japan. Estuar. Coast. Shelf Sci. 78, 796–810.

Okada, T., Furukawa, K., 2005. Mapping sediment condition and benthos of shoreward area in Tokyo Bay. Annu. J Coast. Eng JSCE Vol. 52, pp. 1431–1435.

Okada, T., Furukawa, K., 2005. Mapping Sediment Conditions of Shoreward Area in Tokyo Bay Using Echo Features. Proc. Civ. Eng. Ocean 21, 749–754.

Patankar, S., 1980. Numerical Heat Transfer and Fluid Flow. CRC Press.

Phillips, N., 1957. A Coordinate System Having some Special Advantages for Numerical Forecasting. J. Meteorol. 14, 184–185.

Pochai, N., 2009. A numerical computation of a non-dimensional form of stream water quality model with hydrodynamic advection–dispersion–reaction equations. Nonlinear Anal. Hybrid Syst. 3, 666–673.

Rasmeemasmuang, T., 2007, Integrated Modeling of Multi-Class Sediment Dynamics in a Semi-Enclosed Coastal Sea, PhD Dissertation, Yokohama National University, 147pp.

Rasmeemasmuang, T., Sasaki, J., 2008. Modeling of mud accumulation and bed characteristics in Tokyo Bay. Coast. Eng. J. 50, 277–307.

Sano, H., 2014. Spatial Characteristics of Organic Rich Sediment Accumulation in the inner part of Tokyo Bay, Master dissertation, The University of Tokyo, 71pp.

Sasaki, J., Isobe, M., 2000. Development of a long-term predictive model for baroclinic circulation and its application to Blue Tide phenomenon in Tokyo Bay, in: Coastal Engineering 2000. ASCE, pp. 3870–3883.

Sasaki, J., Kanayama, S., Nakase, K., Kino, S., 2009. Effective Application of a Mechanical Circulator for Reducing Hypoxia in an Estuarine Trench. Coast. Eng. J. 51, 309–339.

Sasaki, J., Koibuchi, Y., Isobe, M., 2002. Realistic Numerical Simulation of Water Quality and Ecosystems in Tokyo Bay, in: Proc. of the Third Joint Meeting of the Coastal Environmental Science and Technology Panel of the United States-Japan Cooperative Program in Natural Resources. pp. 143–157.

Sohma, A., Sekiguchi, Y., Kuwae, T., Nakamura, Y., 2008. A benthic–pelagic coupled ecosystem model to estimate the hypoxic estuary including tidal flat—Model description and validation of seasonal/daily dynamics. Ecol. Model. 215, 10–39.

Sohma, A., Sekiguchi, Y., Yamada, H., Sato, T., Nakata, K., 2001. A new coastal marine ecosystem model study coupled with hydrodynamics and tidal flat ecosystem effect. Mar. Pollut. Bull. 43, 187–208.

Tufford, D.L., McKellar, H.N., 1999. Spatial and temporal hydrodynamic and water quality modeling analysis of a large reservoir on the South Carolina (USA) coastal plain. Ecol. Model. 114, 137–173.

Wan, Y., Ji, Z.-G., Shen, J., Hu, G., Sun, D., 2012. Three dimensional water quality modeling of a shallow subtropical estuary. Mar. Environ. Res. 82, 76–86.

Zhang, W., Watson, S.B., Rao, Y.R., Kling, H.J., 2013. A linked hydrodynamic, water quality and algal biomass model for a large, multi-basin lake: A working management tool. Ecol. Model. 269, 37–50.

Zhang, Z., Sun, B., Johnson, B.E., 2015. Integration of a benthic sediment diagenesis module into the two dimensional hydrodynamic and water quality model – CE-QUAL-W2. Ecol. Model. 297, 213–231.

Zhao, L., Li, Y., Zou, R., He, B., Zhu, X., Liu, Y., Wang, J., Zhu, Y., 2013. A three-dimensional water quality modeling approach for exploring the eutrophication responses to load reduction scenarios in Lake Yilong (China). Environ. Pollut. 177, 13–21.

Zhao, L., Zhang, X., Liu, Y., He, B., Zhu, X., Zou, R., Zhu, Y., 2012. Three-dimensional hydrodynamic and water quality model for TMDL development of Lake Fuxian, China. J. Environ. Sci. 24, 1355–1363.

Zheng, L., Chen, C., Zhang, F.Y., 2004. Development of water quality model in the Satilla River Estuary, Georgia. Ecol. Model. 178, 457–482.

PUBLICATIONS

1. Amunugama, A.A.W.R.R.M.K., Sasaki, J., Nakamura, Y. and Suzuki, T. : Development of a benthic-pelagic coupled model for reproducing water quality in Tokyo Bay, *J. JSCE B3(Oceanic Eng.)*, Vol., 71, 2015.

2. Amunugama, A.A.W.R.R.M.K., Sasaki, J., Nakamura, Y. and Suzuki, T. : Spatial distribution of sediment quality in Tokyo Bay through benthic-pelagic coupled modeling approach, *J. JSCE B2(Coastal Eng.)*, Vol., 71, 2015. (in press)